A BIOMECHANICAL INVESTIGATION OF A DISLOCATION SPINAL CORD INJURY IN A RAT MODEL

by

Stephen Frank Ernesto Mattucci

B.A.Sc., The University of British Columbia, 2008

M.A.Sc., The University of Waterloo, 2011

A THESIS SUBMITTED IN PARTIAL FULFILLMENT OF

THE REQUIREMENTS FOR THE DEGREE OF

DOCTOR OF PHILOSOPHY

in

THE FACULTY OF GRADUATE AND POSTDOCTORAL STUDIES

(Biomedical Engineering)

THE UNIVERSITY OF BRITISH COLUMBIA

(Vancouver)

December 2017

Abstract

Traumatic spinal cord injuries clinically occur in a heterogeneous fashion, including at different spinal levels, injury velocities, and injury mechanisms. Clinical treatment options, such as early surgical decompression produce inconsistent recovery outcomes in the patient population, despite demonstrating effectiveness in preclinical animal models. The most common biomechanical factors, such as cervical level, high-energy impact and dislocation injury mechanism, are not adequately represented in preclinical models, which may explain the lack of agreement between clinical studies. The overall objective of this thesis was to investigate the biomechanics of a high-speed cervical dislocation rat model at acute stages, refine the model, and incorporate residual compression. The temporal progression of acute SCI was investigated in different injury mechanisms, where dislocation injuries demonstrated the fastest loss of white matter tissue. To refine the dislocation model, new vertebral injury clamps were designed with a feature allowing the clamps to pivot and self-align when tightened. The vertebral kinematics during a dislocation injury were analysed using high-speed x-ray and clamp slippage was significantly reduced with the self-aligning clamps, compared to the existing clamps. This study also emphasized the importance of validating injury displacements against input parameters, particularly when comparing results or reproducing injuries. In order to implement residual compression within the dislocation model, injury parameters were independently investigated. Electrophysiology techniques were implemented to determine a minimum residual compression depth that affects signal conduction following a traumatic injury. Continuously holding the residual compression following the initial injury induced a significantly different physiological response compared to when the injury was immediately reduced. Behavioural outcome was used to identify severities following a range of displacements, and four hours of residual compression was survivable following a ‘mild’ traumatic injury, indicating suitable parameters for future studies. Rats of the same weight were identified to have different anatomical dimensions and structural properties of the spinal column, potentially influencing injury outcomes in closed-column models. The continued development and implementation of the cervical dislocation injury model in the rat will deepen understanding of SCI biomechanics and provide an additional clinically-relevant injury model for testing the robustness of potential treatment therapies.

Lay Summary

The overall objective was to investigate the biomechanics of spinal cord injury (SCI) in a rat model. Some of the most common factors in human injuries are currently underrepresented in preclinical SCI research. These include: a high speed injury, in the neck, and where the spinal cord is pinched between two displaced vertebrae; known as a ‘dislocation injury mechanism’.

The progression of tissue damage over time was observed to be faster after a dislocation compared to other injury mechanisms. Custom spine clamps were redeveloped to produce consistent spine motion during the dislocation injury, which was analysed using high speed x-ray. Finally, the spinal cord was held in compression following the initial traumatic injury, which is particularly clinically relevant to the timing of surgery after SCI.

These improvements to the dislocation model will provide future researchers a robust avenue to further investigate the importance of biomechanical factors contributing to SCI.

Preface

A version of Chapter 1 has been submitted for publication: Mattucci S., Speidel J., Liu., Kwon B.K., Tetzlaff W., and Oxland T., (submitted September 2017) Basic biomechanics of SCI – how injuries happen in people and how animal models have informed our understanding. This was a review article based primarily on the literature reviewed in the Introduction. I was responsible for writing the manuscript, with editing assistance from my co-authors.

A version of Chapter 2 is in preparation for publication: Mattucci S., Liu J., Kwon B.K., Tetzlaff W., and Oxland T., Temporal progression of acute spinal cord injury mechanisms in a rat model: contusion, dislocation, and distraction. I was responsible for conducting the experiments, collecting the data, analyzing the data, performing statistical analyses and writing the chapter. I had assistance in the design of the experiment (Drs. Tetzlaff, Kwon and Oxland). I received assistance in preparing the specimens (Dr. J. Liu), and producing and analyzing the histological data (C. Fournier). I also received assistance editing the chapter (Drs. Tetzlaff and Oxland). Ethical approval was provided by the University of British Columbia Animal Care Committee under certificate A13-0075.

A version of Chapter 3 has been published: Mattucci S., Liu J., Fijal P., Tetzlaff W., and Oxland T., (2017) Repeatability of a dislocation spinal cord injury model in a rat – a high speed biomechanical analysis (Journal of Biomechanical Engineering). I was responsible for designing the study, designing the injury clamps, conducting the experiments, collecting the data, analyzing the data, performing statistical analyses and writing the manuscript. I received assistance in preparing the specimens (Dr. J. Liu) and analyzing the data (P. Fijal). I received editing assistance of the manuscript from all of my co-authors. Ethical approval was provided by the University of British Columbia Animal Care Committee under certificate A13-0075.

A version of Chapter 4 is in preparation for publication: Mattucci S., Speidel J., Liu J., Kwon B.K., Ramer M., Tetzlaff W., and Oxland T., The development of a cervical dislocation spinal cord injury rat model with residual compression. I was responsible for designing the study, conducting the experiments, collecting the data, analyzing the data, performing statistical analyses and writing the manuscript. I received assistance in designing the experiment (Dr. Oxland, J. Speidel), preparing the specimens (Dr. J. Liu, J. Speidel), designing experimental

devices and collecting the data (J. Speidel), and operation of electrophysiology equipment (Dr. M. Ramer). I also received assistance editing the chapter (Drs. Oxland and Ramer). Ethical approval was provided by the University of British Columbia Animal Care Committee under certificate A16-0268.

Table of Contents

List of Tables

List of Figures

List of Abbreviations

ALL - Anterior longitudinal ligament

AMS - ASIA Motor Score

ANOVA - Analysis of variance

ASIA - American Spinal Injury Association

CL - Capsular ligament

CNS - Central nervous system

CSF - Cerebrospinal fluid

CST - Corticospinal tract

EC - Eriochrome cyanine

ISL - Interspinous ligament

LF - Ligamentum flavum

LVDT - Linear variable differential transformer

MBP - Myelin basic protein

NF - Neurofilament-H

NYU - New York University

OCT - Optimal cutting temperature

OSU - Ohio State University

PBS - Phosphate buffered saline

PEEK - Polyether ether ketone

PLL - Posterior longitudinal ligament

PNS - Peripheral nervous system

RNS - Reactive nitrogen species

ROS - Reactive oxygen species

SCI - Spinal cord injury

SCIWORA-ET - Spinal cord injury without obvious radiographic abnormality or evidence of trauma

SD - Standard deviation

SSEP - Somatosensory evoked potentials

Tub - β-tubulin III

UBC - University of British Columbia

WM – White matter

Glossary

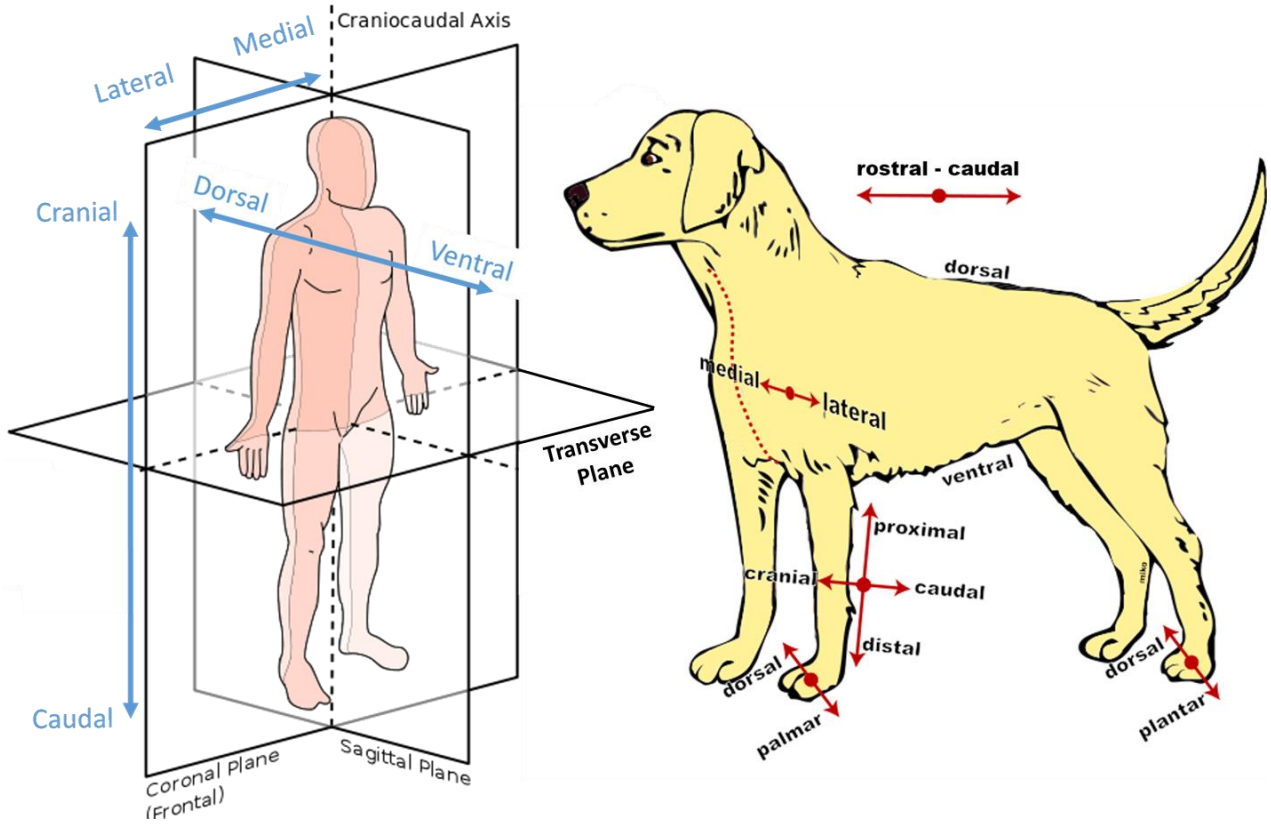

Cranial / rostral – toward the head

Caudal – toward the feet or tail

Ventral – toward the anterior or surface of an animal opposite the back

Dorsal – toward the posterior or back of an animal

Medial – toward the midline of the body

Lateral – away from the midline of the body

Distal – away from the centre of the body or point of attachment

Proximal – toward the centre of the body or point of attachment

Coronal (or frontal) plane – subdivides the body into ventral and dorsal halves

Sagittal plane – subdivides the body into lateral halves

Transverse plane – subdivides the body into cranial/rostral and caudal halves

Acknowledgements

I wish to first acknowledge the support of my research supervisor, Dr. Thomas Oxland. Before joining the lab, Dr. Oxland, I remember you telling me about the growth that one undergoes while completing a Ph.D., and it truly is remarkable to look back on how I've grown as an academic and as a person. I'd like to thank you for helping me see the value in the process. Lastly, thank you for always having an open door, your willingness to talk about anything from project difficulties, to career decisions. Your perspective has been invaluable. And of course "The data are the data."

I wish to graciously acknowledge the Wings for Life Spinal Cord Research Foundation, the Canadian Institutes of Health Research, and the Blusson Integrated Cures Partnership for the research funding that made this project possible.

I would like to thank my committee: Drs. Wolfram Tetzlaff, Brian Kwon, and Peter Cripton. Thank you for taking my simple questions seriously, and taking the time out of your busy schedules to meet, provide direction, and challenge me. After some recent conference experiences I have realized how lucky I have been to have such a diverse network to draw from.

Of course I need a separate paragraph to acknowledge the support and contributions of Dr. Jie Liu. Jie, there were many days when I felt exhausted or discouraged, but your passion and excitement for research gave me the energy to push on.

I would like to thank all of my colleagues at ICORD, whom I have had the pleasure of working with over the past several years. This environment relies on the support of one another, and I believe I have gained so much from my peers beyond what I could ever return. To those who came before me, Drs. Seth Gilchrist, Robyn Newell, Tim Bhatnagar, and Hannah Gustafson, thanks for ensuring that I've never been the smartest person in the room. Thanks for all the rousing discussions over the years. Thanks to Jason Speidel for challenging the ideas in our projects, helping to balance the workload of running such large experiments. Thanks to all of you who were able to provide quick answers and share a laugh when needed: Dr. Oscar Seira, Dr. Peggy Assinck, Cameron Lam, Greg Duncan, Caron Fourner, Andrew Yung, Angela Melnyk, and Nicole Janzen.

Lastly I would like to thank my family for the continued love and support throughout this journey. To my parents, Kathy and Domenic Mattucci, for always listening, and not asking when I'll be done. Mom, you are the strongest person I know. Thanks for always giving me advice, especially when it's the advice I'm looking to hear. Dad, thanks for teaching me the value of hard work. To my sister Aly, thanks for always reminding me appreciate the simple pleasures in life. Thanks so much to my grandparents, Teresa Mattucci, and the late Ernesto Mattucci and Frank Ridler. I often think about the challenges you each had to overcome over your lives, which inspires me to confront the unknowns in my own future. Thanks to Jasper, for simultaneously being the (2nd) biggest source, and relief of stress these past two years. And most importantly, thanks to my roommate, Mhairi. For keeping your head up through best and worst of times these past several years. A wise friend once told me that there isn't enough support for the significant other, and he was right. Mhairi, I could not have done this without you. I love you, and look forward to recalling many stories with "remember during Ph.D…".

Dedication

I would like to dedicate this work to my sister Aly Mattucci. The challenges you overcome on a daily basis make me believe that anything is possible. You provide me with more inspiration and motivation than you could ever know.

Chapter 1: Introduction

1.1 Overview

In this chapter the anatomy and physiology of the spine and spinal cord will be introduced. Clinical aspects relating to traumatic spinal cord injury (SCI) will be reviewed, including epidemiology, etiology, injury severity, and the timing of surgical decompression. Spinal column injury patterns and spinal cord injury mechanisms will be described with respect to relevant biomechanical parameters. A brief background of secondary SCI pathology will be introduced including the relationship between humans and rodent models. Preclinical animal injury models will be reviewed and discussed with respect to relevance to clinical injury biomechanics. Finally the chapter will conclude with the specific objectives of this thesis.

1.2 Anatomy and Physiology

1.2.1 Spinal Column Anatomy

The human spinal column consists of 24 aligned bones, known as vertebrae, which form the support structure of the human body and protect the spinal cord (Moore & Dalley, 1999). The spinal column is divided into four regions: cervical, thoracic, lumbar, and sacral (Figure 1-1). The seven most superior vertebrae comprise the cervical spine or the neck, and provide motion while supporting the head. The thoracic spine has twelve vertebrae, each connected to two ribs, which limit the mobility of these vertebrae (McKinley & O'Loughlin, 2008). The lumbar region has the five largest vertebrae, making up the lower back region. The sacrum is the most inferior region of the spine, consisting of five vertebrae fused together (Moore & Dalley, 1999).

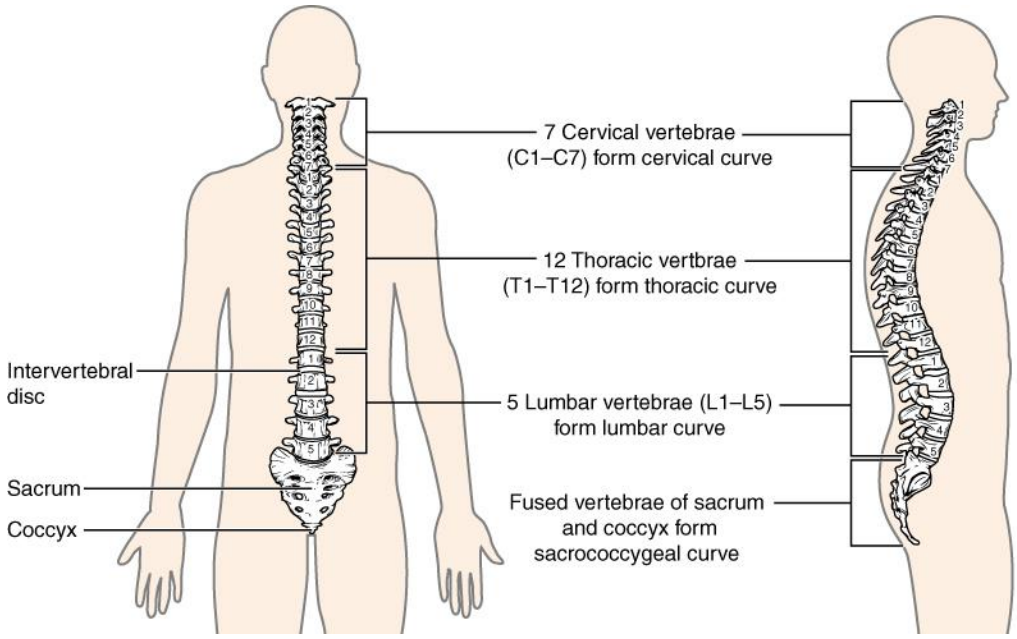

Figure 1-1– Anterior and sagittal views of the vertebral column. Image from: https://cnx.org/contents/4CMef3D9@4/The-Vertebral-Column (Creative Commons Attribution 4.0 License)

The main functions of each vertebra are to support axial loading and protect the spinal cord; thus there are some common anatomical features (Figure 1-2) (Moore & Dalley, 1999). All vertebrae consist of a vertebral body, the largest bony section, which transfers load between adjacent vertebrae via the intervertebral discs. Posterolateral bony structures called pedicles extend from the vertebral body and support bony pillars, which connect to adjacent vertebrae at superior and inferior articular joints called facet joints. The lamina extends posterior-medially from both facet joints, forming the vertebral arch (Moore & Dalley, 1999). These features together form the vertebral foramen, and with adjacent vertebrae, align to form the spinal canal, which protects the spinal cord. Additional bony protrusions from the vertebrae are processes, and serve as attachment points for ligaments and muscles, and additional foramina (or holes) allow passage of vertebral arteries or veins (Moore & Dalley, 1999).

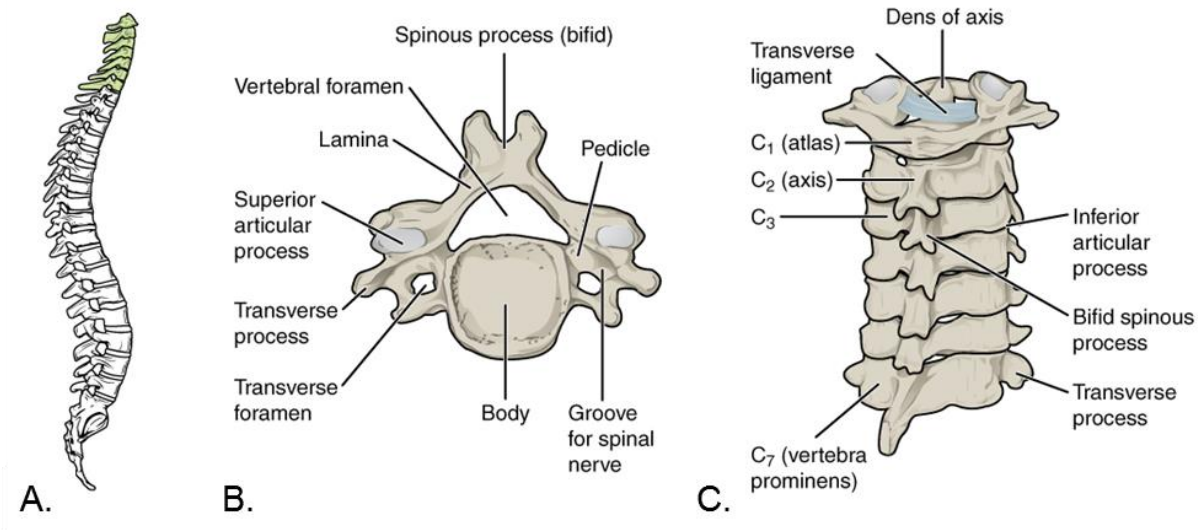

Figure 1-2 - Typical cervical vertebra. A. sagittal view of the spine, with cervical region highlighted, B. superior view of a typical cervical vertebra, C. posterior view of the cervical spine. Image from: https://cnx.org/contents/4CMef3D9@4/The-Vertebral-Column (Creative Commons Attribution 4.0 License)

This research primarily focuses on the cervical spine, so this region will be discussed in detail. The cervical vertebrae are referred to as C1 through C7, where the number corresponds to the spinal level; C1 being the most superior. C1 and C2, also known as the atlas and axis, respectively, have unique features, and C3 through C7 share very similar characteristics (Figure 1-2). C1, the atlas, has two large concave superior articular surfaces supporting the occipital condyles of the skull, allowing the head to move in flexion and extension (Moore & Dalley, 1999). C1 does not have a vertebral body, but a foramen that supports the bony odontoid process, or dens, from C2. The odontoid process extends superiorly from the vertebral body of C2, and is held in place within C1 by the transverse, alar, and apical ligaments (Moore & Dalley, 1999). This feature allows C1 and the head to rotate about C2, the axis.

Intervertebral Discs

The intervertebral discs are located between the vertebral bodies, and are responsible for supporting the loading on the spine and enabling movement (Roaf, 1960; White & Panjabi, 1990). The disc has three parts: the nucleus pulposus, annulus fibrosis, and the cartilaginous endplates (Figure 1-3). The nucleus pulposus is a gel-like substance within the disc, comprised mostly of water, where the water content degenerates with age (Moore & Dalley, 1999). The

annulus fibrosis surrounds the nucleus pulposus with layers of fibrous collagen bands and fibrocartilage, where the fibers are oriented at approximately 30 degrees from the transverse plane. The intervertebral discs of the cervical region are different: alternating layers of the annulus fibrosis do not exhibit alternating oblique orientations, and the thickness is crescent shaped – thickest anteriorly, and tapering towards lateral regions (Mercer & Bogduk, 1999). The posterior annulus consists of only a thin layer of longitudinal collagen fibers (Mercer & Bogduk, 1999). The lateral region consists of a thin layer of periosteofascial tissue covering the fibro-cartilaginous core (Mercer & Bogduk, 1999). Finally, uncinate processes extend superiorly from the lateral edges of the vertebral bodies to form uncovertebral joints with the superior vertebra, which affect motion coupling of the cervical spine (Clausen et al., 1997).

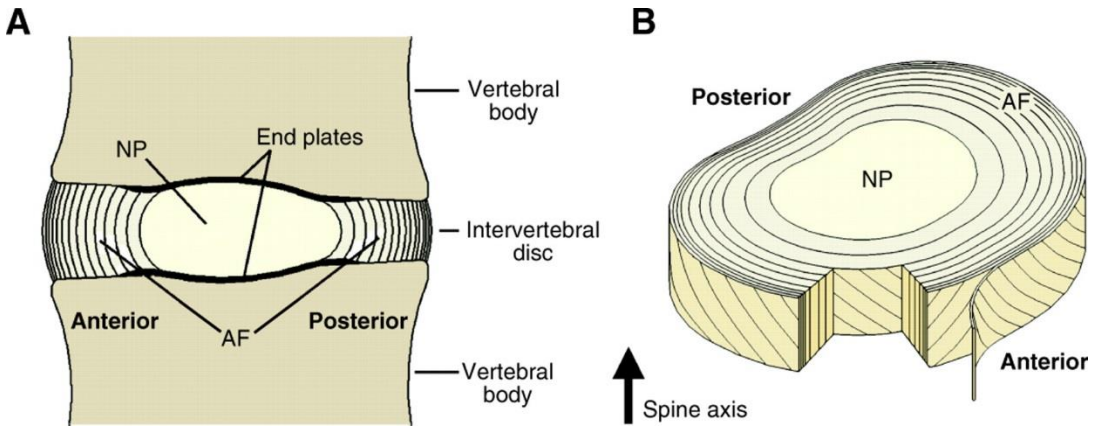

Figure 1-3 - Schematic of the intervertebral disc. A. sagittal cross section of disc between vertebral bodies, B. Three dimensional representation of fibrous layers surrounding nucleus pulposus. (Smith et al., 2010) (Creative Commons Attribution 3.0 License)

When a compressive load is applied to the disc, the nucleus becomes pressurized, causing the endplates and annulus to deform. The annulus bands resist this loading in tension. Similarly when the disc undergoes bending, it experiences both tension and compression, where the side in compression bulges outwards.

The outer annular fibers are thought to be the primary load bearing elements when adjacent vertebrae experience pure shear loading (Yingling & McGill, 1999). Further, the lateral annular fibers likely resist most of the shear loading due to disc geometry and fiber orientation, however in the lateral regions only half of the fibers are engaged (Yingling & McGill, 1999). The lateral fibers are also the first structures to fail, usually by endplate avulsion. When subjected to pure

shear loading, the lumbar intervertebral disc exhibits a linear displacement response under small loads, progressing to a stiffening, non-linear response under increasing loads – likely due to the increased activation and resistance of collagen fibers (Schmidt et al., 2015). Without a nucleus pulposus, annular fibers are relaxed and result in increased strain at low shear loading, compared to when the nucleus is present (Lantz et al., 1980). When vertebral segments experience pure shear loading, the articular facets are also responsible for load sharing (Lantz et al., 1980; Yingling & McGill, 1999).

Facet Joints

The facet joints are symmetrical pairs of synovial joints located posterolaterally to the vertebral bodies (Figure 1-4). The joints stabilize the spine and restrict motion, when the articular surfaces of adjacent vertebrae come into contact. The joint consists of articular cartilage surfaces from adjacent vertebrae, surrounded by a capsular ligament with synovial fluid inside acting as lubrication. The capsular ligament holds the articular surfaces together under tension. The facet joints are oriented at approximately 45 degrees from the transverse plane in the cervical spine, with the orientation differing along the length of the spinal column. When the spine moves in rotation or extension, the articular surfaces make contact, sliding over each other, limiting vertebral motion.

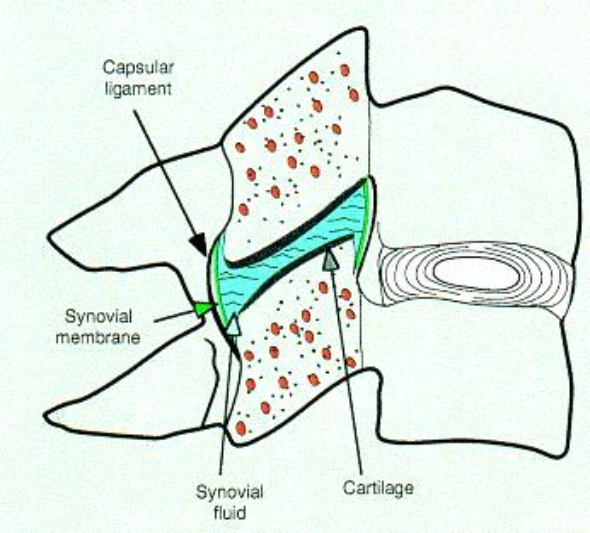

Figure 1-4 – Cross sectional view of facet joint. Articular cartilage surfaces from adjacent vertebrae are surrounded by capsular ligament, with synovial fluid contained in the joint. (reprinted with copyright permission) (Yoganandan et al., 2001)

Ligaments

Ligaments are fibrous bands that connect between bones and carry a tensile load in the direction of fiber orientation (Figure 1-5) (White & Panjabi, 1990). Ligaments are primarily comprised of collagen, elastin, proteoglycans, and water (Oza et al., 2006). Ligaments have four major functions (White & Panjabi, 1990): to allow proper motion of the vertebrae using minimal energy from surrounding muscles, provide spinal stability, protect the spinal cord by restricting motion and prevent the disc from protruding, and they must protect the spine in traumatic circumstances. When large loads are applied, the ligaments must restrict motion as well as absorb large amounts of energy applied to the system (White & Panjabi, 1990). The anterior longitudinal ligament (ALL) is a long, continuous band that runs the entire length of the spine along the anterior surface of the vertebrae and intervertebral discs and provides stability and prevents hyperextension of the vertebral column (Moore & Dalley, 1999). The posterior longitudinal ligament (PLL) is similar to the ALL in that it runs the length of the spine, only it is located within the spinal canal on the posterior surface of the vertebral bodies and intervertebral discs, and it helps to prevent hyperflexion and herniation of the discs. The ligamentum flavum (LF) are elastic ligaments connecting adjacent vertebral arches posterior to the vertebral canal, and preserve the normal curvature of the spine by helping to return vertebrae to the normal position following movement (Moore & Dalley, 1999). The capsular ligaments (CL) surround the facet joints, containing the synovial fluid, and limit flexion movements of the spine. The interspinous ligament (ISL) connects the spinous processes and also limits flexion of the spine.

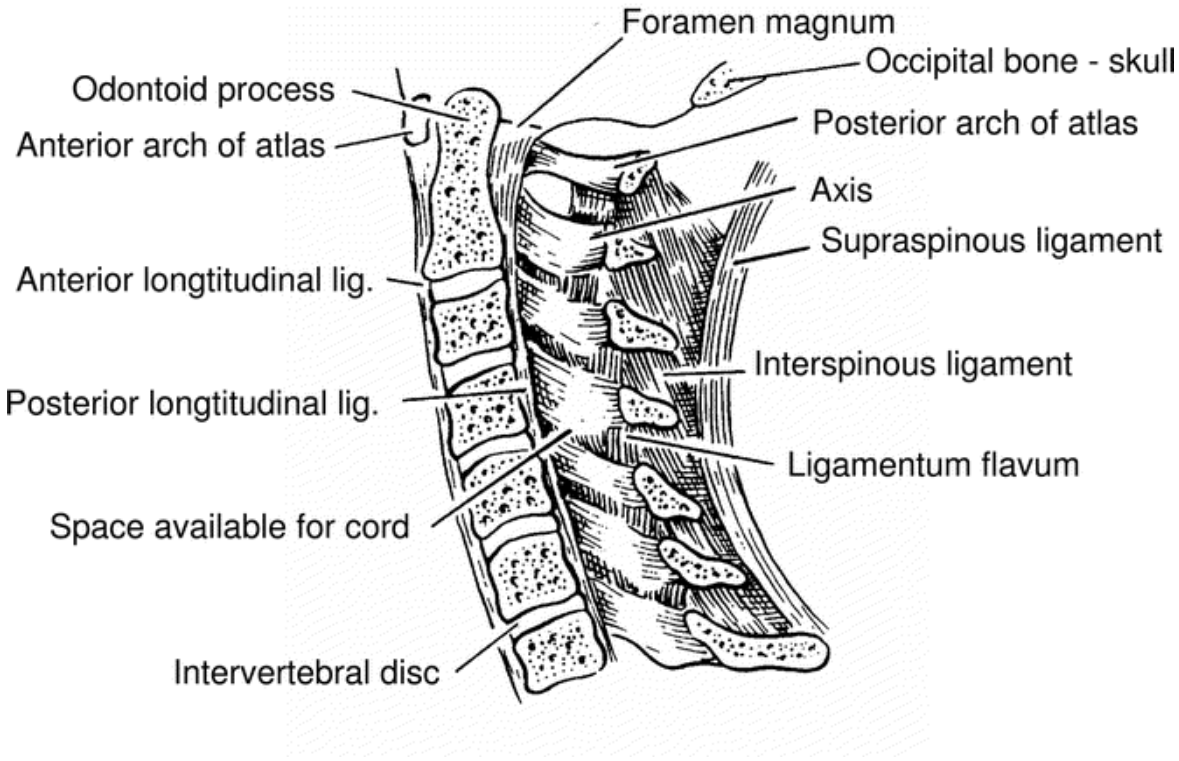

Figure 1-5 – Cross sectional sagittal view of cervical spine ligaments. (reprinted with copyright permission) (Crosby, 2006)

1.2.2 Spinal Cord Anatomy

The spinal cord is responsible for allowing the brain to communicate with the entire body. It communicates sensory information to the brain, conducts signals away from the brain to regulate motor and autonomic function, and manages reflexes at spinal levels (Barr & Kiernan, 1988). Together, the brain and spinal cord comprise the central nervous system (CNS), while afferent and efferent neurons comprise the peripheral nervous system (PNS). The CNS is responsible for processing signals received from the PNS, known as afferent signals, and if an action is required, the CNS sends a signal to the efferent neurons of the PNS to communicate with the body (Silverthorn, 2010). There are two types of efferent neurons: the somatic motor division controls skeletal muscle, and the autonomic division controls the autonomic nervous system (body functions not consciously directed such as heart beat, respiration, digestion, etc.) (Silverthorn, 2010).

The spinal cord extends from the brain at the base of the skull down to the lumbar spine where it becomes the cauda equina. It is a cylindrical structure, slightly flattened dorsoventrally (Moore & Dalley, 1999). It is surrounded by three meninges (covering layers): the dura, arachnoid, and pia mater (Figure 1-6) (Moore & Dalley, 1999). The dura mater is the thickest of the three membranes, continuous with the dura covering the brain and associated with veins draining blood (Barr & Kiernan, 1988). The arachnoid mater is adjacent to the inner surface of the dura, forming the outer boundary of the cerebrospinal fluid-filled subarachnoid space. The pia mater adheres to the surface of the spinal cord as the innermost meninge layer. The spinal cord is suspended within the dura by the denticulate ligaments, attaching laterally to the spinal cord (Moore & Dalley, 1999).

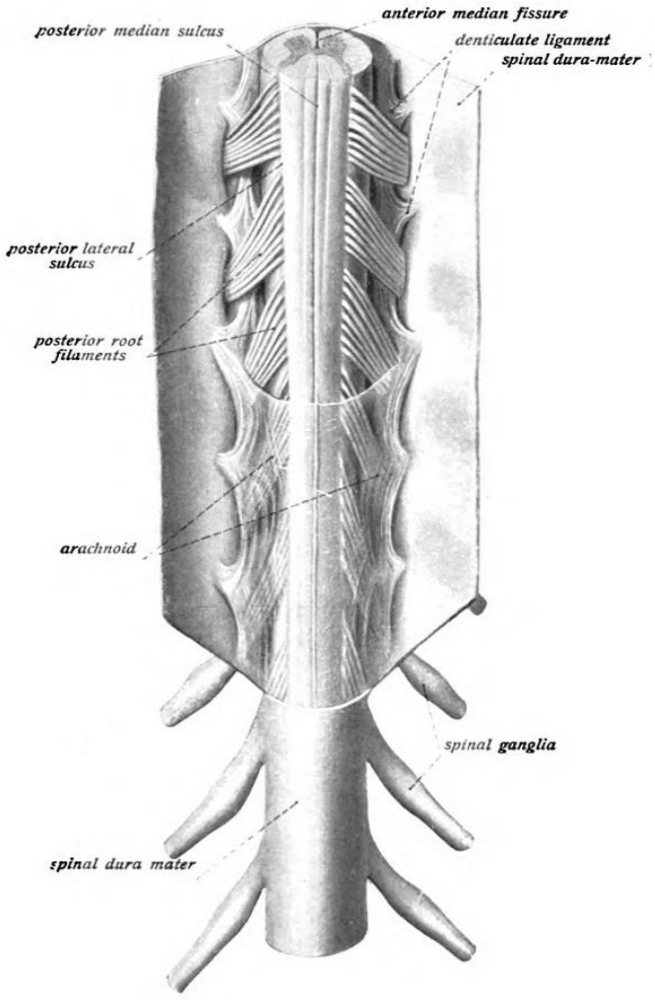

Figure 1-6 - The spinal cord, with surrounding meninges. (Public domain) (Sobotta 1908)

The spinal cord is segmented based on vertebral level, with nerves exiting the spinal cord bilaterally at each level through the intervertebral foramina (Barr & Kiernan, 1988). Each spinal nerve corresponds to the vertebral level in which it exits: in the cervical spine they correspond to the rostral vertebral level, and in the thoracic, lumbar and sacral regions, they correspond to the rostral level, where the C8 spinal nerve exits between the C7 and T1 vertebrae. Each spinal nerve consists of a dorsal root (carrying afferent neurons) and a ventral root (carrying efferent neurons) (Moore & Dalley, 1999). The level at which a spinal nerve exits the spinal column is directly related to which part of the body it innervates, including the sensory signal regions on the skin called dermatomes (Figure 1-7) (Barr & Kiernan, 1988). The nerves overlap areas, so if one nerve is lost, sensation in a dermatome is not necessarily lost. The spinal cord is enlarged in the cervical (C4 – T1) and lumbar (L2 – S3) regions for innervation of the arms and legs, respectively (Moore & Dalley, 1999).

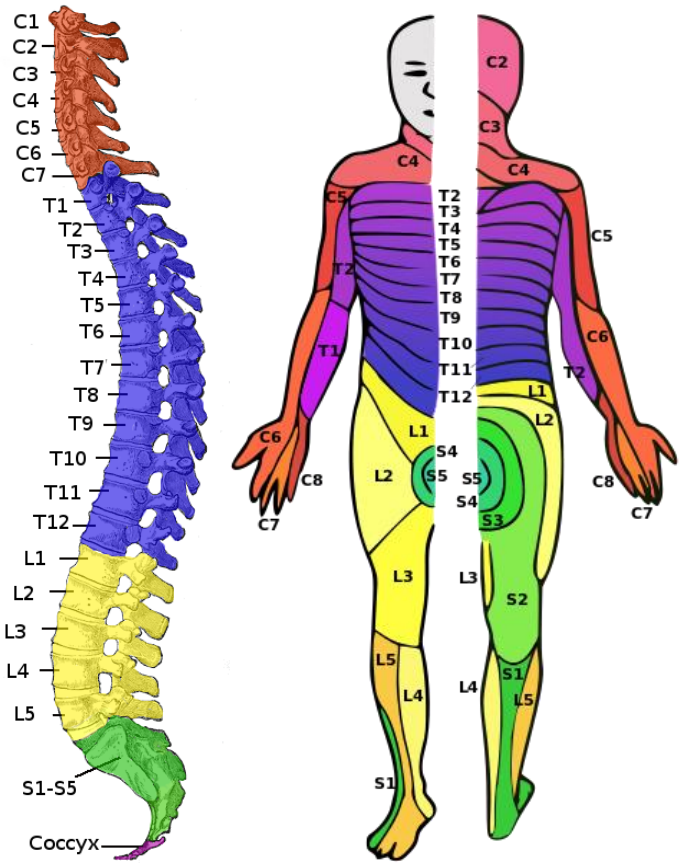

Figure 1-7 - Spinal cord innervation levels with corresponding dermatomes. (Public domain) (Stephan 2005)

When a transverse section of the spinal cord is observed, two distinct areas are present: the butterfly-shaped gray matter in the centre, and the surrounding white matter (Barr & Kiernan, 1988). The gray matter consists of unmyelinated nerve cell bodies, dendrites, and axon terminals. Cell bodies are assembled in an organized fashion to form groups with similar functions. The gray matter on each side consists of a dorsal horn, a ventral horn and an intermediate zone (Figure 1-8), with three categories of neurons present: interneurons, motor neurons, and tract neurons (Barr & Kiernan, 1988). Interneurons are the smallest cells, responsible for local communication and facilitating reflex response. Motor neurons of the ventral horn communicate with skeletal muscles. Cell bodies of tract neurons exist in the dorsal horn, where the axons make up the ascending white matter (Barr & Kiernan, 1988). The white matter consists of ascending and descending groups of mostly myelinated axons with very few cell bodies, bundled into tracts or fasciculi that connect different regions of the CNS. A grouping of more than one fasciculus is called a funiculus. The dorsal funiculus (medially from the dorsal gray horn) consists of a lateral fasciculus cuneatus and medial fasciculus gracilis (Barr & Kiernan, 1988). The lateral funiculus runs between the dorsal and ventral roots, and the ventral funiculus is located between the ventral roots and the large anterior median fissure. The central canal runs through the centre of the spinal cord and contains cerebrospinal fluid.

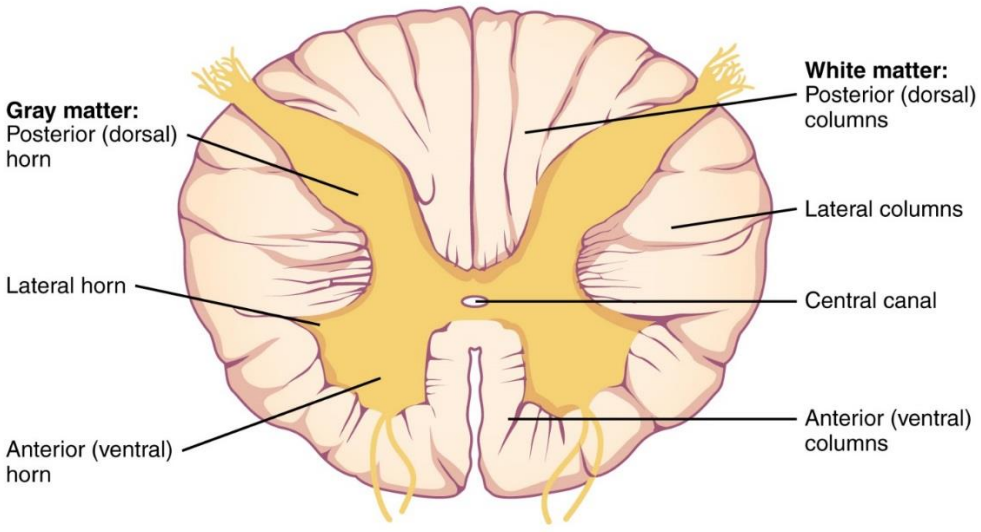

Figure 1-8 – Cross sectional view of regional anatomy of the spinal cord. Note the gray matter is yellow in this image. This cross section is from C7. (Image from: https://cnx.org/contents/FPtK1zmh @8.25:94lv8wHH@4/The-Central-Nervous-System)(Creative Commons Attribution 4.0 License)

Cellular level

There are two primary types of cells in the nervous system: neurons and glial cells. Neurons conduct the signals throughout the body, and glial cells support the proper functioning of the nervous system (Silverthorn, 2010).

Neurons

Neurons have a main cell body that contains the nucleus and organelles and act as the control centre, producing the necessary proteins to keep the cell functioning properly (Figure 1-9). Several branches extend from the cell body: dendrites or axons. Dendrites are the terminals that receive signals from neighbouring neurons, and axons are the long branches that carry outward signals to other neurons or tissues (Silverthorn, 2010). Neurons can be classified functionally into interneurons, sensory (afferent), or motor (efferent). Interneurons exist only in the CNS and only communicate with other neurons. When the long axons of neurons are grouped together in fibre bundles, they are referred to as nerves (Silverthorn, 2010). Sensory nerves carry afferent signals to the CNS, motor nerves carry efferent signals to limbs and organs, and mixed nerves carry signals in both directions.

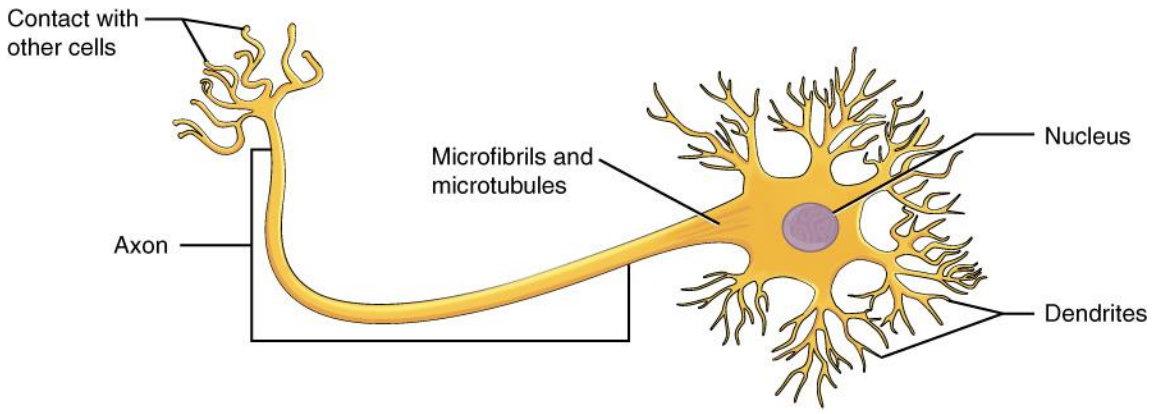

Figure 1-9 – Typical multipolar motor neuron. (Image from: https://cnx.org/contents/FPtK1zmh @8.25:nhY2Qahd@6/Nervous-Tissue-Mediates-Percep)(Creative Commons Attribution 4.0 License)

If an axon is damaged and separates from the cell body it will likely deteriorate, resulting in loss of function of the neuron. The severed distal portion lacks the required organelles to survive, and the neuron no longer is in contact with the target tissue to which to carry its signals (Silverthorn,

2010). A damaged efferent neuron will result in loss of function of the tissue, a muscle for example, and a damaged afferent neuron will result in a sensory loss, temperature for example.

Dendrites act to increase the surface area of the neuron by extending from the cell body in a branch-like fashion to receive information signals from many other neurons (Silverthorn, 2010). Neurons within the PNS have relatively few dendrites, and typically relay a signal from one tissue in the body to another. Neurons in the CNS have a more elaborate dendrite system and often contain dendritic spines. Dendritic spines are small bulbous growths from the dendrite branches with a head and neck, which allow for more communication points with other neurons and can easily change shape over relatively short periods of time (Silverthorn, 2010).

Axons are the opposite of dendrites; they carry signals away from the cell body to the target neurons or tissues. Axons can range in length from a few micrometers to longer than a meter, and neurons typically have one primary axon to carry the signals (Silverthorn, 2010). The signal is initiated at the most proximal end of the axon to the cell body in a region called the axon hillock. Along the length of the axon, any branches of the axon are referred to as collaterals, where each collateral ends at an enlargement called the axon terminal, where the signal is transmitted to the target at the synapse (Figure 1-10) (Silverthorn, 2010). The neuron transmitting the signal is the presynaptic cell, the neuron receiving the signal is the postsynaptic cell, and the space in between is the synaptic cleft. When the signal travelling down the axon reaches the axon terminal, it triggers the synaptic vesicles to release neurotransmitters into the synaptic cleft, causing them to be absorbed by receptors in the target cell (Silverthorn, 2010).

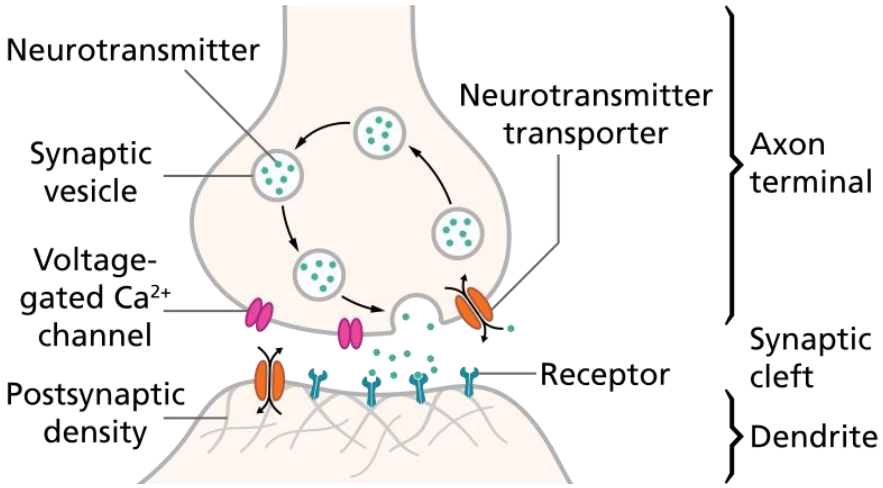

Figure 1-10 – Schematic of a synapse. Neurotransmitters are released from synaptic vesicles where they bind to target receptors. Image from: https://commons.wikimedia.org/wiki/File:SynapseSchematic_en.svg (Creative Commons Attribution 4.0 License)

Glial Cells

Glial cells act to support neurons, despite the fact they outnumber neurons by almost 50:1 (Silverthorn, 2010). They respond to neurotransmitters and help develop, maintain, and repair neurons. The CNS has four types (oligodendrocyte, astrocyte, microglia, and ependymal cells), and the PNS has two types of glial cells (Schwann and satellite cells). Oligodendrocytes (and Schwann cells) support neurons by forming a myelin sheath over the axons, by wrapping several concentric layers of a phospholipid membrane around the axon (Figure 1-11) (Silverthorn, 2010). The glial cells communicate with the neurons via chemical signals and provide biochemical support, and the myelin insulates the axons, providing protection and increasing signal transmission speed. Each oligodendrocyte can myelinate several axons. Nodes of Ranvier are the unmyelinated gaps along the axon, between adjacent myelin wrapped sections (Figure 1-11) (Silverthorn, 2010). These nodes allow the cell to be in contact with the extracellular fluid, where ion channels permit the electrical signal to jump from node to node.

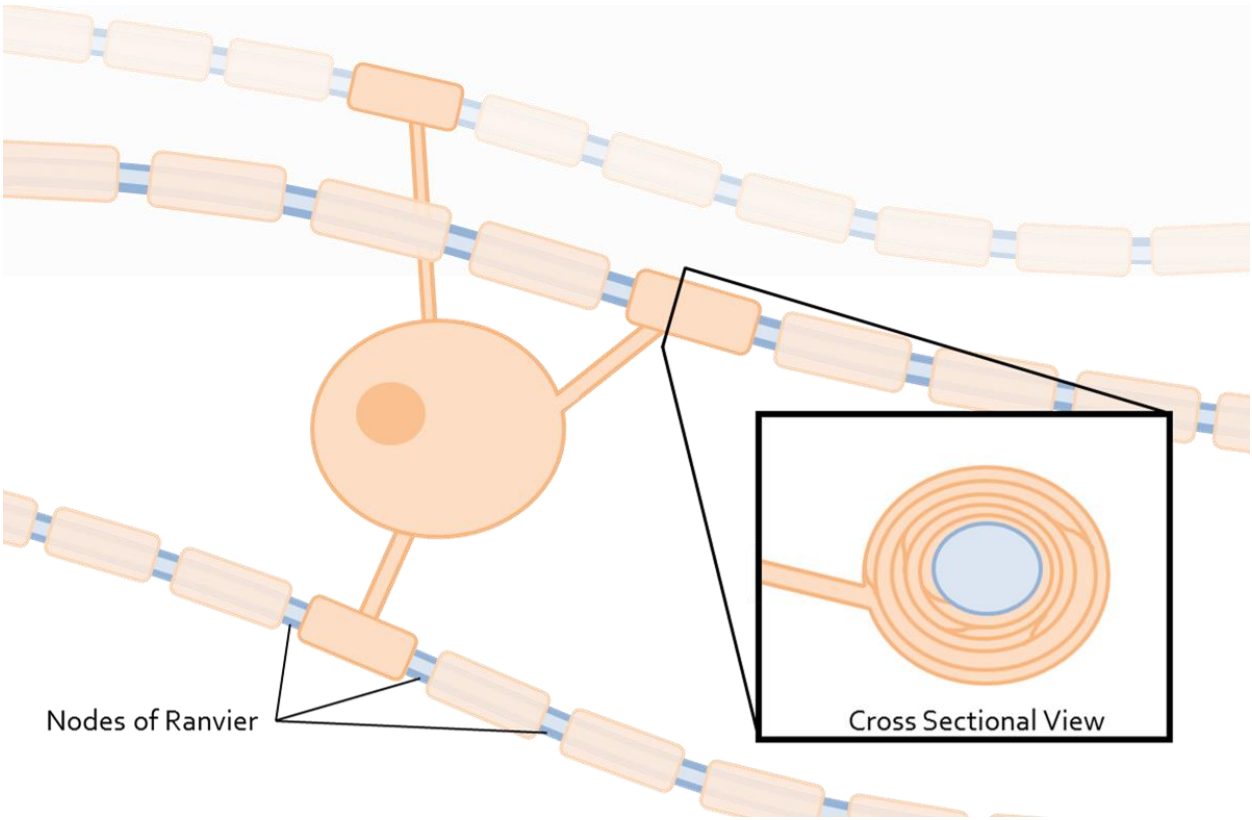

Figure 1-11 - Oligodendrocyte myelinating multiple axons. Cross sectional view shows the myelin sheath wrapping many layers around the axon. Nodes of Ranvier are identified as the unmyelinated gaps along the axon.

Astrocytes exist in the CNS and are highly branched glial cells that play several roles in maintaining the environment (Figure 1-12) (Silverthorn, 2010). They provide neurons with substrates for ATP production, take up water and potassium to maintain homeostasis in the extracellular fluid, and also form part of the blood-brain-barrier, regulating the transport of ions between blood and extracellular fluid (Silverthorn, 2010). Microglia are immune cells that act to clean the CNS of dead cells and foreign debris; however, they are not always helpful, as some diseases are a result of the microglia releasing free radicals that can damage neurons (Silverthorn, 2010). Ependymal cells act to separate the CNS fluid compartments with semi-permeable epithelial layers (Silverthorn, 2010).

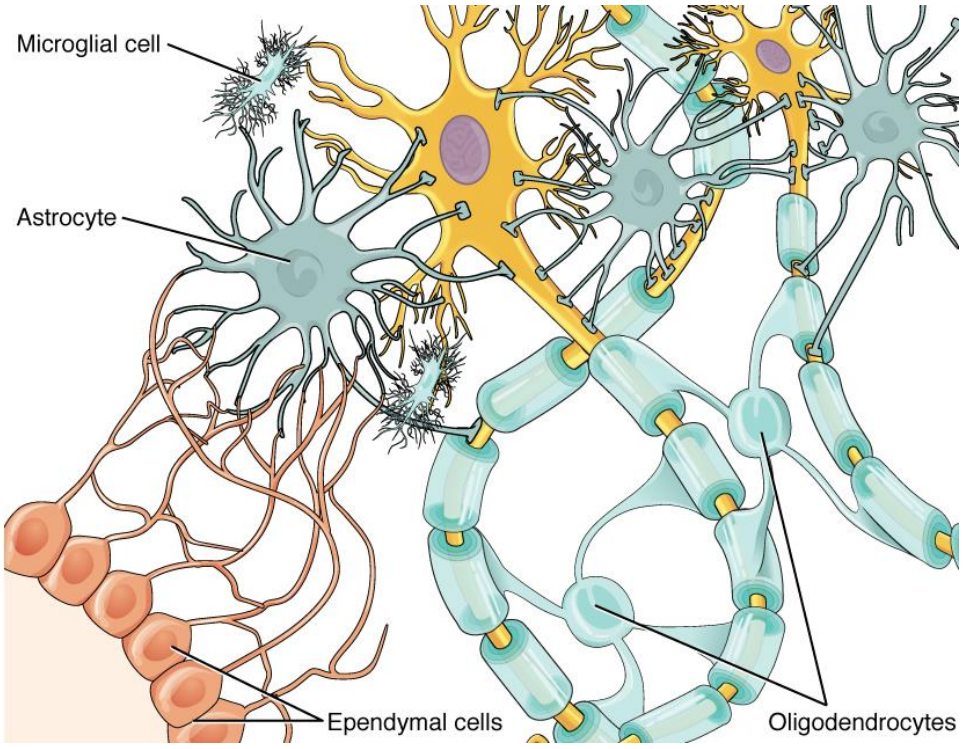

Figure 1-12 - Glial cells supporting neurons. Astrocytes maintain the environment, oligodendrocytes myelinate axons, microglia clean the environment, and ependymal cells form semi-permeable epithelial layers. Image from: https://cnx.org/contents/FPtK1zmh@8.25:mYoZvS9p@3/Nervous-Tissue (Creative Commons Attribution 4.0 License)

1.2.3 Electrical Signal Conduction within Neurons

Neurons transmit signals by propagating an electrical charge along the cell. These electrical charges are initiated by ions moving in and out of the cell, across the cell membrane and influenced by the permeability of the membrane to ions such as potassium (K^+), sodium (Na^+), and chlorine (Cl^-). If the membrane becomes more permeable, and ions enter the intracellular fluid, the cell membrane will depolarize (i.e. Na^+ enters the cell) (Silverthorn, 2010). A cell can also hyperpolarize, moving the cell membrane potential in the opposite direction (i.e. K^+ leaves the cell). Three types of gated ion channels regulate the ion permeability of a cell (Silverthorn, 2010). Voltage gated ion channels respond to the cell's membrane potential, and are involved in the initiation and conduction of electrical signals. Chemically gated ion channels respond to a host of ions and molecules such as neurotransmitters and signal molecules. Mechanically gated ion channels open in response to a physical stimulus (i.e. pressure).

There are two basic types of electrical signals within a cell: graded potentials and action potentials (Silverthorn, 2010). Graded potentials are variable-strength signals that travel short distances and lose signal strength as they travel – like a ripple in a pond. These graded potentials occur when a chemical signal is received from another cell, and the strength is dependent on the stimulus. If a signal is strong enough when it reaches the axon hillock, it initiates an action potential (Figure 1-13). Action potentials are brief, but large, depolarizations that travel long distances without losing signal strength, and are triggered by a high concentration of voltage gated channels in the axon hillock, if the graded potential is greater than the threshold (Silverthorn, 2010). The strength of the axon potential is binary – it either triggers or it does not, and is not influenced by the strength of the graded potential. Cells have a refractory period after an action potential (of about 2 ms), to limit the rate of signals and to prevent signals from travelling backwards.

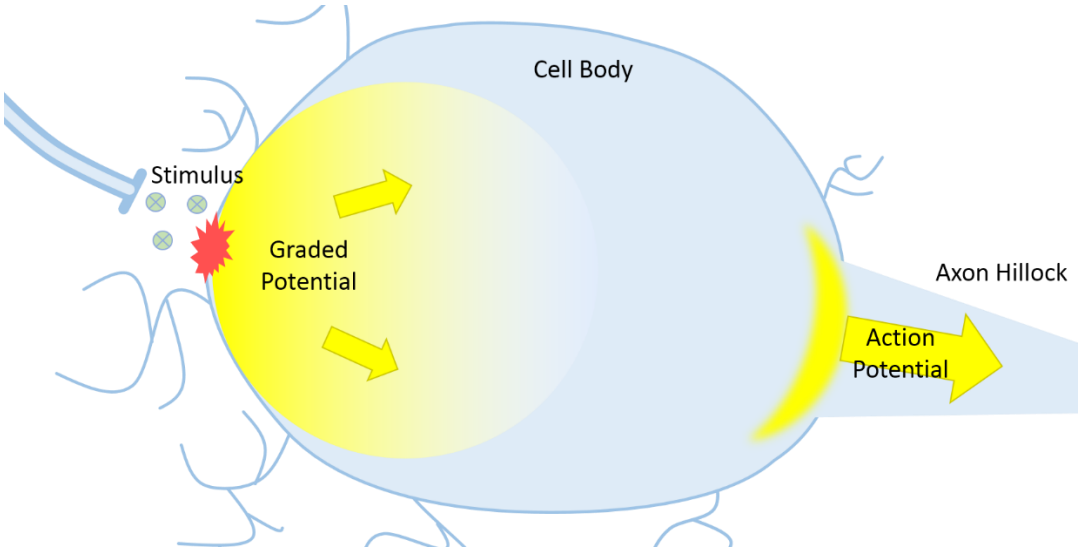

Figure 1-13 - A stimulus triggers a graded potential within a neuron cell body, which in turn will trigger an axon potential if the signal is greater than the threshold.

Action potentials do not lose strength as they are transmitted, as they are reinforced by voltage-gated channels along the axon (Figure 1-14). Two key parameters influence the speed of an action potential: axon diameter (where a larger diameter conducts a faster signal), and insulation of the cellular membrane. The myelin surrounding segments along an axon acts similarly to insulation on an electrical wire. The small gaps between myelinated segments are known as nodes of Ranvier, where voltage-gated channels are concentrated to keep the signal amplitude

high. The apparent jump of the action potential between nodes is called saltatory conduction (Barr & Kiernan, 1988; Silverthorn, 2010). The myelin sheath increases the transverse resistance and reduces the capacitance of the membrane, increasing conduction speed (Susuki, 2010). Demyelination slows signal conduction and since there are no voltage-gated channels at these sites, the signal may no longer be above the triggering threshold at the next node of Ranvier.

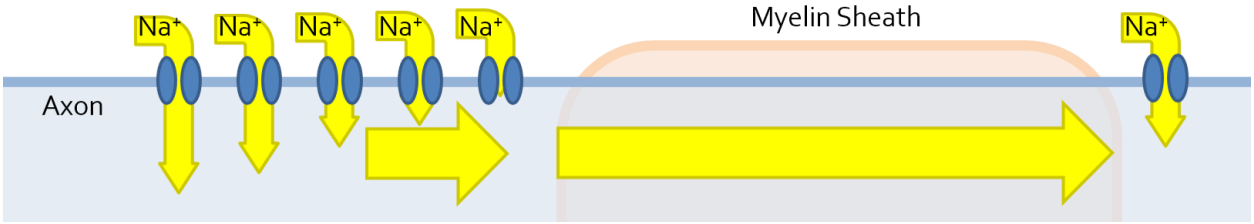

Figure 1-14 - Action potential travelling the length of an axon. Voltage-gated channels reinforce the action potential, and myelin sheaths act as insulation to allow saltatory conduction and keep the signal from losing strength.

Neurons communicate to other neurons at the axon terminus, known as the synapse. Electrical synapses very rapidly pass the electrical signal of one cell to the next through gap junctions. Chemical synapses use neurotransmitters released from the presynaptic cell, which bind to receptors on the postsynaptic cell. One neuron can synapse on multiple cells, or multiple neurons can synapse on one cell. The synapse can release excitatory transmitters, or inhibitory transmitters to prevent an axon from generating an action potential.

Different types of axons serve different functions, and have different diameters which help to dictate how fast the signal travels (Table 1-1).

Table 1-1 - Different types of axons and their function, size, and velocity of signal conduction (Purves et al., 2001)

	Type	Function	Diameter	Velocity
Sensory axons	Ia, II	Proprioception	13 – 20 µm	80 – 120 m/s
	Aβ	Touch	6 – 12 µm	35 – 75 m/s
	Aδ	Pain, temperature	1 – 5 µm	5 – 30 m/s
	C	Pain, temperature	0.2 – 1.5 µm	0.5 – 2 m/s
Motor Axons	α	Generate muscle force	13 – 22 µm	70 – 120 m/s
	γ	Set muscle length	3 – 8 µm	15 – 40 m/s

Neurofilaments are the most abundant cytoskeletal structural element in large, myelinated axons. They run in parallel along the length of the axon and interact through a combination of electrostatic and steric repulsive forces, mediated by their unstructured side arms (Purves et al., 2001). Neurofilaments provide support for the cell's radial growth and diameter. Microtubules run along the length of the axon and function as the main cytoskeletal tracts for transportation of mitochondria, lipids, synaptic vesicles, proteins, and other organelles and enzymes to and from the cell body along the axon. When microtubules are compromised, the distal portion of the cell is unable to receive vital components from axonal transport and will degenerate.

1.2.4 Spinal Cord Tracts

Groups of ascending and descending neurons in the spinal cord make up distinct tracts, each responsible for particular functions. Descending tracts travel down the spinal cord and synapse on motor neurons, which exit the spinal cord to reach their target tissues, while ascending tracts begin at a tissue, and end at the brain. Most tracts are two or three neurons in length, synapsing in the gray matter and the brain. Spinal tracts also can decussate (cross to the opposite side of the body) through the anterior commissure, and travel contralateral within the spinal cord to the organs they innervate. Spinal cord tracts have an organized layout within the spinal cord (Figure 1-15), and details from some of the prominent tracts are summarized in Table 1-2.

.

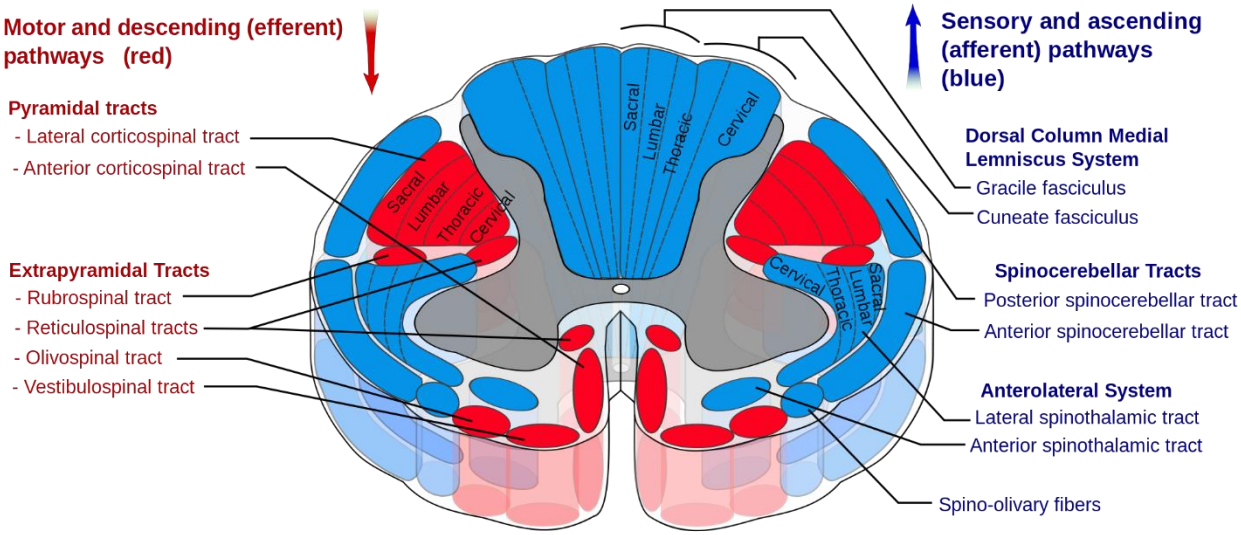

Figure 1-15 - Spinal cord descending (red) and ascending (blue) tract layout within a transverse cross sectional schematic of the spinal cord. Image from: https://commons.wikimedia.org/wiki/File:Spinal_cord_tracts_-_English.svg (Creative Commons Attribution-Share Alike 3.0 Unported License)

Table 1-2 – Details of prominent human spinal cord tracts.

	Tract	Type of signal	Spinal cord position relative to cord exit	Nerves	Fiber Type
Ascending	Dorsal White Column: Gracile fasciculus (lower body), Cuneate fasciculus (upper body)	Discriminative touch, proprioception	ipsilateral	3	Ia, II, Aβ
	Posterior spinocerebellar	Non-conscious status (length and velocity) of individual and groups of muscles	ipsilateral	2	Ia, II
	Anterior spinocerebellar	Whole limb and trunk coordination	contralateral	2	Ia, II
	Lateral spinothalamic	Noxious (pain and temperature) and nondiscriminative (crude) tactile	contralateral	3	Aδ, C
	Anterior spinothalamic	Autonomic, endocrine, motor, pain, temperature, simple tactile sensations and activation of pain-inhibiting mechanisms	contralateral	2 - 3	Aδ, C
Descending	Corticospinal	Conscious control of motor system and fine movement. Ventral (trunk), lateral (limb)	Lateral: ipsilateral, ventral: contralateral	2	α, γ
	Rubrospinal	Influences general locomotion	ipsilateral	2	α, γ
	Vestibulospinal	Coordinate posture and balance. Lateral (body), medial (head)	ipsilateral	2	α

1.3 Traumatic Spinal Cord Injury – Clinical

1.3.1 Epidemiology and Etiology

Spinal cord injury (SCI) causes severe neurological dysfunction such as motor and sensory deficits, chronic severe pain, bladder, bowel and sexual dysfunction, and autonomic dysreflexia, with few proven treatment options available (Ahuja et al., 2017; Hagg & Oudega, 2006). SCIs are devastating to the injured individuals and their families, with over 85,000 Canadians living with SCI (Noonan et al., 2012), and up to 347,000 individuals in the United States (NSCISC, 2016). Each year there are over 1,700 new traumatic injuries occurring in Canada (Noonan et al., 2012), approximately 17,000 cases in the United States, not including those who die at the accident scene (NSCISC, 2016), and almost 180,000 cases globally (Fitzharris et al., 2014). The economic costs associated with SCIs represent a significant burden to society, estimated in the billions of dollars per year in North America (Krueger et al., 2013; NSCISC, 2016). The average age at time of injury has increased from 28.7 in the 1970s to 42.2 during the 2010s (Chen et al., 2016B).

The region of the spine sustaining an SCI is important, as higher spinal level injuries have the potential for greater functional loss. Cervical SCIs are the most common, occurring in 59% of new SCI cases, and have demonstrated an increasing proportion of SCIs since 1972 in the United States (Figure 1-16) (Chen et al., 2016B).

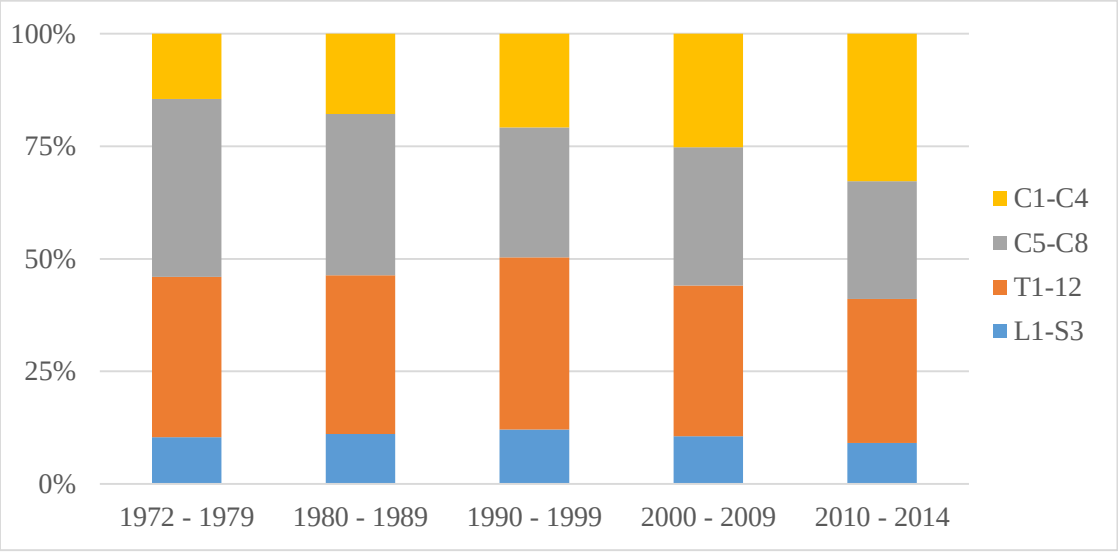

Figure 1-16 – Spinal level of new traumatic SCI over the past 5 decades. (Chen et al., 2016B)

SCIs are caused by a multitude of different events such as motor vehicle collisions, falls, and sports related injuries. SCIs most commonly occur as high energy injuries from motor vehicle accidents, but recent demographic data indicates a rising incidence in elderly individuals who sustain SCI after low energy incidents such as a fall from a standing height (Figure 1-17) (Chen et al., 2016B; Pickett et al., 2006). These different causes of SCI may involve different magnitudes and directions of forces and impact velocities, and therefore may be causing different patterns of injury.

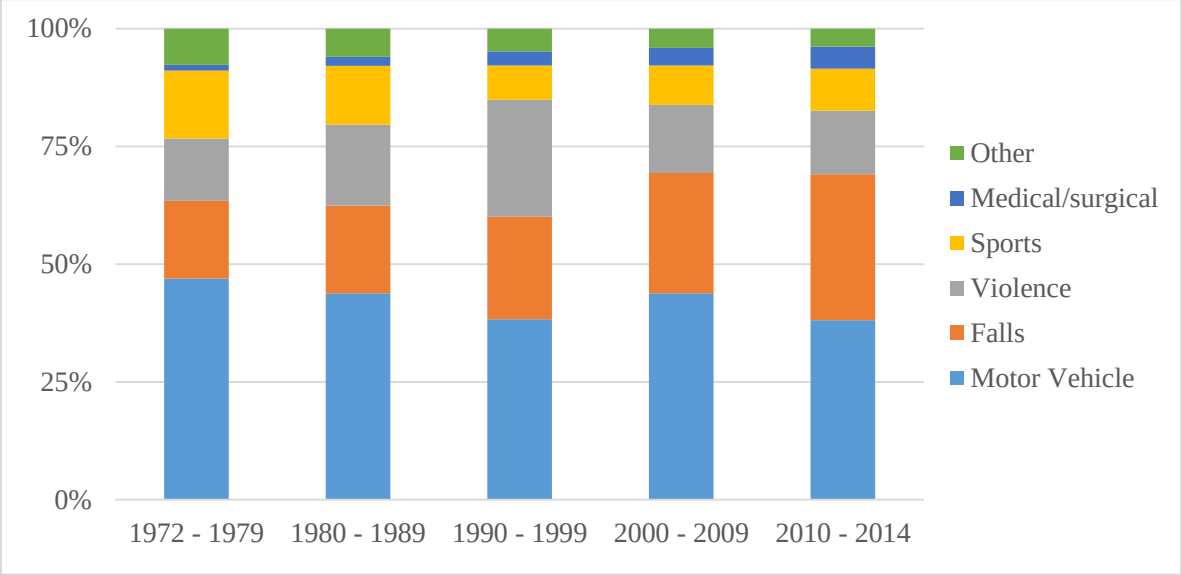

Figure 1-17 - Etiology of new traumatic spinal cord injury over the past 5 decades (Chen et al., 2016B)

1.3.2 Severity of Injury

ASIA classification

To classify the severity of a spinal cord injury, clinicians relate a patient's motor and sensory function to the American Spinal Injury Association (ASIA) Impairment Scale (AIS) (Table 1-3). Ideally the AIS evaluation is completed within 72 hours of injury to establish a patient baseline, which can help to determine future rehabilitation strategies. Forty-five percent of SCIs are complete ASIA Grade A level of severity (Sekhon & Fehlings, 2001).

Table 1-3 - ASIA Impairment Scale (AIS) with respective incidence levels (Sekhon & Fehlings, 2001). Adapted from www.asia-spinalinjury.org

Grade	Definition	Incidence	Details
A	Complete	45 %	No sensory or motor function is preserved in the sacral segments S4 – S5
B	Sensory incomplete	15%	Sensory but not motor function is preserved below the neurological level and includes the sacral segments. No motor function is preserved more than 3 levels below the motor level on either side of the body.
C	Motor incomplete	10%	Motor function is preserved below the neurological level, and less than half of key muscles below the neurological level have a muscle grade ≥ 3 (active movement, full range of motion against gravity)
D	Motor incomplete	30%	Motor function is preserved below the neurological level, and more than half of key muscles below the neurological level have a muscle grade ≥ 3
E	Normal		Normal motor and sensory function (patient had prior deficits)

Canal Size

Existing spine morphology influences SCI severity. Previous studies have demonstrated a significant correlation between spinal canal diameter at uninjured levels and the degree of neurologic deficit, where those with smaller canal diameters were more prone to severe deficits than those with large canals (Eismont et al., 1984; Kang et al., 1994) (Figure 1-18). When comparing patients following acute cervical SCI, those with neurological deficits had significantly smaller Torg-Pavlov ratios (sagittal spinal canal-to-vertebral body ratio) than those with no neurologic symptoms (Aebli et al., 2013). Similarly, contact-sport athletes with developing spinal stenosis have demonstrated a high sensitivity for transient neurapraxia (Torg et al., 1996). These results are not surprising as spinal cord diameters vary to a smaller degree (Elliott, 1945; Nordqvist, 1964; Nouri et al., 2017) compared to spinal canal diameters. From a biomechanical perspective, a smaller spinal canal requires less canal occlusion to compress the

spinal cord, where the initial canal occlusion in a larger spinal canal may not compress the spinal cord.

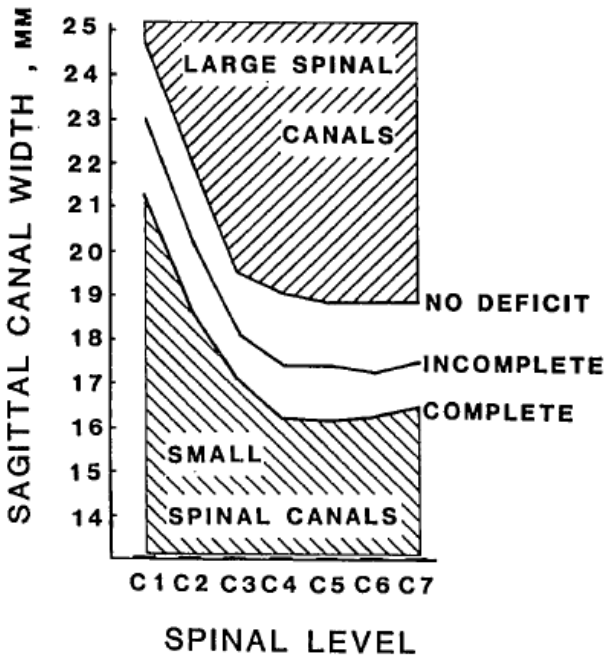

Figure 1-18 - Relationship between large and small sagittal spinal canal diameters to neurological deficit (reprinted with copyright permission) (Eismont 1984)

1.3.3 Timing of Decompression

Despite surgeons' ability to agree on cervical spine injury morphology as seen on MRI and injury classification, there are still significant differences of opinion regarding management of the injury and treatment implications (Arnold et al., 2009; Liu et al., 2015; Nassr et al., 2008; van Middendorp et al., 2013; Yousefifard et al., 2016). Following the initial primary injury mechanism to the spinal cord, the SCI is often accompanied by persistent residual compression of the cord from fragments of the surrounding bone and soft tissue (Dumont et al., 2001). The initial injury is a dynamic event, while the residual compression is static. The acute treatment of this injury may involve surgery to stabilize the injured spinal column with implants and to remove compression on the spinal cord. It has been established that the initial, primary injury from physical trauma results in significant damage to the spinal cord (Beattie et al., 2002), however the influence of residual compression remains controversial (Cadotte & Fehlings, 2011; Fehlings et al., 2010; Furlan et al., 2011; Wilson, et al., 2012B).

In the context of SCI treatment, the issue of surgical decompression is of particular importance, if for no other reason than the disappointing fact that it is one of the few interventions that clinicians can offer patients. The Surgical Treatment of Acute Spinal Cord Injury Study (STASCIS), was a large, multicentre, international, prospective cohort study involving 313 patients (with 222 follow-up) to investigate the effects on the timing of surgical decompression (Fehlings et al., 2012). The results suggest that early surgical decompression may enhance the functional improvement of patients; as 19.9% of patients who were treated surgically within 24 hours of injury saw a ≥ 2 grade improvement in AIS (ASIA Impairment Scale) 6 months post-surgery, compared to only 10.2% in those treated late (Figure 1-19) (Fehlings et al., 2012). However, there was no difference between groups with a 1 grade improvement, and 42% of patients treated early did not show any functional improvement. A major limitation behind non-randomized comparative studies, such as STASCIS, is the susceptibility to confounding by indication (van Middendorp, 2012) – a bias may be introduced, as treatment decisions may be influenced by prognostic factors. Nevertheless, STASCIS suggests that there are predisposing factors influencing the outcomes of early decompression surgery. For example, the early group included younger, more severely injured patients, which may lead surgeons to be more aggressive in decompression treatment, and also leaves the potential for greater functional recovery.

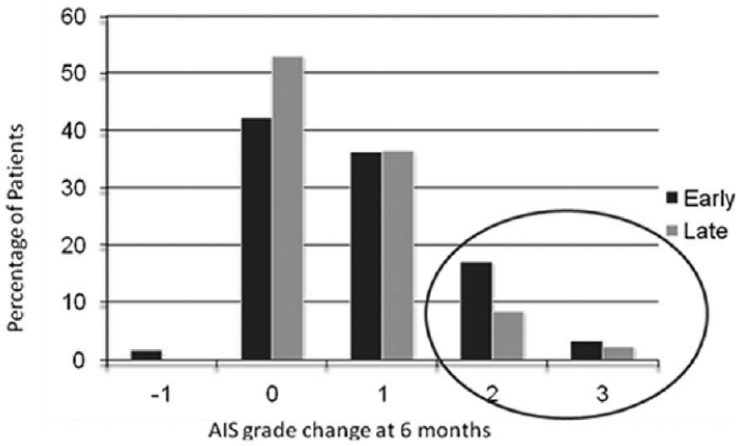

Figure 1-19 - Improvements in AIS functional outcome at 6 months following early vs late decompression surgery from STASCIS (Fehlings et al., 2012). Despite the early group demonstrating more patients experiencing a 2+ AIS grade recovery, 42% of patients still saw no improvement following early decompression. (Image use: Creative Commons Attribution 4.0 International License)

More recent studies have reduced the threshold definition of 'early' decompression to 12 hours (Burke et al., 2016; Dobran et al., 2015), or even 8 hours (Grassner et al., 2016; Jug et al., 2015; McCarthy et al., 2011), and observed a greater improvement in the early treatment group. Two separate systematic review and meta-analysis studies have recently been published with conflicting results. Yousefifard et al. (2016) deemed that results from 22 studies on the timing of decompression indicate that early decompression surgery can improve neurologic recovery and is associated with fewer post-surgical complications, particularly when performed within 12 hours after injury. van Middendorp et al. (2013) argued that despite finding amongst 18 studies that early decompression was significantly associated with neurological and length of stay outcomes, the evidence lacks robustness as a result of heterogeneity within and between the original studies. One recent study even recommends delaying surgery beyond 72 hours post-injury, due to the increased risk of mortality and neurological deterioration experienced by the early surgery group (Liu et al., 2015). A randomized control trial is needed to provide more direct evidence on the effectiveness of early decompression, however, this presents ethical dilemmas by potentially denying early treatment to some patients. With no consensus on the timing of decompression, further research is needed to better understand the influence of early decompression and other relevant, potentially confounding variables.

While the danger of early intervention is less of a concern due to refinements in surgical and medical management, there remain substantial issues surrounding early surgical intervention after acute SCI (Fisher et al., 2005). Treating all patients 'as early as possible' dilutes the effectiveness for the patients who need it most, and creates a larger demand of patients needing the 'earliest possible treatment'. If a patient arrives at a hospital with an acute SCI at 2:00 am, should that patient be treated immediately or is it acceptable to wait until the morning? Starting a complex 4 to 5 hour operation with the potential for significant blood loss in the middle of the night with a tired surgeon and a team of nurses unfamiliar with spine surgery is not ideal for the patient, but would be justified if there were a solid neurologic rationale to do so. If an injury occurs to someone away from home, or far from a specialized spinal cord injury centre, is it worth the wait to transit them to a preferred hospital? If two patients simultaneously arrive at the hospital with acute SCIs, and there is only one available operating room, which patient should be treated first? Feasibility studies report that less than 50% of recent SCI patients are able to undergo decompression within 24 hours, but speculate a drastic increase in these proportions if proper modifications are made to pre-hospital logistics (Furlan et al., 2011). Further analyses are needed to more accurately define which patients stand to benefit the most from early operative intervention (Wilson, et al., 2012B).

The lack of definitive results from the literature suggests that there are predisposing factors as to why only some people improve after decompression. This is consistent with the argument presented by Dr. Charles Tator in his seminal review of clinical trials for SCI in which he noted that the disregard for the heterogeneity of human SCI patients may be a key reason for the lack of success in clinical studies (Tator, 2006). Clearly there is a need for "personalized medicine", which begins with a thorough understanding of the injury mechanism, as it could be a confounding factor with respect to the effectiveness of early decompression. For example, patients with facet dislocation SCIs demonstrated less potential for motor recovery 1 year following injury compared to patients without, despite the facet dislocation group having significantly earlier decompression (25.1 vs 41.3 hours) (Wilson et al., 2013).

The energy involved in the SCI event is also related to injury mechanism. A SCI from a 'high-energy event' such as a motor vehicle accident, would likely have greater cord impact velocities than an injury caused by a fall from standing. Patients with low-energy injuries had a 5.5 fold

improvement in functional recovery compared to high energy injuries (Fisher et al., 2005). Most STASCIS patients involved in a high-energy injury (64%) were part of the early treatment group (Fehlings et al., 2012), potentially introducing a confounding variable. Patients from high-energy injuries were also associated with greater likelihoods of complications during the hospital stay (Wilson, et al., 2012A). Experimental results have also shown a correlation between cord impact velocity and tissue damage (Kearney et al., 1988; Sparrey et al., 2008). Soft tissues, including the spinal cord, are viscoelastic; meaning that the response to a deformation is dependent upon the velocity of loading, due to the presence of fluid in the material. The fluid can easily escape at slow injury rates without causing damage, however at fast injury rates, the fluid cannot escape in time, resulting in the development of high internal pressures; potentially causing more damage.

1.4 Spinal Column Injury Patterns and Spinal Cord Injury Mechanisms

SCI typically occurs when external forces on the spinal column cause failure of hard and soft tissues, effectively reducing or eliminating their capacity to protect the spinal cord. The anatomic damage to the spinal column occurs as specific *injury patterns*, which include compression fracture, burst fracture, dislocation (with or without fracture), and distraction injuries (Oxland et al., 2011; White & Panjabi, 1990). The most common injury patterns to the spinal column that result in SCI are dislocation and burst fracture (Figure 1-20), occurring in 32 – 58% and 9 – 35% of instances, respectively (Sekhon & Fehlings, 2001; Tator, 1983; Tator et al., 1987; Vaccaro et al., 2016; Wilson et al., 2013) (Figure 1-21). When specific spinal column injury patterns are associated with spinal cord injury, they are referred to as *injury mechanisms*. A burst fracture involves a fragment of bone impacting the spinal cord, where axial compression causes the nucleus pulposus to penetrate and fracture the vertebral body. It is most closely associated with a contusion mechanism of SCI. A dislocation involves substantial relative translation of one vertebra with respect to an adjacent vertebra. It is most closely associated with a dislocation or shear mechanism of SCI. For more than thirty years, it has been noted that dislocations result in the most severe neurological injuries, with the direction and magnitude of the dislocation being important variables (Marar, 1974; Tator, 1983). Other less common injury mechanisms include SCI without obvious radiographic abnormality or evidence of trauma (SCIWORA-ET), lamina or spinous process fracture, or spinal cord injury due to foreign bodies or projectiles.

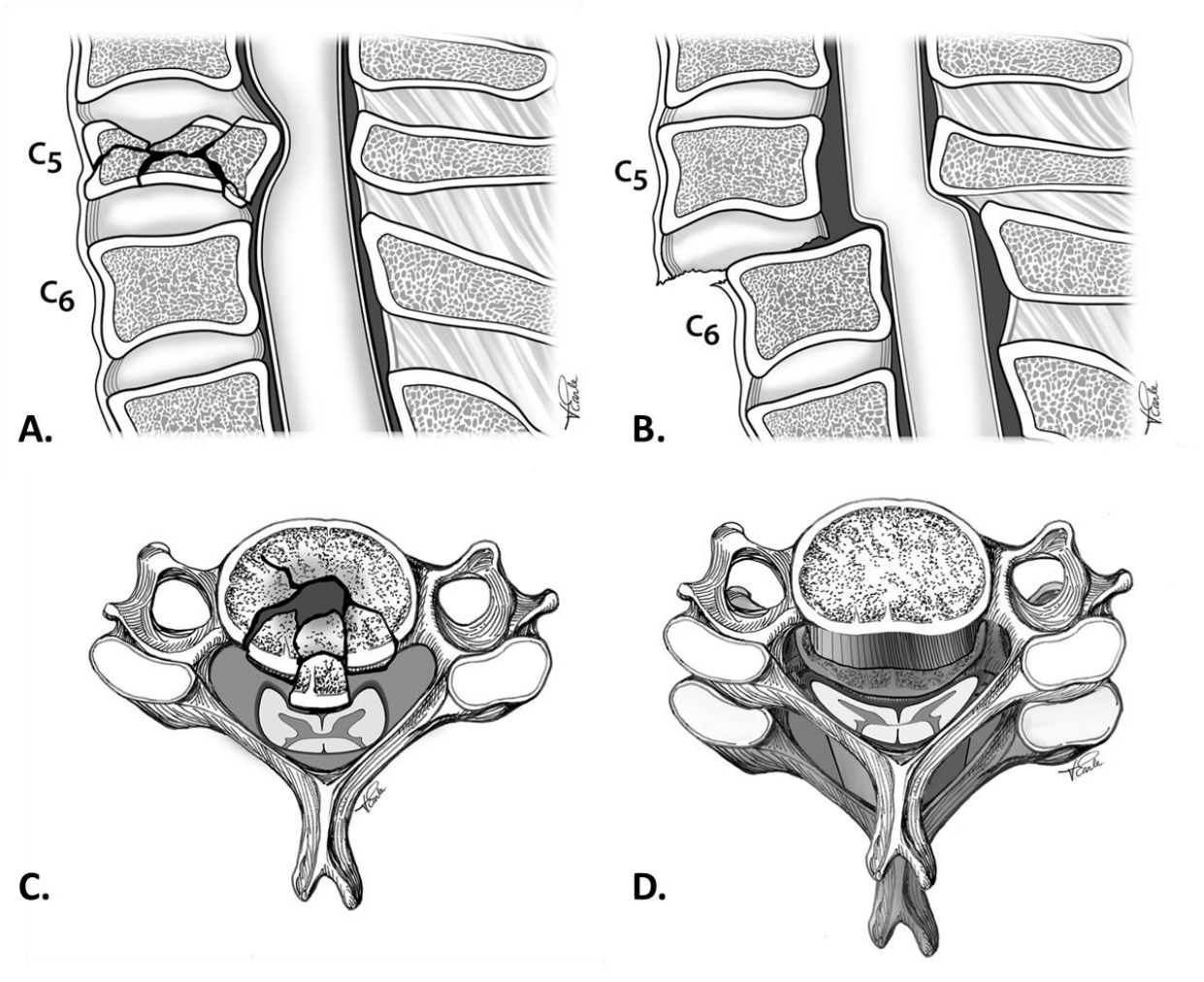

Figure 1-20 - Cross-sectional and transverse schematics of burst fracture and dislocation injury patterns. A. Sagittal cross-sectional view of a burst fracture injury. Compressive force increases pressure in the intervertebral disc nucleus, which penetrates through the superior endplate of the inferior vertebral body. A fragment of bone from the posterior vertebral wall fractures into the spinal canal, contusing the spinal cord. B. Sagittal cross-sectional view of a dislocation injury. The intervertebral disc ruptures at the vertebral endplate as the superior vertebra translates anteriorly. The spinal canal narrows and a shearing force is applied to the spinal cord by the posterior vertebral arch of C5, and the vertebral body of C6. C. Transverse view of a burst fracture injury. The bone fragment fractures from the vertebral body at high-velocity and impacts the anterior surface of the spinal cord. D. Transverse view of a dislocation injury. Where the spinal canal is narrowest, the spinal cord is pinched between the posterior vertebral arch of C5 and the vertebral body of C6. Additionally, the facets of C5 are dislocated anterior to the facets of C6.

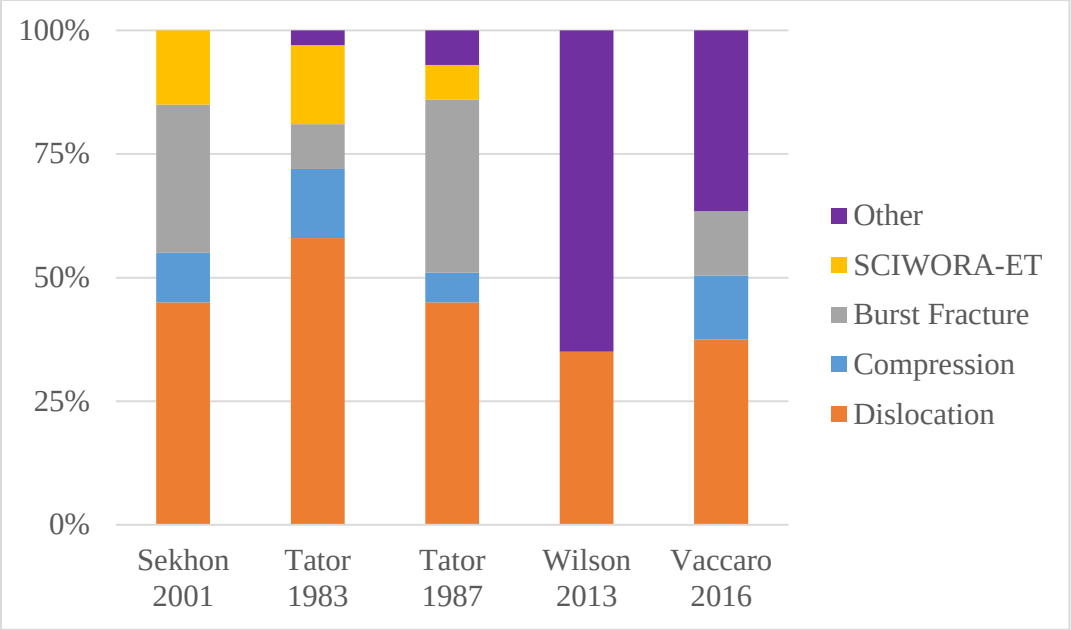

Figure 1-21 – Relative frequency of various spinal cord injury mechanisms as reported by clinical etiological studies. (Data from: Sekhon & Fehlings, 2001; Tator, 1983; Tator et al., 1987; Wilson et al., 2013, Vaccaro et al., 2016)

1.4.1 Injury Mechanism Biomechanics

Clinicians have devised classification systems for spinal column and spinal cord injuries to aid with treatment strategies and communication; however, there is no consensus in the literature. One early classification of cervical spine injuries simply categorized the injuries as fractures, dislocations, or fracture dislocations (Durbin, 1957). Classifications then began to add a descriptor relating to the anatomical motion of the injury, for example: pure flexion, flexion and rotation, extension, vertical compression, or direct shearing force (Holdsworth, 1963, 1970).

Allen et al., (1982) developed a classification system incorporating both musculoskeletal and neurologic damage, where each group exhibits a progression of stages based on severity. While this classification took a thorough approach to describe the diverse injuries, it is quite complex and inaccessible to those not intimately familiar with the subtleties of spinal column injury patterns. This system was also one of the first to add a biomechanics approach by attempting to deduce the modes of failure for the spinal components based on radiographic images, and associated ‘injury vectors’. In an attempt to classify injuries based on the structural failure of the spinal column, a ‘three column spine’ concept was hypothesized (Denis, 1983). This concept

divides the sagittal structures of the spine into three distinct load bearing columns, each comprised of various aspects of the vertebrae and soft tissues. The injury pattern can be defined by the mode of failure of these three columns.

More recently injury classification systems have been developed based on the spinal region sustaining injury, including the Subaxial Cervical Spine Injury Classification System (SLIC) (Vaccaro et al., 2007) and the Thoracolumbar Injury Classification and Severity Score (TLICS) (Vaccaro et al., 2005). These systems consider injuries based on three main categories: injury morphology (i.e. pattern of spinal column disruption), integrity of the disco-ligamentous complex, and neurological status. Injuries are assigned points in each category, where greater points correspond to more severe injuries, and the points are summed to numerically classify the injury and guide treatment. Due to disagreements on injury morphology and lack of international adoption, these systems have since been revised to the AOSpine classification systems (Vaccaro et al., 2013, 2016). These systems adjusted the main morphology types: compression, tension band, and translational, with the addition of facet injuries for the cervical classification.

Many of these classifications are primarily based on patient radiographic evidence and clinician experience, where the exact directions and magnitudes of forces can only be inferred. Experimental tests are required to verify these hypotheses.

1.4.1.1 Burst Fracture

Vertebral compression fracture occurs when the vertebral body fails due to axial load, and generally occurs due to vertical compression or compressive flexion of the spine (Allen et al., 1982). According to the three column concept, the anterior and middle column fail in compression, while the posterior column is often still intact (Denis, 1983). When the vertebral body endplate fails under compression due to the increased pressure within the intervertebral disc (Perey, 1957), the nucleus may be forced into an the adjacent vertebral body, fracturing the posterior aspects of the vertebral body, with bony fragments ‘bursting’ into the vertebral canal (Hall et al., 2006; Holdsworth, 1963; Magerl et al., 1994). These projected fragments transfer energy to the spinal cord tissue causing injury (Hall et al., 2006). The term ‘burst fracture’ was first described by Holdsworth (1963) due to the apparent shattering of the vertebral body from within. The basic difference between a compression and burst fracture is that the posterior

vertebral wall remains intact in a compression injury, and fails in a burst fracture (Denis, 1983) (Figure 1-22). Burst fractures have been experimentally reproduced by subjecting cadaveric vertebral bodies to dynamic axial compressive forces, where bone fragments severely encroached into the spinal canal (Fredrickson et al., 1992; Panjabi et al., 1994; Willén et al., 1984). Burst fractures are associated with increased range of motion (Panjabi et al., 1994; Willén et al., 1984), resulting in clinical instability and increased risk of further neurological damage (Denis, 1983).

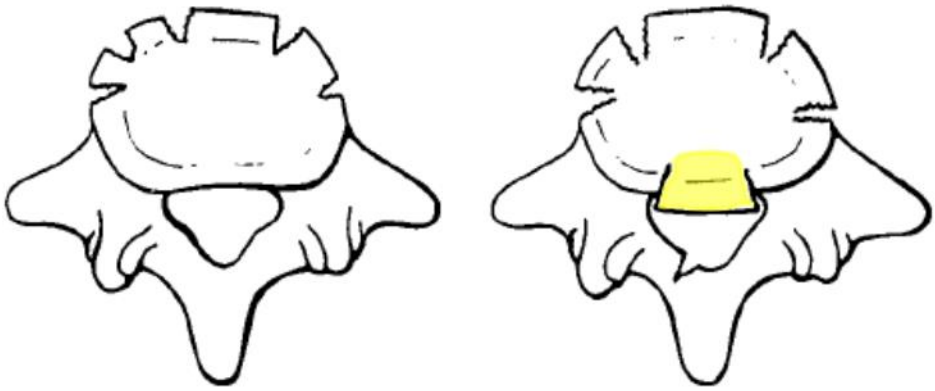

Figure 1-22 - Compression fracture compared to a burst fracture. In a burst fracture the posterior vertebral wall fails (highlighted in yellow), forcing bony fragments into the vertebral canal. (reprinted with copyright permission) (Denis, 1983)

Importantly, vertebral burst fracture fragments may remain in place, applying residual compression to the spinal cord, or may withdraw from the vertebral canal (White & Panjabi, 1990). Canal encroachment is greatest during a dynamic injury (Carter et al., 2000; Chang et al., 1994; Panjabi et al., 1995; Tran et al., 1995; Wilcox et al., 2002, 2003), and post-injury canal measurements do not correlate with peak dynamic occlusions (Carter et al., 2000; Chang et al., 1994; Panjabi et al., 1995; Wilcox et al., 2004). These findings provide explanation as to why neurologic outcome is not related to the degree of canal occlusion observed in post-injury radiographic images (Boerger et al., 2000; Herndon & Galloway, 1988; Mohanty & Venkatram, 2002). Soft tissues play a role in the reduction of the canal occlusion, including the attachment of the disc annulus to the fragment (Fredrickson et al., 1992), the tension of the posterior longitudinal ligament (Hall et al., 2006), and the spinal cord dura (Wilcox et al., 2003).

Higher energy impacts produce greater canal encroachments (Panjabi et al., 1995; Wilcox et al., 2003), where fractures progress from end-plate to wedge to burst with increasing energy (Panjabi et al., 1995), and also lead to higher pressures within a surrogate spinal cord (Wilcox et al., 2003). A similar progression occurs with increasing loading rate (Carter et al., 2000) – even when the impact energies were equivalent (Tran et al., 1995). These findings raised some important questions, namely, postulating whether there is a cut-off loading rate at which burst fracture occurs, or if occlusion is directly proportional to loading rate for all magnitudes (Tran et al., 1995).

1.4.1.2 Dislocation

In its most basic form, a vertebral dislocation injury occurs with substantial relative transverse translation of one vertebra relative to an adjacent vertebra (Figure 1-23). Most commonly this occurs in the sagittal plane (White & Panjabi, 1990), in the anterior direction (Tator, 1983). The spinal canal narrows between edge of the posterior arch of one vertebra (usually superior) and the posterior corner of the adjacent vertebral body (usually inferior). The annular fibers are the most effective structures resisting translation in the sagittal (and coronal) plane, and are ruptured or torn from the vertebral end plate, destroying the anterior and posterior longitudinal ligaments and posterior elements (White & Panjabi, 1990). Dislocation exhibits clinical variability, and may occur with only the failure of soft tissues, known as facet dislocation, or may occur with fracture of one or more aspects of the vertebrae, known as fracture-dislocation (Figure 1-24). Additionally, dislocation may be bilateral (i.e. both facets), or occur from unbalanced forces, causing non-symmetrical injuries, such as the unilateral dislocation of only one facet.

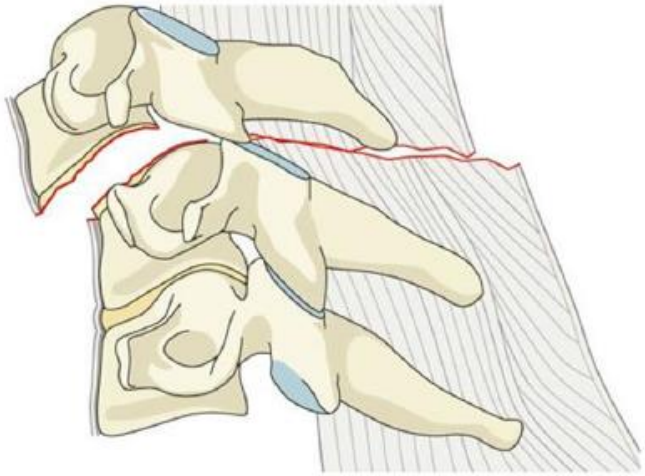

Figure 1-23 – Dislocation injury involves the substantial relative transverse translation of one vertebra relative to an adjacent vertebra. (Image reprinted with permission) (Vaccaro et al., 2016)

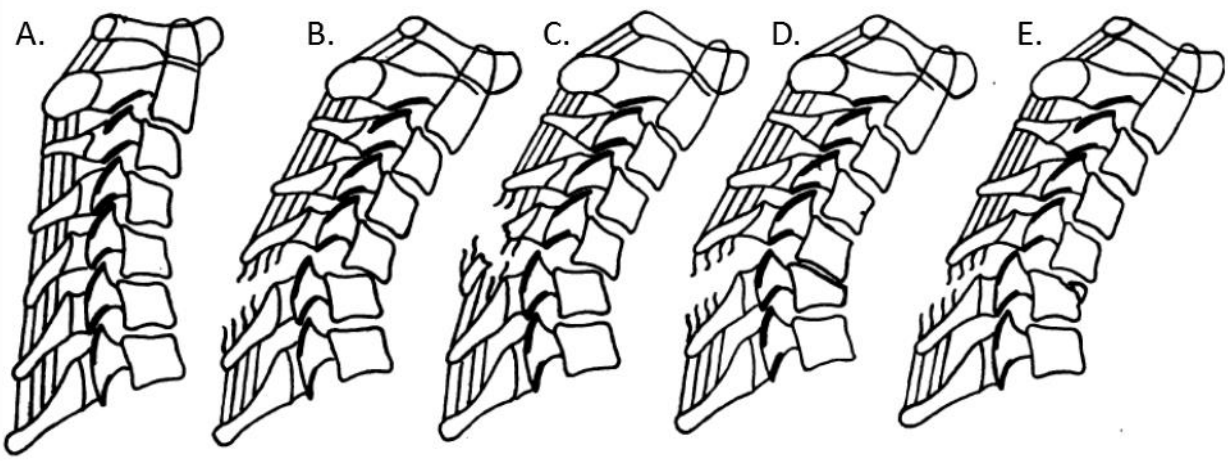

Figure 1-24 - Common types of dislocation (Durbin, 1957). A. Normal flexed cervical spine. B. Dislocation without fracture. C. Dislocation with fracture of spinous process. D. Dislocation with compression fracture of inferior vertebral body. E. Dislocation with fracture of anterior surface of inferior vertebral body. (reprinted with copyright permission)

For two adjacent vertebrae with normal anatomical orientation, the inferior facet joint surface of the superior vertebra is posterior to the superior facet joint surface of the adjacent, inferior vertebra (Figure 1-25-A). A facet dislocation occurs when the superior vertebra's inferior facet slides over, and becomes locked anterior to the inferior vertebra's superior facet (Figure 1-25-B) (Edwards et al., 1988; Leite et al., 1997).

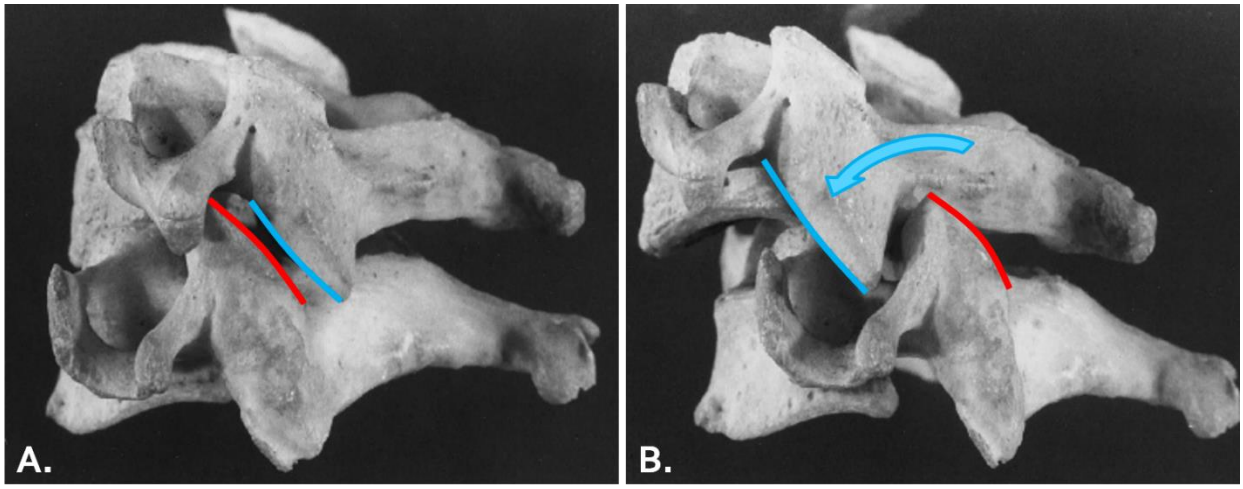

Figure 1-25 - Lateral view of the anatomic orientation of facet joint surfaces of adjacent vertebrae. A. The inferior facet joint surface of the superior vertebra (blue) is posterior to the superior facet joint surface of the inferior vertebra (red). B. The superior vertebra's inferior facet (blue) slides over, and becomes locked anterior to the inferior vertebra's superior facet (red), resulting in facet dislocation (reprinted with copyright permission) (Leite et al., 1997)

Facet dislocations are most common in the cervical spine and require less force, as the articular facet surfaces are relatively flat and easily slide over each other (compared to thoracic or lumbar facet surfaces) (Holdsworth, 1970). Dislocation may occur at any of the cervical spinal levels, however typically occurs at C5-C6 or C6-C7 (Table 1-4) (Anissipour et al., 2017; Du et al., 2014; Durbin, 1957; Harrington & Park, 2007; Isla et al., 2002; Johnson et al., 2004; Ordonez et al., 2000; Reinhold et al., 2006; Vaccaro et al., 2001; Wilson et al., 2013). The frequency of dislocations occurring in the lower cervical spine may be due to morphometric differences in the orientation of the superior articular facets (i.e. more horizontally oriented, lower height, smaller A-P facet diameter) at these levels (Ebraheim et al., 2008).

Table 1-4 - Distribution of clinical dislocation injuries by spinal level as reported by previous clinical studies. Dislocations are combined unilateral and bilateral, with and without fracture. The spinal levels where dislocation most commonly occurs are C5-C6 (35%) and C6-C7 (36%).

Study	Total	C2-C3 / C3-C4	C4-C5	C5-C6	C6-C7	C7-T1
Durbin 1957	53	9	17	19	5	3
Ordonez 2000	10	0	1	4	5	0
Vaccaro 2001	48	0	7	20	19	2
Isla 2002	42	3	5	13	16	5
Johnson 2004	87	6	12	33	33	3
Reinhold 2006	124	14	19	43	43	5
Harrington 2007	22	2	4	6	10	0
Wilson 2013	135	9	19	45	57	5
Du 2014	22	1	2	6	8	0
Anissipour 2017	21	1	5	7	8	0
Total	564	45 8%	91 16%	196 **35%**	204 **36%**	23 4%

Dislocation injuries are typically both mechanically and neurologically unstable, meaning further displacements and neurological damage are likely to occur without proper precautions of surgical decompression and stabilization (Denis, 1983; Tator, 1983). From a multicentre study, cervical SCI patients with facet dislocations were significantly associated with more severe neurological deficits at time of injury, high-energy injury etiology, and longer hospital stays (Wilson et al., 2013). Additionally, they demonstrated significantly less functional recovery after 1 year, despite earlier decompression times (Table 1-5) (Wilson et al., 2013).

Table 1-5 - Characteristics exhibited by cervical SCI patients with and without facet dislocation (Wilson et al., 2013)

Characteristic	Facet Dislocation	Other Column Injury Patterns	P
Total patients	135 (32%)	286 (68%)	
Presenting AIS grade A	69 (51.1%)	80 (28.0%)	< 0.01
High energy	81 (60.5%)	131 (46.6%)	0.01
Time to decompression (hours)	25.1 (±34.8)	41.3 (±44.6)	< 0.01
Acute hospital stay (days)	41.2 (±75.2)	30.0 (±38.5)	0.04
Change in AMS at 1-year follow-up	18.0 (±21.4)	27.9 (±25.1)	<0.01

AIS: American Spinal Injury Association (ASIA) impairment scale

AMS: American Spinal Injury Association (ASIA) motor score

Allen et al. (1982) categorized dislocation as 'distractive flexion', where increasing stages of severity correspond to different injury features. A stage-2 injury corresponds to unilateral facet dislocation, stage 3 consists of bilateral facet dislocation with anterior displacement approximately 50% of the vertebral body width, and stage 4 involves anterior displacement of an entire vertebra width with an unstable "floating" vertebra (Allen et al., 1982). They postulated major injury vectors as tension and shear to the posterior ligamentous complex, and compression to the inferior vertebral body. According to Denis' three-column spine hypothesis, fracture dislocation likely occurs as a result of compression, rotation and shear on the anterior column, and distraction, rotation and shear on the middle and posterior columns (Denis, 1983). Similarly, White and Panjabi (1990) hypothesized a combination of forces causing a dislocation, where the main vector is a moment in acting in the sagittal plane.

Dislocation is often clinically described as being caused by compression and/or flexion (Beatson, 1963; Edwards et al., 1988; Norton, 1962; White & Panjabi, 1990). Previous studies that subjected motion segments to unconstrained flexion or compressive-flexion loads found failure due to vertebral wedge or compression fracture with disc and ligament ruptures, but not typical facet dislocations (Crowell et al., 1993; Nightingale et al., 2002; Roaf, 1960; Zhu et al., 2008). These compressive flexion descriptions more accurately describe the external forces applied to the spine, and not necessarily the forces causing failure at the vertebral level (Bauze & Ardran, 1978; Edwards et al., 1988; Nightingale et al., 1996, 2016). Depending on the orientation of the spine and kinematics during loading, external forces can result in different local forces at each individual vertebra (Nightingale et al., 1996) (Figure 1-26). Dislocation injuries are most consistently produced when there is a large transverse shear component acting at the level of dislocation. This is often achieved when experimental testing conditions have motion constraints relevant to injury scenarios. Dislocation injuries were consistently produced in whole cervical spine vertical compression tests, when the skull was constrained from rotation but free to translate (Figure 1-27) (Bauze & Ardran, 1978; Nightingale et al., 1991), and in multi-segment thoracic flexion-compression tests with constrained ends (Zhu et al., 2008). Compared to loads required for vertebral compression fracture, the relatively low vertical loads causing dislocation indicate the spine is particularly vulnerable in these orientations (Bauze & Ardran, 1978; Nightingale et al., 1991).

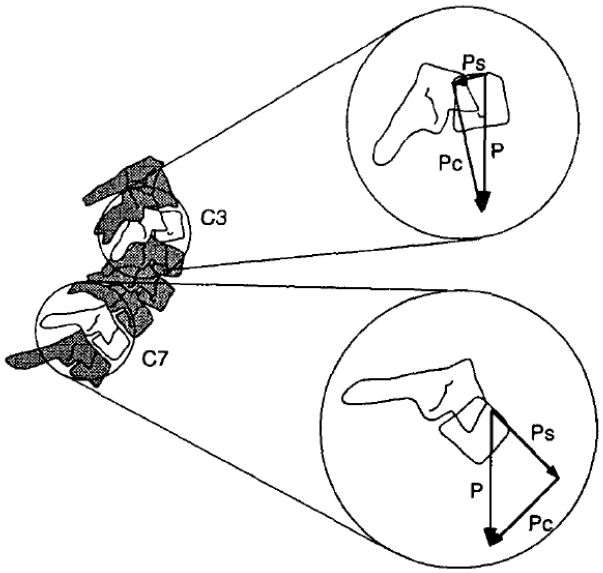

Figure 1-26 – Local vertebral forces. The external compression force (P) results in different local shear (Ps) and compression (Pc) at local vertebrae depending on spine orientation. (reprinted with copyright permission) (Nightingale et al., 1996)

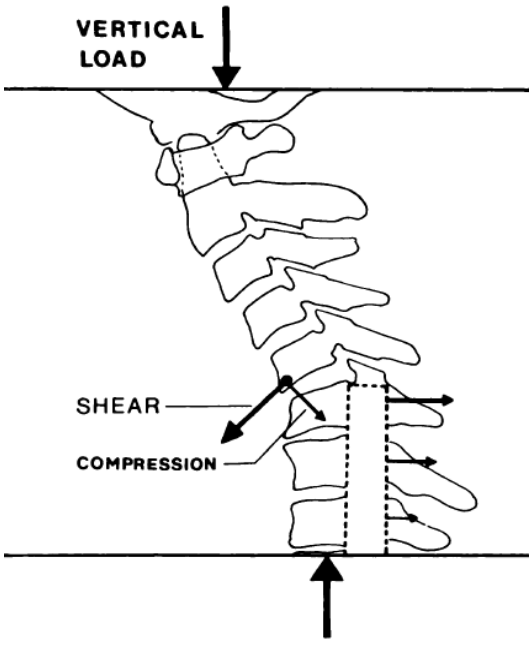

Figure 1-27 – External compressive flexion loading results in significant shear at the level of dislocation. (reprinted with copyright permission) (Bauze & Ardran, 1978)

A bench-top sled apparatus was used to produce bilateral facet dislocations in motion segments to quantify dynamic canal narrowing (Ivancic et al., 2007), facet joint kinematics (Panjabi et al., 2007), and forces and moments during loading via inverse dynamics (Ivancic et al., 2008) (Figure 1-28). The post-impact narrowing of the spinal canal diameter (0.8 mm) was significantly less than the dynamic canal narrowing (6.2 mm). Average canal narrowing velocity was 0.23 m/s. These results align with previous burst fracture findings (Chang et al., 1994; Panjabi et al., 1995; Tran et al., 1995; Wilcox et al., 2002, 2003), in that canal narrowing observed in the clinic substantially underestimates the maximum dynamic narrowing that occurred during injury. Extrapolation of these results with soft tissue geometries indicated dynamic spinal cord compression of up to 35% (Ivancic et al., 2007). Additionally, since dislocations were induced using progressively greater impacts, typical clinical dislocations likely exceed the velocities and occlusions seen in this study. Following impact, specimens displayed the same chronological order of kinematic events (Panjabi et al., 2007). Using inverse dynamics, the moment and shear required to cause dislocation was lowest in C5/C6 (Ivancic et al., 2008): one of the most common spinal levels where dislocation injuries occur (Table 1-4). Although these experiments involved detailed analyses of bilateral facet dislocations, the reported kinematics are a product of the specific experimental testing scenario, and may not be representative of all clinical dislocations.

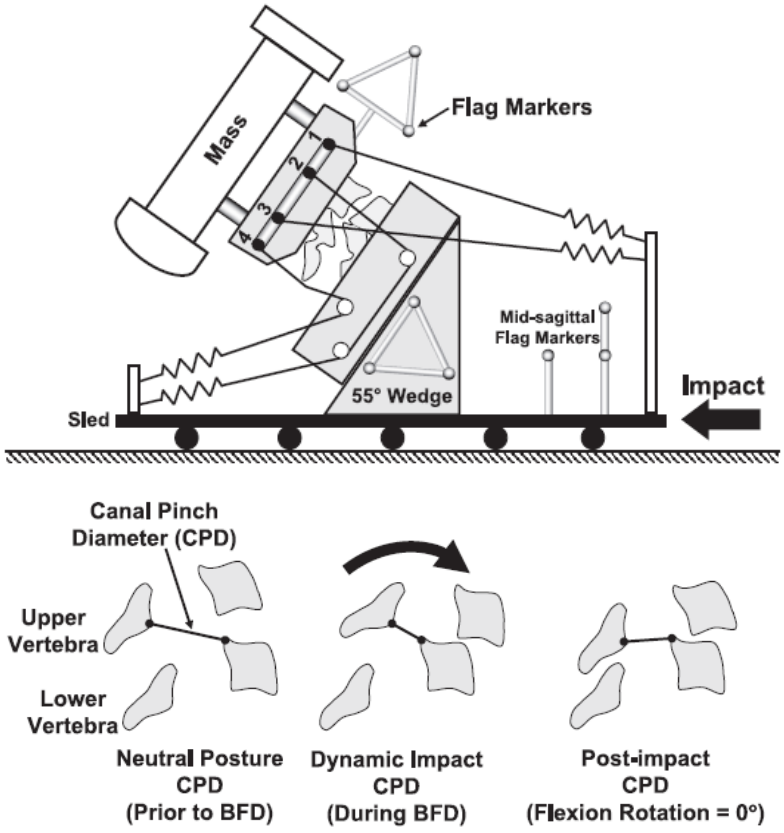

Figure 1-28 - Experimental sled setup of Ivancic et al., (2007) and schematic of canal narrowing during impact. (reprinted with copyright permission)

1.4.2 Velocity of Canal Occlusion

It is impossible to measure the velocity of an impact to the spinal cord in a clinical scenario, so we must rely on velocity measurements from relevant biomechanical studies. Whole cervical spine cadaveric specimens subjected to relevant horizontal rear (3.5 – 8 g, Ito et al., 2004) or frontal impact (4 – 10 g, Ivancic et al., 2006) accelerations, both found that spinal canal pinch velocity generally increased as impact acceleration increased. Although not tested statistically, of note was the largest increase in canal pinch velocity occurred between the 8 and 10 g impacts (Ivancic et al., 2006) (Table 1-6), suggesting a threshold at higher energies at which the spinal cord is injured more catastrophically. There is still a disconnect between spinal cord injury as these studies were not able to track soft tissue protrusions, and impacts did not produce typical SCI mechanisms of burst fracture or facet dislocation.

Table 1-6 - Relationship between impact acceleration and peak velocity of spinal canal narrowing at each spinal level during whole cervical spine simulated frontal impact (Ivancic et al., 2006). Spinal canal narrowing velocity generally increased as impact acceleration increased, particularly at higher impact accelerations.

	Spinal Canal Narrowing Velocity (m/s)						
Impact	C0 - dens	C1 – C2	C2 – C3	C3 – C4	C4 – C5	C5 – C6	C6 – C7
4 g	0.09 (0.04)	0.04 (0.02)	0.05 (0.02)	0.02 (0.01)	0.02 (0.01)	0.03 (0.01)	0.04 (0.02)
6 g	0.21 (0.08)	0.11 (0.04)	0.08 (0.04)	0.03 (0.01)	0.03 (0.01)	0.04 (0.02)	0.03 (0.02)
8 g	0.23 (0.04)	0.08 (0.03)	0.12 (0.08)	0.03 (0.01)	0.03 (0.01)	0.04 (0.01)	0.03 (0.01)
10 g	0.98 (0.11)	0.15 (0.07)	0.22 (0.13)	0.12 (0.09)	0.14 (0.04)	0.08 (0.09)	0.17 (0.08)

Many previous studies investigating the velocity of canal occlusion had one obvious limitation: the absence of the spinal cord. A biofidelic surrogate spinal cord (Kroeker et al., 2009) quantified spinal cord deformation within whole cervical spine specimens during dynamic head-first impacts (Saari et al., 2011). The injuries produced from the 0.6 m drop test (~3 m/s impact) were either hyperextension or atlantoaxial dislocation, and resulted in cord compression ranging from 19% to 78%, with larger compressions associated with the dislocations. The average velocity of cord compression was 1.1 m/s for hyperextension and 3.7 m/s for dislocation.

A summary of measured velocities of canal occlusion from relevant biomechanical studies is presented in Table 1-7.

Table 1-7 - Comparison of measured velocity of canal occlusion from previous cadaveric studies.

Study	Specimen details	Measurement details	Measured velocity
Panjabi et al. 1995	Drop-weight on 3 human thoracolumbar segments to produce burst fracture	Strain gauge within canal	~ 1 m/s (calculated as peak displacement/event time)
Wilcox et al. 2004	Drop-weight on 3 bovine segments to produce burst fracture	High speed video of mirror reflected canal	1 – 10 m/s (reported observed range)
Ivancic et al. 2006	Sled impact on whole cervical spine specimens to simulate frontal impact	High speed camera measurement of markers correlated to rigid body canal pinch diameter	0.08 – 0.98 m/s
Ivancic et al. 2007	Sled impact on human cervical FSUs to produce bilateral facet dislocation	High speed camera measurement of markers correlated to rigid body canal pinch diameter	0.23 m/s (SD: 0.06)
Saari et al. 2011	Whole cervical spine with surrogate spinal cord in dynamic head-first impact simulation	High speed cineradiography of surrogate spinal cord within whole spine specimens under head first impacts	0.3 – 5 m/s

1.4.3 Biomechanics of Neural Tissue

A detailed understanding of the response of spinal cord tissue under various mechanical loading conditions can provide insight into traumatic spinal cord injury mechanisms and thresholds, however the few studies on spinal cord material properties report a wide range of variability (Clarke, 2011). Most spinal cord material property tests have been performed in tension, to investigate stress-strain relationships and are typically performed below yield, as the physiological threshold of injury is much lower than yield, and often stress-relaxation properties are of interest (Clarke, 2011).

There is a wide range of reported mechanical property values of spinal cord in the literature, with elastic modulus varying from 0.012 to 1.37 MPa (Bilston & Thibault, 1996; Clarke et al., 2009; Fiford & Bilston, 2005; Hung & Chang, 1981; Hung, et al., 1981A; Hung, et al., 1981B; Oakland et al., 2006; Tunturi, 1978); however, this range may be attributed to the variety of methodological differences, such as tissue species, age, testing environment, and loading conditions. There are relatively few studies that have investigated the influence of these different testing variables. Of particular importance is the testing environment, where in vivo tests obviously provide properties as close to natural state as possible, but are much more difficult to perform. Thus it is critical that in vitro tests closely mimic in vivo conditions (temperature, hydration, etc.). Additionally, spinal cord tissue degrades rapidly post-mortem, with the modulus increasing dramatically in the first 72 hours (Oakland et al., 2006). Age has been demonstrated to have a significant difference, as neonatal rats have significantly softer spinal cords compared to adult rats (Clarke et al., 2009). These differences emphasize the need for experimental spinal cord tests to mimic as closely as possible the scenario they are trying to represent.

Identifying 'failure' properties of spinal cord is not straightforward, as the spinal cord may still be able to structurally support load, however its physiological function may be greatly compromised. This relationship between injury thresholds and mechanical properties are not well understood. Bain et al. (2001) investigated the relationship between axonal stretch and both physiological, and morphological signs of injury. Physiological damage occurred prior to structural damage, as electrophysiology signals were lost prior to any evidence of structural damage. Importantly, this study demonstrates that distinct mechanical thresholds corresponding to injury exist in the white matter. These results also diminish the importance of defining structural failure properties of spinal cord tissue.

Spinal cord tissue is viscoelastic, so it is sensitive to loading rate and exhibits stress relaxation properties. Several studies, despite differing testing methodologies, have demonstrated spinal cord stiffness increases with increased strain rate, in both tension (Clarke et al., 2009; Fiford & Bilston, 2005) and compression (Fradet et al., 2016; Sparrey & Keaveny, 2011). Additionally, greater damage has been observed at fast strain rates compared to slow rates when strain magnitude is equivalent (Shi, 2006). In spinal cord injury models, the load relaxation characteristics have been shown to be dependent on initial impact velocities, where the interface

pressure between the impactor and the spinal cord relaxes more rapidly following a high-rate injury compared to a slow-rate (Carlson, et al., 1997A, 1997B; Sjovold et al., 2013). These variables are critically important when considering how spinal cord injuries most frequently occur in the human population: at high rates, with residual compression.

The two distinct regions of the spinal cord, gray and white matter, are defined by their different morphologies and neuronal arrangement. These differences would inherently imply different mechanical properties, but there are few studies in the literature differentiating the two. Early studies have reported conflicting results (Ichihara et al., 2001; Ozawa et al., 2001). Ichihara et al. (2001) reported gray matter to be significantly stiffer when tested in tension, however failed at lower strains, while Ozawa et al. (2001) found no significant differences when evaluated using pipette aspiration. More recently, sections of mouse spinal cord were tested using atomic force microscopy, and gray matter was found to be significantly stiffer than white matter regardless of directionality, and both stiffened with increasing strain (Koser et al., 2015). Stiffness distributions under compression were found to strongly correlate to the direction of axons in both the gray and white matter. Tissue was generally stiffer perpendicular to axons or with a greater proportion of cell nuclei. Longitudinal axons were the major load-bearing structures within lamprey spinal cords for high longitudinal strains, as they have a much greater elastic modulus compared to the surrounding extracellular matrix (Luna et al., 2013). Although these were small-scale tests, and properties may not be relevant on a larger scale, the relationships between directionality, cell orientation and structure are still likely important in relating to injury.

1.5 Secondary Spinal Cord Injury Pathology

Following the initial physical trauma, or primary injury mechanism, the spinal cord undergoes a cascade of biological responses to the injury, many of which can cause further damage. These biological processes are referred to as secondary spinal cord injury and are responsible for the progression of the injury from hours to days to months.

Neurogenic shock

Neurogenic shock is generally referred to as a loss of sympathetic innervation following spinal cord injury (Dumont et al., 2001; Taylor et al., 2017). The trauma causes the sympathetic nervous system to stop stimulating the blood vessels, which leads to vasodilation (relaxation of

blood vessels), and a drop of blood pressure. The outcomes are bradycardia (slowed heart rate due to lack of blood flow to the heart), reduced cardiac output, hypothermia, and can lead to ischemia (insufficient oxygen and glucose from blood to tissue) of the nervous tissue. Neurogenic shock typically occurs within the first few hours following injury, and can last from days to months (Tator, 1995), making it difficult to gauge initial functional impairments. This leads to further questions related to neurological function as it is difficult to tell if functional recoveries are due to neural repair and plasticity, or simply the neurogenic shock wearing off.

Vascular Effects

Vascular effects are present immediately at the time of trauma at the lesion, and become worse in the ensuing hours. It is mainly the microcirculation vessels that are affected (venules and capillaries near the injury site), while larger vessels are often undamaged (Tator & Fehlings, 1991). The rupture of these small vessels is due to the mechanical trauma or from intravascular coagulation (Norenberg et al., 2004). This leads to small areas of hemorrhage that progress to necrosis, particularly in the gray matter (Dumont et al., 2001; Hausmann, 2003; Norenberg et al., 2004; Tator, 1995). The lack of blood flow causes ischemia and local edema (swelling from accumulation of fluid in interstitial space) in the nervous tissue and worsens in the first few hours following injury (Norenberg et al., 2004; Tator & Fehlings, 1991). The trauma has been shown to cause vasospasm (muscles contract, vessels vasoconstrict) and thrombosis (blood clots) (Tator, 1995).

Reperfusion, or restoring blood flow to the tissue, can worsen the damage from increased production of reactive free radicals and toxic byproducts that lead to oxidative stress in the cells, particularly at the early stages of reperfusion (Dumont et al., 2001).

Glutamate Excitotoxicity

Under normal conditions, the major excitatory neurotransmitter, glutamate, is removed from the synaptic cleft to prevent accumulation (Hausmann, 2003). Beginning in the immediate phase of injury and continuing into the acute phase (0 – 48 hours), glutamate is released in large quantities, resulting in direct and indirect damage (Dumont et al., 2001). Glutamate receptors are activated, and Na^+ accumulates within the cell, leading to intracellular acidosis and cytotoxic edema. Reverse activation of the Na^+-Ca^{2+} exchanger leads to accumulation of calcium within

the cell. Excitotoxicity also triggers a cascade that results in production of reactive oxygen and nitrogen species. Oligodendrocytes are particularly vulnerable to glutamate excitotoxicity as they have a full array of glutamate receptors, leading to demyelination of axons around the injury site (Bernal-Chico et al., 2015), directly affecting signal transmission.

Increased Calcium Influx

High calcium concentrations within the cell lead to damage from several mechanisms, and continue for hours to weeks (Liverman et al., 2005). Calcium interferes with mitochondrial processes, including respiration, already weakened by ischemia. Calcium also activates an array of enzymes (proteases, kinases and lipases), including calpains, which degrade important structural proteins of the axon-myelin unit (Dumont et al., 2001). Other proteases and kinases destroy cell membranes and contribute to inflammatory response, lipid peroxidation and reduced blood flow by causing blood clots and vasoconstriction. Lipid peroxidation produces more free radicals, speeding the process, as a positive feedback loop (Dumont et al., 2001).

Free Radicals and Lipid Peroxidation

Free radicals such as reactive oxygen and nitrogen species (ROS and RNS) are produced after SCI as a consequence of insufficient oxygenation (Hausmann, 2003). These free radicals cause lipid peroxidation and oxidative and nitrative damage to proteins and nucleic acids, which leads to the death of neurons and glia (Oyinbo, 2011; Rowland et al., 2008). The free radical takes an electron from a lipid molecule, which then becomes less stable, triggering a chain reaction leading to the breakdown of the cell membrane and death by necrosis (Hagg & Oudega, 2006). The oxidative damage also promotes mitochondrial dysfunction and contributes to intracellular calcium overload, which activates enzymes that damage cytoskeletal proteins. The production of ROS is associated with both ischemia and subsequent reperfusion following injury, and the detection of ROS peaks at about 12 hours following injury and remains elevated for about 1 week (Rowland et al., 2008).

Inflammation and Immune Response

Following a spinal cord injury, the immune system is responsible for clearing cellular debris (Oyinbo, 2011) and maintaining homeostasis in the central nervous system by regulating amino

acid levels and pH (Dumont et al., 2001). The immune response involves the recruitment of numerous cell types, including astrocytes, microglia, T cells, neutrophils and invading monocytes (Rowland et al., 2008), and can occur over hours or weeks (Donnelly & Popovich, 2008) (Figure 1-29). The cumulative effect of immune cells and regulatory proteins is inflammation (Oyinbo, 2011). Immune cells secrete proinflammatory cytokines (signaling molecules), as inflammation is crucial to clear cellular debris. Over-activation of inflammation, however, can damage healthy tissue and cause further injury (Oyinbo, 2011).

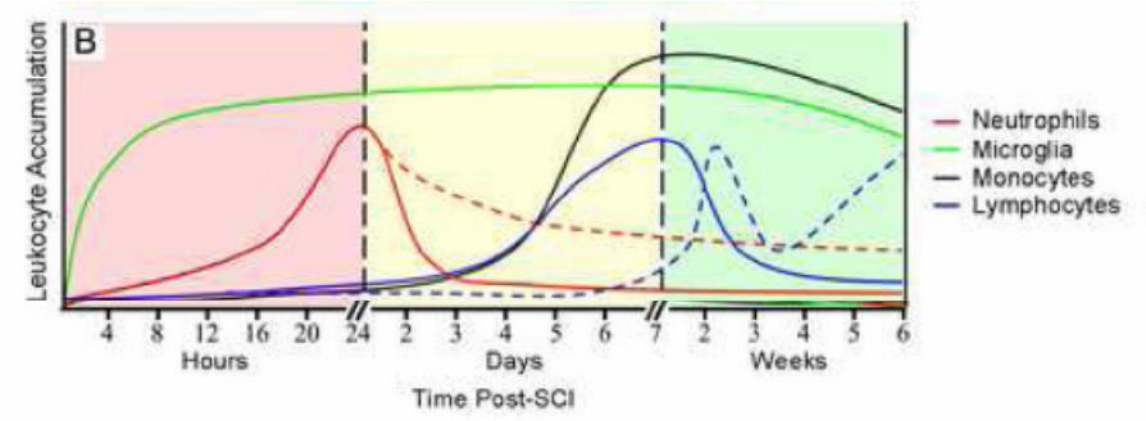

Figure 1-29 - Immune cell accumulation in the spinal cord and progression over time (reprinted with copyright permission) (Donnelly & Popovich, 2008)

Insult to the CNS triggers ‘danger cells’ (ATP or heat-shock proteins) to be released, which communicate and recruit circulating leukocytes and coordinate local inflammation (Popovich & Longbrake, 2008). The initial inflammatory response after injury is biphasic (Dumont et al., 2001). The first phase involves predominantly neutrophils, which arrive first from the blood stream, and remove intruders and tissue debris to prevent infection, but may increase damage to CNS cells by release of enzymes and free radicals (Norenberg et al., 2004). The next phase involves the recruitment and migration of macrophages, and activated microglia transforming into macrophages, which ingest damaged tissue but also release enzymes and free radicals (Hagg & Oudega, 2006). Macrophages can persist within the lesion site for weeks to months and are crucial to the removal of lipids within necrotic debris, which are potential sources of oxidative free radicals (Norenberg et al., 2004).

The functional significance of some immune cells is controversial in the CNS after injury (Dumont et al., 2001; Norenberg et al., 2004). Macrophages and microglia have been seen as important to neural regeneration, but also have been thought to contribute to oligodendrocyte death, neuronal death and demyelination. The demyelination is thought to begin within 24 hours of injury and continue for days. Injury and repair seem to go hand in hand, which could explain why various experimental models of neuroinflammation elicit both injury and repair in the CNS (Popovich & Longbrake, 2008).

Apoptosis

Apoptosis is cell suicide: an energy-consuming programmed death from biochemical changes, and is activated in neurons, oligodendrocytes, microglia, and possibly astrocytes (Dumont et al., 2001). It can be triggered by a variety of insults including cytokines, inflammatory injury, free radical damage, and excitotoxicity. Apoptosis contributes to different factors depending on the cell in which it occurs: microglia (inflammatory secondary injury), oligodendrocytes (demyelination), and neurons (signal loss) (Dumont et al., 2001). Two pathways of apoptosis are defined as extrinsic (receptor-dependent, triggered by extracellular signals), or intrinsic (receptor-independent, triggered by intracellular sources) (Dumont et al., 2001; Hausmann, 2003).

Demyelination

Glutamate excitotoxicity, free radical assaults, and inflammatory response lead to the death of oligodendrocytes, causing demyelination of the neurons (Oyinbo, 2011). Demyelination occurs in the acute phases at the epicentre of the primary injury (Donnelly & Popovich, 2008), but distal white matter oligodendrocytes continue to undergo apoptosis for many weeks (Casha et al., 2001; Crowe et al., 1997). Activated microglia, which are abundant after SCI, have been demonstrated to induce oligodendrocyte apoptosis (Hagg & Oudega, 2006). Demyelination is characterized by the swelling of the myelin sheaths, followed by fragmentation and phagocytosis by macrophages (Norenberg et al., 2004).

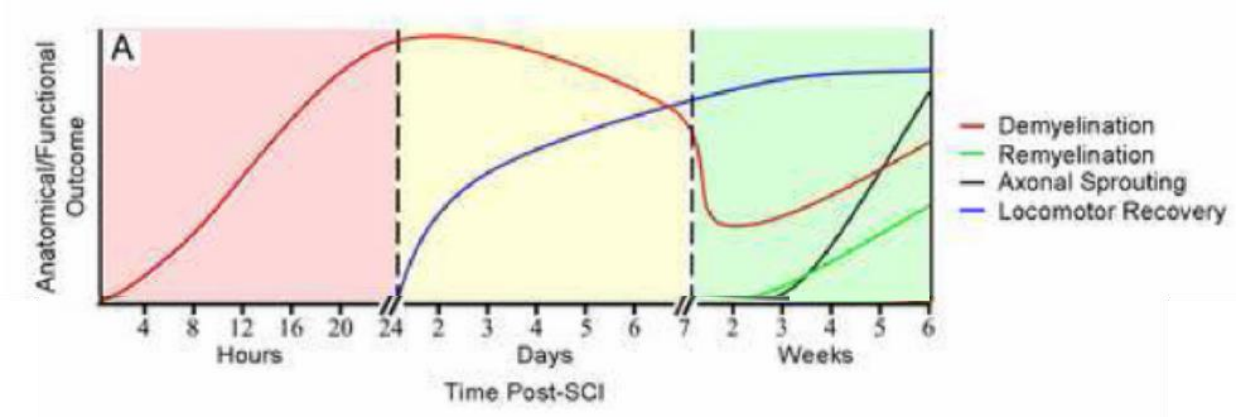

Figure 1-30 - Acute demyelination following SCI (reprinted with copyright permission) (Donnelly & Popovich, 2008)

Without myelin, neuron signals are delayed, and axons are exposed to damaging effects of free radicals and inflammatory cytokines, leading to neuron death due to necrosis or apoptosis (Oyinbo, 2011). The degeneration of fibers characterized by the disruption of their myelin sheaths is known as Wallerian degeneration (Hausmann, 2003). It is accompanied by activation of microglia in ascending tracts above the lesion, and descending tracts below the lesion, and is partly responsible for the delayed sensory-motor dysfunction.

Astroglial Scar

Delayed astrocytic response occurs in the sub-acute phase (2 days – 2 weeks), where reactive astrocytes at the periphery of the lesion become hypertrophic and proliferative, as they grow multiple, large cytoplasmic processes that interweave to form the astroglial scar (Rowland et al., 2008). The astrocytes support the physiology in the injured spinal cord by promoting reestablishment of ionic homeostasis and the integrity of the blood-brain-barrier, which is important for reducing the edema and limiting the infiltration of immune cells. Without the glial response after SCI, the extent of cavitation of the lesion is increased (Hagg & Oudega, 2006). The scar continues to mature in the intermediate phase (2 weeks to 6 months) and isolates the intact neural tissue from inflammatory cells, which is advantageous as it reduces neuroinflammation and neurodegeneration (Popovich & Longbrake, 2008).

The astroglial scar potentially represents both a chemical and physical barrier to axon regeneration (Hagg & Oudega, 2006; Rowland et al., 2008), however this is under debate (Anderson et al., 2016). Chemically, the astrocytes secrete a number of growth inhibitory extracellular components. Astrocytes also act as a physical barrier, as their protein core interacts with other extracellular matrix components such as laminin, fibronectin, and neural cell adhesion molecules (Rowland et al., 2008).

1.5.1 Relationship Between Humans and Animal Models

Animal models are essential in order to better understand the biological processes behind SCI and evaluate treatment interventions. Animal models allow in vivo studies where independent injury variables can be adjusted to represent human SCI (Erbayraktar et al., 2013). Animals used in SCI research include rats, mice, guinea pigs, cats, dogs, rabbits, pigs, and non-human primates (Zhang et al., 2014). The rat is one of the most common, due to the anatomical (Flynn & Bolton, 2007; Watson et al., 2009) and physiological similarities to the human spinal cord (Kwon et al., 2002; Metz et al., 2000). Additionally the rat model is desirable because rats are relatively inexpensive, easy to care for, cope with surgical infections, can be studied in large numbers, and behavioural and histological analysis techniques are well established (Talac et al., 2004).

Individuals living with SCI have increased expectations for the results of preclinical studies, and are more likely than researchers to suggest that effective rodent model results are sufficient to proceed with clinical trials, so long as the studies were robust (Kwon et al., 2012). Animal models have recently focused on injury to the cervical region, which result in distinct neurological deficits, and are more representative of clinical injuries (Cheriyan et al., 2014). However, both similarities and differences exist between the nervous system of rodents and humans, in terms of size, anatomical and physiological characteristics, and pathological responses (Courtine et al., 2007). Additionally, there are unavoidable environmental discrepancies such as the anesthesia involved during injury to animal models, and the multiple drug treatments that humans are typically subjected to relating to other trauma sustained in the injury event, creating a different pharmacological environment (Kwon et al., 2002). Therefore it is important to understand the differences between human and rat SCI which may lead to limitations in scientific research.

1.5.1.1 Anatomy

Size difference: gross and cellular

Human and rat spinal cords have an obvious size difference, both in diameter and length. At the cellular level, human corticospinal tract fibers are both larger and more numerous than in rodents (Courtine et al., 2007). This does not include other potential differences in cell types, distributions, morphologies and extracellular matrix composition. These variables may also change during aging or pathological conditions. These factors may introduce differences with respect to the distribution of stress due to an applied load. Additionally, there are also substantial differences between rodents and humans in the distances over which neural fibers might be required to regenerate after injury due to species size.

Spinal tract layout differences

The anatomical layout of the spinal tracts between human and rat are remarkably similar. There are no fundamental differences between rat and human organization of the respiratory nervous system, making rodents a suitable model for evaluating respiratory affects after SCI (Kastner & Gauthier, 2008). However, there is one important exception. The motor cortex and its descending output – the corticospinal tract (CST) – are different between rodents and humans, both qualitatively and quantitatively (Courtine et al., 2007). In humans, the corticospinal tract is one of the most important tracts, responsible for fine motor control in the forelimbs, and is located in the lateral funiculus. In rats, the corticospinal tract is primarily located in the medial region of the dorsal column (Figure 1-31). This is of particular importance when evaluating the spinal cord injury model, and whether particular tracts are affected from specific injury mechanisms.

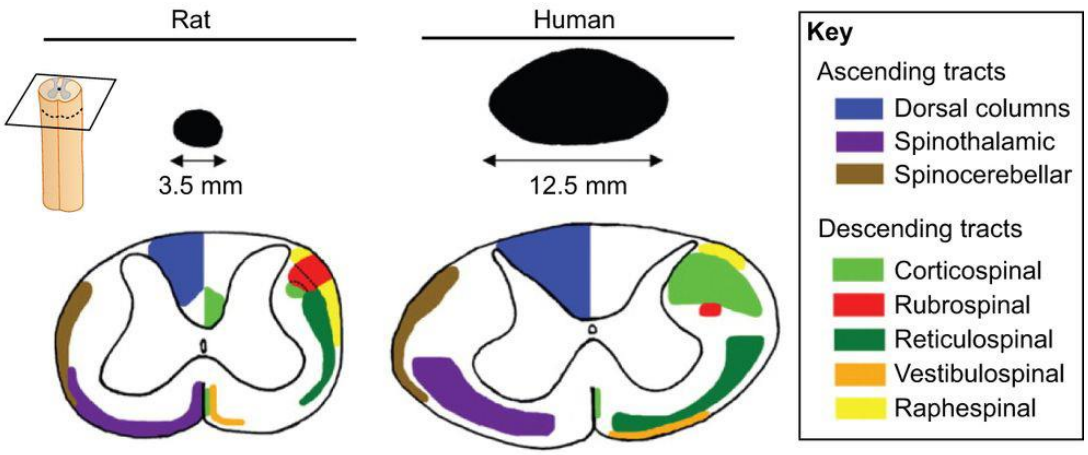

Figure 1-31 – Sensory (ascending) and motor (descending) spinal tract layout comparison between rat and human. Note the corticospinal tract (light green) exists entirely in the lateral white matter in humans, but primarily in the medial dorsal column in rats. (reprinted with copyright permission) (Watson et al., 2009)

Humans have direct connections between CST and motoneurons to innervate limb muscles, where rodents have no direct connections between corticospinal neurons and the motoneurons – interneurons relay input to motor neurons (Courtine et al., 2007). There is also a strong correlation between the number of direct connections between cortex and motor neurons and the level of manual dexterity (Figure 1-32) (Courtine et al., 2007). Lesions to the corticospinal fibers cause major impairments in fine motor function of the hands and feet, where the magnitude is most severe in humans due to the increase in the size and number of CST fibers. Lesions to the CST do impair fine motor function in rodents, however injuries are less sensitive since overall dexterity is lesser in rodents compared to humans. These lesions also have a lesser effect on stepping in rodents, indicating the motor cortex is not essential for creating the muscle synergies that sustain simple locomotion in rats and mice (Courtine et al., 2007).

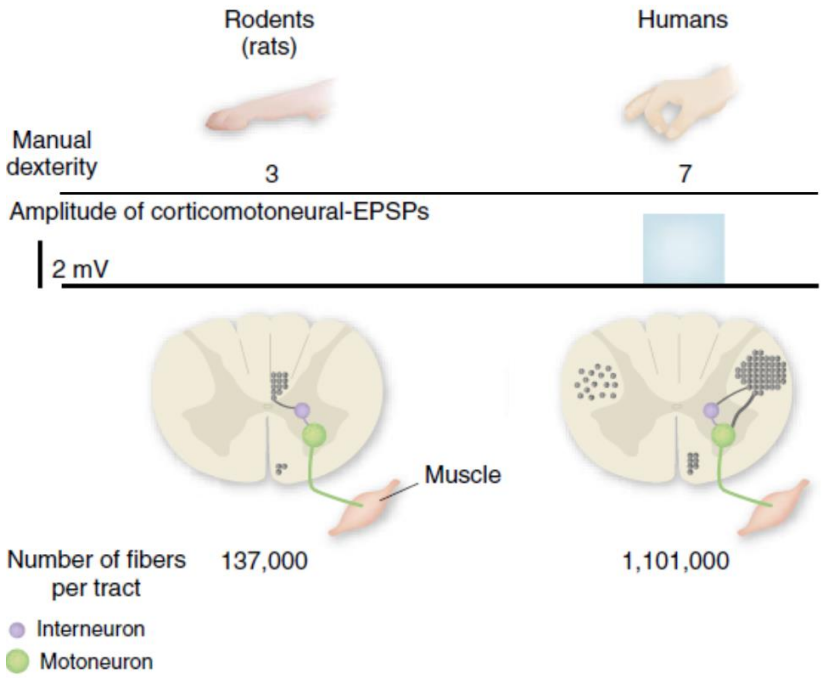

Figure 1-32 – Comparison of the corticospinal tract between rats and humans. In rodents, interneurons relay cortical input to motor neurons, whereas in humans, corticspinal neurons also directly synapse on motor neurons innervating forelimb muscles. Additionally, humans have an increased size and number of corticospinal fibers. These developments correlate with improved dexterity (reprinted with copyright permission) (Courtine et al., 2007)

1.5.1.2 Physiology

It is difficult to relate physiologic time in a rat to that of a human. Studies have attempted to identify relationships between ages, but this is difficult given the developmental phases. One study related the adolescent and adulthood phase of a rat's life as 10.5 – 11.8 rat days equivalent to one human year (Sengupta, 2013). These cannot be directly scaled down to measure equivalent smaller time scales, as physiological processes are not correlated with age, and differ between species. For example, the heart rate of a rat is approximately 260 - 400 beats per minute (Sengupta, 2013), compared to that of a human at approximately 60 – 80 beats per minute. These metabolic time difference ratios vary from 1:35 (based on age) to 1:4 (based on heart rate). In the context of spinal cord injury, it is conceivable that the duration of different pathophysiological processes would vary between species as well.

The morphological response to spinal cord injury in rat models are qualitatively very similar to those seen in humans, for example the development of large cavities in the spinal cord following SCI (Norenberg et al., 2004), however there are differences that may challenge the translation of therapies (Table 1-8) (Hagg & Oudega, 2006). The inflammatory response is lesser in humans, with only a minor neutrophil response, but the rapid expression of cytokines is very similar. In rats, the astroglial response is faster and a more pronounced astroglial scar forms. It is thought that demyelination of spared axons is reduced in humans, however the pathology results require higher resolution to detect degeneration accurately.

Table 1-8 - Similarities and differences in response to spinal cord injury between the rat and human. (Hagg & Oudega, 2006)

	Rat	Human
Degenerative processes		
Vascular response	Hemorrhage, angiogenesis	Hemorrhage, angiogenesis
Inflammation	Extensive	Much less pronounced, despite similar cytokine expression
Demyelination	Yes	Yes, but perhaps less pronounced
Axonal degeneration	Some die-back and Wallerian degeneration	Wallerian degenerations much more protracted
Glial scar	Extensive	Not extensive
Cyst formation	Yes	Yes
Schwann cell resposnse	Some invasion	Extensive Schwannosis
Regenerative processes		
Sprouting	Yes	Yes
Remyelination	Yes	Yes
Plasticity of uninjured systems	Yes	Yes

Despite the limitations of the rat model, few other models of neurological disorders are translationally as relevant or robust (Kjell & Olson, 2016). The additional benefits of the rat

model being readily available at specified ages and weights, relatively inexpensive compared to other larger animal models, requiring minimal housing space requirements; and the existence of a wide range of validated behavioural outcome techniques make it a suitable animal model for SCI research. However, any SCI treatments demonstrating promising results should be validated against multiple animal models (Filli & Schwab, 2012; Hilton et al., 2016).

1.6 Animal Injury Models

Animal injury models have evolved significantly since the original weight-drop injury model was developed in 1911 (Allen, 1911; Cheriyan et al., 2014). Injury models can be classified based on injury mechanism, such as contusion, residual compression, dislocation, distraction, transection, or chemical. Contusion injuries apply a focal force to the exposed spinal cord to elicit damage by using weight-drop, electromagnetic, stepping motor, or pressurized air devices. Residual compression models apply a sustained force or displacement on the spinal cord over a length of time. Dislocation models induce injury via the displacement of the vertebrae in the transverse plane. Distraction models stretch the spinal cord axially. Transection models either partially or completely slice the spinal cord in the transverse plane, and chemical models investigate targeted aspects of the secondary injury pathology; however, since this work is focused on mechanical injury mechanisms, transection and chemical models will not be discussed.

Injury models strive to achieve consistency and precision of the biomechanical displacements or forces applied during injury by precisely controlling input parameters, with the goal of producing consistent neurological and functional deficits (Kwon et al., 2002). No single injury model is representative of all spinal cord injuries, as spinal cord injury is heterogeneous in the human population. Instead, injury models are used to address specific research questions, where it is important that the injury represents the specific clinical condition as closely as possible. The existing models do not encompass all clinical injury scenarios, and there is a need to further develop models. For example, more emphasis on modeling cervical spine injury and upper limb dysfunction is crucial, as it most commonly seen in human SCIs, and is currently under-represented (Filli & Schwab, 2012).

1.6.1 Contusion

Weight drop

The original preclinical spinal cord injury device was developed by Allen in 1911 as a weight drop impactor (Allen, 1911, 1914). The injury parameter was classified as a product of the weight in grams, and the drop height in centimeters, where the impact units are gram-centimeters. This method allowed for consistent injury input parameters between animals, in this case dogs.

The weight-drop model, adapted for use in rats, was implemented in the NYU impactor (Gruner, 1992). After laminectomy to expose the spinal cord, the device used a 10 g impactor dropped from a height of 6.25 – 75 mm above the surface of the cord, and accelerated by gravity to produce injuries ranging from mild to severe. The impactor was a cylindrical rod of 2.5 mm diameter with chamfered edges to avoid rupturing the dura mater. The NYU device supported the adjacent vertebrae to the injury level (T10) to minimize the amount of impact energy absorbed by the surrounding tissue and prevent movement of the animal (Gruner, 1992). The device monitors impact parameters to allow unexpected values to be discarded (Gruner, 1992). The impactor rebounds after impact, striking the cord a second time, but the height is generally less than 10% the original height with a reduced velocity. This second impact has been a concern within the field (Cheriyan et al., 2014), and should also be considered when comparing results between other contusion devices (Kwon et al., 2002). The NYU device was adopted by the Multicentre Animal Spinal Cord Injury Study (MASCIS) in 1993, and many of the conditions were standardized (Basso et al., 1996). However, in practice, different centres using the NYU impactor invariably deviated from the recommended conditions (anesthesia, rat strain, etc.) (Kwon et al., 2002).

When comparing results from a weight-drop model to other contusion devices, it is important to be aware of the biomechanical implications associated with the interaction between the kinetic energy of the impactor, the mass, and the velocity at impact (Kwon et al., 2002). Of note is the linear relationship between height and mass with kinetic energy ($E = mgh$), and the nonlinear relationship between height and velocity ($v^2 = 2gh$) (Kwon et al., 2002). The coupling between

mechanical injury variables make it challenging to investigate the independent influence of these factors on injury outcome.

Force controlled

The commercially available Infinite Horizon (IH) impactor (Precision Systems and Instrumentation, LLC, Fairfax Station, VA) produced contusion SCI in rodents (Scheff et al., 2003). The IH implemented a force-controlled approach using an external computer and a stepper motor to produce injury. The impactor velocity was 130 mm/s, and after reaching the predetermined force threshold, the tip was immediately withdrawn; however, inertial effects result in overshoot of desired force. The IH also had a position sensor, and calculated injury displacement based on characteristics of the force-time plot. One of the common limitations of the IH was that the forceps provided were often variable in how rigidly they hold the vertebrae stable during injury, potentially allowing the spine to slip during injury (Cheriyan et al., 2014). However, some researchers have developed custom clamps to hold the vertebrae during injury (Choo et al., 2009; Streijger et al., 2013). The IH produces consistent injuries with a significant correlation between locomotor performance and force applied to the spinal cord ($p < 0.001$) (Scheff et al., 2003).

The air gun impactor (Marcol et al., 2012) used a high-pressure stream of air to produce a contusion SCI in a rat model at a precise location on the spinal cord. A 2 mm hole was drilled in the lamina at the injury level, where an injector was inserted. It was positioned to touch the dura, before an ‘air shot’ was initiated. The air gun could produce a range of pressures from 10 to 500 kPa, and the exposure time could be adjusted from 0.1 seconds to 15 minutes (Marcol et al., 2012). The air gun model is limited in that the exact force and displacement imparted to the spinal cord are unknown, making it challenging to compare to other contusion devices without an explicit comparison study.

Displacement controlled

To independently control the amount of cord compression and the initial velocity of compression, a pneumatic stroke impactor was developed to induce SCI (Anderson, 1982). The

actuator used a constrained pneumatic cylinder, with an adjustable crosshead and interchangeable impact tip, and produced injury velocities from 1 to 6 m/s, with an accuracy of approximately 5% (Kearney et al., 1988). Stiff rubber stops within the pneumatic cylinder controlled the stroke length. Accuracy of locating the surface of the spinal cord or 'zero' point, was accurate within 0.1 mm, corresponding to variability of cord compression of approximately 5%.

The Ohio State University (OSU) impactor used a feedback-controlled impactor to produce displacement controlled spinal cord injuries. It was originally developed in 1987 (Bresnahan et al., 1987; Noyes, 1987; Somerson & Stokes, 1987), but refined in 1992 to improve repeatability (Stokes, 1992; Stokes et al., 1992). Imperative to displacement controlled devices is determining the surface of the spinal cord, or 'zero' point. The OSU device oscillated the impactor tip at 60 Hz at an amplitude of 30 μm, which was slowly lowered until contact with the spinal cord was detected by force signal. The device then impacted the cord to a predetermined displacement, at a peak velocity of 160 mm/s (Stokes et al., 1992), and held the cord compressed for ~ 5 ms before retracting. The device measured force and displacement.

The UBC Multi-mechanism SCI device was used to produce contusion injuries in a rat model (Chen et al., 2016A; Choo et al., 2007, 2009, 2008; Lam et al., 2014; Sjovold et al., 2013). The device consisted of an electromagnetic linear actuator (TestBench ELF LM-1, TA Instruments, New Castle, DE) with internal linear variable differential transformer (LVDT), with a nominal operating range of 12 mm, and dynamic positional accuracy within 30 μm (Figure 1-33). Force and acceleration transducers were coupled in series between the actuator and the specimen, where the accelerometer was used to compensate for intertial loads during the high-speed injury event, and data was sampled at 8 kHz. C4 and C5 were held stable using a custom vertebral clamp during injury to prevent the spine from displacing during impact, and the initial surface of the spinal cord, or the 0 mm datum was established prior to injury by a touch force of 0.03 N. Contusion injury was performed at C4/5 using a 2 mm spherical head actuator tip (Figure 1-34) to a depth of 1.1 mm (SD: 0.06) at a velocity of 96.7 cm/s (SD: 4.8) to produce a moderate-severe injury (Choo et al., 2007).

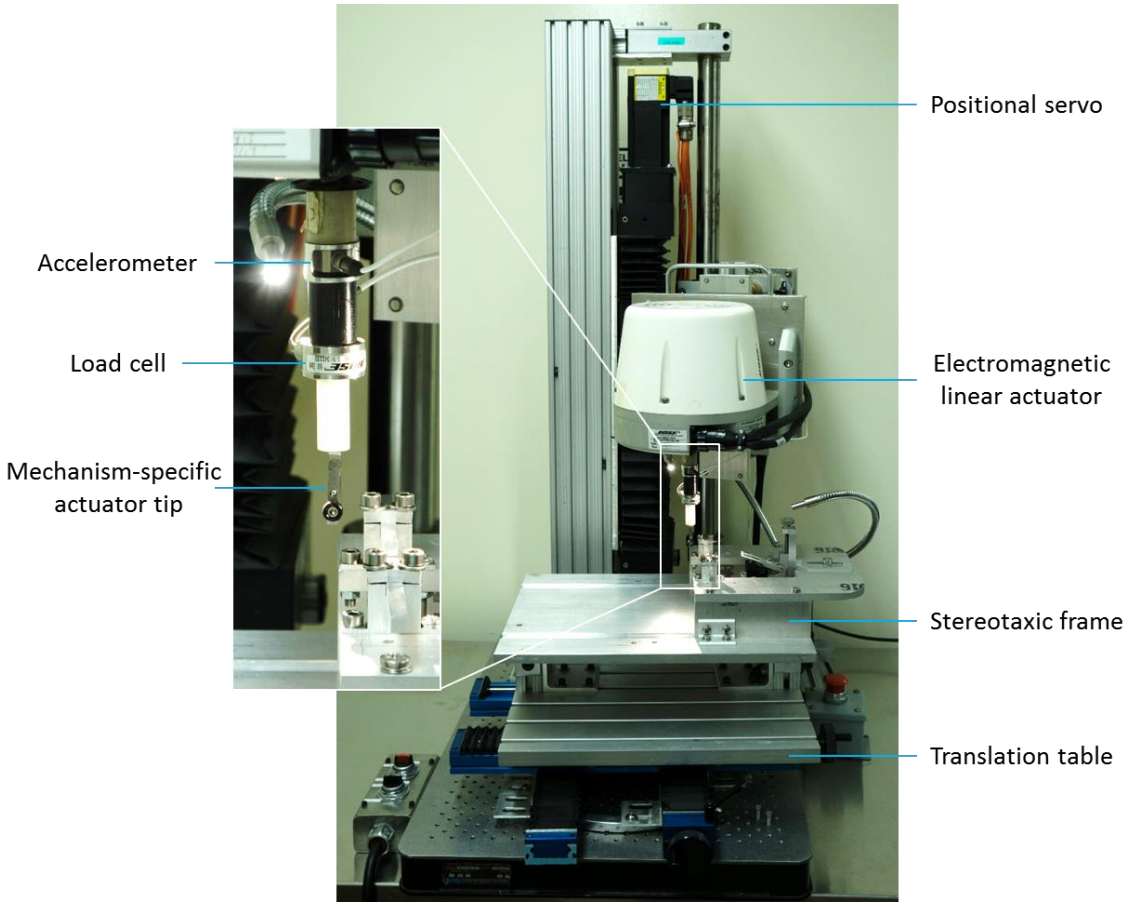

Figure 1-33 - UBC Multi-Mechanism SCI Device. The electromagnetic linear actuator was mounted to a positional servo, and the stereotaxic frame was mounted to a translation table. Displacement was measured by an LVDT within the electromagnetic actuator, and force and acceleration were measured via transducers mounted in series to the actuator. Transducers and actuator tip were interchangeable and injury mechanism specific.

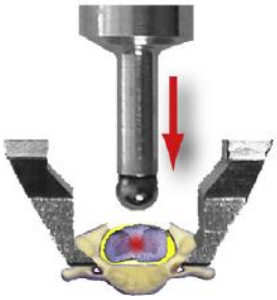

Figure 1-34 - UBC injury system contusion schematic. Vertebrae were secured using custom clamps, and injury was produced using a 2 mm spherical actuator tip. (Choo et al., 2009) (reprinted with copyright permission)

The Louisville Injury System Apparatus (LISA) used a pneumatically powered impactor to induce a contusion injury in a rat (Zhang et al., 2008). It used a laser system to measure the reflected beam from the surface of the spinal cord to detect distance to an accuracy of ± 0.005 mm. It measures the position to the target tissue, compression of the spinal cord, and impactor velocity. The impactor was accelerated using compressed air to a velocity of 0.5 – 2 m/s, and the spine was stabilized during impact using a custom spine stabilizer, which held the facets of T8, suspending the spine to prevent movements.

1.6.2 Residual Compression

Residual compression models are intended to replicate the sustained compression of the spinal cord that is often present following a spinal cord injury. One of the earlier residual compression models used a modified aneurysm clip to produce a prolonged SCI (Rivlin & Tator, 1978). Following laminectomy, the compression clip was closed around the spinal cord and left to compress the cord for a specified amount of time, where longer compression times generally resulted in more severe injury outcomes. The compression clips were designed with a range of closing forces to independently produce different levels of injury, for example 2.3, 16.9, or 53.0 grams (Guha et al., 1987). The clip compression model was advantageous in that it was relatively inexpensive, produced varying severity levels of SCI, and could be used in all regions of the spine (Cheriyan et al., 2014). However, since the only injury variables available were the closing force of the clip and the duration of clip compression, other important variables were unknown, such as velocity of the clip at contact, actual force imparted on the cord, the extent of cord compression (Cheriyan et al., 2014), or how comparable the delivery of force to the cord is compared to contusion models (Kwon et al., 2002). Similar models involved forceps with a spacer of specific width to produce graded injuries (Blight, 1991; Plemel et al., 2008), where the spacer limited the compression to a maximum displacement.

A balloon catheter device has been widely used as a method for applying residual compression to the spinal cord in a variety of animal models (Fukuda et al., 2005; Nesathurai et al., 2006; Tarlov et al., 1953; Vanický et al., 2001). A catheter was inserted into the spinal canal, usually caudal to the desired injury site, then when in place the balloon was filled with saline or air to a fixed

volume, compressing the spinal cord. The balloon model was more representative of chronic spinal cord injury conditions since it lacks the acute traumatic aspect.

Most studies have demonstrated that the neurological deficit is determined by the magnitude and duration of the compression (Carlson et al., 1997A, 2000, 2003; Delamarter et al., 1995; Dolan et al., 1980; Guha et al., 1987; Hashimoto & Fukuda, 1990; Tarlov & Klinger, 1954), and many have demonstrated improved outcomes with early decompression times (Carlson, et al., 1997A, 2003; Delamarter et al., 1995; Dimar et al., 1999; Dolan et al., 1980; Guha et al., 1987; Rabinowitz et al., 2008). However, the vast majority of studies addressing early decompression utilized slow compression devices such as aneurysm clips (Dolan et al., 1980; Guha et al., 1987), nylon cables (Delamarter et al., 1995; Rabinowitz et al., 2008), balloon catheters (Tarlov & Klinger, 1954), screws (Hashimoto & Fukuda, 1990) or slow mechanical pistons (Carlson et al., 1997A, 2000, 2003; Ouyang et al., 2009). The slow and precise application of pressure upon the spinal cord clearly does not reproduce the sudden, violent impact typically sustained by the spinal cord in the acute setting, which can immediately sever axons (Sparrey et al., 2008), potentially limiting the possibility of recovery. Many studies that implemented more diverse animal models have reported negative results with respect to early timing of decompression (Aki & Toya, 1984; Croft et al., 1972; Delamarter et al., 1991; Furlan et al., 2011), emphasizing the possibility that predisposing factors influence effectiveness of surgical timing. Additionally, only one study investigated residual compression in a cervical SCI model (C7/T1, Guha et al., 1987).

A high-speed contusion model was used to compare tissue damage from different magnitudes of residual compression (0%, 40%, 90%) (Sjovold et al., 2013). The actuator was held at a specified level of residual compression following the initial 700 mm/s impact. The degree of residual compression was important in the rostral-caudal extent of spinal cord tissue damage, most notably in the gray matter, where deeper residual compression resulted in further gray matter damage in the rostral and caudal directions. Of particular interest to the high velocity nature of the injury, the force under the impactor decreased dramatically to less than 10% of the peak force within 5-10 seconds of the initial impact (Figure 1-35) (Sjovold et al., 2013). This was counter to the force-time characteristics reported previously (Carlson et al., 2003), where the loading did not reduce to 10% until 3 hours after the initial impact. These findings suggest that the dynamic

nature of the injury event plays a considerable role in the response of the spinal cord during subsequent residual compression.

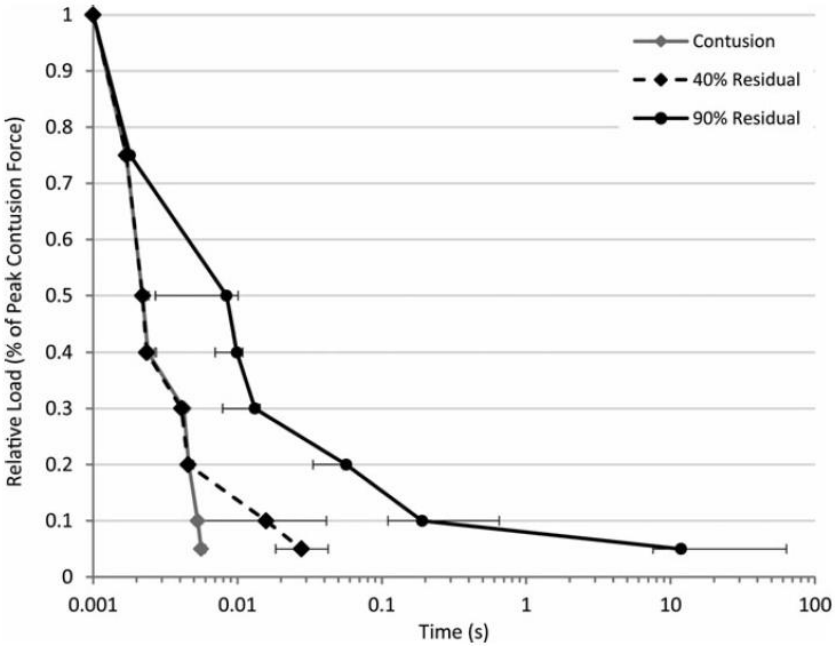

Figure 1-35 - Load relaxation following a contusion injury and residual compression on the spinal cord. Residual compression was held at 90% or 40% peak displacement, or with no residual compression. The graph shows the median times taken for the force on the spinal cord to relax as a percentage of peak force. For the 90% residual compression group, less than 10% of the peak force remains at ten seconds post impact. (reprinted with copyright permission) (Sjovold et al., 2013)

The most clinically relevant studies to evaluate the effects of timing of residual compression used a weight-drop technique to dynamically contuse the cords of rats before inserting variable sizes of spacers (Dimar et al., 1999; Shields et al., 2005). They reported that longer decompression times (> 24 hours) significantly reduced motor scores compared to early timing (< 6 hours). A major limitation of these studies was that there was a brief time interval after the initial impact where there was zero cord compression before the spacers were inserted. This may have allowed blood perfusion to the damaged tissue, and was not representative of clinical residual compression scenarios. Additionally, the original study inserted spacers adjacent to the injury epicentre; compressing the tissue that may not have been damaged by the initial impact (Dimar et al., 1999). Although the injuries were dynamic, these limitations prevent these studies from being completely representative of real-life injury scenarios.

1.6.3 Dislocation

To more closely replicate clinical SCI and the closed-column injury, a lateral dislocation model was developed by Fiford et al. (2004) (Figure 1-36). Injury was produced without the need to expose the spinal cord for impactor access, as all transfer of force was achieved through the interface between the vertebrae and the spinal cord, similar to human SCI. The device consisted of two adjustable clamps, attached to the lateral surfaces of the vertebrae, and rigidly attached to horizontal beams. The rostral clamp attached to T12, and the caudal clamp attached to L2, allowing L1 to move freely. The rostral beam was fixed to the base-plate, while the caudal beam translated laterally by a linear actuator and was monitored by a feedback controller to produce the specified speed and displacement. The device was capable of producing a lateral displacement of 1 to 20 mm, at a desired speed of 50 to 150 mm/sec. Injury displacements ranged from 3.2 to 7.5 mm, with peak loads ranging from 17 to 28 N, with greater displacement correlating with greater degree of injury. Axonal injury was found further from the injury epicentre, similar to human SCI, with the injury pattern consistent with regions of higher strain. The authors recognized further evaluation of the model is required to confirm repeatability, and that survival studies are required to fully characterize the model.

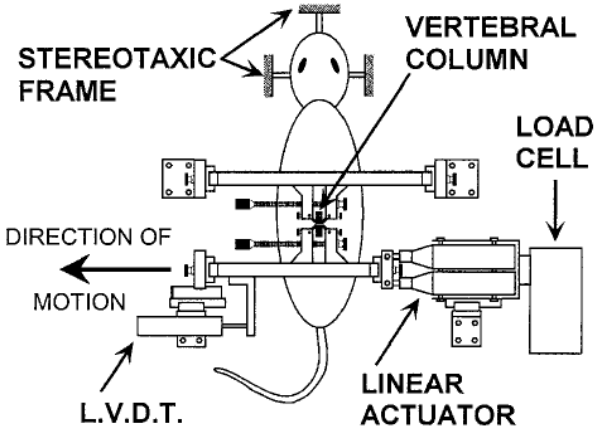

Figure 1-36 - Schematic of lateral dislocation device. (reprinted with copyright permission) (Fiford et al., 2004)

The lateral dislocation model has been used to investigate the contrasting neuropathology of spinal cord injury based on age in rats (Clarke & Bilston, 2008), helping to explain the greater initial severity of SCI in infants as axonal injury density was higher. The lateral dislocation was

also compared to an anterior dislocation, where anterior dislocations to the same displacement were more severe (Clarke et al., 2008). Between lateral and anterior loading directions, both had similar vertebral fracture and maximum loads, both demonstrated a 45 degree diagonal band of tissue damage corresponding to the direction of loading, and each had a different distribution of axonal damage. These findings illustrate the sensitivity of loading direction in the dislocation model, and the biomechanical importance of modeling spinal cord injury in the most clinically relevant manner.

Custom vertebral clamps (Figure 1-37A) were developed and characterized to produce dislocation injuries in conjunction with the UBC SCI device (Choo et al., 2009). The clamps were designed to wedge into a lateral groove that runs rostrocaudal along the rat spine between the lateral masses of the facet joints and the transverse processes. It was important for the vertebral clamps to be both stiff (minimal deflection caused by applied force) and have a high failure load (force required to cause slippage or fracture), as unintended movement in the vertebrae during the injury introduces errors into the intended compression of the spinal cord (Dohrmann et al., 1978). To evaluate the mechanical characteristics of the vertebral clamps, cadaveric rat cervical spine specimens (n = 6) were held securely as a load was applied to the lamina in the dorso-ventral direction (the weaker direction) (Choo et al., 2009). Force was applied until the vertebrae fractured or slipped from the clamps at a maximum load, defined as the failure load, which corresponded to the usable limit of the clamps. The stiffness was defined as the steepest region of the force-displacement curve. The failure load was 64.7 ± 10.2 N, and occurred with the fracture of the C4 lamina, and the stiffness was measured as 83.6 ± 18.9 N/mm. Deflections found at 2 N (0.03 ± 0.01 mm), 10 N (0.16 ± 0.05 mm), 20 N (0.30 ± 0.09 mm), and 30 N (0.48 ± 0.11 mm), were considered to be insignificant, and that the clamps held the vertebrae rigidly to produce vertebral column injuries without slippage or fracture. To attach the clamps, the spine was surgically exposed and a facetectomy was performed at C4/C5 to reduce the possibility of residual dislocation following injury. The rostral clamp held C3 and C4 stationary while the caudal clamp, coupled to the actuator, dislocated C5 and C6 dorsally 2.5 mm (SD: 0.16) at a velocity of 95.1 cm/s (SD: 9.5) (Choo et al., 2007).

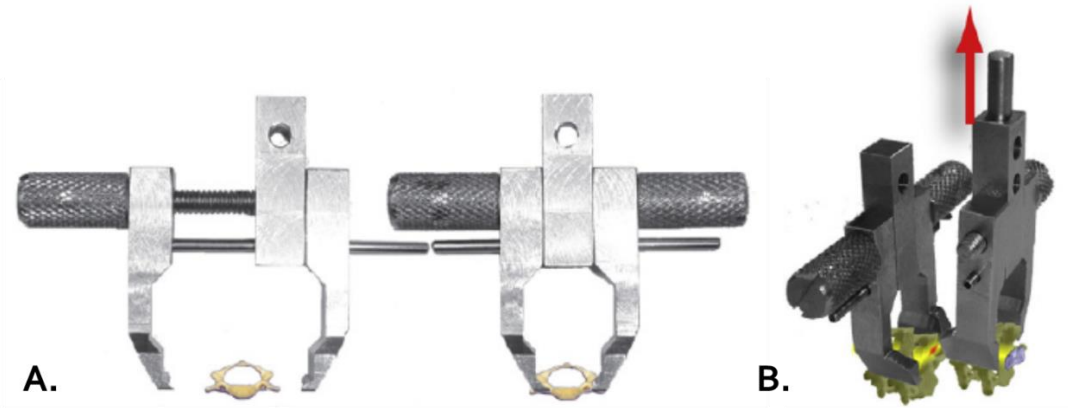

Figure 1-37 - A. Custom vertebral clamps for producing dislocation injuries. Clamps gripped adjacent vertebrae in a rostral-caudal groove between the transverse processes and facet joints. B. The rostral clamp was rigidly secured to the stereotaxic frame, while the caudal clamp was dislocated dorsally using the UBC injury system. (reprinted with copyright permission) (Choo et al., 2009)

1.6.4 Distraction

Distraction injuries involve the application of axial tensile forces to the spinal cord, and since they are closed-column models, require the force to be transferred via the vertebrae. During static axial loading, the coupling between the spine and spinal cord has been observed to be greatest during moderate loads (Maiman et al., 1989). The lesser coupling observed at low and high loading were attributed to initial slack in the spinal cord and neuronal disruption, respectively, suggesting that the threshold of neurologic injury is directly related to the end of the spinal cord's elastic range (Maiman et al., 1989). Additionally, in dynamic axial tensile loading, the level of peak strain in the spinal cord did not always occur at the level of column fracture (Kroeker & Ching, 2013). Thoracic distraction models in the rat used hooks placed under the lamina (Dabney et al., 2004) or custom surgical forceps secured between lateral processes (Bell et al., 2017; Seifert et al., 2011) to induce bidirectional distraction at low velocities (< 9 mm/s).

To produce distraction injuries, the UBC multi-mechanism injury device was mounted to a custom frame with seven degrees of freedom, allowing any desired orientation of the actuator relative to the position of the animal (Chen et al., 2016A; Choo et al., 2007, 2009, 2008). Distraction injuries were procedurally similar to dislocation, with the same custom vertebral clamps attached to the spine (Figure 1-38). The rat was positioned in the stereotaxic frame with

15° of flexion at C4/C5, and the actuator was rotated 90° to pull the C5/C6 clamp caudally by 4.1 mm (SD: 0.01) at a velocity of 91.9 cm/s (SD: 2.9) (Choo et al., 2007).

Figure 1-38 - A distraction injury produced by the UBC multi-mechanism injury device, where the rostral vertebral clamp was rigidly secured at 15 degrees flexion, and the caudal vertebral clamp was distracted caudally. (reprinted with copyright permission) (Choo et al., 2009)

1.6.5 SCI Model Summary

A summary of the previously described SCI models is presented in Table 1-9. Weight-drop and force controlled contusion models are the most widely used, and typically produce reproducible injuries. Weight-drop devices are limited in that force and displacement are coupled with velocity, limiting the ability to determine the independent influence of these important variables. Force controlled devices are limited by sensor feedback, where velocity must be restricted to prevent force overshoot – an impactor travelling at high speeds typically requires more distance to stop after reaching a target force. Displacement controlled contusion devices allow for precise and independent control of both displacement and velocity to evaluate the independent effects. However, such wide adjustment possibilities of these variables can lead to different complex injury mechanics making comparisons within the field difficult. Displacement controlled devices also require rigid stabilization of the spine to prevent potential vertebral movement during impact. Pneumatic impactors have the potential for reaching high velocities, but are often unable to measure exact spinal cord injury parameters (such as force), without additional complex measurement techniques. Residual compression models such as the clip compression, balloon catheters and nylon straps allow for consistent compression of the spinal cord over time, but each model differs by means of compression, such as constant force or displacement or direction.

Additionally, these compression models lack the initial traumatic aspect responsible for the primary injury, as occurs in most clinical SCI scenarios. Closed-column dislocation and distraction models are advantageous as they more closely replicate clinical injuries, however they require complex procedures, the exact injury parameters experienced by the spinal cord (i.e. injury depth and force) are unknown, and they require validation to ensure consistent vertebral kinematics.

Table 1-9 - Summary of SCI models.

Model		Mechanism	Animal	Velocity	Strengths	Weaknesses
Weight drop / NYU impactor	Allen 1911, Gruner et al. 1992	Weight-drop contusion	Rodents	0.3 – 0.9 m/s	Widely used, reproducible injury	Weight bounce, coupled velocity and displacement
Infinite Horizons	Scheff et al. 2003	Force controlled contusion	Rodents	130 mm/s	Widely used, reproducible injury, commercially available	Vertebral forceps not rigid, Injury displacement calculation not validated
Air gun impactor	Marcol et al. 2012	Air pressure contusion	Rats	Unknown	Minimally invasive	Unknown displacements or velocities, injury severities not validated
Pneumatic stroke impactor	Anderson 1982	Displacement controlled contusion	Ferrets	1 – 6 m/s	Independent control of velocity and displacement	No force measurement
OSU impactor	Noyes 1987	Displacement controlled contusion	Rodents	Up to 160 mm/s	Widely used, reproducible injury	
UBC multi-mechanism device	Choo et al. 2007	Displacement controlled contusion, dislocation, distraction	Rats	Up to ~1 m/s	Produces multiple clinically relevant injury mechanisms, independent control of velocity and displacement	Injury severities not validated, complex procedure
LISA impactor	Zhang et al. 2008	Displacement controlled contusion	Rodents	0.5 – 2 m/s	Independent control of velocity and displacement, precise parameters	
Clip compression	Rivlin & Tator 1978	Compression	Rodents	N/A	Widely used, reproducible injury, simple procedure, inexpensive	Velocity and compression magnitude not recorded
Balloon catheter	Tarlov et al. 1953	Compression	Dogs, rats, monkeys	N/A	Inexpensive	Injury parameters not recorded, inconsistent
Lateral dislocation	Fiford et al. 2004	Dislocation	Rats	50 – 150 mm/s	Clinically relevant injury mechanism	Injury reproducibility not validated, complex procedure
Harrington distractor	Dabney et al. 2004	Bi-directional distraction	Rats	Up to 9 mm/s	Clinically relevant injury mechanism	complex procedure, kinematic motion not validated
UTA distractor	Seifert et al. 2011	Bi-directional distraction	Rats	1 mm/s	Clinically relevant injury mechanism	complex procedure, kinematic motion not validated

1.6.6 Effects of Impact Velocity and Energy

All tissues of the spine, including the spinal cord, are viscoelastic, which means that they exhibit time-dependent behaviour under loading. Gray matter is more vascularized, with dense dendritic connections between neurons, while white matter is structurally anisotropic due to the axial alignment of myelinated axons (Bilston, 2016). The stress-strain sensitivity in neural tissue likely reflects both interstitial fluid flow within the tissue, and inherent viscoelasticity in the nerve fibres and other constituents (Cheng et al., 2008). Studies investigating the viscoelastic properties have reported that increased strain rate typically results in an increased modulus of the non-linear stress-strain response (Bilston & Thibault, 1996; Clarke et al., 2009; Fiford & Bilston, 2005; Oakland et al., 2006). Spinal cord tissue exhibits significant stress relaxation, to different degrees dependent on applied strain and strain rate (Clarke et al., 2009; Fiford & Bilston, 2005; Oakland et al., 2006; Tunturi, 1980). There are wide variations in results between studies, due to the methodological differences, such as: species, in vivo vs. ex vivo tissue, strain magnitude, strain rate, hydration, and preconditioning. The sensitivity of the mechanical behaviour of spinal cord tissue to loading conditions highlights the importance of animal injury models replicating clinical injury scenarios as closely as possible, with respect to impact velocity and method of residual compression.

Several studies have demonstrated that SCI severity is sensitive to impact velocity (Kearney et al., 1988; Lam et al., 2014; Maikos & Shreiber, 2007; Sparrey et al., 2008). There are also interaction effects between impact velocity and depth in contusion models in that injury outcome is primarily dependent upon displacement at low velocities (Kearney et al., 1988), and similarly injury velocity has been shown to only affect outcome beyond an impact depth threshold (Lam et al., 2014). Conversely, speed of injury has been reported to not have a significant effect on spinal cord damage in both contusion (Kim et al., 2009) and dislocation models (Lau 2013); however, this may be due to the smaller range of velocities (contusion: 100 – 400 mm/s, dislocation: 100 – 250 mm/s) compared to those studies that reported velocity effects [1.5 – 6 m/s (Kearney et al., 1988), 3 – 300 mm/s (Sparrey et al., 2008), 8 – 800 mm/s (Lam et al., 2014)]. The lack of observed differences between velocities at lower magnitudes also supports a threshold effect based on the relationship between injury displacement and velocity, such as the viscous response (product of displacement and velocity) proposed by Kearney et al. (1988).

The velocity effects have been speculated to be a result of increased energy imparted to the spinal cord (Gerber & Corrie, 1979; Kearney et al., 1988), in that the quantity of injured spinal cord tissue is proportional to the energy transmitted to the spinal cord (Gerber & Corrie, 1979). This assumption however is dependent on the definition of injury. Spinal cord tissue could potentially be damaged to the point of complete loss of cellular function, and still structurally continue to absorb energy. Conversely, energy could be dissipated throughout the spinal cord, but tissue deformation never reaches an injurious threshold. Although not significant, trends have been observed where impacts of similar energy had different outcomes, suggesting that injury is more closely related to viscoelastic effects and tissue strain (Lam et al., 2014).

1.6.7 Effects of Injury Mechanism

Contusion, dislocation, and distraction injuries have demonstrated distinct differences in patterns of tissue damage and behavioural functional outcomes (Chen et al., 2016A; Choo et al., 2007, 2009, 2008). At acute time points, contusion caused localized increases in membrane permeability, compared to dislocation and distraction, which were asymmetrical with damage extending further rostrally. Hemorrhage was similar between contusion and dislocation, with no hemorrhage following distraction. Relative to contusion, dislocation accelerated neurofilament degeneration, produced a wider zone of axonal degeneration, and extended the rostro-caudal area of microglial and astrocyte activation. In contrast, the distraction injury exhibited only modest secondary pathological changes at 3 hours post-injury, suggesting that a broader therapeutic time-window may exist following this type of SCI. A finite element approach was also used in conjunction with the experimental data to identify correlations between principal strain and tissue damage for the contusion ($R^2 = 0.86$) and dislocation ($R^2 = 0.52$) mechanisms (Russell et al., 2012). At 8 weeks post-injury, contusion caused the greatest loss of myelinated axons in the dorsal white matter (Chen et al., 2016A). Dislocation resulted in the greatest overall loss of white matter, in both the rostrocaudal and lateral directions, and greatest neuronal cell loss in the gray matter horns. Distraction spared the most myelinated axons, but caused enlarged extracellular spaces and alterations in the white matter – contrary to the mild injuries observed at early time points. Behaviourally, the distraction injury was the only group to not recover grip strength over time, and the dislocation injury was the only group to not recover grooming ability. One

limitation of the dislocation injury model, is the large variability in outcomes compared to the precise injury parameters (Figure 1-39): 1.84 ± 0.02 mm displacement, 870 ± 11 mm/s velocity, and 18.0 ± 1.9 N maximum force (Chen et al., 2016A). The distinct patterns of tissue damage and behavioural recovery associated with the different injury mechanisms is relevant to the heterogeneity observed in the human SCI population. Of note from these injuries was the variability of behavioural outcomes following the dislocation injury despite consistent input parameters. The closed column nature of this model relies upon the relative movement of the vertebrae to injure the spinal cord, potentially introducing extra factors which influence the relationship between the displacement input parameter and compression of the spinal cord (such as slipping at the vertebra-clamp interface). Potential therapeutic interventions should be evaluated across multiple injury mechanisms, as the distinct pathologies likely require specific treatments.

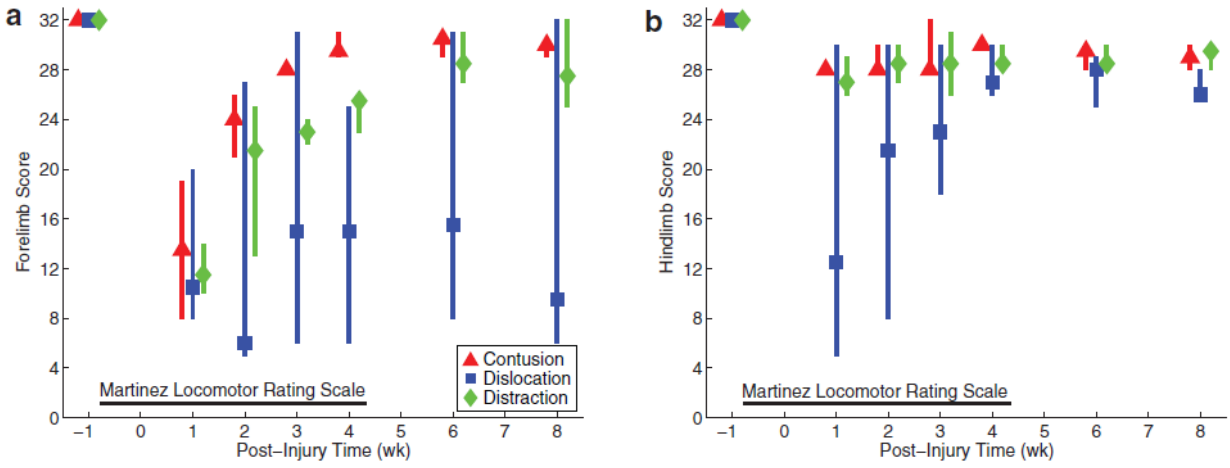

Figure 1-39 - Martinez locomotor rating scale for forelimb (a) and hindlimb (b). Data are presented as medians with quartiles and offset horizontally for clarity. In some instances the dislocation injuries demonstrate a range from severe motor deficits to almost uninjured. (reprinted with copyright permission) (Chen et al., 2016A).

A recent comparison between two different injury models with respect to treatment efficacy reported a difference based on injury mechanism (Geremia et al., 2017). The treatment, a CD11d monoclonal antibody, was compared between a clip compression SCI and a hemi-contusion, both cervical, and only the clip compression group demonstrated recovery. To determine if the

differences were due to the difference in mechanism or spinal level, the experiment was repeated at the T12 spinal level where the results were the same: the T12 clip compression demonstrated improved recovery, while the T12 contusion did not. The authors hypothesized the increased hemorrhaging due to contusion may play a role in the differences, as the treatment specifically targets the interaction between activated white blood cells and the intact vascular endothelium to reduce neutrophil and monocyte invasion. These results are of particular importance as they are the first to directly investigate the effect of injury mechanism on a treatment, and to find significant differences, emphasizing the importance of the distinct pathophysiological mechanisms to both injury and treatment processes.

1.7 Thesis Objectives

Traumatic spinal cord injuries occur in a heterogeneous fashion, including at different spinal levels, injury velocities, and injury mechanisms. Injuries typically occur at the cervical level due to high-velocity events, such as motor vehicle accidents, and the most common injury mechanism is dislocation. One of the few treatment options available following SCI is surgical decompression to remove residual compression on the spinal cord. However, the timing of performing the decompression is controversial. Clinical study results do not match preclinical experimental evidence, which demonstrates the beneficial neurological outcome of early decompression. The lack of agreement between preclinical and clinical results may be attributed to the heterogeneity in the human population in that some of the most common clinical SCI factors, such as injury mechanism and velocity, are often not represented in preclinical animal models. Recent studies have demonstrated the importance of injury mechanism, emphasizing the need for preclinical models to represent the clinical scenario as closely as possible.

The overall objective of this thesis was to investigate the biomechanics of a high-speed cervical dislocation rat SCI model at acute stages, refine the model, and incorporate residual compression. This was achieved through the following chapter-specific objectives:

2.1 Evaluate the temporal progression of injury at specific tracts within the white matter, for acute time points of 3 hours, 24 hours, and 7 days, for three distinct injury mechanisms, contusion, dislocation, and distraction;

3.1 Design new vertebral injury clamps to reduce relative motion between the clamps and vertebrae;

3.2 Precisely measure clamp and vertebral kinematics during a high-speed dislocation injury in an in-vivo rat model using the existing and redesigned clamps;

3.3 Quantify slippage (i.e. relative motion) at the vertebra-clamp interface to determine which clamps provide the most rigid connection;

4.1 Determine the minimum residual compression depth that affects spinal cord signal conduction following traumatic dislocation SCI;

4.2 Determine the acute effect on spinal cord signal conduction following dislocation SCI, with and without immediate residual compression;

4.3 Determine if 4 hours of residual compression following a dislocation injury is survivable;

4.4 Establish the behavioural outcome sensitivity to different dislocation depths using validated injury clamps; and

4.5 Determine the relationship between rat weight at time of injury and spinal canal geometry to better inform closed-column injury models.

This research will help to better understand the biomechanics of spinal cord injury. The process will provide critical details for the systematic development and validation of clinically relevant SCI models, and progress towards a more repeatable dislocation injury model. Refinement of the dislocation model, which closely represents the most common and severe clinical SCI mechanism, will provide robust avenues for evaluating treatments, and further biomechanical understanding of neural tissue response and injury as a result of mechanical loading.

Chapter 2: Temporal Progression of Acute Spinal Cord Injury Mechanisms in a Rat Model: Contusion, Dislocation, and Distraction

2.1 Introduction

Traumatic spinal cord injury (SCI) causes severe neurological dysfunction, such as motor and sensory deficits, and sometimes including chronic pain. Few treatment options are currently available (Ahuja et al., 2017; Hagg & Oudega, 2006). SCIs are heterogeneous in terms of the spinal level at which they occur, the cause of the injury, and the anatomical damage to the spinal column. Of particular interest is the trauma to the spine, which occurs as specific injury patterns, such as burst fracture, flexion-distraction, and most commonly, dislocation (Sekhon & Fehlings, 2001; Tator, 1983; Tator et al., 1987; Vaccaro et al., 2016; Wilson et al., 2013). These injury patterns result in different insults to the spinal cord, termed injury mechanisms. During a vertebral burst fracture, fragments from the vertebral body can occlude into the spinal canal producing a contusion type injury, subjecting the spinal cord to compressive stresses in the transverse plane. A flexion-distraction injury occurs when the vertebrae separate axially, inducing distractive tensile forces on the spinal cord. A dislocation injury involves the relative transverse displacement of adjacent vertebrae and narrowing of the spinal canal, effectively imparting a combination of shear, tensile and compressive stresses on the spinal cord.

These injury mechanisms have demonstrated different histological patterns of injury at acute and chronic time points (Chen et al., 2016A; Choo et al., 2007, 2008). Choo et al. (2007) showed that differences in primary damage were observed at 5 minutes post injury. Contusion injuries produced focal lesions, with localized increased membrane permeability around the epicentre. In contrast, dislocation injuries produced lesions that extended further rostrocaudally, with increased axonal damage in the lateral columns, and hemorrhaging similar to contusion. Distraction injuries produced diffuse damage that extended rostrocaudally, with little observed hemorrhaging. At 3 hours post injury, dislocation injuries exhibited accelerated neurofilament degeneration (dephosphorylation), produced a wider zone of axonal degeneration (amyloid precursor protein accumulation), and extended the rostrocaudal area of microglial and astrocyte activation, relative to contusion injuries. Distraction injuries had modest secondary pathological changes (Choo et al., 2008). A longer term survival study found that at 8 weeks post injury,

distraction injuries resulted in the most extensive lesion cavity and structural alteration in white matter (WM) with widening of extracellular spaces, while sparing the most myelinated axons overall (Chen et al., 2016A). In that study, dislocation caused the greatest overall loss of WM tissue, especially in the lateral columns, and neuronal cell death in both ventral and dorsal horns. Contusion injuries caused the most severe loss of myelinated axons in the dorsal WM (Chen et al., 2016A). Additionally, the different injury mechanisms induce distinct strain patterns in specific regions of the spinal cord (Bhatnagar, et al., 2016A), which have been shown to correlate with histological damage (Bhatnagar, et al., 2016B; Russell et al., 2012).

This temporal progression of tissue damage following the initial insult to the cord has been investigated in contusion and clip compression injuries in a rat model. These studies have demonstrated the rostral and caudal progression of the lesion over time (Andrade et al., 2008; Crowe et al., 1997; Grossman et al., 2001; Ling et al., 2013; Ling & Liu, 2007; Ward et al., 2014), different rates of progression of necrosis and apoptosis within neural and glial cells (Crowe et al., 1997; Grossman et al., 2001; Ling et al., 2013; Ling & Liu, 2007), and the acute inflammatory response (Carlson et al., 1998; Ward et al., 2014). These findings have led to further understanding of the progression of secondary pathologies and potential targets for pharmacological interventions and therapeutic windows following contusion injuries (Andrade et al., 2008; Carlson et al., 1998; Ling et al., 2013; Ling & Liu, 2007; Shuman et al., 1997). However, different progressions of tissue damage and glial reactivity have been observed to be severity dependent in contusion injuries (Andrade et al., 2008). Therefore, the localized damage due to different injury mechanisms may induce secondary pathology responses that progress at different rates in specific regions of the spinal cord. Quantifying the loss and demyelination of axons, which occurs at the acute phases of primary injury (Casha et al., 2001; Donnelly & Popovich, 2008), can allow for regional comparisons of the progression of damage within the WM. Therefore, the objective of this study was to evaluate the temporal progression of injury at specific tracts within the WM, for acute time points of 3 hours, 24 hours, and 7 days, for three distinct injury mechanisms, contusion, dislocation, and distraction. Different rates of injury progression at specific regions of the spinal cord may provide insight towards the pathologies that are initiated by specific primary injury mechanisms.

2.2 Methods

All procedures were approved by the Animal Care Committee of the University of British Columbia in accordance with the guidelines published by the Canadian Council on Animal Care. Eighty-four male Sprague-Dawley rats were used for the experiment with an average weight of 311 g (SD: 14 g) at the time of surgery. Animals were anesthetized with inhalational isoflurane (1.5 – 3% / L O_2), and their backs were shaved and disinfected. Marcaine (0.25%, 0.3 mL) was injected subcutaneously at the incision site to relieve pain, and buprenorphine (0.05 mg/kg in 0.3 mL PBS) and Ringer's lactate solution was injected under the back skin to also provide fluid. Lacrilube ophthalmic ointment was applied to the eyes to prevent drying. Animals were kept warm between 36 – 37 °C on a heating pad, while temperature, heart rate and blood oxygenation were monitored throughout surgery and injury procedures. The spine was surgically exposed dorsally from C3 to T1 along the midline, and the musculature removed from the posterior processes of the vertebrae. Moderate contusion (n = 25), dislocation (n = 28), and distraction (n = 28) injuries were produced at C5/C6, using the UBC multi-mechanism SCI device (Chen et al., 2016A; Choo et al., 2007, 2009, 2008).

For contusion injury preparation, a partial laminectomy was performed on both C5 and C6 to expose the dura mater covering the spinal cord. Care was taken to not injure the dura mater. A custom vertebral clamp was attached to the spinal column beneath the transverse processes and rigidly connected to a stereotaxic frame to secure the spine during injury (Figure 2-1A). The 2-mm spherical injury tip was lowered towards the spinal cord to contact the surface of the dura mater, stopping at a position defined by a small measured force (0.03 N), relative to the expected injury load (~2 N, Choo et al., 2007). To produce the injury, the actuator tip was retracted from the spinal cord/dura mater, then was accelerated towards the spinal cord, and progressed to a maximum depth of 1.30 mm (SD: 0.01 mm) at a maximum velocity of 724 mm/s (SD: 9 mm/s), then immediately retracted to a non-contact position.

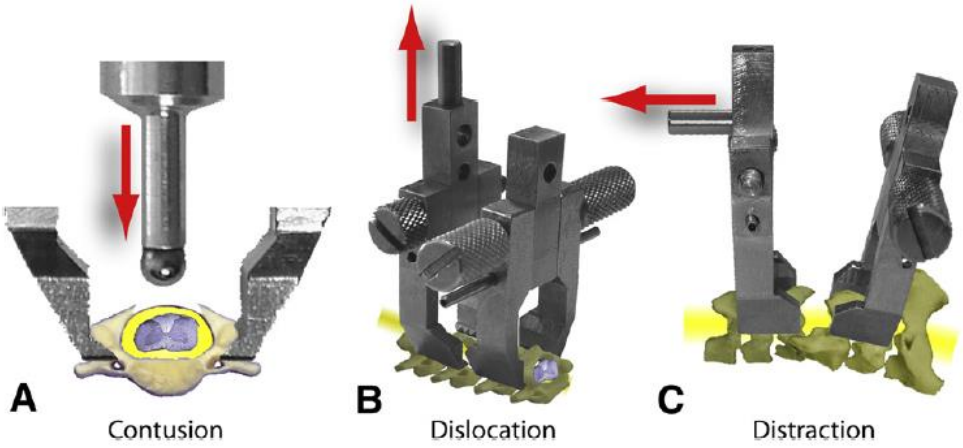

Figure 2-1 - Schematic diagrams of the three cervical SCI mechanisms produced. A. Contusion was produced by holding the vertebrae secure, and striking the spinal cord with a 2 mm diameter spherical impactor through a laminectomy between C5 and C6. B. Dislocation was produced by holding C4 and C5 rigid, and dislocating C5 and C6 dorsally using custom injury clamps. C. Distraction was produced by holding C4 and C5 rigid, and translating C5 and C6 caudally using the same custom injury clamps as for dislocation. (reprinted with permission) (Choo et al., 2008)

For dislocation and distraction injury preparation, a facetectomy was performed at the C5/C6 spinal level. Custom vertebral injury clamps (Choo et al., 2009) were attached to the C4/C5 and C6/C7 vertebrae, the rostral clamp was rigidly secured to a customized stereotaxic frame, and the caudal clamp attached to the actuator. An initial tensile preload of 2 N was applied to the spine in both cases. For dislocation, the actuator dynamically translated the caudal clamp (C6/C7) 1.77 mm (SD: 0.07 mm) dorsally at a maximum velocity of 824 mm/s (SD: 27 mm/s) (Figure 2-1B). For distraction, the rostral clamps were oriented at 15° flexion (Choo et al., 2007), and the caudal clamp (C6/C7) was translated 4.37 mm (SD: 0.14 mm) at a maximum velocity of 1039 mm/s (SD: 40 mm/s) (Figure 2-1C). Sham animals underwent the same procedure for a dislocation, but no dislocation injury was induced following the preload.

The injury parameters were initially based on a previous study (Chen et al., 2016A), and pilot tests were performed to determine similar functional deficits between mechanisms (i.e. flexed paws, paralysis) to approximate similar injury severities between mechanisms. It is challenging to compare equivalent severities between mechanisms, but this was not a focus since the objective of this study was to compare the progression of injury within each mechanism.

Post-injury, a custom vertebral clamp was used to stabilize the spine following the closed-column dislocation and distraction injuries (Shahrokni et al., 2012). Musculature and skin was sutured, and animals were placed in an incubator (37 °C) until consciousness was fully regained. Animals were housed singly for three days post injury, with access to regular food, sugared cereal, water and hydrogel if needed. Three doses of buprenorphine (0.05 mg/kg) and Ringer's lactate (10 mL) were given subcutaneously for three days post injury, and Ringer's lactate was continued if animals exhibited signs of dehydration.

One distraction-, and two contusion-injured animals perished immediately following injury. Two dislocation-injurued animals perished within 24 hours post-injury. Four dislocation-injured animals reached humane end-point prior to the 7-day post injury time point, demonstrating severe weight loss, respiratory issues, and/or porphyrin. Additionally, five dislocation-injured animals had a broken lamina following the injury, and the injury clamp slipped from one animal during a distraction injury. These animals were sacrificed, and not included in the reported data (Table 2-1).

2.2.1 Histological Analysis

Animals were euthanized at predetermined time points (3 hours, 24 hours, or 7 days) post-injury by an overdose of 5% chloral hydrate (intraperitoneal injection), and perfused with fixative solution (4% paraformaldehyde in phosphate buffered saline 0.1 M). Spinal cords were harvested and post-fixed for 24 hours in fixative solution. Spinal cords were submerged in sucrose solutions with increasing concentrations (12%, 18%, 24%) every 24 hours, then frozen on dry ice while immersed in cutting compound (OCT). Cords were cut in the transverse plane on a cryostat at a thickness of 20 µm. Sections at the epicentre and ± 1, 3, and 5 mm from the epicentre were used for all analyses.

One set of sections was stained with eriochrome cyanine (EC) for myelin / white matter sparing analysis. Sections were imaged under a light microscope (Axioplan 2, Carl Zeiss, Jena, Germany) (2.5 x), and images were blinded and manually thresholded for spared WM (Figure 2-2) (SigmaScan Pro 5, Systat Software Inc., Chicago, IL).

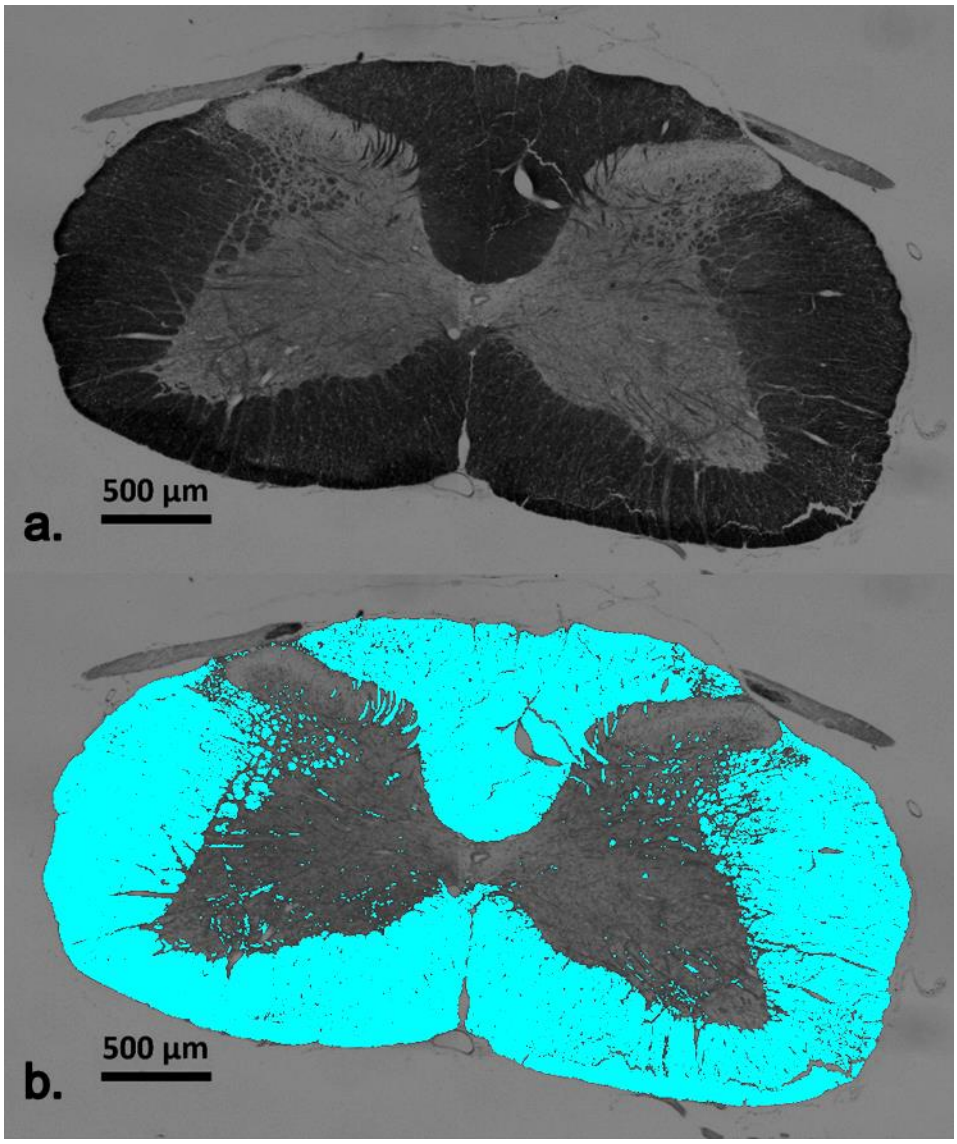

Figure 2-2 - a. Eriochrome cyanine stained spinal cord section from an uninjured sham animal. b. Thresholded area of white matter.

For immunofluorescence, one set was washed in 0.01 M phosphate buffered saline (PBS) for 10 minutes, before being delipidized by dehydrating in an ascending series of ethanol concentrations (EtOH, 50%, 70%, 90%, 95%, 100%), followed by rehydration in a descending series of ethanol concentrations. Sections were blocked for 30 minutes in normal donkey serum (1:10, Jackson ImmunoResearch Laboratories, West Grove, PA) before incubation overnight at room temperature in primary antibodies diluted in 0.01 M PBS with 0.1% Triton X-100. Primary antibodies were used to target myelin basic protein (MBP) (chicken host, 1:200, Aves Labs,

Tigard, OR), Neurofilament-H (NF-H) (mouse host, 1:500, Abcam, Toronto, ON), β-tubulin III (Tub) (mouse host, 1:500, Abcam, Toronto, ON), and SMI-312 (SMI) (mouse host, 1:500, Covance, Princeton, NJ). Sections were then washed 3 x 5 minutes in 0.01 M PBS and incubated for 2 hours in secondary antibodies conjugated with DyLight 488 (donkey host, chicken antigen, Jackson ImmunoResearch Laboratories, West Grove, PA) and DyLight 594 (donkey host, mouse antigen, Jackson ImmunoResearch Laboratories, West Grove, PA). Sections were washed 3 x 5 minutes in 0.01 M PBS then mounted with Fluoromount-G (SouthernBiotech, Birmingham, AL). Each set of sections was stained at the same time and under the same conditions to avoid procedural variation. Sections were imaged under a fluorescence microscope (Axio Observer Z1 inverted confocal, Carl Zeiss). Brightness and contrast were kept constant for all images within each set of sections.

For analysis of the immunofluorescence images, regions of interest (57.25 µm x 57.25 µm, 3278 μm^2) were manually placed at the following locations: gracile fasciculus (G, placed 50 µm from midline, small axons), cuneate fasciculus (C, placed 50 µm from gray matter dorsal horn and dorsal corticospinal tract, very large axons), dorsal corticospinal tract (CST, placed 50 µm from gray matter, very small axons), dorsolateral WM (D, placed 50 µm from gray matter dorsal horn), lateral WM (L, placed lateral to the gray matter, at the dorsoventral midline), and ventrolateral WM (V, placed midway between the lateral gray matter ventral horn and spinal cord surface, avoiding ventral nerve root axons) (Figure 2-3). The position of the boxes was adjusted to avoid artifacts, while still remaining in the same tract. Within each region of interest, the total number of axons was counted, and the total number of myelinated axons was counted.

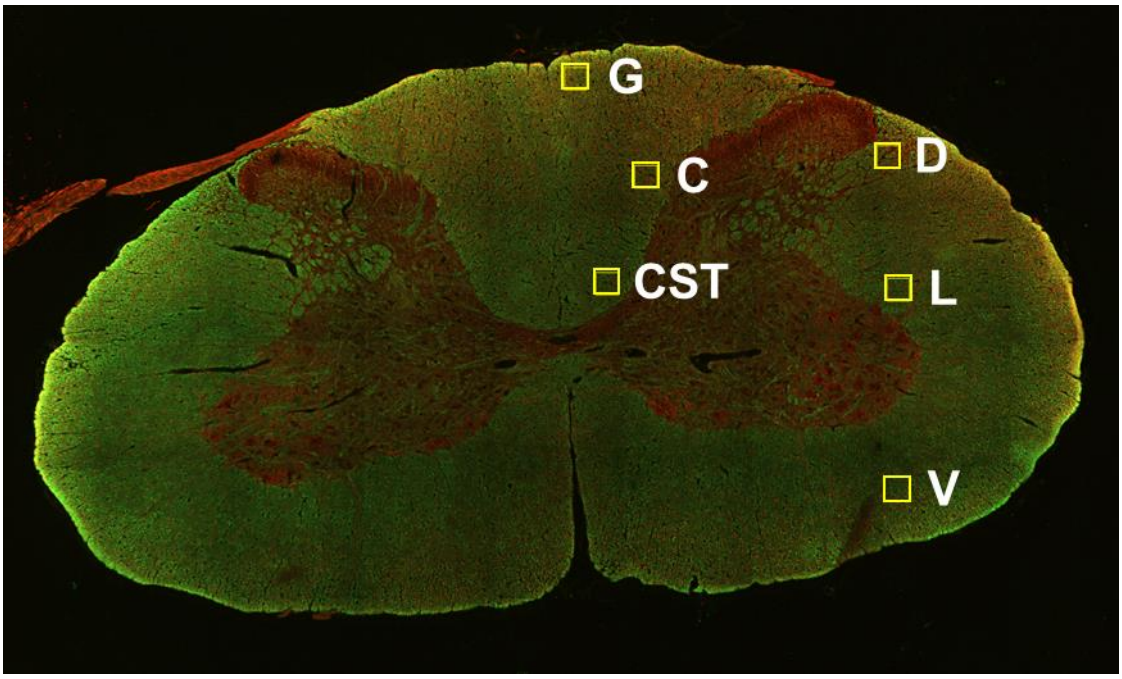

Figure 2-3 - Locations of regions of interest for counting axons and myelinated axons in an uninjured spinal cord section. G: Gracile fasciculus – placed 50 µm from midline, small axons. C: Cuneate fasciculus – placed 50 µm from gray matter dorsal horn and dorsal corticospinal tract, very large axons. CST: Dorsal corticospinal Tract – placed 50 µm from gray matter, very small axons. D: Dorsolateral white matter – placed 50 µm from gray matter dorsal horn. L: Lateral white matter – placed lateral to the gray matter, at the dorsoventral midline. V: Ventrolateral white matter: placed midway between the lateral gray matter ventral horn and spinal cord surface, avoiding ventral nerve root axons.

2.2.2 Statistical Analyses

To analyse the progression of injury within each injury mechanism, a two-way mixed ANOVA was used to compare the injury time points (i.e. 3 hours, 24 hours, 7 days and sham) at each rostrocaudal spinal location (i.e. epicentre, ± 1, 3, 5 mm). Injury sub-groups (i.e. specific mechanism, time point and rostrocaudal location) were tested for normality using the Shapiro-Wilk test (Graphpad Prism, GraphPad Software, Inc., La Jolla, CA). The vast majority (86%) of the injury sub-groups were normally distributed, and ANOVA is considered to be fairly robust to deviations from normality (Feir-walsh & Toothaker, 1974; Norman, 2010; Schmider et al., 2010). Specific differences between time points were evaluated at rostrocaudal spinal locations using Tukey's test to correct for multiple comparisons, and adjusted P-values are reported.

2.3 Results

2.3.1 Injury Parameters

Injury parameters from each of the nine injury groups are reported in Table 2-1. All injuries were displacement controlled, and the same input parameters were used for each injury of the same injury mechanism. The maximum impact force on the spinal cord is reported for contusion, where the maximum forces for dislocation and distraction relate to the failure of the connecting soft tissues of the spinal column (i.e. intervertebral disc and ligaments). Similarly, maximum displacement is reported for cord compression in contusion, and vertebral displacement for dislocation and distraction. The entire injury event was approximately 10 ms in each injury case, and typical injury-time curves are shown in Figure 2-4. There were no significant differences between time point groups for any of the injury parameters within each injury mechanism ($p > 0.05$).

Table 2-1 - Injury parameters for each injury group. Values are reported as means (SD).

Injury	Time point	n	Weight (g)	Maximum Displacement (mm)	Maximum Force (N)	Maximum Velocity (mm/s)
Contusion	3 hr	9	313 (17)	1.30 (0.01)	1.75 (0.35)	729 (8)
	24 hr	8	316 (28)	1.29 (0.01)	2.05 (0.30)	713 (7)
	7 day	8	301 (8)	1.30 (0.00)	1.86 (0.11)	727 (6)
Dislocation	3 hr	8	304 (10)	1.74 (0.02)	24.1 (3.7)	806 (14)
	24 hr	9	311 (8)	1.78 (0.04)	25.2 (4.5)	832 (17)
	7 day	11	313 (10)	1.77 (0.05)	26.2 (4.2)	830 (36)
Distraction	3 hr	8	312 (17)	4.41 (0.12)	45.7 (4.9)	1039 (35)
	24 hr	9	308 (7)	4.48 (0.33)	46.6 (7.2)	1053 (54)
	7 day	11	317 (9)	4.35 (0.12)	45.0 (13.6)	1026 (28)
Sham	-	3	305 (15)	-	-	-

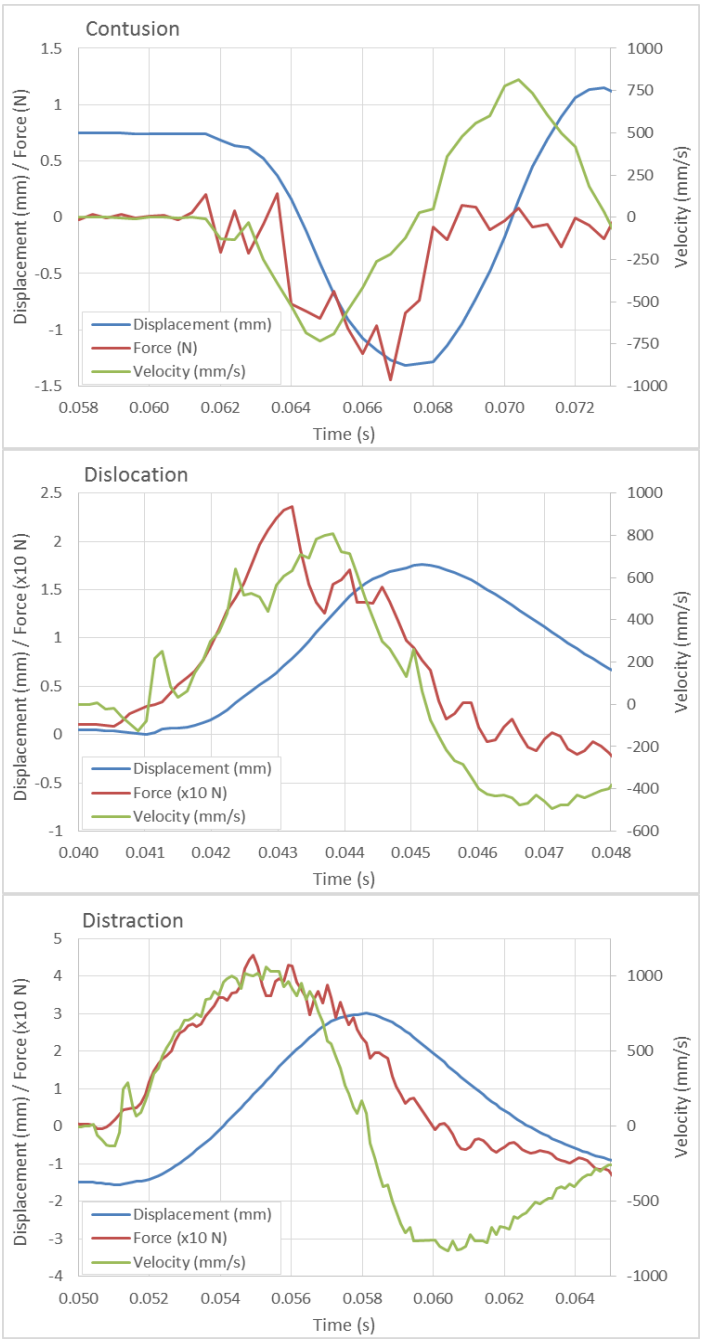

Figure 2-4 - Typical injury-time curves for contusion, dislocation, and distraction injury mechanisms. Unfiltered displacement (mm), force (N), and velocity (mm/s) signals are shown. All data were sampled at 5000 Hz. Displacement was measured at the linear differential transformer within the actuator, force was compensated for inertial loading using acceleration, and velocity was calculated from the displacement signal data. Contusion: the impactor starts at approximately 0.75 mm, and accelerates towards the surface of the spinal cord (0 mm). Dislocation: the force plot typically drops immediately after peak force, as the intervertebral disc shears from the endplate of the vertebral body. Distraction: the actuator begins at -1.5 mm, reaching a total stroke of ~4.5 mm.

2.3.2 Histological Analyses

All graphs from histological data and full statistical results are presented in Appendix A .

Overall white matter sparing (EC)

Contusion injuries demonstrated significant WM loss at 1 mm rostral ($p < 0.05$) and at the injury epicentre ($p < 0.01$) at all three time points post injury (Figure 2-5A). Additionally, at 1 mm caudal, the loss of WM progressed significantly between 3 hours and 7 days ($p < 0.01$). Dislocation also demonstrated a significant loss of WM at the injury epicentre ($p < 0.01$) at all three time points (Figure 2-5B). By 24 hours post-injury, the damage was significantly greater than 3 hours at 1 mm rostral ($p < 0.05$) and 1 mm caudal ($p < 0.01$) from the epicentre. By 7 days post injury the spared WM at 3 mm caudal was significantly less than after 24 hours ($p < 0.05$). The distraction injuries demonstrated significantly less spared white matter from 1 mm caudal to 1 mm rostral ($p < 0.05$) for all three time points (Figure 2-5C). There was no significant difference in WM loss across injury time points following distraction injury, except that at 5 mm rostral, the WM loss at 3 hours was significantly different from 24 hours ($p < 0.05$).

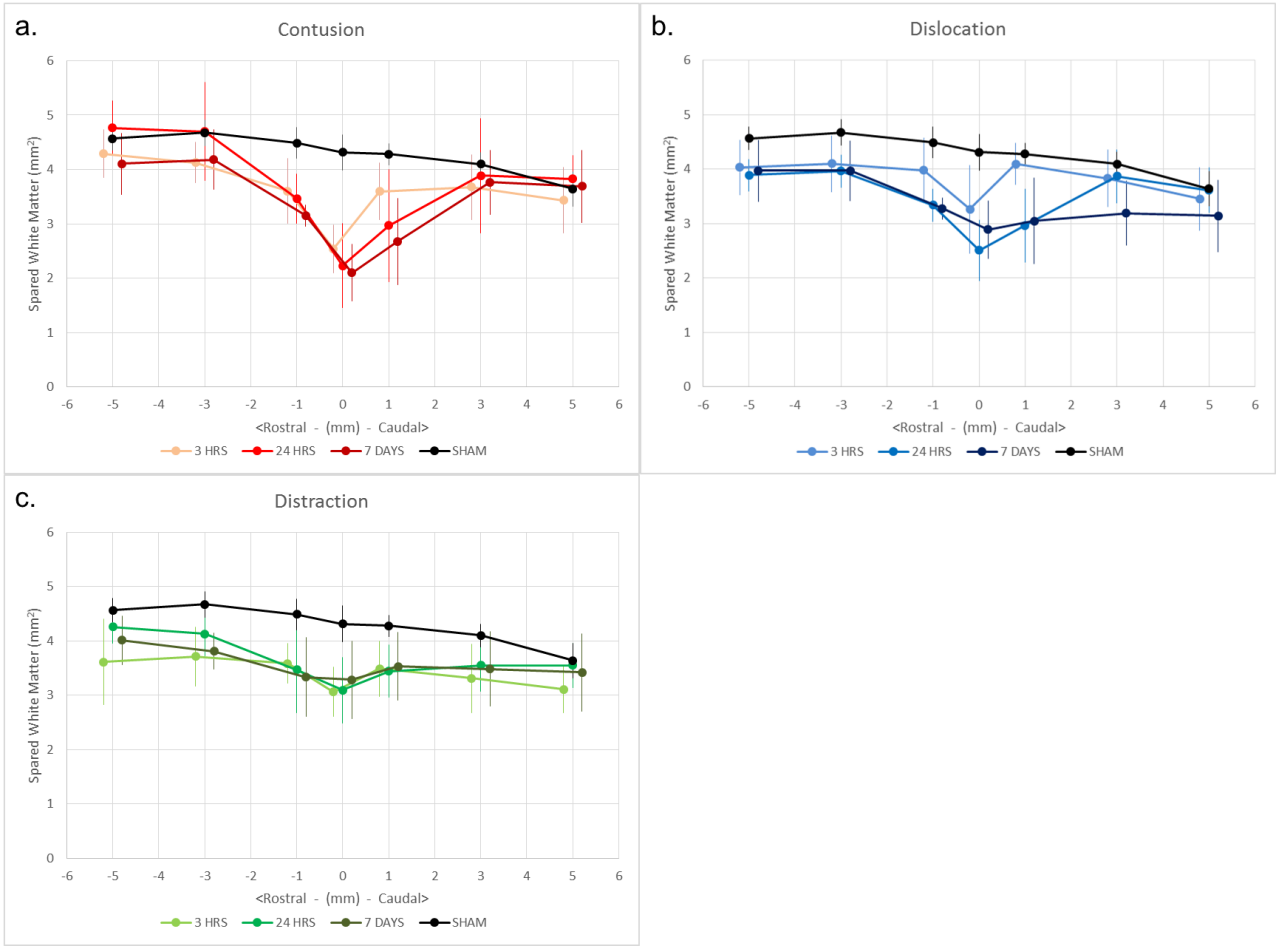

Figure 2-5 - Area of overall spared white matter (mm^2). Mean values (± standard deviation) are shown for each location along the spinal cord. The different time points post-injury are compared for each injury mechanism to observe the progression of injury. All data are presented as means and standard deviations and offset horizontally for clarity.

Loss of axons and myelinated axons (NF/Tub/SMI/MBP)

All three injury mechanisms demonstrated a decrease of myelinated axons along the length of the spinal cord for dorsolateral, ventrolateral and lateral tracts. This loss continued over time for contusion and dislocation, although not significantly. Quantified myelinated axon counts and representative micrographs for each time point for the cuneate fasciculus are presented for contusion (Figure 2-6), dislocation (Figure 2-7), and distraction (Figure 2-8) injuries.

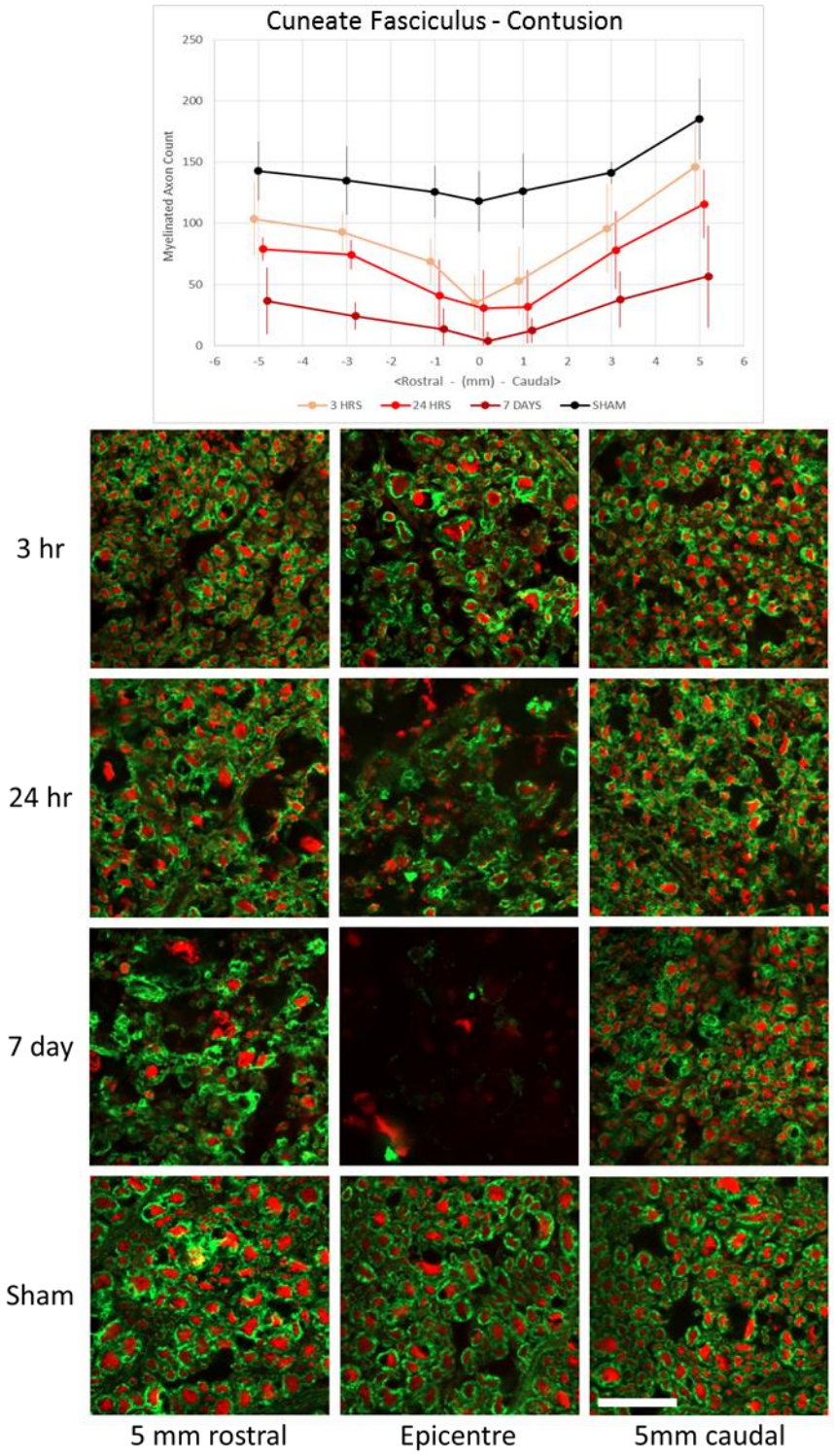

Figure 2-6 - Cuneate fasciculus following a contusion injury mechanism. The loss of myelinated axons is most pronounced at the injury epicentre and progresses over time. Scale bar 20 µm.

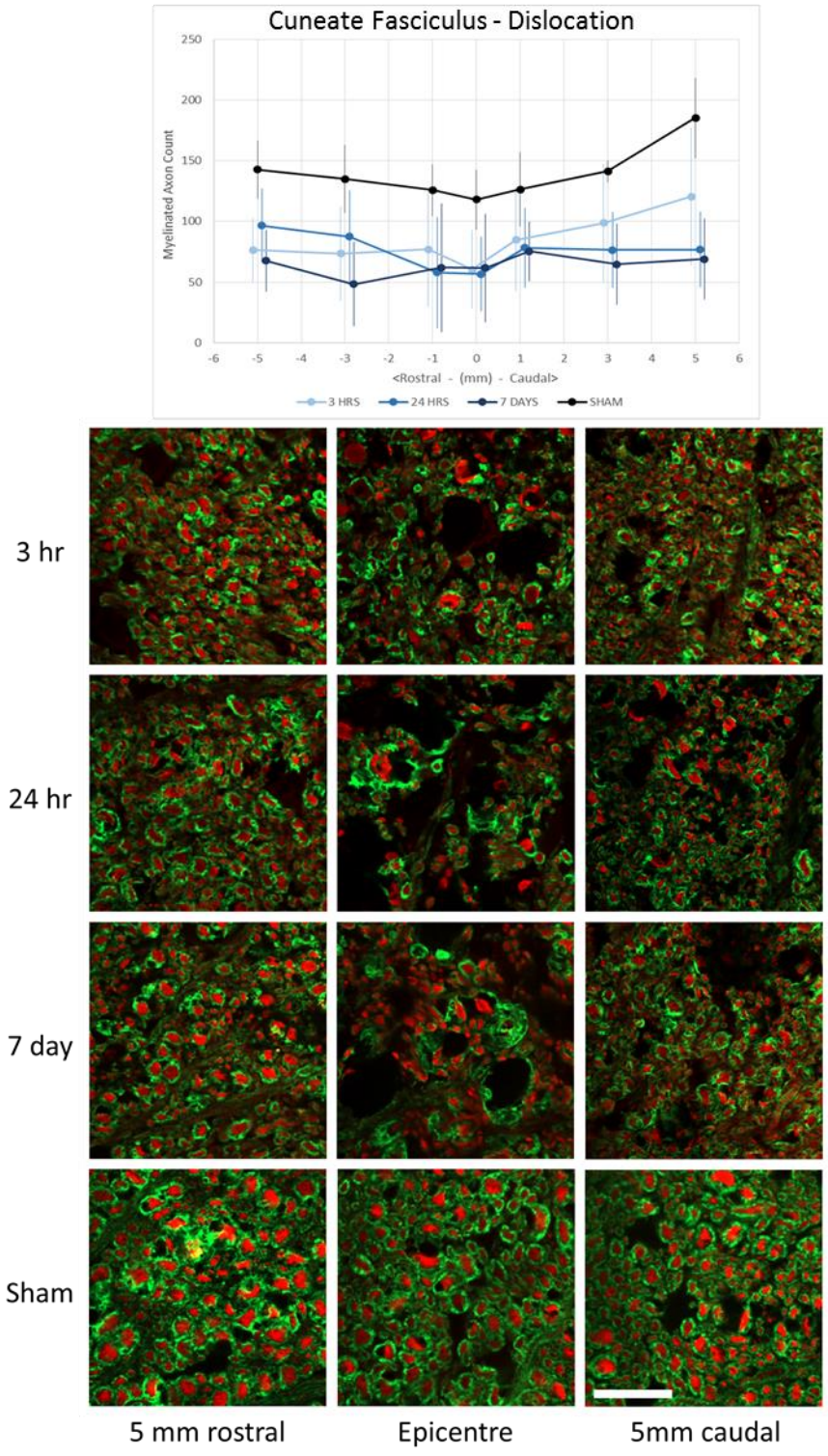

Figure 2-7 - Cuneate fasciculus following a dislocation injury mechanism. Qualitatively the injury appears most severe at epicentre. There was no significant loss of myelinated axons over time.

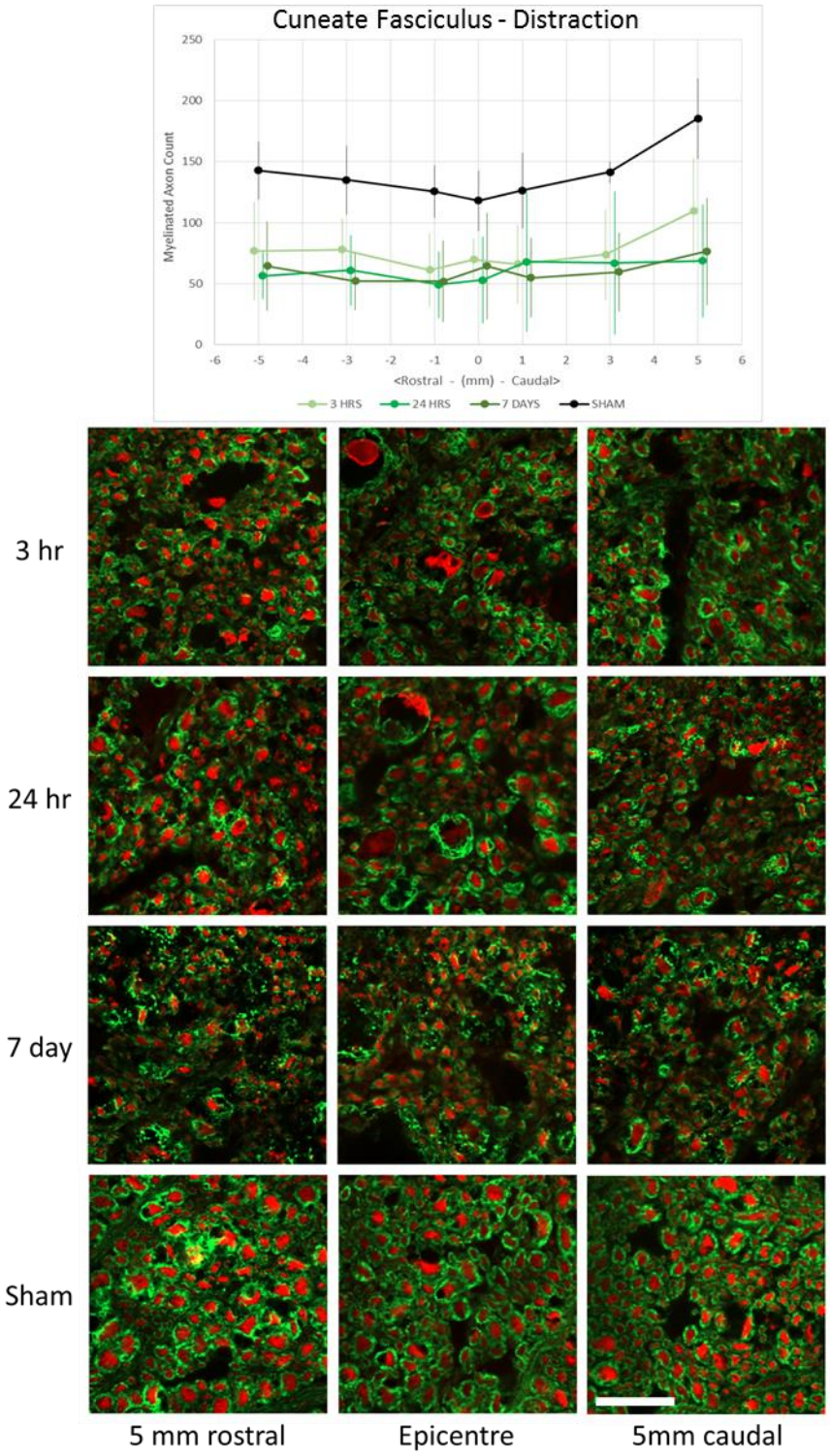

Figure 2-8 - Cuneate fasciculus following a distraction injury mechanism. The injury demonstrates similar rostro-caudal distribution, with no significant loss of axons over time. Scale bar 20 µm.

Following contusion injuries, all three dorsal column tracts (gracile, cuneate, and CST) exhibited significantly fewer axons ($p < 0.05$) and myelinated axons ($p < 0.01$) at the epicentre than those from sham experiments at all three time points, except for axon count in the cuneate fasciculus, which was only significantly less than sham data at 7 days post injury ($p < 0.01$) (Figures A1 – A3). There was a progressive decrease in both axons and myelinated axons over time throughout the dorsal column. In the gracile fasciculus, there was a significant loss of axons and myelinated axons between 3 hours and 24 hours 1 mm rostral ($p < 0.01$), and a significant loss of axons between 24 hours and 7 days at 3 and 5 mm rostral ($p < 0.01$) (Figure 2-9A). In the corticospinal tract, there was a significant loss of axons and myelinated axons between 24 hours and 7 days at 3 and 5 mm rostral ($p < 0.01$) (Figure 2-9B and Figure 2-11). The cuneate fasciculus demonstrated a focal loss of axons and myelinated axons at the lesion epicentre, where axons and myelinated axons increased symmetrically at further rostral and caudal locations from the epicentre (Figure 2-9C).

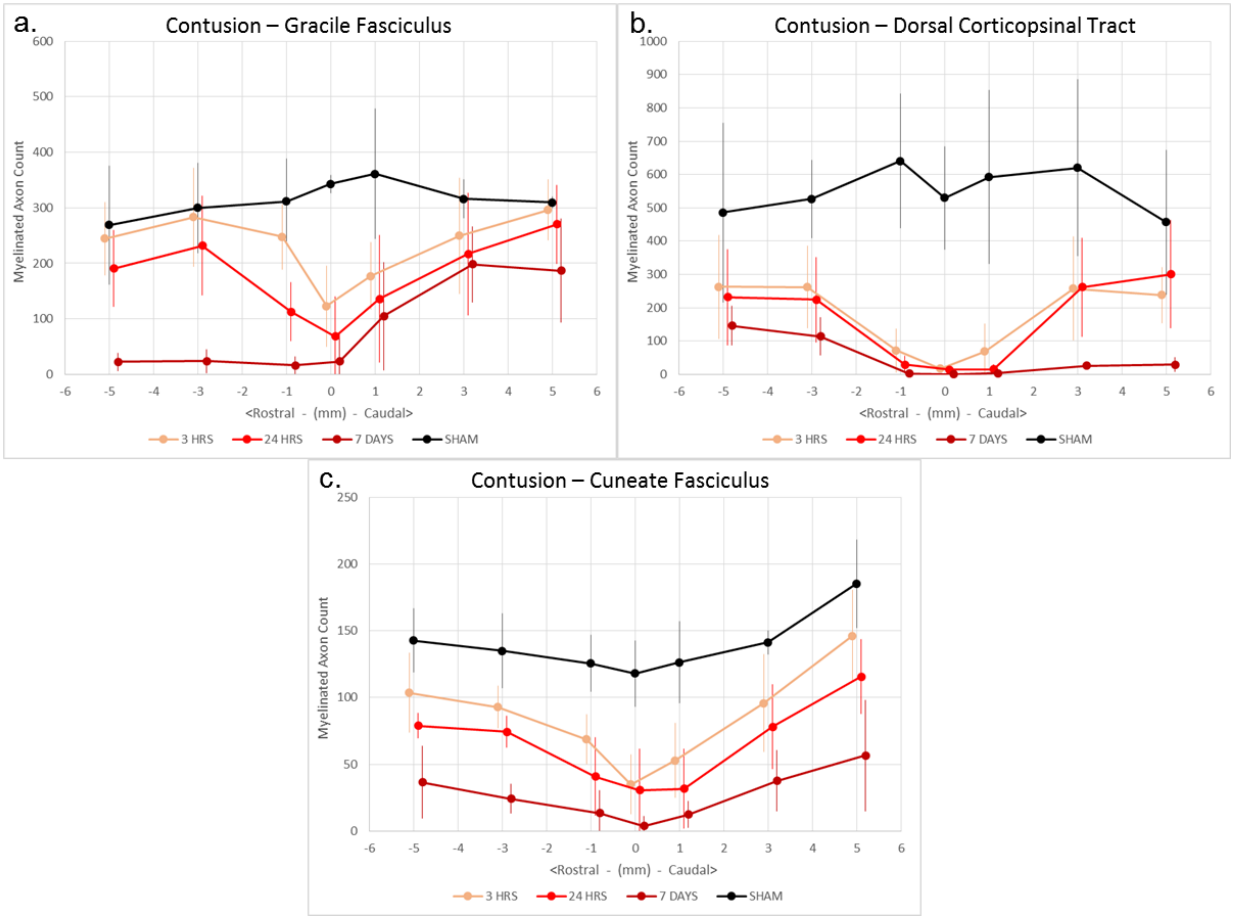

Figure 2-9 - Myelinated axon count (per 3278 µm^2) along the length of the spinal cord from rostral (-) to caudal (+) for contusion injury mechanism at specific regions of interest. a. Gracile fasciculus – focal lesion, with decline rostral to the epicentre which progresses over time, particularly between 24 hours and 7 days. b. Corticospinal tract – focal lesion, with decline caudal to the epicentre which progresses over time, particularly between 24 hours and 7 days. c. Cuneate fasciculus – focal lesion, with proportionate rostro-caudal loss of myelinated axons over time. All data are presented as means and standard deviations and offset horizontally for clarity.

The dislocation injuries did not exhibit a significant decline in axon counts at any time point in the gracile or cuneate fasciculi. There was a focal decrease of myelinated axons at the epicentre in the gracile fasciculus (Figure 2-10A). Dislocation injuries demonstrated patterns similar to contusion injuries in the corticospinal tract – a focal lesion at the epicentre, expanding caudally over time (Figure 2-10B and Figure 2-11). From 3 hours to 24 hours there was a loss of both axons ($p = 0.06$) and myelinated axons ($p = 0.05$), at 1 mm caudal to epicentre. There was a focal

loss of axons and myelinated axons at the epicentre in the ventrolateral and dorsolateral regions at 3 and 24 hours post injury (Figure 2-10 C & D).

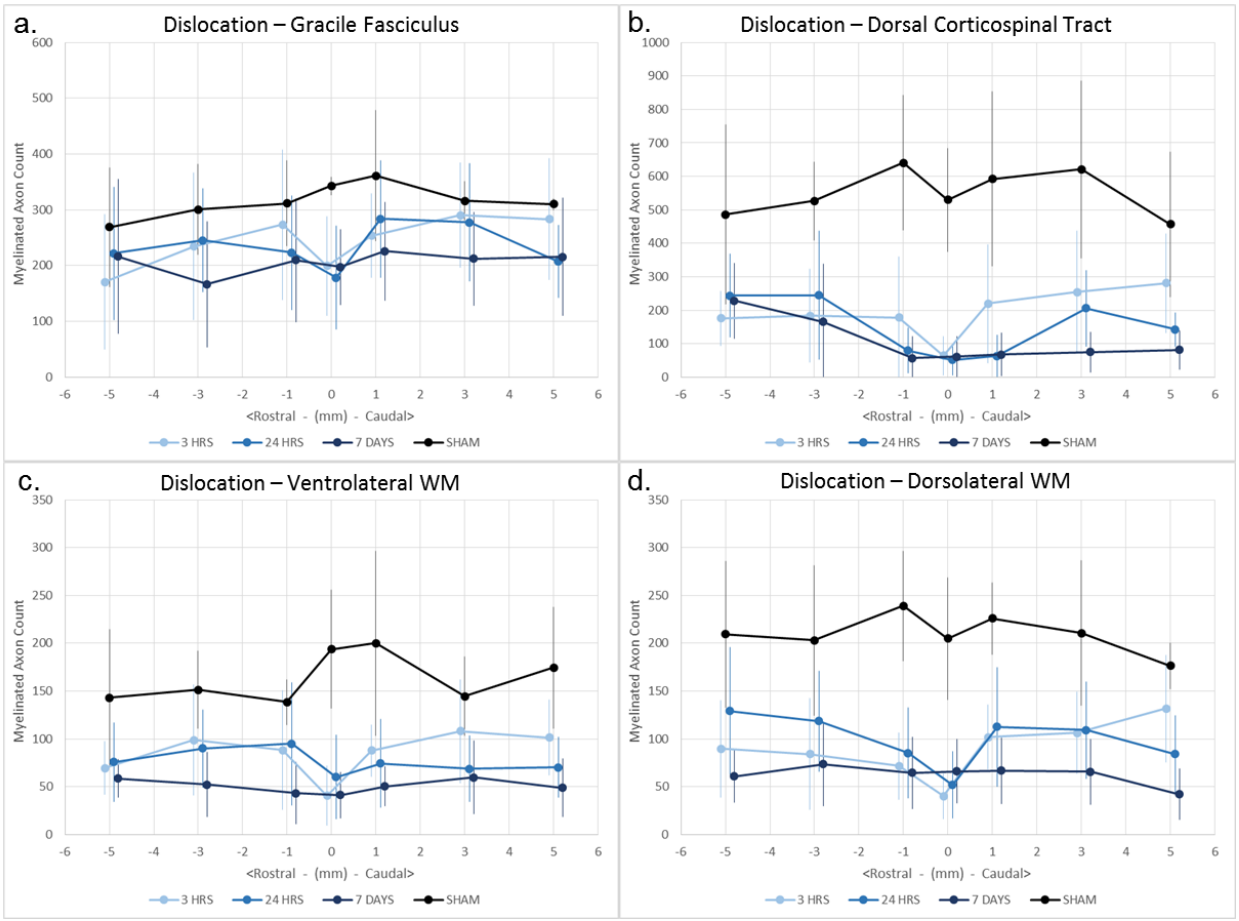

Figure 2-10 - Myelinated axon count (per 3278 µm^2) along the length of the spinal cord from rostral (-) to caudal (+) for dislocation injuries. a. Gracile fasciculus – focal loss of myelinated axons at the epicentre for early time points, but loss spreads by 7 days post-injury. b. Corticospinal tract – similar pattern to contusion, with progressive decline caudal to the epicentre, particularly between 3 hours and 24 hours. c and d. Ventrolateral, dorsolateral WM – focal loss of myelinated axons at the epicentre for early time points, but loss spreads by 7 days post-injury. All data are presented as means and standard deviations and offset horizontally for clarity.

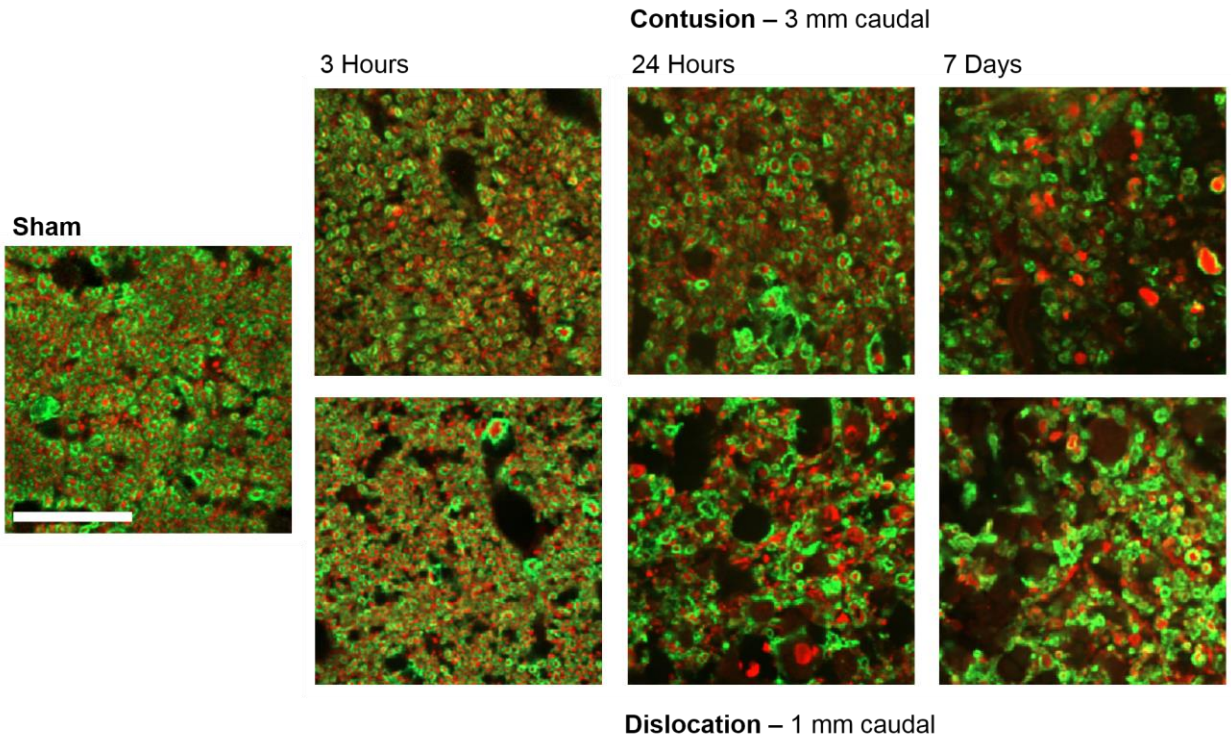

Figure 2-11 - Representative confocal micrographs of myelinated axons in the dorsal corticospinal tract (CST) used for quantitative analysis of white matter damage following contusion injuries (3 mm caudal) and dislocation injuries (1 mm caudal). Axons/axon debris are stained in red (NF/Tub/SMI), and myelin/myelin debris are stained in green (MBP). The sham micrograph shows densely configured axons surrounded by tight myelin sheaths. At 3 hours post injury, axons are still tightly packed in both contusion and dislocation, but show less defined myelin sheaths surrounding the axons. At 24 hours post-injury following a contusion injury myelin sheaths are beginning to unravel from the axons, as clearly defined voids become apparent between the axons and surrounding myelin. By 7 days post contusion injury, significant loss of both axons and myelin has occurred, many axons have become swollen, and axon and myelin debris are present throughout the CST. At 24 hours after a dislocation injury, significant loss of myelin has occurred, and many axons can be seen without surrounding myelin. 7 days following a dislocation injury the CST is still filled with axon and myelin debris. Scale bar 20 µm.

Distraction injuries demonstrated no significant loss of axons in the gracile, or cuneate funiculi or significant loss of myelinated axons in the gracile fasciculus at any time point. There was significant loss of axons in the corticospinal tract, and myelinated axons in the cuneate fasciculus (Figure 2-8), although not significant at all rostrocaudal locations. There was significant loss of myelinated axons at most rostro-caudal locations, and at all time-points for the corticospinal

tract, lateral WM, dorsolateral WM, and ventrolateral WM ($p < 0.05$) (Figure 2-12). There were no significant differences between time points for any of the regions.

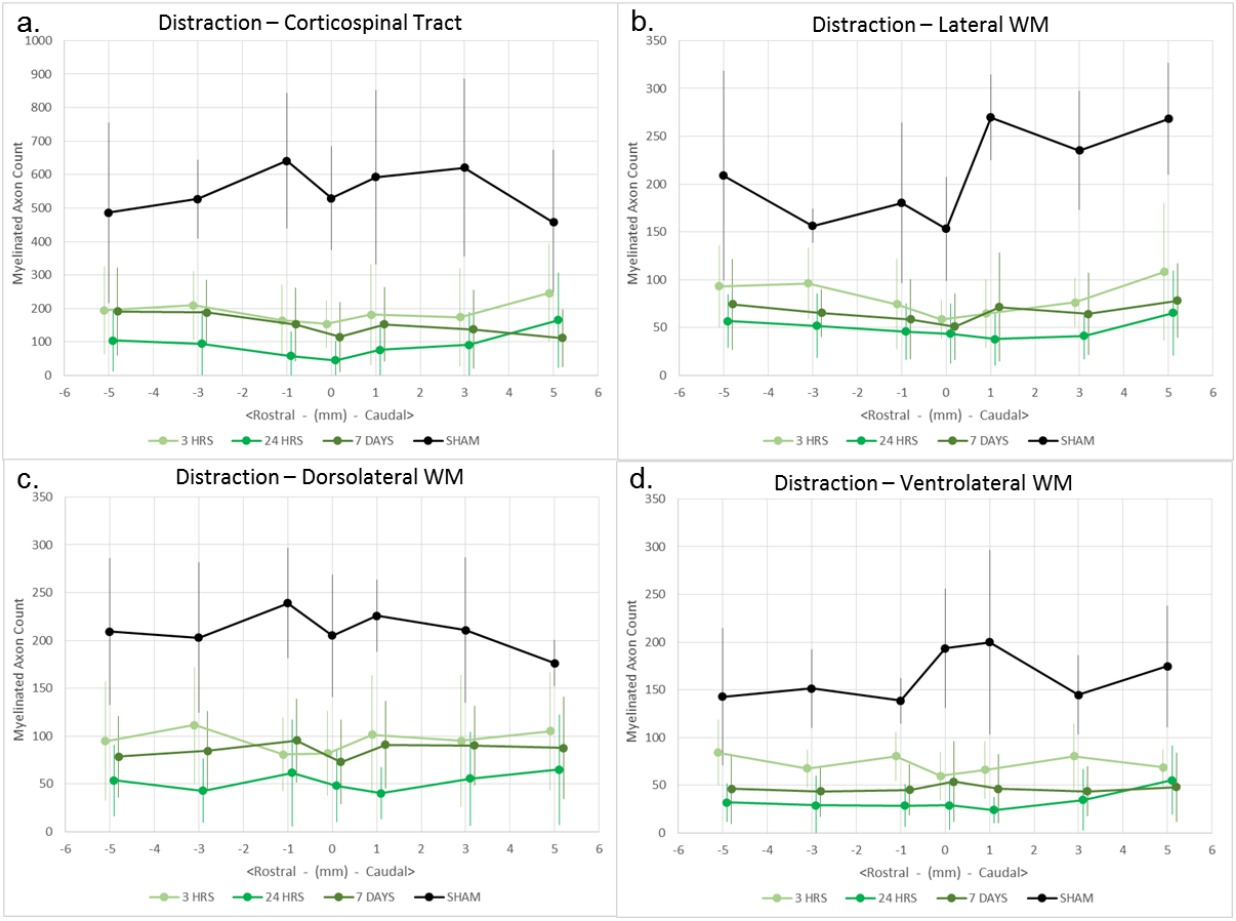

Figure 2-12 - Myelinated axon count (per 3278 µm^2) along the length of the spinal cord from rostral (-) to caudal (+) for distraction injuries. The corticospinal tract (a), lateral white matter (b), dorsolateral white matter (c), and ventrolateral white matter (d), demonstrated uniform rostro-caudal loss of myelinated axons, and no significant progression of injury over time. All data are presented as means and standard deviations and offset horizontally for clarity.

2.4 Discussion

The objective of this study was to evaluate the progression of injury, through analysis of WM loss, at acute time points of 3 hours, 24 hours, and 7 days, for three distinct injury mechanisms, contusion, dislocation, and distraction. Contusion injuries resulted in focal damage at the epicentre, particularly in the dorsal column tracts, with injury significantly progressing between 24 hours and 7 days post injury rostrally from the epicentre in the gracile, and caudal from the

epicentre in the CST. Dislocation injuries were more widespread rostrocaudally from the injury epicentre, with significantly less overall spared white matter observed between 3 hours and 24 hours 1 mm caudal to the epicentre. Distraction injuries were the most diffuse, and demonstrated little progression of injury between 3 hours and 7 days. These results provide insight that specific rates and locations of degradation in the white matter may be injury mechanism dependent, suggesting a potential temporal difference between injury mechanisms.

The rostrocaudal shape patterns for myelinated axons in the different injury mechanisms were similar to those reported at 8 weeks post injury (Chen et al., 2016A). For contusion, the gracile fasciculus and CST had few remaining myelinated axons at 7 days, very similar to that observed at 8 weeks post injury. This was similar for the CST in the dislocation injuries, however the rostral gracile fasciculus exhibited more damage at 8 weeks post injury, suggesting the continued loss of WM beyond 7 days. The loss of myelinated axons was more focal at the injury epicentre at 8 weeks than at 7 days in the dorsolateral and ventrolateral WM for all three injury mechanisms, perhaps indicative of further progression of secondary pathologies beyond 7 days. This is most likely reflected in reports of axonal die-back from the lesion epicentre (Evans et al., 2014). However, these discrepancies may also be due to different injury severities between the studies.

Interestingly, several tracts demonstrated no progression of injury over the 7 days, particularly for the distraction injury mechanism. These results may indicate that the damage is primarily mechanical, in this case due to tensile loading, and may not initiate the same secondary injury cascades as the localized compression in contusion injuries for example. These findings may have potential implications with respect to neuroprotective strategies. If damage caused by certain mechanisms is limited to the acute phase post-injury, the timing window may be shorter for applying neuroprotective treatments to prevent further secondary injury. Therefore, future research is justified to further investigate the effects of mechanistic loading patterns on the progression of secondary injury pathologies.

Spinal Cord Biomechanics and Regional Loading

The different mechanisms subject the spinal cord to distinct loading patterns during injury. The contusion tip impacts the dorsal surface of the spinal cord, subjecting the spinal cord to

compressive stress in the transverse plane, particularly in the dorsal column. The histological results correlate with this loading pattern by demonstrating focal axon and myelinated axon loss in the dorsal column tracts (Figure 2-9). The distraction injury relies on the various connection points between the vertebrae and spinal cord (denticulate ligaments, nerve roots, dura mater) to apply tension to the spinal cord. This results in a uniform distribution of axial tensile stress throughout the transverse spinal cord cross section, and along the rostro-caudal length (Greaves et al., 2008; Khuyagbaatar et al., 2016). The histological results correlate with this loading pattern as axon and myelinated axon loss was uniformly distributed rostro-caudally, and observed in all of the analysed tracts (although to a lesser degree in the gracile fasciculus). The dislocation injury applies the most complex loading pattern to the spinal cord; a combination of shear, compressive, and tensile stress. The relative transverse displacement of the vertebrae induces a plane of shear stress within the spinal cord (Choo et al., 2007, 2009, 2008; Clarke et al., 2008). There would also be transverse compressive stress where the spinal cord is pinched between the lamina of C5 and the vertebral body of C6 (Figure 2-13). Additionally, there is likely tensile stress along the ventral and dorsal surface, where the spinal cord is forced to follow a curved path as it is bent around the vertebrae (Fiford et al., 2004). If different modes of loading are responsible for distinct pathologies, the dislocation injury therefore likely exhibits localized similarities with both contusion and distraction injuries.

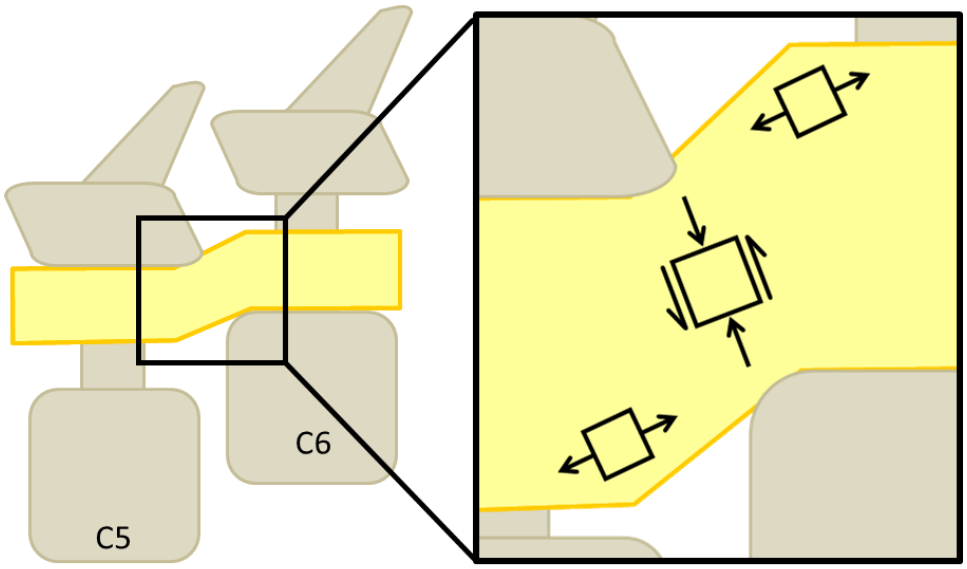

Figure 2-13 - Regional stress patterns due to the loading on the spinal cord from a dislocation injury. The relative translation of vertebrae would induce a plane of shear stress, as well as compressive loading where the spinal cord is pinched between vertebrae. There is also likely tensile stress at the ventral and dorsal surface where the spinal cord is bent around the vertebrae.

The dislocation injury did not induce greater damage to the lateral region of the WM compared to the other mechanisms, as observed in previous studies (Chen et al., 2016A; Choo et al., 2007, 2008). This may be due to the greater observed injury severity in some previous animals (Chen et al., 2016A). Additionally, these studies performed analyses on the entire lateral column of the spinal cord, whereas results from the current study were from a specific, smaller region within the lateral column. The damage from the dislocation injuries reported in previous studies may be located outside of the area of interest used in the current study, or may be more diffuse throughout the lateral column, making it more detectable with larger-area WM analyses.

An interesting trend was observed in the gracilis, dorsolateral and ventrolateral tracts following the dislocation injury: a focal loss of axons and myelinated axons at the lesion epicentre at 3 and 24 hours, which spread both rostral and caudal by 7 days. During the injury, the vertebrae directly contact the perimeter of the spinal cord near epicentre, likely inducing this damage to the most superficial tracts (Figure 2-14). Due to this loading mechanism on the spinal cord, we observed that the dorsolateral tract was slightly more damaged rostrally than caudally at 3 hours (Figure 2-10D). A similar relative difference between rostral and caudal aspects of the

ventrolateral tract was expected, but was not observed (Figure 2-10C). This may be due to the presence of the posterior longitudinal ligament at the ventral spinal canal, perhaps further distributing loading on the spinal cord.

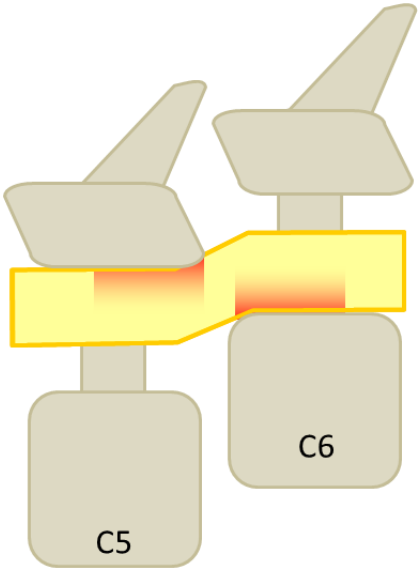

Figure 2-14 - Dislocation injury schematic, where the dorsal tracts would be expected to be more damaged rostrally due to contact with the C5 lamina, and ventral tracts would be expected to be more damaged caudally due to contact with the C6 vertebral body.

Dorsal Column Tract Differences – Axon Size

In contusion injuries, the loss of axons and myelinated axons in the gracile fasciculus extended rostrally, indicating the gradual distal degeneration of ascending sensory axons. Conversely, the loss of axons and myelinated axons in the corticospinal tract extended caudally, affecting the distal descending axons of the corticospinal neurons. These findings are expected, as when axons are damaged, the distal portion often degenerates due to the disruption of axonal transport and disconnection from the cell body, called Wallerian degeneration (Lubińska, 1977). Despite the ascending cuneate fasciculus being located lateral to the gracile fasciculus and dorsolateral to the corticospinal tract, it displayed considerably less rostral degeneration following injury. This difference in response could be due to the bifurcation of cuneate axons after entering the spinal cord to both ascend to the dorsal column nuclei and descend for several segments, which would explain the uniform rostrocaudal degeneration over time. Additionally, this difference could also be due to the cuneate fasciculus being comprised of larger diameter axons than the adjacent

gracile fasciculus and corticospinal tract (Figure 2-15) (Dula et al., 2010; Niu et al., 2013; Ong et al., 2008). This effect in the contusion model is of particular importance, because the compressive stresses would likely be very similar in these adjacent regions within the dorsal column. This supports the theory that the diameter of the axons influences the injury threshold, in this case, associated with compressive, transverse plane stresses. Contrary to the preservation of large-diameter axons at acute stages in the present study, a selective loss of large-diameter axons has been observed at chronic stages (i.e. 2 – 5 months post injury) (Blight, 1991; Blight & De Crescito, 1986). Therefore smaller axons may be more vulnerable to damage at acute stages, and large axons may be more vulnerable over time. These findings may be similar to small-fiber neuropathy observed in peripheral nerves, where the high surface-to-volume ratio makes small-diameter axons particularly sensitive to influx of ions (Hoeijmakers et al., 2012; Rolyan et al., 2016).

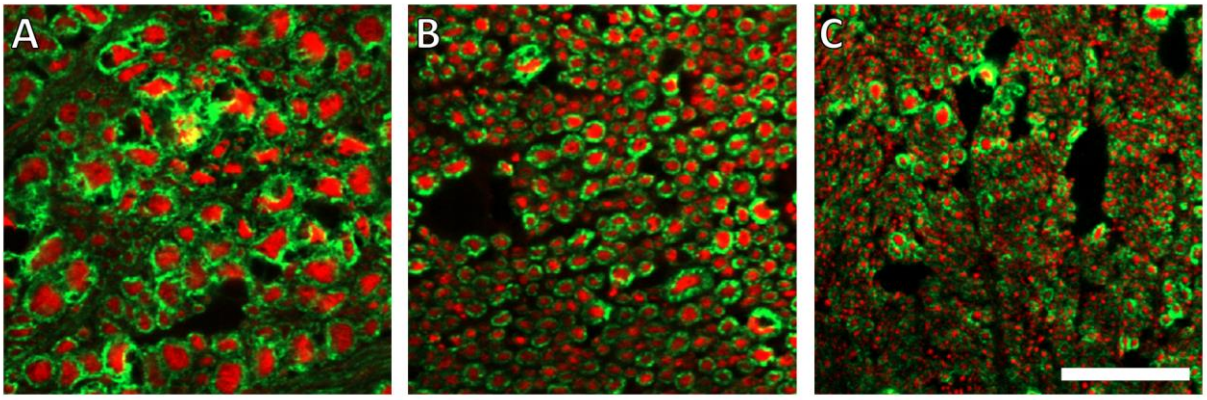

Figure 2-15 – Micrographs of relative axon diameters of the dorsal column tracts: cuneate fasciculus (A), gracile fasciculus (B), and dorsal corticospinal tract (C).Micrographs from a single sham animal. Scale bar: 20 µm.

There were no observed differences in axon damage or loss between the cuneatus, gracilis, and corticospinal tracts due to the distraction injury, although the overall counts were greatly reduced in all three tracts. This suggests that axon diameter may not have an effect on the injury threshold of the axon, due to axial tensile stress. It is possible that the localized dorsal column tensile stress, due to the distraction injury, was below injurious levels for all three regions. Previous studies have reported there is no selective vulnerability of axons based on diameter under compression (Shi & Blight, 1996; Shi & Borgens, 1999) or stretch (Shi & Pryor, 2002), however

these studies were performed in vitro, and absence of pathologies related to vascular damage may not represent the secondary pathways initiated by the physical trauma.

The differences in stresses and strains at different regions of the spinal cord due to different injury mechanisms are therefore important to consider, given the varying diameters of axons in different regions. The effect of axon size also introduces similarities with respect to translational efforts to the human spinal cord. Relative axon size distribution is generally conserved in the dorsal column across mammalian species, including human, where small-diameter axons are mostly located medially and large diameter axons are mostly located laterally (Niu et al., 2013), indicating that overall stress distribution patterns may be conserved. If injury sensitivities are influenced by interactions between axon diameter and localized stresses, perhaps other injury variables such as velocity may have interaction effects with axon size (or other anatomical differences). Similar to axon diameter, other spinal cord microstructure variations between axons such as myelin thickness and axon density (Dula et al., 2010) may also affect stress-based injury thresholds of axons and other cells such as oligodendrocytes and astrocytes. Further testing on the injury sensitivity of spinal cord microstructure and interactions between other variables, such as velocity, could provide additional understanding of spinal cord tissue biomechanics.

Limitations

Injury displacement, force, and velocity were consistent between dislocation injuries; however, the animals exhibited a wide range of outcome severities from essentially uninjured to severely injured to the point of humane endpoint. The variability observed in the outcome severity of the dislocation injuries may be due to a number of factors including slipping at the vertebra-clamp interface, anatomical size differences, blood pressure, or respiratory movement. In five instances the lamina fractured during injury (no apparent difference in injury metrics), indicating the need for specific tightening parameters to prevent over-tightening (or under-tightening) of the clamps and to ensure consistent attachment parameters. In order to implement the dislocation model into future studies to investigate the effects of other variables or potential treatments, more consistent injuries are required.

Injury displacements were slightly reduced compared to a previous study to limit the outcome severities, where difficulties were experienced in long term care and survival of the most

severely injured animals (Chen et al., 2016A). Despite the displacement reduction, four animals reached humane endpoint prior to the 7-day time point following a dislocation injury, introducing a 'survival bias'. The loss of the most severe range of animals in the 7-day group likely reduced the observed severity in the histological analyses compared to the 3- or 24-hour time points. Additionally, the more severe nature of these injuries likely had greater characteristic damage patterns due to the injury mechanism, and the loss of these animals may have obscured further regional injury progression. No other animals reached humane endpoints.

Differences in velocities between mechanisms were due to relative stroke lengths of the actuator for each injury displacement. These differences likely did not introduce a velocity effect as differences up to 300 mm/s have previously not introduced differences in injury severity in a high speed contusion model when of the same order of magnitude (velocity range 100 – 400 mm/s) (Kim et al., 2009).

Six of the eight spinal cords from the distraction 24-hour group, and three shams were mistakenly exposed to 24% sucrose for several weeks longer than prescribed. These spinal cords were observed under microscope with no obvious abnormalities detected. However, the sucrose-exposed sham spinal cords had substantially lower axon counts than the normal sham counts, and thus were discarded from the analysis. The large standard deviations in the sham counts are likely due to the small sample size (n = 3). Similarly, the exposed cords from the 24-hour distraction group generally demonstrated lower axon and myelinated axon counts than the two cords of proper sucrose exposure time. Comparisons with the 24-hour distraction group were made with caution. Tight adherence to methodological protocols is important in future studies, since slight deviations can affect metrics of WM damage, as sucrose overexposure is known to destroy antigens and weaken the immunostainings.

There are also methodological factors that may contribute to the variability across injury mechanisms. The epicentre was histologically identified as the section with the greatest observed damage. This technique is effective for contusion injuries, where the injury is focal, and the epicentre is easily identified. This technique, however, is more difficult for the more diffuse closed-column injury mechanisms, particularly distraction. Region-of-interest boxes were placed as close as possible to the predetermined locations, however may have been placed in slightly

different locations when the tissue was severely damaged, or to avoid artifacts. Neither of the factors are considered to be a significant cause of variability as the rostrocaudal WM damage profile matched those observed previously, particularly in the gracile fasciculus and dorsal corticospinal tract (Chen et al., 2016A).

Additional analyses such as gray matter damage and immune response may provide further insight towards mechanistic differences of injury progression, however this was outside of the scope of this thesis. The differences in loading patterns between the injury mechanisms were hypothesized to produce different spatial damage patterns, to potentially be best observed by similar analyses at different locations, thus white matter tracts were analysed for axonal and myelin loss.

The differences in group sizes are due to the challenges associated with SCI survival studies. Animals can potentially be lost at several stages of the experiment. For example, animals may experience adverse reactions to anesthesia during surgery, the injury event may lead to immediate death, or the injury severity may lead to euthanasia during the survival period. Additional animals were added to the 7-day dislocation and distraction groups in anticipation of animal drop out (due to injury severity). A detailed power analysis can typically provide appropriate sample sizes, however accurate estimates of the variances and critical differences are not realistic given the early stage of this research. Previous studies have demonstrated that 8 animals per group was sufficient to determine significant differences between mechanisms (Chen et al., 2016A), therefore, this was the minimum quantity of animals required for each group.

Several non-significant trends that were observed may have been significant with greater sample sizes or reduced variability in the model. These trends were reported when the tissue damage measures corresponded to regions of the spinal cord where damage was expected based on the biomechanics of the injury model, for example, reduced myelinated axon counts in the tracts where the vertebrae contact the surface of the spinal cord in the dislocation model. These trends were highlighted as they may require further attention in future studies involving these injury models.

2.5 Conclusions

Contusion, dislocation, and distraction not only demonstrate distinctly different injury patterns, but also elicit injuries that progress at different rates. Contusion injuries demonstrated significant loss of white matter between 24 hours and 7 days. Dislocation demonstrated significant loss of white matter between 3 and 24 hours, indicating this injury mechanism may initiate a faster pathological response in specific spinal tracts. Distraction injuries did not demonstrate any significant progression of injury within 7 days, suggesting a slower pathological response. The dislocation model warrants further development and refinement to reduce variability in order to better design more specific tests to investigate the associated injury biomechanics and provide an additional avenue to evaluate potential treatment therapies. Additionally, the severe injury outcomes associated with dislocation are analogous to what is observed clinically, further increasing the clinical relevance of this model (Marar, 1974; Tator, 1983; Wilson et al., 2013).

Chapter 3: Repeatability of a Dislocation Spinal Cord Injury Model in a Rat – A High-Speed Biomechanical Analysis

3.1 Introduction

Traumatic SCI is a devastating injury often resulting in significant physical, social, and financial impact on individuals (Ackery et al., 2004; Krueger et al., 2013; Sekhon & Fehlings, 2001). SCI is heterogeneous, with individuals being injured at different spinal levels, by different injury mechanisms, and to varying degrees of severity (Filli & Schwab, 2012; Tator, 2006). The spinal level sustaining the injury is important, as not only do cervical injuries have the potential for greater functional loss, they are the most common (59%) with this trend increasing over recent decades (Chen et al., 2016B). A better understanding of injury mechanism may help to guide therapeutic decision making, leading to more patient-specific treatments (Wilson & Fehlings, 2011).

The most common injury mechanism is dislocation, occurring in roughly 32 – 58% of SCI cases (Sekhon & Fehlings, 2001; Tator, 1983; Tator et al., 1987; Vaccaro et al., 2016; Wilson et al., 2013). Dislocation involves one vertebra sliding past an adjacent vertebra, exerting a combination of compressive, tensile and shear forces on the spinal cord (Russell et al., 2012). Dislocations typically result in the most severe neurological injuries, with the direction and magnitude of the dislocation being important variables (Marar, 1974; Tator, 1983; Wilson et al., 2013). Further, patients with SCI caused by facet dislocation have significantly longer hospital length of stay, and less functional improvement after long-term follow-up (Wilson et al., 2013). The rate of occurrence, severity, and lack of recovery associated with dislocation SCI warrant further work into understanding this injury mechanism better.

Typically, most pre-clinical SCI injury models use a contusion or a transection to injure the spinal cord. Recent models have adopted a ‘closed-column’ approach, where the spinal cord is injured by controlled motion of the vertebrae, such as in dislocation and distraction models (Dabney et al., 2004; Fiford et al., 2004; Seifert et al., 2011; Wu et al., 2016). The limited pre-clinical dislocation studies show different patterns of tissue damage (Choo et al., 2007, 2009, 2008; Clarke et al., 2008; Clarke & Bilston, 2008; Fiford et al., 2004; Lau et al., 2013) and behavioural outcomes (Chen et al., 2016A), suggesting these mechanisms are deserving of

further research with respect to therapeutic treatments. Additionally, finite element models have demonstrated different patterns of maximum principal strain and von-Mises stress between injury mechanisms that are directly associated to neurological damage (Khuyagbaatar et al., 2016; Maikos et al., 2008; Ouyang et al., 2008; Russell et al., 2012). Several studies have recommended further work towards investigating variables contributing to injury and mechanical response of neural tissue, hoping to provide additional insight into the pathophysiology of SCI (Cheriyan et al., 2014; Filli & Schwab, 2012; LaPlaca & Prado, 2010; Miele et al., 2012; Orr et al., 2017).

Although the UBC SCI dislocation model (Bhatnagar et al., 2014; Chen et al., 2016A; Choo et al., 2007, 2009, 2008) closely approximates clinical SCI, the main limitation is the variability in injury outcomes (Cheriyan et al., 2014). Despite consistent dislocation injury displacement parameters (1.84 mm ± 0.02), both tissue damage and behaviour demonstrated more variable outcomes than contusion (Chen et al., 2016A). The consistent injury parameters suggest there is a source of variability that exists where injury clamps grip the vertebrae to perform the controlled dislocation, warranting the design of new injury clamps. From an engineering perspective, once attached, each injury clamp and the respective gripped vertebra should behave as a rigid body, so that the displacement parameters as recorded from the injury device correlate to what is experienced by the spinal cord. Since the dislocation injury mechanism is sensitive to loading directions (Clarke et al., 2008), consistent injury kinematics are essential to develop a better biomechanical understanding of the relationship to injury. The SCI research community recognizes the importance of developing clinically relevant cervical injury models (Filli & Schwab, 2012; Kwon et al., 2010), and the refinement of a dislocation model is important to provide additional avenues for testing neuroprotective strategies and further pursue personalized treatments according to specific primary injury mechanisms (Hilton et al., 2016).

The overall objective of this study was to improve the biomechanical repeatability of a dislocation model for SCI in a rat model, through the following specific aims:

i. Design new vertebral injury clamps to reduce relative motion between the clamps and vertebrae;

ii. Precisely measure clamp and vertebral kinematics during a high-speed dislocation injury in an in vivo rat model using existing and redesigned clamps; and

iii. Quantify slippage (i.e. relative motion) at the vertebra-clamp interface to determine which clamps provide the most rigid connection.

3.2 Methods

3.2.1 Design of Self-Aligning Clamps

In order to design new dislocation injury clamps, one must understand the existing clamp design (Choo et al., 2007) (Figure 3-1), and how it holds the rat vertebrae. Following surgical exposure of the spine, a facetectomy performed at the spinal level of the dislocation helps to align the clamps and prevent residual dislocation following injury (Choo et al., 2007). The clamps are attached to the spine, with the rostral clamp gripping the two vertebrae rostral to the level of the dislocation and holding both together and stationary, while the caudal clamp grips the two vertebrae caudal to the dislocation level, to be displaced dorsally. The rostral and caudal clamps are identical, and mirrored to each other when attached. Each clamp consists of two arms, where the vertebral interface is a wedge shape at the end of each arm, designed to fit into a lateral groove running rostral-caudal between the facet joints and transverse processes (Figure 3-2A). A ridge at the ventral edge of each arm allows the clamps to align into the space produced by the facetectomy for consistent clamp orientation. The two arms are tightened together about a centre post, which limits the narrowest possible clamping distance to prevent over-tightening of the vertebrae, reducing the risk of fracture.

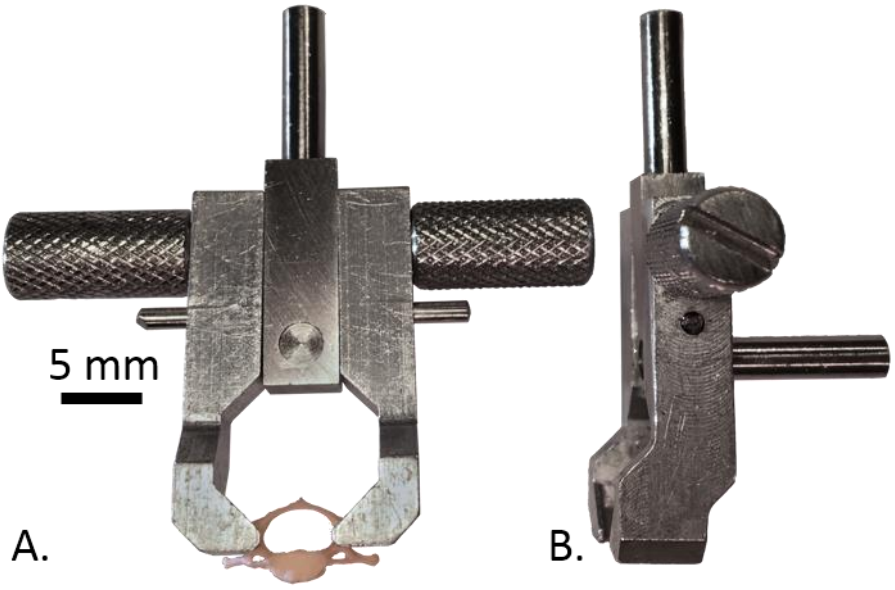

Figure 3-1 - Original dislocation clamps (Choo et al. 2007). A. Transverse plane of clamp holding vertebra, where clamp grips vertebra in the lateral groove between the transverse process and facet joints. B. Sagittal plane view of clamp.

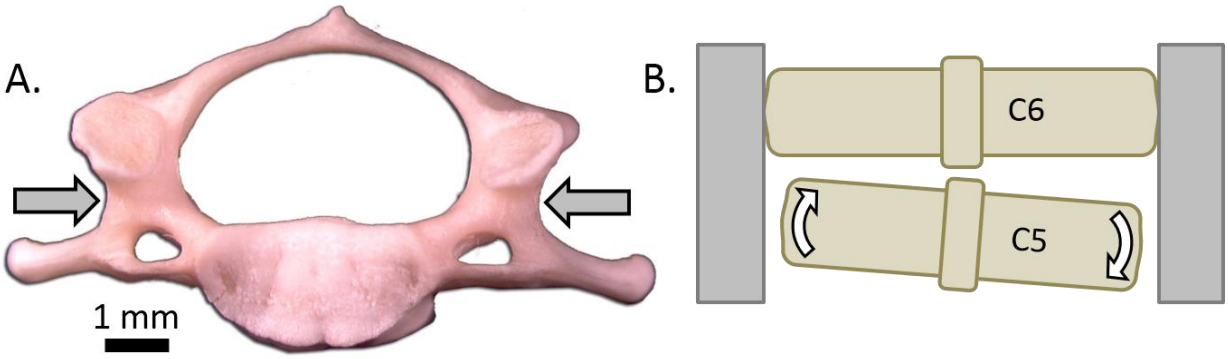

Figure 3-2 - A. The lateral ridge between the articular and transverse process. This ridge runs the length of the cervical spine, and is where the injury clamps are tightened. B. Existing injury clamps tightening to hold two adjacent vertebrae. Since the vertebrae are different widths, the clamps can only securely hold one vertebra, allowing the narrower vertebra to move.

To inform the new vertebral clamp design, the rat cervical spine anatomy was investigated quantitatively with attention to how the existing clamps held each vertebra. The soft tissue was dissolved from six post-mortem male Sprague-Dawley (350 – 400 g) rat cervical spines (5%

solution of NaOH (Onwuama et al., 2012)). The large weight range was intentional, as redesigned dislocation clamps must be able to fit a wide variety of spine sizes. The width of each vertebra (C4 – C7) at the lateral ridge between the articular and transverse processes (Figure 3-2A) was measured with digital calipers (Table 3-1) as this is the location where the vertebral clamps are tightened. In addition, existing clamps were attached to all individual vertebra to qualitatively assess fit.

Table 3-1 - Width measurements in mm of cadaver cervical spines of Sprague-Dawley rats, measured with digital calipers. The existing clamps were also tightened to each vertebra to ensure proper hold.

Spines	C4	C5	Difference	C6	C7	Difference
1	6.38*	6.50	0.12	6.45*	6.72	0.27
2	6.51	6.65	0.14	6.66	6.88	0.22
3	6.66	6.71	0.05	6.87	6.87	0.00
4	6.76	6.89	0.13	7.00	7.30	0.30
5	6.26*	6.38*	0.12	6.41	6.67	0.26
6	6.43*	6.61	0.18	6.75	7.07	0.32
Average	6.50	6.62	0.12	6.69	6.92	0.23
SD	0.18	0.18	0.04	0.23	0.23	0.12

*Fully tightened clamp could not hold vertebra

The existing clamps acted as two parallel ridges attempting to simultaneously grab two adjacent vertebrae. This could only be achieved if the vertebrae were the exact same width. However, different widths of adjacent vertebrae within a spine would limit the clamp to only be tightened to the wider of the two vertebrae, allowing the narrower vertebra to move independently (Figure 3-2B). Additionally, when the original clamps were adjusted to the tightest setting (6.45 mm), they were unable to grip five of the 24 total vertebrae (Table 3-1).

The primary design criterion for the new clamps was to enable each clamp to grip both vertebrae independently for both the rostral and caudal pair, as width differences between adjacent vertebrae were found to be up to 0.32 mm (Table 3-1). New clamps were designed to allow the clamp ‘arms’ to pivot on contact around a dorsal-ventral axis (Figure 3-3). A custom saddle washer matches the curvature of, and rests against, a rounded outer surface, allowing the arm to self-align as the clamp is tightened. The saddle washer was manufactured from polyether ether ketone (PEEK) to minimize friction at the interface and thereby assist with alignment. This design ensures that each clamp holds both intended vertebrae, instead of only the widest vertebra. The minimum clamp width was reduced to 5.97 mm to allow the clamps to grip smaller vertebrae. The clamps were machined from 7075 T651 aluminum to allow visibility through the x-ray.

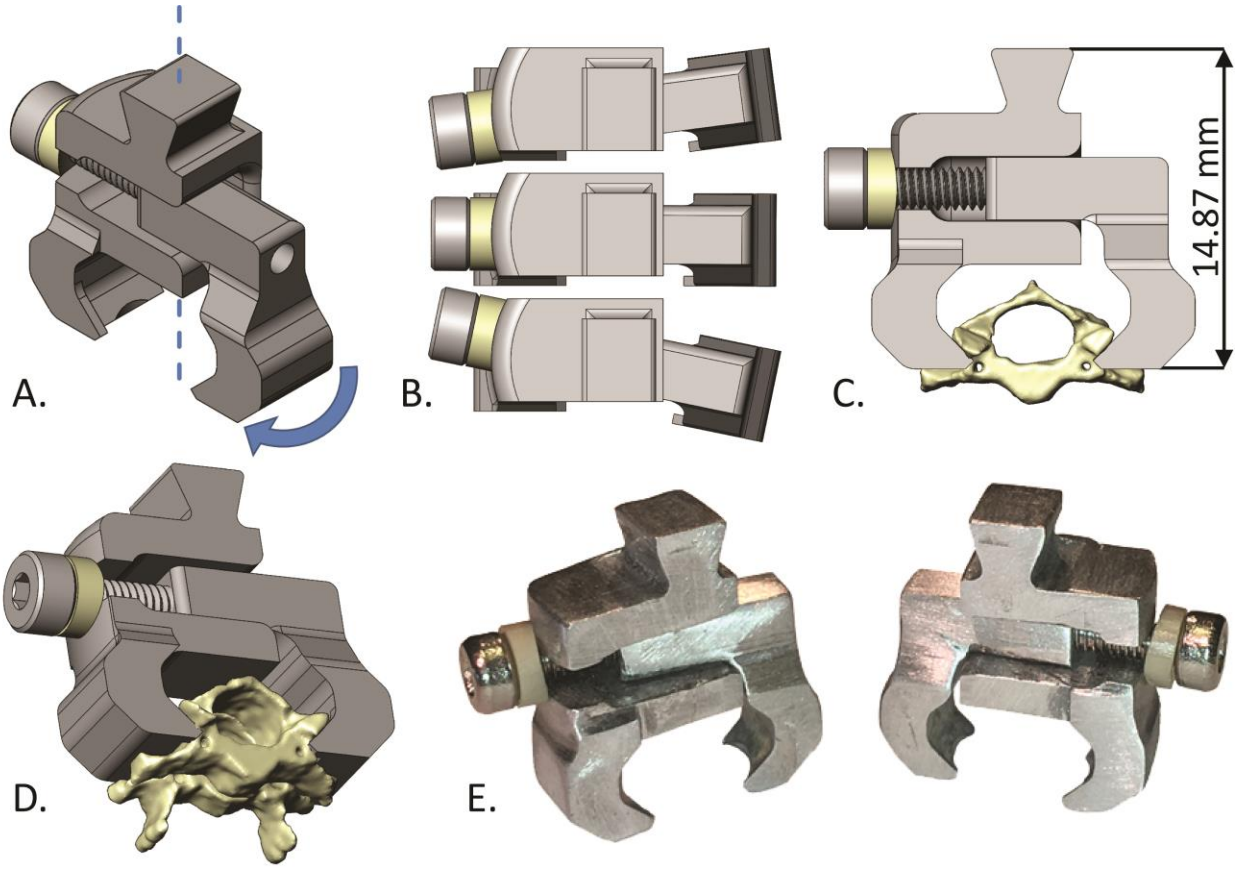

Figure 3-3 - Self-aligning dislocation injury clamps. A. Clamp arm pivoting about dorsoventral axis. B. Saddle washer slides on exterior surface of clamp, which enables clamp arm to pivot. Three positions shown. C. Dimensioned front view of clamp holding C5. D. Front-bottom view of clamp simultaneously holding C5 and C6. E. Photo of clamp prototype. Saddle washers are constructed of PEEK to reduce friction at the interface and remain aligned during tightening. Images drawn to scale.

3.2.2 Measurement of Vertebral Kinematics using High-Speed X-Ray

To measure the relative motions of the vertebrae and vertebral clamps during a dislocation injury, 400 µm radio-opaque tantalum beads (Bal-tec, Los Angeles, CA) were fixed to the vertebrae and injury clamps (Figure 3-4). A minimum of two markers were placed on each vertebra and clamp to quantify both translation and rotation in this sagittal plane analysis. Translation was tracked by averaging the marker coordinates on each rigid body, and compared to subsequent frames. Rotation was tracked as the angle of the line formed by two of the markers relative to the first image.

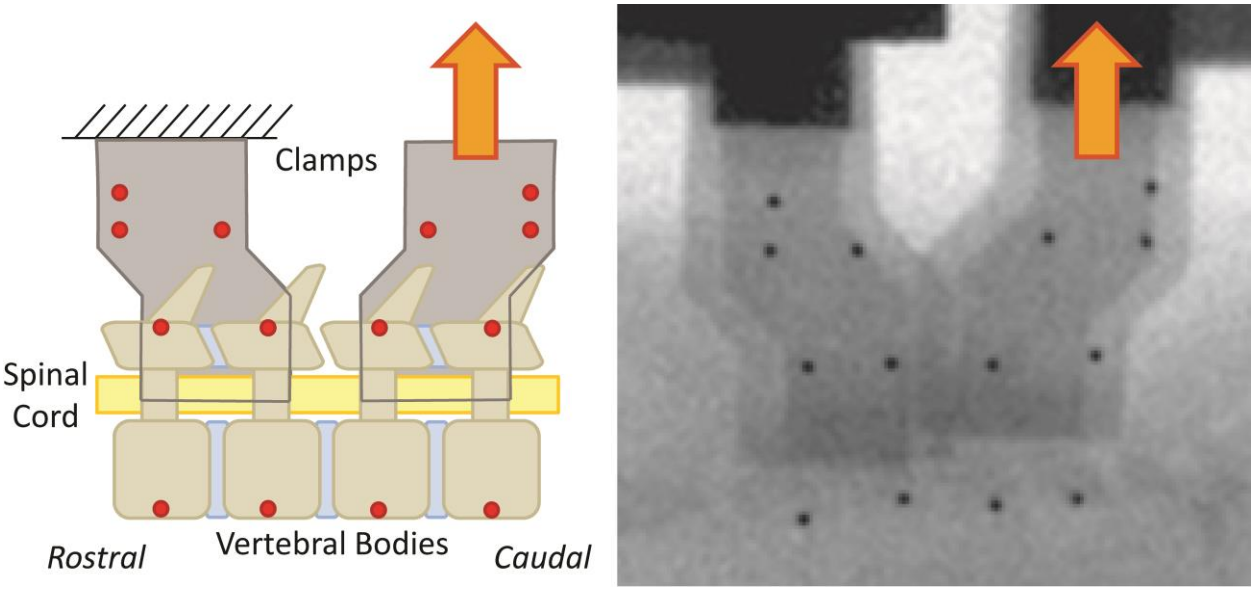

Figure 3-4 - Schematic of the location of the fiducial markers on the vertebrae and injury clamps, with a corresponding high-speed x-ray image (enhanced for clarity). The clamps are represented as outlines on the schematic to visualize the marker locations on the vertebrae. The rostral clamp was held rigid while the caudal clamp was dislocated dorsally.

The injury was performed within a high-speed x-ray system consisting of an x-ray tube and generator (Comet MXR-160 and Gulmay FC-160 640W, TSG X-Ray, Atlanta, GA) operated at 120 - 125 kV and 2.2 - 2.5 mA, and an image intensifier (PS93QX-P20, Precise Optics, Bay Shore, NY) with a high-speed camera (Phantom V12, Vision Research, Wayne, NJ). The stereotaxic frame that holds the animal and the rostral clamps was aligned parallel to the image intensifier. The source to image intensifier distance was 100 cm, and the camera recorded at 8000 frames per second and 512 x 512 image resolution, with a spatial resolution of 0.12 mm/pixel. Magnification error due to the vertebrae and clamp markers moving in different (but parallel) planes was less than 0.01% and was neglected.

All procedures were approved by our institution's Animal Care Committee in accordance with the guidelines published by the Canadian Council on Animal Care. Thirty-four male Sprague-Dawley rats (n = 17 for existing clamps, n = 17 for self-aligning clamps, mean weight 315 g, SD: 18 g) were used to investigate the relative motion between vertebrae and vertebral clamps during a dislocation injury. Rats were anesthetized to a state of deep anesthesia using isoflurane (1-2%/L/min) inhalant for the preliminary surgery. Once the spine was exposed, a surgical drill was

used to make shallow holes (nominally 500 µm diameter, 200 µm deep) on the dorsal surface of the laminae and the dorsal surface of the transverse processes of C3-C6, to fix the fiducial markers using cyanoacrylate. The injury was shifted one level rostral, as initial pilot tests secured the fiducial markers to the ventral surface of the vertebrae, but could not access C7 due to the interference from the ribs. A facetectomy was performed at the dislocation spinal level (C4/C5), and the existing injury clamps were attached to the spine by tightening the clamps into the groove between the transverse processes and facet joints. The self-aligning clamps were attached in the same manner, but a torque screwdriver was used to tighten the clamps to 2.7 N·cm to ensure consistent grip strength and prevent over-tightening.

The rats were given an intraperitoneal injection of ketamine (72 mg/kg) and xylazine (10 mg/kg) as the isoflurane was removed. Surgical plane was verified before the animal was relocated to the UBC multi-mechanism SCI device and high-speed x-ray setup (Figure 3-5). The animal was positioned into a stereotaxic frame, which was fixed beneath the actuator and used ear bars to secure the head, and custom pieces to hold the rostral clamp rigid. The actuator was carefully lowered onto the caudal clamps, and tightened into place without altering the neutral position of the spine. The caudal spine was preloaded to 3 N, adding tension to the surrounding soft tissue to ensure a consistent starting location and load on the spine between animals before inducing the injury. The C3/C4 clamp was held stationary while the C5/C6 clamp was dislocated dorsally to a prescribed displacement of 2.30 mm. For the self-aligning clamps, the dislocation displacement was reduced to 2.00 mm, as the injury was expected to be too severe if the new clamps had a more rigid connection. Animals were sacrificed immediately post-injury.

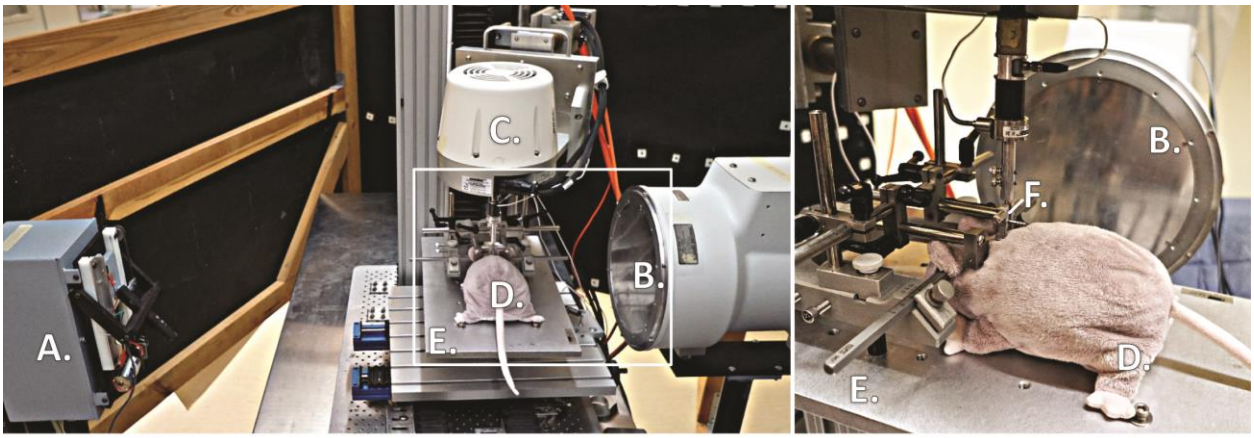

Figure 3-5 - Experimental setup of the UBC multi-mechanism SCI device within the x-ray system. A. X-ray source. B. X-ray image intensifier. C. Electromagnetic actuator. D. Rat (model). E. Stereotaxic frame. F. Dislocation injury clamps.

The x-ray video distortion was corrected using an open source x-ray undistortion algorithm (Brainerd et al., 2010) within Matlab (The Mathworks 2012b 32-bit, Matick, MA) and denoised using custom verified 3D curvelet denoising software developed with the open source CurveLab toolkit (V2.0, curvelet.org, Candès et al., 2006). The motion of the fiducial markers attached to each vertebra and clamp was semi-automatically tracked using TEMA (Version 3.0, Image Systems AB, Linköping, Sweden) to determine the translation and rotation. Images were scaled based on a known dimension in the image plane, and the dorsoventral motion axis was aligned with the caudal clamp. A low-pass Butterworth filter with cutoff frequency of 1250 Hz was applied to the motion data to reduce the high-frequency x-ray image noise, and translation and rotation was calculated from the markers on each rigid body (clamps and vertebrae) throughout the injury.

The dislocation displacement was compared for both injury clamps for each available measurement: the prescribed actuator motion, the linear variable differential transformer (LVDT) recorded actuator motion, and motion tracking of the caudal clamp, C5, and C5 with respect to C4. Example images of dislocation injuries with each clamp are shown in Figure 3-6. The maximum relative anterior-posterior motion of C5 with respect to C4 was averaged for each clamp and compared using Levene's test for the homogeneity of variances to determine if the clamps had significantly different variability. Motion of C4 with respect to the rostral clamp and C5 with respect to the caudal clamp in both translation and rotation were analysed. Maximum

absolute relative motion values between the vertebrae and clamps were averaged for each case, and an unequal-variance t-test was performed to determine if differences were significant between the clamps. Additionally, the combined rotation of C4 and C5, which represents the integrity of the spinal canal, was plotted and evaluated for significant difference between the clamps.

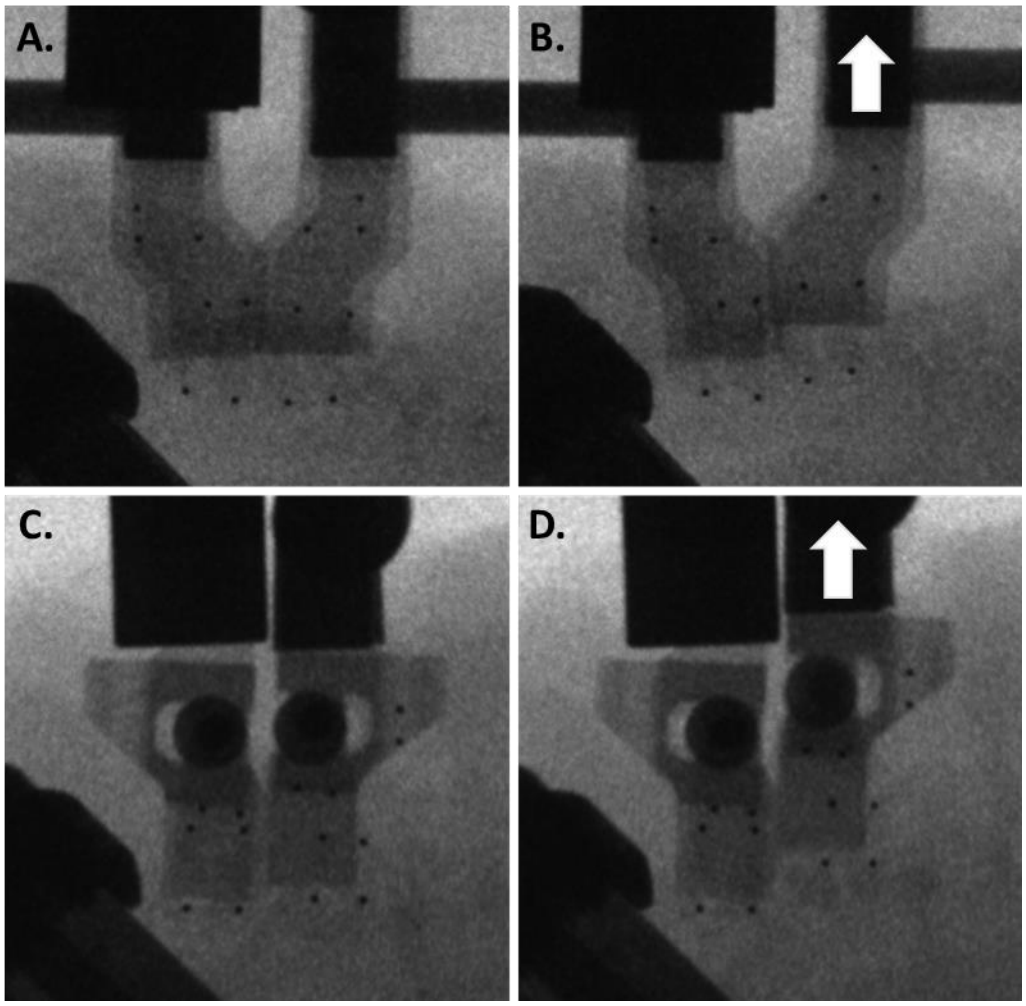

Figure 3-6 – Example images from dislocation injuries from both clamps. A. Existing clamp pre-dislocation. B. Existing clamp post-dislocation. C. Self-aligning clamp pre-dislocation. D. Self-aligning clamp post-dislocation. Fiducial markers have been enhanced for clarity.

3.3 Results

The measurement of vertebral kinematics using high-speed x-ray demonstrated that the dislocation displacement experienced by the spine was less than what was measured at the

LVDT for both clamps (Table 3-2). For the existing clamps, the motion of the actuator as measured by the LVDT was 2.31 mm (SD: 0.09) and the motion tracking of the caudal clamp was 2.29 mm (SD: 0.11), while the dislocation experienced by the spine at C5 displacing relative to C4 was 1.93 mm (SD: 0.29). For the self-aligning clamps the actuator motion was 2.05 mm (SD: 0.06), the motion tracking of the caudal clamp was 2.02 mm (SD: 0.06), and the relative displacement of C5 with respect to C4 was 1.81 mm (SD: 0.10).

Table 3-2 - Dorsoventral motion during dislocation with the different injury clamps, as measured by the LVDT or motion tracking. The injury displacement as experienced by the vertebrae was reduced from the prescribed injury parameters in both cases. The reduction was larger and more variable in the existing injury clamps.

Dorsoventral Displacement	Existing clamps mm (SD)	Self-aligning clamps mm (SD)
Prescribed actuator motion	2.30	2.00
LVDT	2.31 (0.09)	2.05 (0.06)
Motion tracking: caudal clamp	2.29 (0.11)	2.02 (0.06)
Motion tracking: C5	2.09 (0.22)	1.98 (0.07)
Motion tracking: C5 w.r.t. C4	1.93 (0.29)	1.81 (0.10)

The translations of C5 with respect to C4 in the anterior-posterior direction during the dislocation test for all animals are shown in Figure 3-7. Of note is the rather narrow band of translation trajectories for the self-aligning clamps, in contrast to the wide variability in the tests with the existing clamps. There was no significant difference in variances between the different clamps for this parameter when compared using Levene's test for homogeneity of variances ($p = 0.08$). However, the standard deviation was almost threefold greater, and the range was 0.64 mm greater for the existing clamps (SD: 0.29, range: 1.05 mm) compared to the self-aligning clamps (SD: 0.10, range: 0.41 mm).

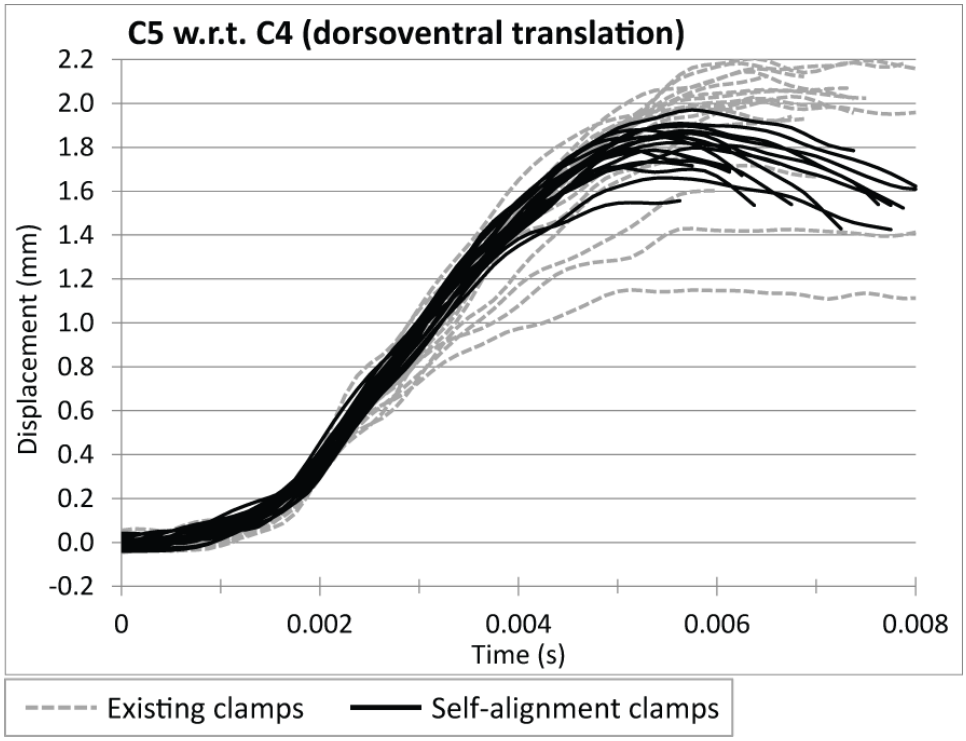

Figure 3-7 - The true measure of the dislocation injury parameter: motion of C5 with respect to C4. The existing clamps had a displacement range of 1.1 to 2.2 mm, while the self-aligning clamps had a range of 1.5 to 1.9 mm.

Relative motions between any vertebra and respective clamp in translation or rotation during the injury indicates slippage and were compared between the existing and self-aligning clamps using an unequal-variance t-test (Table 3-3, Figure 3-8). The relative motion of C5 with respect to the caudal clamp was significantly less ($p < 0.05$) for the self-aligning clamps: 0.09 mm (SD: 0.03) in translation and 1.56 degrees (SD: 0.54) in rotation, compared to 0.25 mm (SD: 0.17) and 4.85 (SD: 3.23) for the existing clamps. In translation, the eleven instances of greatest relative motion between both clamps occurred in the existing clamps (65% of tests), and in rotation, the fourteen instances of greatest relative motion occurred in the existing clamps (82% of tests). The motion of C4 with respect to the rostral clamp was not statistically different between the different clamps. The combined rotation of C4 and C5 was significantly reduced for the self-aligning clamps ($p < 0.05$). The maximum motion observed in the rostrocaudal direction for any case was 0.16 mm (C5 with respect to caudal clamp), so rostrocaudal motion was not investigated further.

Table 3-3 - Average of maximum, absolute relative motions between clamps and vertebrae.

		Existing clamps Mean (SD)	Self-aligning clamps Mean (SD)	P value
C4 w.r.t. rostral clamp	Y translation (mm)	0.11 (0.06)	0.11 (0.06)	0.95
	Rotation (degrees)	2.88 (1.50)	2.99 (1.82)	0.84
C5 w.r.t. caudal clamp	Y translation (mm)	0.25 (0.17)	0.09 (0.03)	0.001*
	Rotation (degrees)	4.85 (3.23)	1.56 (0.54)	0.001*
C4 + C5 combined	Rotation (degrees)	6.46 (4.64)	3.39 (1.71)	0.02*

*Relative motion between clamps was significantly different ($p < 0.05$)

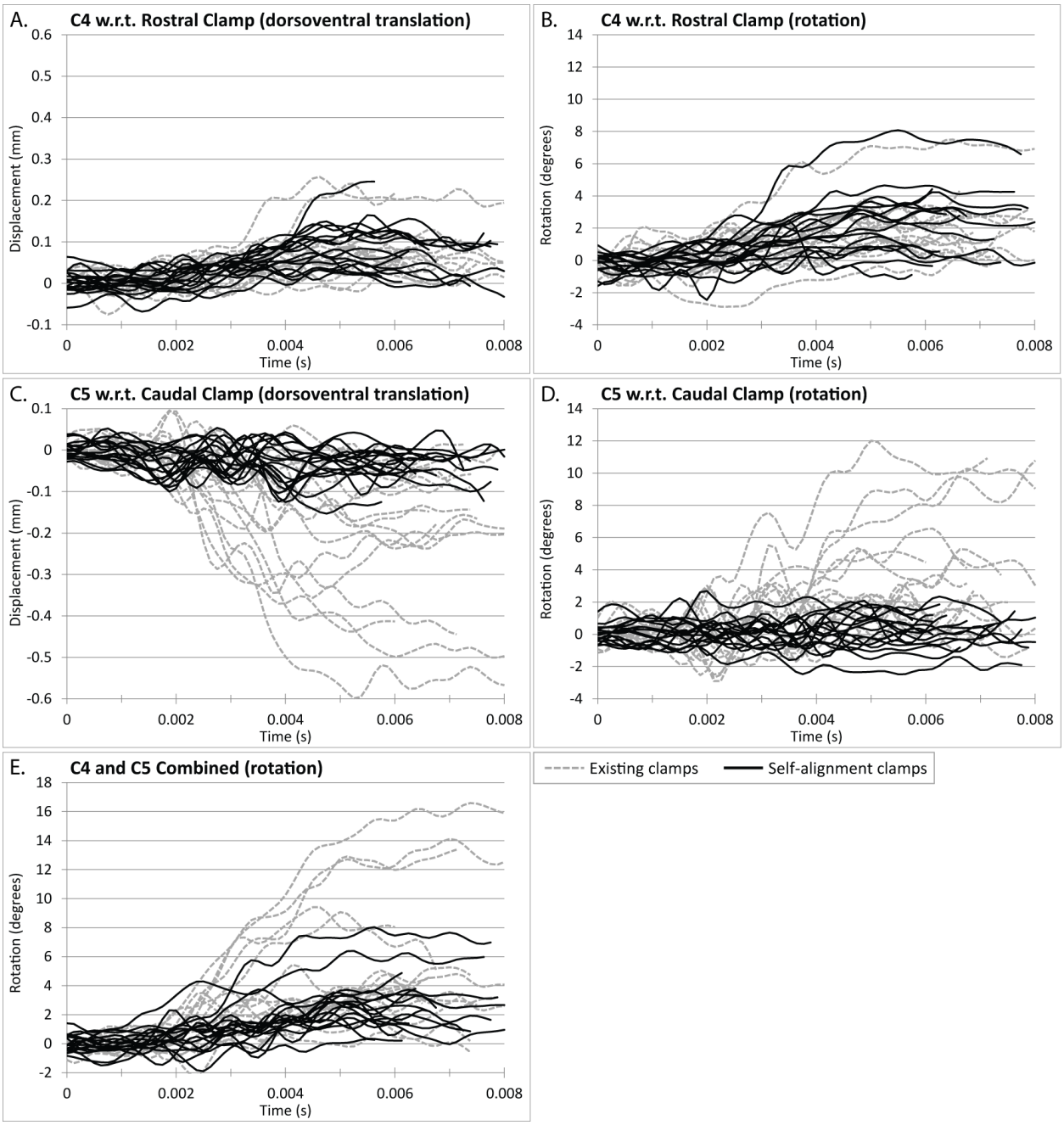

Figure 3-8 - Relative motion compared between existing clamps (grey dashed line) and self-aligning clamps (black solid line). Slipping at the rostral clamp interface was not significantly different between the clamps for both translation (A) and rotation (B). Slipping was most obvious at the caudal clamp interface, and was significantly greater in the existing clamps for both translation (C) and rotation (D). Importantly slipping only occurred in some instances with the existing clamps. The combined rotation of the two vertebrae experiencing the dislocation, C4 and C5: a measurement of maintained spinal canal integrity (E).

3.4 Discussion

To improve the biomechanical repeatability of a rat dislocation SCI model, vertebral injury clamps were redesigned to pivot and self-align to better hold the complex vertebral anatomy. Fiducial markers were attached to the rat vertebrae and the injury clamps, and images were collected via high-speed x-ray to measure the intervertebral kinematics during a dislocation injury. This was the first time high-speed motion of the vertebrae with respect to the clamps has been measured in a dislocation model. The relative motion was significantly reduced for the self-aligning clamps compared to the existing clamps between C5 and the caudal clamp. Of note however, was the inconsistency of the existing clamps: occasionally holding the vertebrae rigid, and occasionally slipping.

A closed-column model of SCI where the injury is induced by relative motion of the vertebrae does not provide information on the loading conditions of the spinal cord, and until now, the kinematics of the vertebrae were also unknown. This study validates a method for measuring vertebral kinematics, and emphasizes the importance of ensuring rigid connections between gripping interfaces in biomechanical testing to avoid relative motion. Considering the difficulty in modeling human traumatic SCI (Filli & Schwab, 2012), and progress of recent models (Cheriyan et al., 2014), similar methods could be adopted by other researchers to validate other closed-column injury models (Dabney et al., 2004; Fiford et al., 2004; Seifert et al., 2011).

The different widths of adjacent vertebrae identified the weakness of the original injury clamps' inability to grip both vertebrae, and provided the primary design requirement of the new clamps: the ability to grip vertebrae of different widths. The implementation of a saddle washer against a rounded outer clamp surface allowed the clamp arms to self-align when tightened, providing a rigid grip of both intended vertebrae. These results help to identify and solve a potential cause of the variability present in the histological and behavioural outcomes in the dislocation model. Kinematic variability in the injury has been significantly reduced, and further studies can be conducted with confidence that injury device parameters correlate to displacements experienced by vertebrae.

This study identifies a major concern in the advancement of clinically relevant closed-column SCI models: the kinematics of the vertebrae are challenging to control with precision, and

variability of injury parameters may be present until verified. Spinal cord injury parameters are often defined as the displacement of the actuator. In existing closed-column models, actuator-based displacement measures are often the only measurement of injury displacement available. However, in reality the displacement imparted to the spinal cord is the relative displacement of the injury-causing vertebra, where if either vertebra slips, the injury displacement will be less than the device-measured displacement. This was verified when comparing measurements from the LVDT to motion tracking of the vertebrae (Table 3-2), and emphasizes the importance of validating a rigid actuator-vertebrae connection. A small amount of slipping was still present at the C4-clamp interface for the self-aligning clamps, indicating the clamp geometry could potentially be further optimized. This was not considered a major concern, given the significant reduction of slipping in both translation and rotation at the C5-clamp interface with the self-aligning clamps.

One of the most interesting measurements in the dislocation model is the combined rotation of C4 and C5. If both vertebrae rotate, they remain open, maintaining the integrity of the canal creating an ‘open pipeline’, instead of shearing or pinching the spinal cord between a narrow opening, as seen clinically (Figure 3-9). The summation of small amounts of slippage at multiple interfaces, typically undetected by the user, could potentially lead to less severe injuries than expected with prescribed injury parameters.

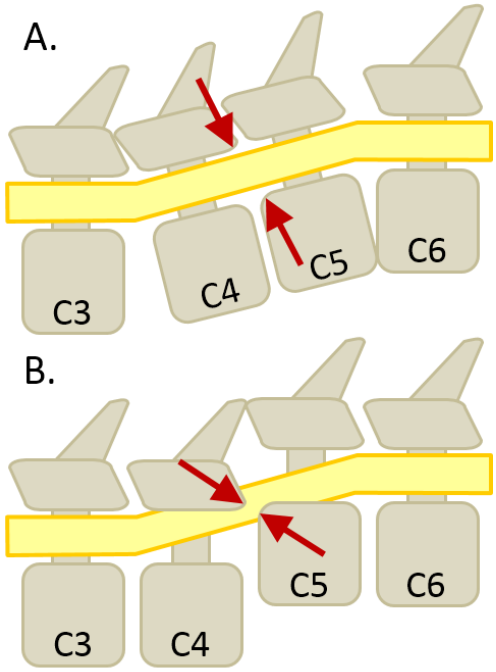

Figure 3-9 – A. When the vertebrae rotate at the site of the dislocation, the canal remains open, with no physical insult on the cord. B. When the vertebrae are restricted from rotation during the dislocation, the canal opening is reduced, causing a shearing or pinching force on the spinal cord.

Although the results were encouraging, in that slippage could be the potential cause of variability in previous studies, and is now reduced, there are limitations with this study. It is unknown if reducing the kinematic variability will correlate to reducing the histological and behavioural variability in the injury outcomes. Histological examination was planned for this study, however the severe nature of the injury resulted in variable biological time points post-injury. Some animals survived to the planned 15 minute time point post-injury, allowing the secondary injury cascade to progress, while some animals perished immediately. Behavioural outcomes were not possible as logistical limitations at our centre prevented any survival studies to be conducted in conjunction with the high-speed x-ray apparatus due to radiation exposure. Future studies with the validated clamps will include these outcomes.

The injuries using the existing clamps were prescribed to 2.3 mm, while the self-aligning clamps were prescribed to 2.0 mm. The existing clamp dislocation was prescribed to 2.3 mm to exaggerate any relative motion as it was unknown if motion would be obvious. However, this produced a very severe injury. Since the self-aligning clamps were expected to hold the vertebrae

with more rigidity, thus increasing severity, the injury depth was reduced to 2.0 mm. The 15% reduction in injury depth is not considered a significant cause of the reduction in relative motion.

3.5 Conclusions

This study has clearly demonstrated the significance of validating vertebral kinematics in a closed-column SCI model, as relative motion (or slippage) was occasionally present between the existing dislocation injury clamps and the vertebrae. By redesigning the injury clamps to pivot and self-align during attachment, relative motion between the vertebrae and injury clamps has been significantly reduced, and thus produced more repeatable spine kinematics during injury. These improvements will serve to address a potential source of variability in the injury model and progress toward a more repeatable rat dislocation model. Refinement of the dislocation model, which closely approximates the most common and severe clinical SCI mechanism, will provide robust avenues for evaluating treatments, and deepen biomechanical understanding of neural tissue response and injury as a result of mechanical loading.

Chapter 4: The Development of a Cervical Dislocation Spinal Cord Injury Rat Model with Residual Compression

4.1 Introduction

Traumatic spinal cord injury (SCI) is a devastating injury often resulting in significant physical, social and financial impact on individuals (Ackery et al., 2004; Krueger et al., 2013; Sekhon & Fehlings, 2001). SCI occurs in a heterogeneous manner, at different spinal levels, by different injury mechanisms, and to varying degrees of severity (Filli & Schwab, 2012; Tator, 2006). Following an initial dynamic trauma event, the spinal cord often remains compressed by surrounding bone fragments and tissue (Dumont et al., 2001), which is often termed 'residual compression'. The appropriate timing of the following surgical decompression intervention remains controversial (Cadotte & Fehlings, 2011; Fehlings & Wilson, 2010; Furlan et al., 2011; Wilson, et al., 2012B), and further work is needed to determine which patients stand to benefit the most from earlier decompression (Fehlings et al., 2012; Wilson, et al., 2012B).

Preclinical residual compression studies have demonstrated the effectiveness of early decompression on improving neuorological outcomes (Carlson, et al., 1997A, 2003; Delamarter et al., 1995; Dimar et al., 1999; Dolan et al., 1980; Guha et al., 1987; Rabinowitz et al., 2008). However, these results do not correspond to clinical evidence. Reviews on clinical surgical decompression indicate that the neurological benefits remain inconclusive (van Middendorp et al., 2013; Yousefifard et al., 2016); some patients benefit from early decompression while others do not. This discrepancy warrants further research into the factors that contribute towards determining which patients may see greatest benefits from early decompression.

Differences between experimental and clinical results may be due to pre-clinical models not closely resembling the wide range of biomechanical factors seen in human injuries, such as spinal level, injury mechanism, velocity of spinal cord impact, and method of residual compression. Only one previous study investigated residual compression in the cervical spine (Guha et al., 1987), the region where more than 50% of human SCIs occur (Chen et al., 2016B). Dislocation is the most common injury mechanism, occurring in 32 – 58% of SCI cases (Sekhon & Fehlings, 2001; Tator, 1983; Tator et al., 1987; Vaccaro et al., 2016; Wilson et al., 2013); however, a residual compression experiment has never been conducted with this injury model. A

cervical dislocation SCI with residual compression would represent a unique pre-clinical model and may help to explain the discrepancy between experimental and clinical results. However, implementing a model with such clinical similarities is challenging (Filli & Schwab, 2012). The parameters that need to be defined for a dislocation residual compression injury model are: velocity of initial injury, peak displacement of initial injury, residual compression displacement, and timing of residual compression.

Traumatic SCI is caused by a high-energy, dynamic event, while most experimental studies have involved slow compression (Carlson et al., 1997A, 1997B, 2000, 2003; Delamarter et al., 1991, 1995; Dolan et al., 1980; Guha et al., 1987; Ouyang et al., 2009). Studies have demonstrated the sensitivity of the spinal cord to impact velocity (Kearney et al., 1988; Lam et al., 2014; Sjovold et al., 2013; Sparrey et al., 2008), and canal occlusion has been measured at velocities up to 5 m/s in ex vivo head impacts (Saari et al., 2011). The only studies to investigate the timing effects of residual compression with a high-rate injury model placed a shim within the spinal canal following a contusion injury (Dimar et al., 1999; Shields et al., 2005). Prior to shim placement, however, there was a period of time when the spinal cord was uncompressed, at a potentially critical acute time point for the onset of secondary injury cascades.

Closed-column SCI models like dislocation resemble human injuries as they rely on the relative movement of vertebrae to injure the spinal cord. Similarly, a closed-column residual compression model more closely mimics human injuries compared to other common techniques such as force clips (Guha et al., 1987; Rivlin & Tator, 1978), or circumferential nylon cables (Delamarter et al., 1991, 1995; Rabinowitz et al., 2008). However, closed-column models have the distinct limitation of the inability to visualize the spinal cord or directly measure spinal cord compression, making it challenging to determine appropriate residual compression displacements. Therefore, an outcome measure to evaluate closed-column dislocation displacements could identify appropriate parameters. Somatosensory evoked potentials (SSEPs) are sensitive to minor spinal cord insults (Agrawal et al., 2009) and provide immediate details on the ability of the spinal cord to conduct signals (Cloud et al., 2012). Previous spinal cord residual compression models have used SSEP amplitude to determine adequate compression levels, where increased compression resulted in a reduction of signal amplitude (Carlson et al., 1997A, 1997B, 2000, 2003). This technique provides an opportunity to evaluate the effect of varying

residual compression displacements in a closed-column model, and to determine the significance of residual compression immediately following traumatic SCI. Additionally, establishing a relationship between animal weight and spinal canal diameter could allow for injury parameter control based on canal occlusion ratios, allowing for better comparisons to human injuries.

Any new SCI model must be characterized to determine the relationship between injury parameters (i.e. displacement or force) and severity. Our previous dislocation injury model typically produced severe injuries (potentially reaching humane endpoint), so the survivability of a dislocation injury with added residual compression remains unknown. A defined dislocation displacement which consistently produces a mild injury would allow for future studies to investigate the effects of timing of residual compression. A residual compression time of 4 hours compared to shorter time points has demonstrated significant effects in a rat clip compression model (Guha et al., 1987). Therefore, in order to make meaningful timing comparisons, rats must be able to survive 4 hours of residual compression following a traumatic dislocation injury.

The overall objective of this study was to develop a rat dislocation spinal cord injury model with immediate residual compression, with the following specific aims:

i. Determine the minimum residual compression depth that affects spinal cord signal conduction following traumatic dislocation SCI;
ii. Determine the acute effect on spinal cord signal conduction following dislocation SCI, with and without immediate residual compression;
iii. Determine if 4 hours of residual compression following a dislocation injury is survivable;
iv. Establish the behavioural outcome sensitivity to different dislocation depths using validated injury clamps; and
v. Determine the relationship between rat weight at time of injury and spinal canal geometry to better inform closed-column injury models.

4.2 Methods

4.2.1 Experimental Overview

Several experimental groups were required to investigate the specific aims. An experimental overview (Figure 4-1) shows how each group contributed to each objective. All procedures were

approved by our institution's Animal Care Committee in accordance with the guidelines published by the Canadian Council on Animal Care.

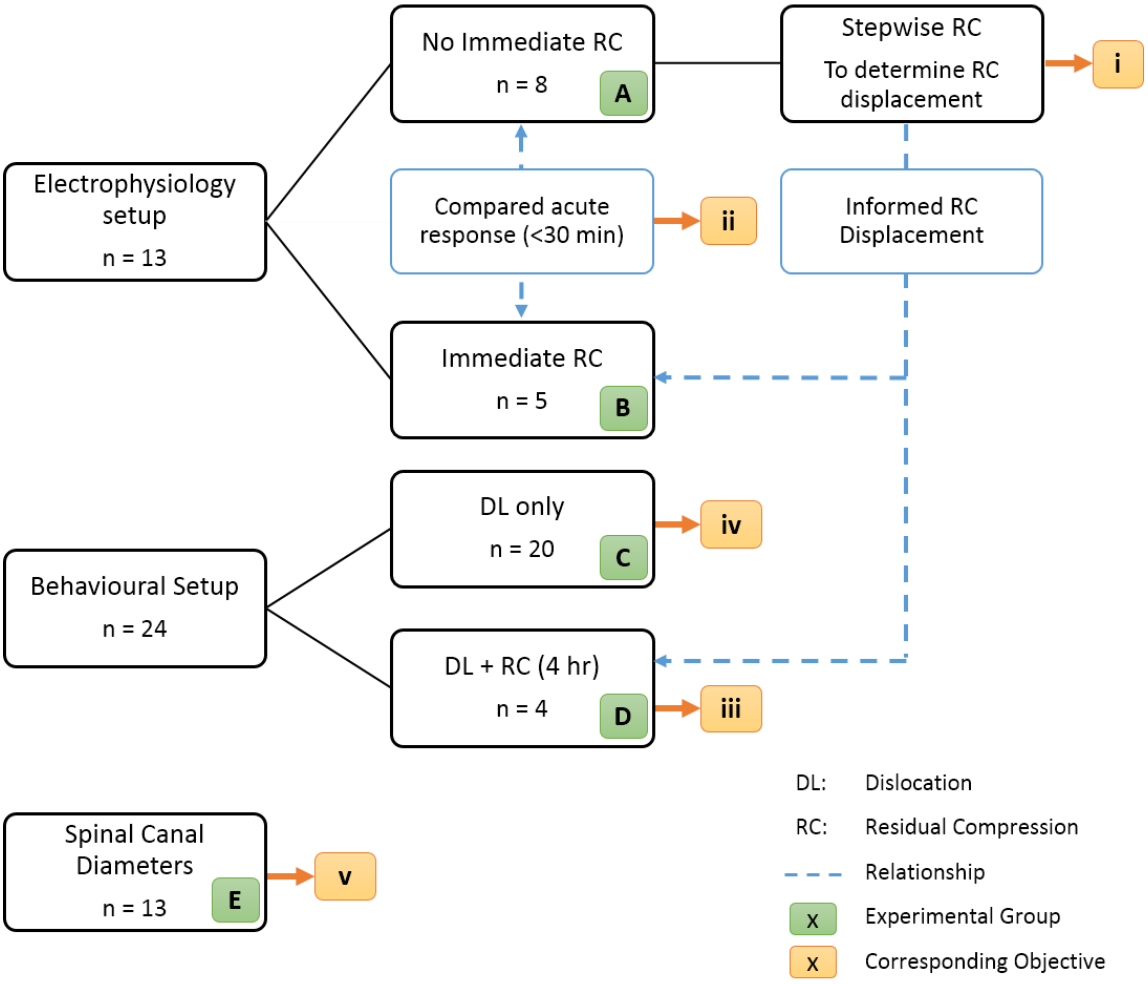

Figure 4-1 - Experimental overview flowchart. Experimental groups are identified by letters, and corresponding objectives by roman numerals. Dashed lines indicate relationships. The results from objective i. informed the injury parameters for groups B and D. The results from groups A and B were compared to determine the effect of immediate residual compression (objective ii).

4.2.2 Electrophysiology Setup and Dislocation Injury

Male Sprague-Dawley rats (n = 13, mean weight 368 g SD: 39 g) were deeply anesthetized (urethane, 2 g/kg), and were kept warm between 36 – 37 °C on a heating pad, while temperature, heart rate and blood oxygenation were monitored throughout surgery and injury procedures. The spine was surgically exposed, and a facetectomy was performed at the dislocation spinal level

(C5/C6). Custom validated vertebral injury clamps which pivot and self-align (see Chapter 3 of this thesis; Mattucci et al., 2017) were attached to the C4/C5 and C6/C7 vertebrae. The skull was exposed, and one hole was drilled 2.5 mm posterior and 2.8 mm laterally from Bregma, on the left side of the skull. Another hole was drilled 3.0 mm to the right of lambda to serve as an intracranial reference, and a grounding wire was inserted into the adjacent musculature (Bazley et al., 2012) (Figure 4-2). Transcranial screw electrodes were implanted to lightly contact the dura mater, and measure contralateral signals as stimulated from the surgically exposed sciatic nerve of the right hindlimb (Cloud et al., 2012). The sciatic nerve was stimulated at an intensity of four times greater than initial twitch threshold (60 – 260 mA), for a duration of 200 μs, and at a frequency of 0.5 Hz. SSEP recordings were collected during the entire procedure and averaged over four-minute intervals. The SSEP magnitude was defined as the greatest peak-to-peak amplitude of the signal, and latency was the time from stimulation to peak amplitude.

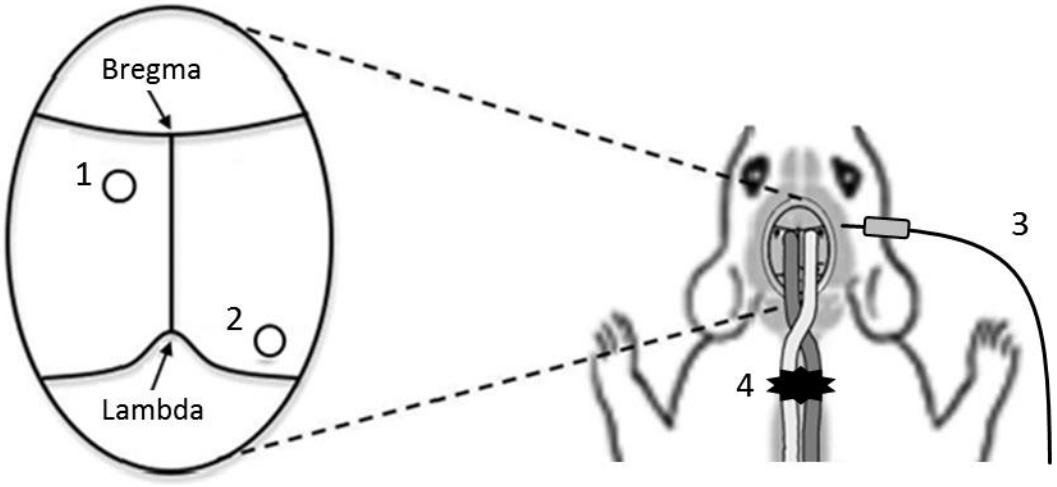

Figure 4-2 - Somatosensory evoked potential electrode placement in skull for measurements of signals initiated at the sciatic nerve of the right hindpaw. Numbers correspond to: right hindlimb region of the cortex electrode (1), reference electrode (2), ground electrode (3), and dislocation injury at C5/C6 (4). Image adapted from Bazley et al., 2012, J Neurosurg.

The rostral clamp was rigidly secured to a customized stereotaxic frame, and the caudal clamp attached to the UBC multi-mechanism SCI device (Choo et al., 2007) (Figure 4-3). Recordings were allowed to reach steady state (three consecutive signal amplitudes over 12 minutes within 10%) prior to injury. The actuator applied a 3 N dorsal preload to the caudal clamp to provide consistent starting tension between animals. The caudal clamp was dislocated dorsally to a peak

displacement of 1.0 mm at 410 mm/s, then either reduced completely (Group A, n = 8) or held at 0.8 mm (Group B, n = 5).

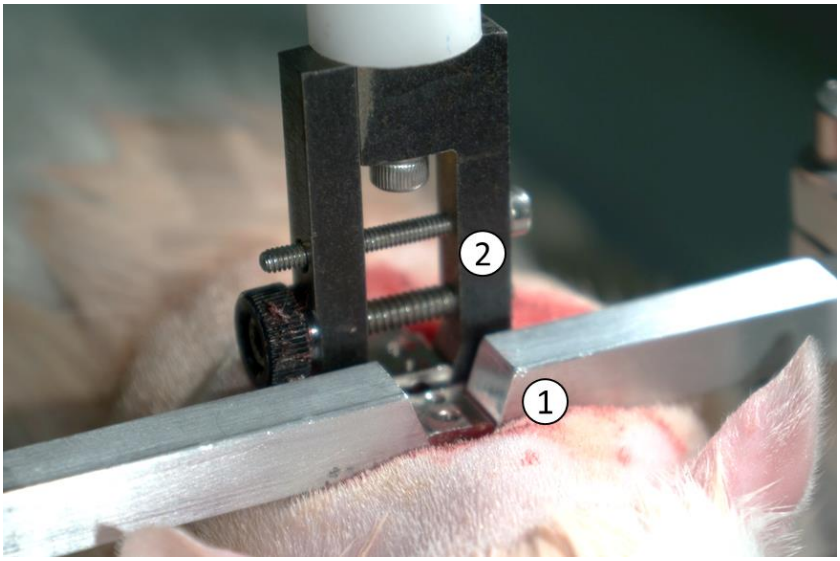

Figure 4-3 - The rostral clamp was held rigid by a custom stereotaxic frame (1), while the UBC multi-mechanism actuator tip was secured to the caudal clamp (2) prior to dorsal dislocation.

4.2.3 Electrophysiology Tests

Following the initial traumatic injury the signal was allowed to stabilize (three consecutive SSEP recordings within 10%), before incremental displacement steps were applied to determine the minimum displacement to affect spinal cord signals (Group A). We hypothesized that signals would remain unchanged until the spinal cord experienced compression (Figure 4-4). The caudal clamps were displaced at 0.5 mm/s to 0.6 mm to apply the first residual compression step. After 30 minutes at 0.6 mm, the displacement was reduced back to 0 mm and held until the signal became steady, as a precaution to avoid a delayed response to the previous compression step. The caudal clamp was then displaced to 0.7 mm, an incremental increase of 0.1 mm, held for 30 minutes, before being reduced to 0 mm again. This procedure was repeated for 0.8, 0.9 and 1.0 mm compression levels. The displacement to cause the SSEP signal amplitude to drop below 50% of baseline was defined to sufficiently compress the spinal cord. The 50% of baseline level is widely adopted as the threshold for injury (American Electroencephalographic Society, 1994; Nuwer et al., 1993). These depths were compared between animals to determine the minimum threshold for residual compression.

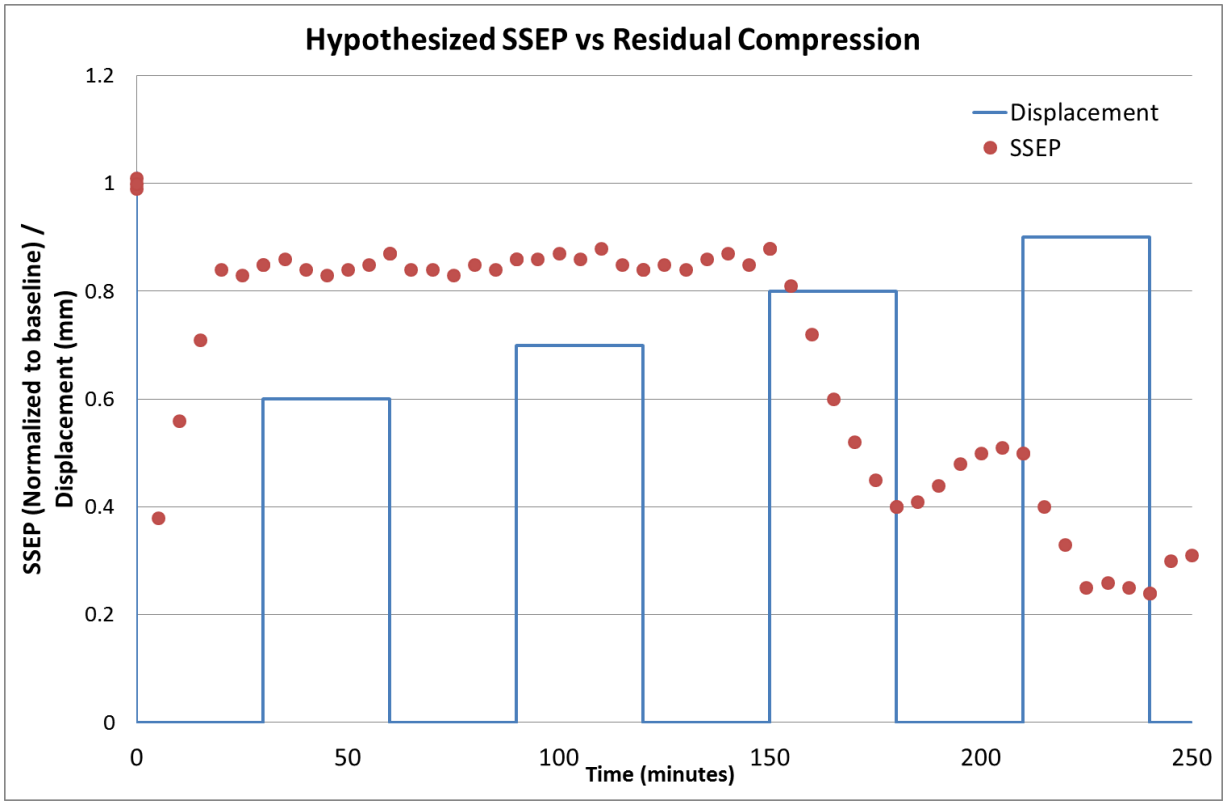

Figure 4-4 - Incremental displacement step approach, with hypothesized SSEP response. The SSEP signal was expected to drop due to the initial trauma at 0 seconds, and remain unaffected if the spinal cord was not compressed by the incremental displacement steps. When displacement of the caudal vertebrae was sufficient to compress the spinal cord, the SSEP would drop below 50% baseline, in this case at 0.8 mm. The signal was allowed to reach a steady state of three consecutive amplitudes within 10% before applying the next step increment. Steps were continued to a maximum of 1.0 mm to determine if further displacement resulted in further signal reduction.

To determine the effect of immediately held residual compression on SSEP signals (Group B), following the initial 1.0 mm traumatic dislocation, the caudal clamps were immediately reduced to and held at 0.8 mm (based on results from Group A). Average response was compared at each 4 minute time interval up to 30 minutes post injury between Group A (no compression) and Group B (residual compression) using a Student's t-test ($p < 0.05$).

4.2.4 Behavioural Outcome Sensitivity and Survivability with Residual Compression

Twenty-four male Sprague-Dawley rats were handled three times per week for two weeks prior to injury. The Martinez open field locomotor rating scale (Martinez et al., 2009) was used to

verify animals did not have any dysfunctional movements prior to injury. The Martinez scale assesses function of forelimb and hindlimb articulations, weight support, digit position, stepping coordination between forelimb and hindlimb, and tail position while the rat is free to walk in an open field arena.

Rats were an average weight of 312 g (SD: 16 g) at the time of surgery. Animals were anesthetized with inhalational isoflurane (1.5 – 3% / L O2), and their backs were shaved and disinfected. Analgesics of 0.25% Marcaine (0.3 mL subcutaneous at incision site), and buprenorphine (0.05 mg/kg) and Ringer's lactate (10 mL) were injected subcutaneously, and Lacrilube ophthalmic ointment was applied to the eyes to prevent drying. Animals were kept warm between 36 – 37 °C on a heating pad, while temperature, heart rate and blood oxygenation were monitored throughout surgery and injury procedures. The spine was surgically exposed, and a facetectomy was performed at the dislocation spinal level (C5/C6). Injury clamps were attached to the C4/C5 and C6/C7 vertebrae, and the rostral clamp was rigidly secured to a customized stereotaxic frame, and the caudal clamp attached to the actuator. Dislocation injuries were produced at displacements between 0.81 mm (290 mm/s) and 1.66 mm (555 mm/s) with no residual compression (Group C, n = 20). Differences were due to the maximum possible velocity within the actuator stroke length. Dislocation injuries were produced to 1.39 mm (SD: 0.03) at 480 mm/s (SD: 21 mm/s), followed by immediate residual compression at 0.8 mm and held for 4 hours (Group D, n = 4).

Post-injury, or post-reduction of the residual compression, the vertebral clamps were fixed together to stabilize the spine (Speidel, 2017) (Figure 4-5), musculature and skin were sutured with the fixed-clamps remaining in the animals, and animals were placed in an incubator (37 °C) until consciousness was fully regained. Animals were housed singly for three days post injury, with access to regular food, sugared cereal, water and hydrogel if needed. Three doses of buprenorphine (0.05 mg/kg) and Ringer's lactate (10 mL) were given subcutaneously for three days post injury, and Ringer's lactate was continued if animals exhibited signs of dehydration. Animals were tested for open-field behaviour by two trained observers at days 4, 7, 14, 21, 28, 35, and 42 days post injury.

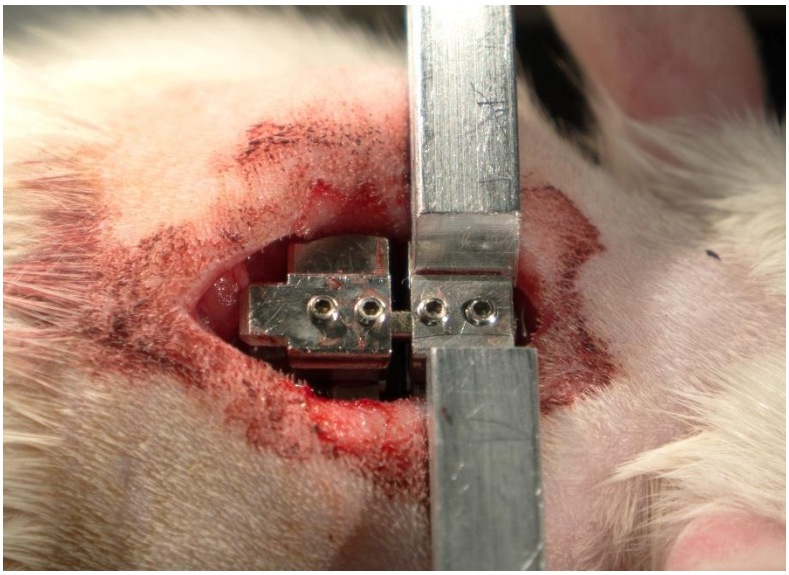

Figure 4-5 - Vertebral clamps fixed together post injury. The clamps have a longitudinal hole where a fixation bar can be held in place by four set screws. (Speidel, 2017)

4.2.5 Relationship Between Rat Weight and Spinal Canal Geometry

Male Sprague-Dawley rats (310 – 372 g) were sacrificed at time of injury for spinal canal measurements (Group E, n = 13). The soft tissue was dissolved from the cervical spines (5% solution of NaOH) (Onwuama et al., 2012). The dorsoventral and lateral diameters of the C5 and C6 spinal canals were measured with digital calipers. Both diameter measurements were used to approximate the spinal canal area as an ellipse (Panjabi et al., 1991). A bivariate Pearson correlation ($p < 0.05$) was used to determine significant correlations between animal weights and spinal canal measurements.

4.3 Results

4.3.1 Electrophysiology

To determine a minimum residual compression depth, seven of eight animals exhibited a SSEP amplitude signal drop to below 50% baseline at the 0.8 mm incremental step or lower (Group A). Four animals had signals drop below 50% baseline at 0.6 mm, one at 0.7 mm, two at 0.8 mm, and one rat never had signals drop below 50% (Figure 4-6). Immediately following the initial peak displacement dislocation injury, five of the eight rats briefly lost SSEP response entirely, while the other three were unaffected (Figure 4-7). The stepwise progression caused SSEP

amplitude response to vary, and sometimes increase above baseline. All eight animals had signals return prior to the first residual compression step. When the dislocation displacement was immediately held at 0.8 mm following initial injury (Group B), no SSEP signal amplitudes dropped below 86% baseline, and three of five increased above baseline (Figure 4-7). The average normalized SSEP signal amplitude was significantly different between Group A (no compression) and Group B (residual compression) at each time point post-injury ($p < 0.05$). There was no effect on signal latency for Groups A or B.

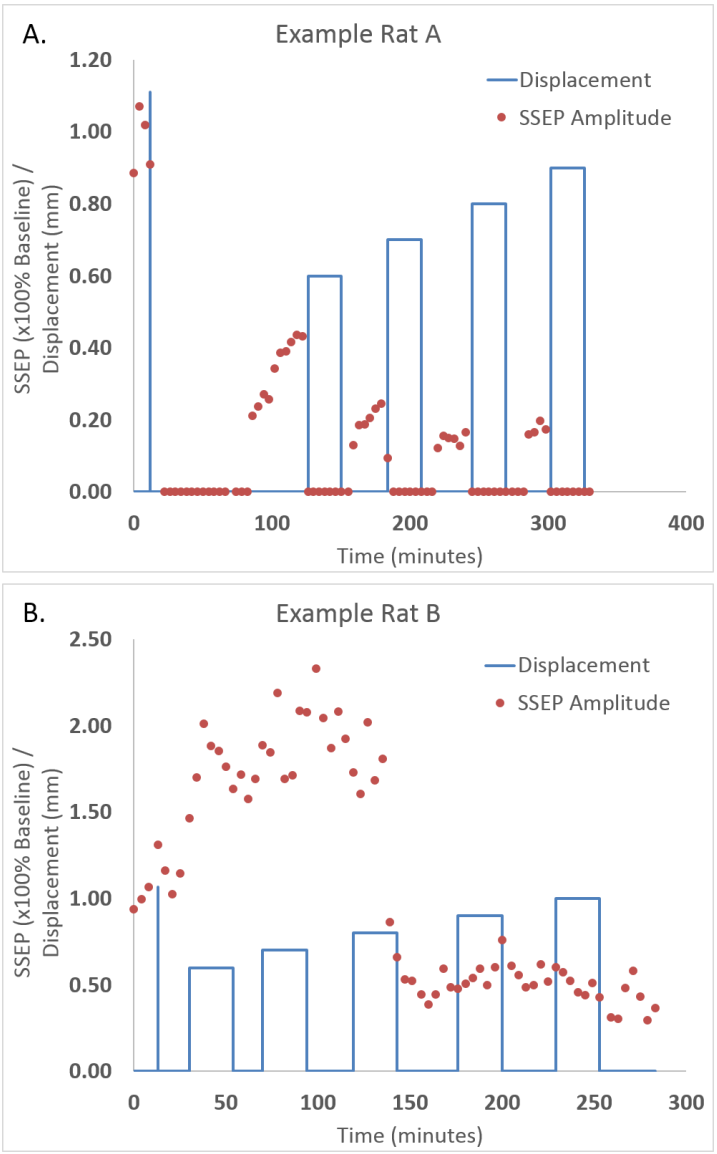

Figure 4-6 – These two examples of SSEP recordings from animals during the incremental stepwise displacement testing represent both extremes of the results. Example Rat A: Signal was absent for 94 minutes post-injury before returning and stabilizing at approximately 45% of baseline signal. Signal disappeared immediately at each incremental step level. Example Rat B: Signal increased briefly following injury then returned to baseline before continuing to increase during the incremental displacements until a displacement of 0.8 mm was reached, where the signal dropped below 50% baseline and remained steady throughout the following incremental steps.

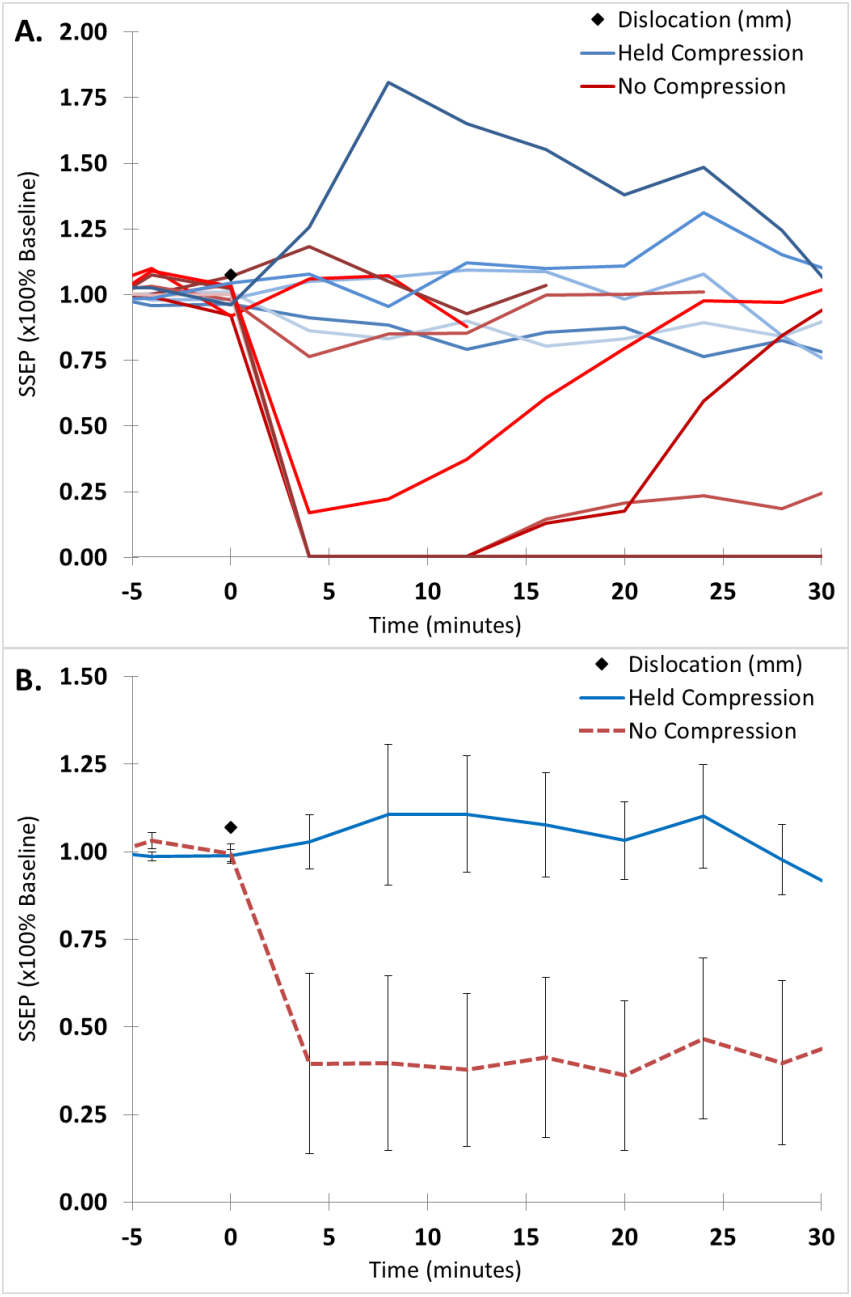

Figure 4-7 - Comparison of initial 30 minutes post-injury of animals with no compression (Group A, red) and held compression (Group B, blue). A. Individual comparisons: five of eight animals no compression had signals immediately drop following initial injury (four were absent), where only two animals with compression had signals drop in the first 30 minutes, and neither below 86% baseline. B. Combined group comparisons: The no compression and held compression groups were statistically significantly different at each time point post-injury ($p < 0.05$). Note: signals from animals in the no compression group were not included once the incremental step procedure began.

4.3.2 Behavioural Outcome Sensitivity and Survivability with Residual Compression

The duration of the dislocation injury for Group C animals (dislocation only) lasted approximately 15 ms, and residual compression was sustained immediately following the initial traumatic displacement for Group D animals (dislocation with residual compression) (Figure 4-8).

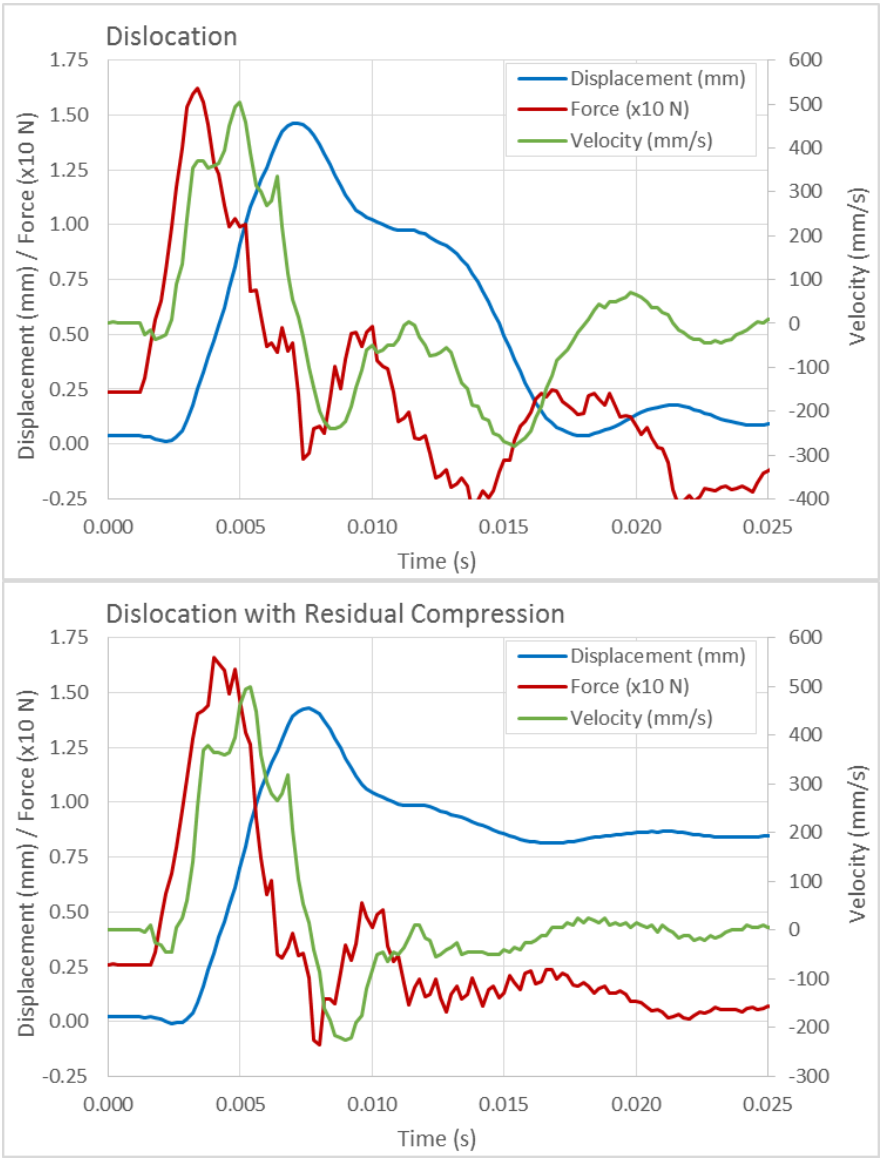

Figure 4-8 – Typical injury-time curves for dislocation injuries with and without residual compression. Unfiltered displacement (mm), force (N), and velocity (mm/s) signals are shown. All data were sampled at 5000 Hz. Velocity was calculated based on displacement signal.

Behavioural outcome scores decreased with increasing dislocation displacement at each time point post-injury (Figure 4-9), however there was wide variability (Group C). A threshold displacement of 1.450 mm consistently produced obvious functional deficits over the initial week post-injury in all animals, and Martinez scores did not recover beyond 35 at 7 days post injury in all animals injured above this threshold. One injury at a displacement of 1.656 mm resulted in immediate death. No animals obtained an 'uninjured' score of 40 on the Martinez open field test on day 4. All four animals with four hours of additional residual compression survived through the six week duration of the study (Group D, diamond outline points in Figure 4-9).

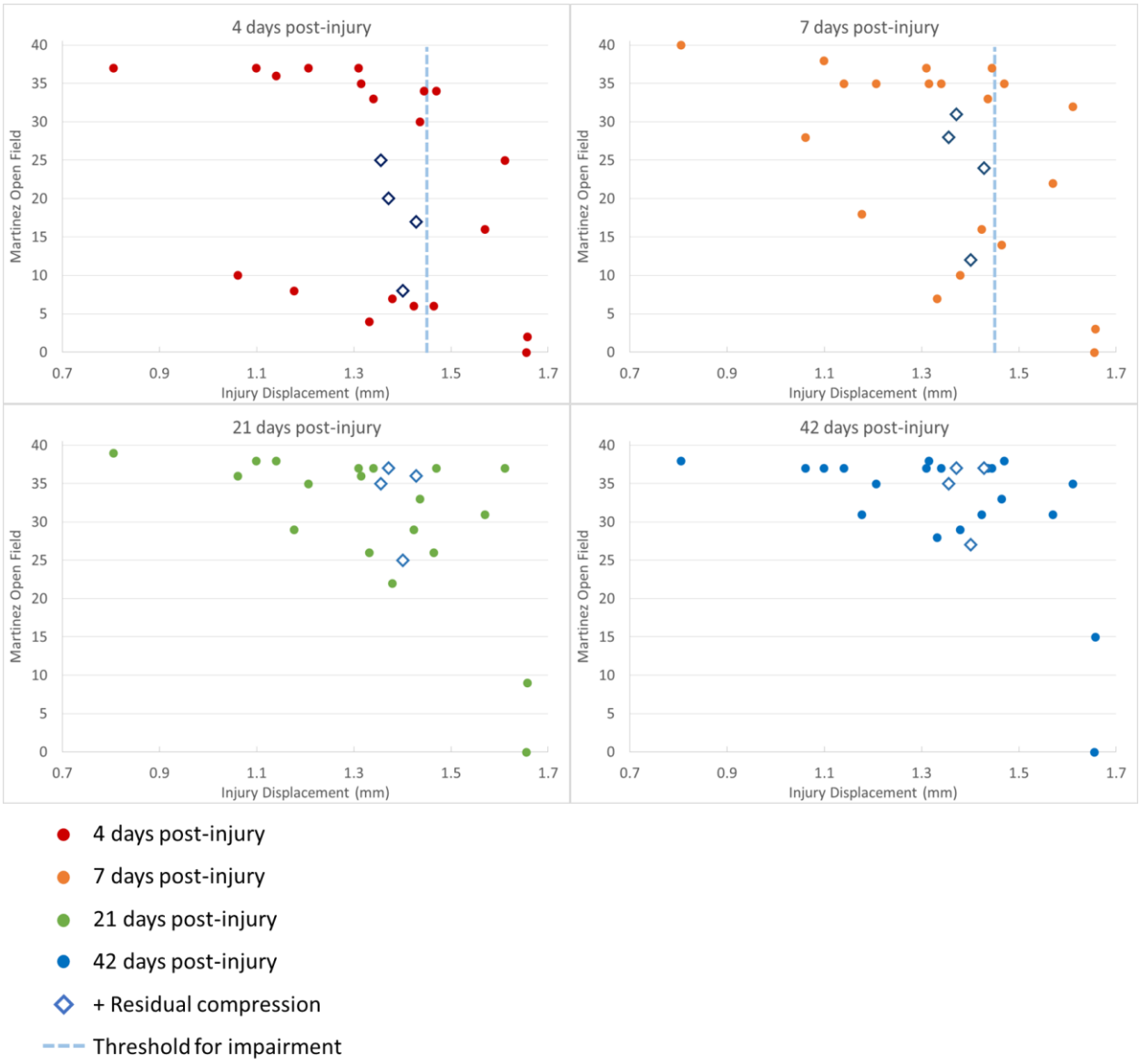

Figure 4-9 - Martinez open field locomotion scores for varying displacement dislocation injuries. Injury severity and variability tended to increase with increased dislocation displacement, and all injury severities demonstrated recovery over the 42 day time period. Circles represent dislocation only, and diamond outlines represent dislocation with 4 hours of residual compression at 0.8 mm.

4.3.3 Relationship Between Rat Weight and Spinal Canal Geometry

The dorsoventral depth of the C5 spinal canal was larger than C6 in eleven of thirteen animals (Group E). There was no significant correlation between rat weight and spinal canal diameter for both the dorsoventral and lateral dimensions (Figure 4-10 A & B, Table 4-1). The largest

difference between canal measurements between animals was: 0.42 mm for C5 and 0.27 mm for C6 dorsoventral diameter, 0.56 mm for C5 and 0.58 mm for C6 lateral diameter, and 8.05 mm^2 for C5 and 6.46 mm^2 for C6 area.

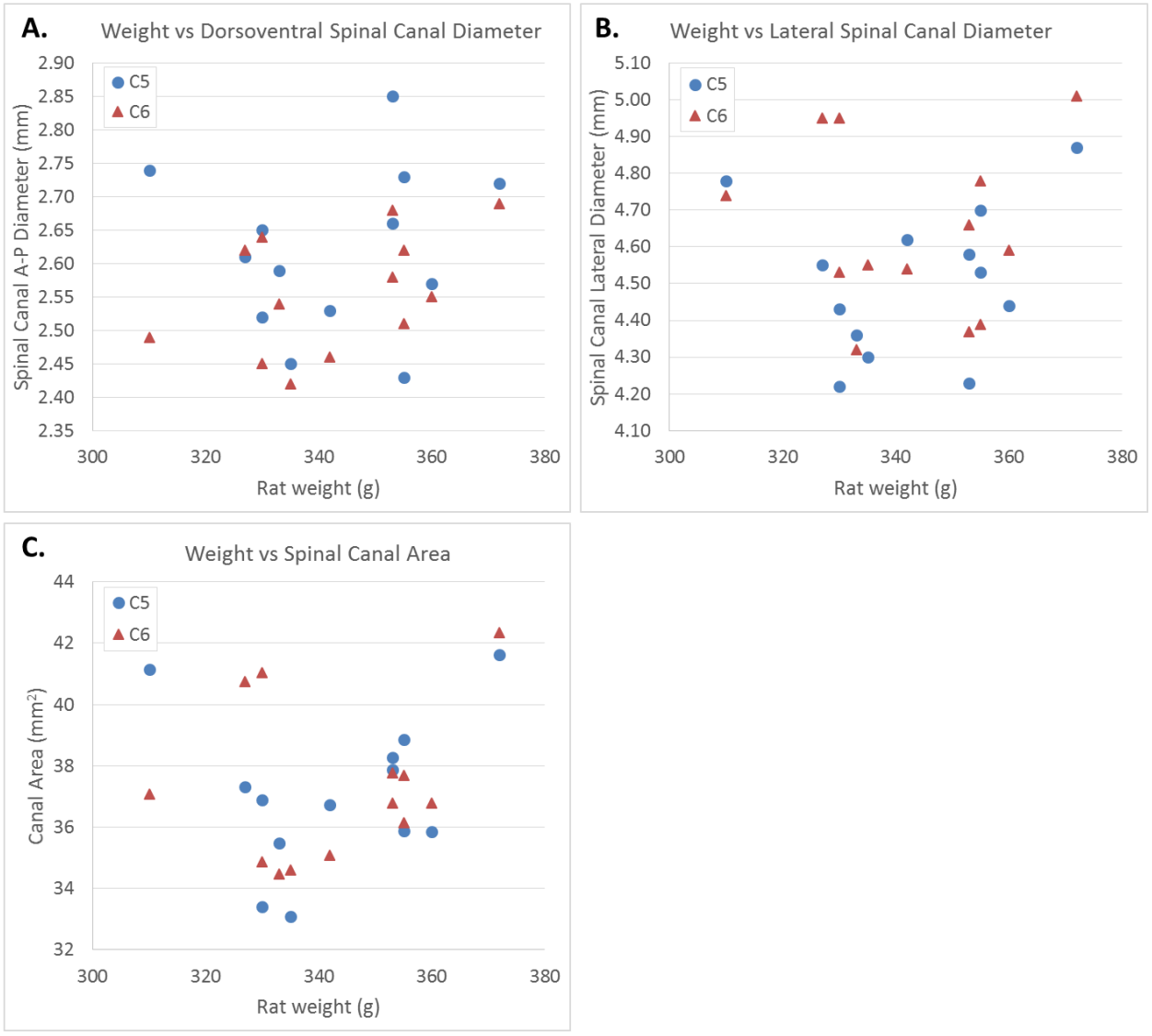

Figure 4-10 - Rat weight vs.C5 and C6 spinal canal measurements. A. Dorsoventral diameter, B. Lateral diameter, C. Area approximated by an ellipse.

Table 4-1 – Bivariate Pearson correlation Values between rat weight and spinal canal geometry

	R^2 Value	
	Rat Weight vs.	
Spinal Canal Measurement	C5	C6
Dorsoventral Diameter	0.106 (p = 0.729)	0.459 (p = 0.117)
Lateral Diameter	0.192 (p = 0.529)	-0.016 (p = 0.958)
Area	0.189 (p = 0.537)	0.218 (p = 0.474)

4.4 Discussion

This study took several critical steps towards developing a rat dislocation spinal cord injury model with immediate residual compression. The electrophysiology aspects determined a residual compression depth that adequately compressed the spinal cord to reduce signal conduction in the majority of animals following a dislocation injury. The differing response when residual compression directly followed traumatic injury emphasized the importance of mimicking clinical circumstances, as pathophysiologic response was significantly different if the compression was briefly removed. From the survival portion of the study, the dislocation injury still demonstrated variable open field behavioural outcomes, and combining 4 hours of residual compression with a traumatic dislocation injury was shown to be survivable. These results identify parameters for future studies to characterize the effects of timing of residual compression, and other relevant biomechanical variables within a dislocation model.

Clinically, neurologic outcome is not related to the degree of canal occlusion observed in radiographs (Boerger et al., 2000; Herndon & Galloway, 1988; Mohanty & Venkatram, 2002). Several ex vivo studies have demonstrated that the maximum extent of canal occlusion occurs during the dynamic injury event (Chang et al., 1994; Ivancic et al., 2007; Panjabi et al., 1995; Wilcox et al., 2002, 2003, 2004). This scenario was reproduced in the dislocation residual compression model by first a high-rate peak displacement, followed by a residual compression at a lesser depth. These ex vivo studies also reported no correlation between peak and post-injury canal occlusions, which motivated the need to determine an independent residual compression depth.

The viscoelastic properties of the spinal cord are important to both the initial injury and the method of residual compression. The spinal cord is sensitive to impact velocity, where injury severity increases with rate (Kearney et al., 1988; Lam et al., 2014; Sparrey et al., 2008). A slow-rate injury is more representative of chronic SCI, and not the common traumatic SCI observed clinically. Different methods of applying residual compression will elicit different viscoelastic behaviours. Under an applied displacement, such as that from displaced vertebrae, the resultant load on the spinal cord relaxes over time (Carlson, et al., 1997B; Fiford et al., 2004; Sjovold et al., 2013) Under a constant force, such as from compression clips, the spinal cord deformation will creep as it continues to deform. These fundamental principles will affect the stresses within the spinal cord tissue, and likely play a role in the progression of the injury.

It is difficult to draw direct comparisons to the literature as each study implements different methodologies for both electrophysiology and residual compression procedures. There are no gold standard procedures for measuring SSEP signals in rats as previous studies implemented various anesthesia techniques, stimulation parameters, and obtained conflicting outcomes.

Anesthesia is known to have a significant effect on electrophysiological signals (Angel & Mason, 1982; Hayton et al., 1999; Koyanagi & Tator, 1996). The anesthetic typically used at our centre for survival surgeries is inhalational isofluorane, which is well documented to suppress SSEP signals (Kortelainen et al., 2014; Liu et al., 2005). Many of the most recent rat SCI studies have used ketamine (Agrawal et al., 2010, 2009; Cloud et al., 2012; Wang et al., 2008). However, the influence of ketamine on sensory and motor evoked potentials is dependent on the depth of anesthesia. Signal amplitude has been shown to decrease by 50% with an increase in variability within 90 minutes of initial induction of anesthesia (Zandieh et al., 2003). Therefore, urethane, which has been shown to be long lasting (6 - 10 hours) and not affect neuronal signal transmission in the central and peripheral nervous system (Maggi & Meli, 1986) was used in the electrophysiology study. Urethane, however, is carcinogenic (Field & Lang, 1988), and animals should not be allowed to recover following anesthesia (Flecknell, 2016).

Most of the rat SCI studies reporting SSEP outcome sensitivity related to injury severity took recordings at non-acute time points (i.e. greater than one day post injury) (Agrawal et al., 2010, 2009; Bazley et al., 2012). The acute measurement studies (< 60 min post injury) reported either

binary (i.e. present or absent) or crude outcomes (i.e. normal, abnormal or absent) (Cloud et al., 2012; Fehlings et al., 1989; Nashmi et al., 1997). One of the previous studies reported that SSEP signals were absent from all 24 animals across three different clip compression severities at 15 minutes post-injury (Nashmi et al., 1997). This is similar to our findings, where five of eight animals had absent signals immediately following SCI, however continuous monitoring demonstrated the return of the signals. Of note, none of the previous rat SCI studies measured SSEP continually post-injury to investigate the temporal response.

Previous studies using other animal models (i.e. dog, monkey) have investigated the time required for SSEP signals to return following varying lengths of slow application of residual compression (Carlson, et al., 1997A, 1997B, 2003; Kobrine et al., 1979). These studies consistently found that longer residual compression times corresponded to longer signal return times. None of these studies involved an initial traumatic impact, and most applied residual compression to a depth based on signal drop.

The stepwise incremental approach to determine the displacement level that affects spinal cord signal conduction demonstrated that 88% of animals had SSEP signals decrease below 50% baseline at or before 0.8 mm, indicating this depth results in spinal cord compression in most animals. The one animal that did not experience an amplitude drop at any compression level did however experience an amplitude increase at a compression level of 0.7 mm, which may indicate some influence of compression. The 0.8 mm depth corresponds to approximately 30% canal occlusion at C5 (average canal diameter of 2.65 mm). This residual compression depth threshold herein is consistent with a previous study seeking to identify a threshold for residual compression (Dimar et al., 1999). Following a traumatic contusion injury at T10, the 35% canal occlusion used in that study demonstrated a dramatic decrease in recovery compared to 20% occlusion. Interestingly, they found that 20% and 35% spacers without an initial SCI did not affect neurologic function, emphasizing the importance of investigating residual compression under clinically relevant conditions. Similarly, canal occlusion was measured to be approximately 41% from radiographs of 28 human patients with complete bilateral facet dislocation injuries (Kang et al., 1994).

Previous residual compression studies that implemented a high-rate initial injury would surgically insert a shim into the spinal canal following injury (Dimar et al., 1999; Shields et al., 2005). This method requires a period of time when the injured spinal cord is not compressed. The electrophysiological results of this study indicate the pathological response at this acute phase is significantly different between an isolated traumatic injury and the same injury with immediate residual compression. Interestingly, the results were counterintuitive, in that the immediate removal of compression resulted in a lost signal in most cases, where continued compression demonstrated signal stability or increased amplitude. Two potential hypotheses that could both explain these findings are that the compression sensitizes the ascending axons, and/or the compression restricts descending inhibitor axons. Mechanical compression potentially sensitizes the ascending firing axons by preferentially activating low-threshold/large diameter dorsal column axons, and also stretch-activated channels (e.g. Piezo 2) (Coste et al., 2010; Woo et al., 2014). Additionally, the compression may also restrict tonic descending inhibitory axons (Dickhaus et al., 1985; Iggo et al., 1985; Kuo et al., 2003), allowing weaker stimuli to initiate action potentials. The increased SSEP signal amplitudes during immediate residual compression do not indicate that the spinal cord is protected, but that signals may be triggering alternative pathologic pathways.

The main limitation of the electrophysiology experiments was the inability to correlate SSEP signals with spinal cord damage or functional outcomes. The incremental step procedure required SSEP signals to stabilize, which took different amounts of time for each animal. This would have allowed the pathological injury progression to advance to slightly different stages, rendering histology results incomparable. Additionally, the stepwise protocol does not allow one to rule out the influence of earlier steps on affecting the signal. This was unavoidable, and allowing the signal to reach steady state between steps was intended to minimize these affects. The longer times needed for the signal to stabilize may have also allowed pathology from the initial injury to progress, also potentially affecting the signal. This likely would have resulted in a gradual signal change, not the immediate drop in signal that was observed – likely caused by the compression of the tissue.

The outcomes from the dislocation model in this study were bimodal, with injuries either minor, or severe, but rarely moderate. Variability in the vertebral kinematics has been reduced

compared to the previous injury clamps (Chapter 3 of this thesis; Mattucci et al., 2017). Dislocation injury outcomes from previous studies would range from no observable injury to severely injured (requiring humane endpoint), despite equivalent peak displacements. In this study, all of the animals with an injury displacement 1.45 mm or greater had obvious functional impairments and scored 35 or less on the Martinez open field test at four and seven days post-injury. This displacement provides a threshold for achieving a mild injury from the initial trauma, from which the residual compression can be added. One of the biggest concerns with incorporating residual compression with a dislocation model was survivability. It was unknown if an animal could survive residual compression for 4 hours following the initial traumatic injury. This scenario was piloted in four animals, with all four animals surviving to 6 weeks post-injury, indicating appropriate parameters for a more extensive study.

The aim of the behavioural portion of the study was to establish a correlation between injury parameters and outcome severity, and particularly identify thresholds for minimal and severe injuries to allow for better planning of future studies. These parameters were adequately identified through the Martinez open field test. From the animal care standpoint, animals sustaining 1.45 mm or greater dislocation injuries consistently demonstrated pain, and qualitative deficits (e.g. flexed paws) for the first few days post-injury before quickly recovering. The most severe animals were not mobile and required extensive care for the first week post-injury (e.g. multiple Ringer's lactate injections daily, hand feeding, washing and drying of urine-soaked fur), and more severe injuries would have likely resulted in humane endpoint. Therefore we recommend limiting severe injuries to 1.6 mm using the new dislocation model. Although histological outcomes would be useful for further correlating injury parameters, this was beyond the scope of this experiment and these outcomes are planned for a future larger study.

Although 4 hours is not a realistic surgical intervention timeframe for human injuries, the time points are likely not directly transferable from the rat model due to species differences (i.e. size and metabolic rate differences). However, four hours of residual compression in the rat model can be compared to shorter durations to allow insight into possible pathological secondary injuries that are affected by residual compression. It is critically important to understand what secondary injury effects are responsible for neurological deficits in order to develop a successful treatment.

Closed-column SCI models rely on the controlled movement of the vertebrae to injure the spinal cord. Therefore the precision of the injury device is limited by the variability of the vertebral anatomy. In the case of our dislocation model, C6 is displaced dorsally with respect to a rigid C5. The compression experienced by the spinal cord is determined by the canal pinch diameter (Ivancic et al., 2006): the distance between the most rostral point on the dorsal aspect of the C6 vertebral body and the most caudal aspect of the lamina of C5 (Figure 4-11). Therefore the dorsoventral canal diameter of C5 is the primary anatomical feature that determines how dislocation displacement relates to relative canal occlusion and spinal cord compression. The largest observed difference in C5 canal diameter was 0.4 mm, which corresponds to 27% of the displacement of a prescribed 1.5 mm dislocation injury. The surrounding soft tissues may also play a role, such as the location of intervertebral disc-vertebral endplate failure. However we have previously observed consistent failure at the rostral vertebra's caudal endplate (Choo et al., 2008, Appendix B). This anatomical variability within a model with sensitive parameters may continue to contribute to injury variability. A method to measure C5 canal diameter immediately prior to injury, such as micro CT or high-resolution ultrasound could potentially allow for dislocation injuries to be controlled based on relative occlusion. Alternatively, the model could be altered to be less sensitive to this ratio, however, the biomechanics of the spinal cord matching the clinical scenario would need to be preserved. The dislocation could be performed on non-adjacent vertebrae (i.e. with a 'floating' vertebra in between) to induce similar stress patterns (Fiford et al., 2004), however this would reduce the pinching effect seen clinically. Potentially, the lamina of C5 could be removed and substituted with an artificial lamina, placed at a constant distance from the spinal cord. However, this may introduce challenges with respect to securely holding C5.

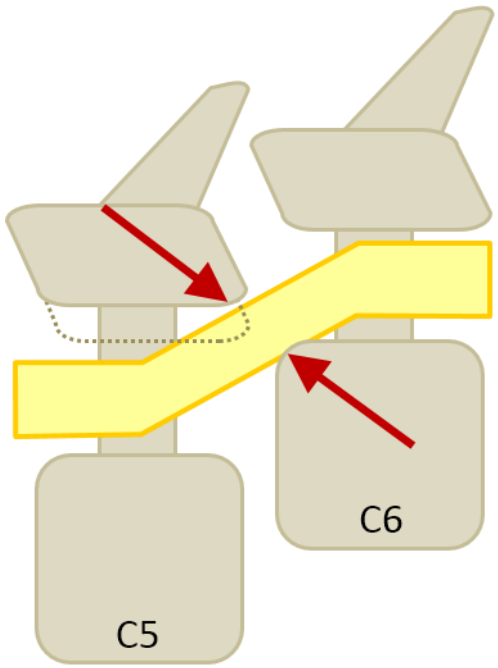

Figure 4-11 - Schematic of C5 and C6 dislocated with lateral aspects removed for visibility with identified canal pinch diameter (arrows). The dotted line represents the dorsal aspect of C5 with a smaller dorsoventral canal diameter, illustrating a smaller canal pinch diameter, likely causing increased damage to the spinal cord.

Other studies have reported similar spinal canal diameter averages and standard deviations for rats of similar size (Jaumard et al., 2015; Laing et al., 2014, 2011), however these studies only provided one grouped measurement despite similar weight ranges. Laing et al., (2014) measured the ratio of spinal cord to spinal canal diameters using MRI in young (182 g, SD: 4 g) and aged (230 g, SD: 25 g) female Fisher rats, and found the ratios to be within 3% at C4, C5, and C6, suggesting the spinal cord and vertebrae grow in parallel. The spinal cord dorsoventral diameter was 89% of the spinal canal diameter, while the spinal cord area was 76% of the spinal canal area. The differences in canal diameter measured in the current study could lead to variable outcomes in both cases. If the spinal canal to spinal cord ratios remain the same, equivalent displacements would produce different relative compressions. If spinal cord diameters are independent, larger spinal canals would provide more space available for the spinal cord to move within.

Severity of SCI in humans has been previously linked to sagittal spinal canal diameter. When patients were grouped based on neurologic deficit, there was a significant correlation between canal diameter and the degree of neurologic deficit, where those with smaller canal diameters were more prone to severe deficits than those with large canals (Eismont et al., 1984; Kang et al., 1994). Since spinal cord diameters in humans vary to a lesser degree (Elliott, 1945; Nordqvist, 1964; Nouri et al., 2017) compared to spinal canal diameters, smaller canals tend to have less space available for the spinal cord, with greater likelihood for injury.

4.5 Conclusions

This study has provided critical details to implement in the development of a closed-column traumatic spinal cord injury model with residual compression. The process has justified individual parameters that may have otherwise been masked by confounding variables if parameters were determined solely by trial and error. A residual compression depth of 0.8 mm was determined to consistently impede signal conduction within the cord, as well as the importance of residual compression following immediately after the initial traumatic insult – which has previously not been done before. An initial dislocation displacement of 1.45 mm was determined to induce a mild injury, and the addition of residual compression was survivable for 6 weeks. Finally, in an attempt to better understand closed-column displacements, it was determined that spinal canal diameters are not correlated to animal weight, and advanced techniques need to be implemented to induce injuries relative to individual anatomical geometries.

Chapter 5: Discussion and Conclusions

5.1 Overview

Spinal cord injuries occur in a heterogeneous fashion, including at different spinal levels, at various injury velocities, and with different combinations of forces and directions, termed injury mechanisms. Most SCIs occur at the cervical level, are high-energy events (e.g. motor vehicle accidents), and the most common injury mechanism is dislocation. Some of the most common biomechanical variables of human SCI, such as injury mechanism and velocity, are often not represented in preclinical animal models. The development and refinement of a clinically representative high-speed cervical dislocation model would provide a better understanding of dislocation injuries and allow for more robust evaluation of treatments across multiple mechanisms.

One of the few treatment options available following SCI is surgical decompression to remove residual compression on the spinal cord and restore anatomical alignment. The timing of performing the decompression is controversial as some clinicians believe it is important to decompress as early as possible and some believe the evidence is insufficient. While preclinical experimental evidence demonstrates the beneficial neurological outcome of early decompression, many patients that undergo early decompression treatment still do not exhibit improvement in neurological outcomes. This disconnect demonstrates that the models used to evaluate residual compression are likely not representative of the specific human injury biomechanics, among other factors. The incorporation of residual compression within a cervical dislocation model would allow for further investigation of the influence of clinically relevant biomechanical variables on neurological recovery.

This thesis work began with a study to investigate the differences between injury mechanisms at acute time points to further understand the progression of injury as a result of contusion, dislocation and distraction injuries. The three injury mechanisms demonstrated significant degradation in white matter tracts at different rates: contusion between 24 hours and 7 days, dislocation between 3 and 24 hours; while distraction had little change over 7 days. These results indicate that distinct injury mechanisms likely initiate pathologies that progress at different rates, and these differences could be important with respect to clinical therapeutic windows. However,

there was significant variability present in the data, particularly with the dislocation injuries. Since equivalent dislocation input parameters produced both uninjured and severely injured animals, it was challenging to draw conclusions from experimental results. It was evident that the dislocation model needed to be refined to provide a robust, clinically-relevant injury model to evaluate treatments in the future, particularly the influence of the timing of decompression.

Dislocation is a closed-column injury model, relying upon the movement of vertebrae to injure the spinal cord. This adds an extra degree of variability in that injury clamps must rigidly hold the vertebrae to produce consistent injury kinematics. The vertebral anatomy was analysed to determine geometric differences between adjacent vertebrae, identifying a major limitation of the existing clamps – each clamp could only grip the wider of the two intended vertebrae. Therefore new injury clamps were designed with a feature allowing the clamps to pivot and self-align when tightened, and thereby grip both intended vertebrae. The vertebral kinematics during a dislocation injury were compared with both the original and redesigned clamps using high-speed x-ray and fiducial markers attached to the vertebrae and clamps. Slipping was identified between the original clamps and vertebrae in some instances but was significantly reduced with the self-aligning clamps. This study emphasized the importance of validating injury displacements against input parameters, particularly when comparing results or reproducing injuries.

The development of new dislocation injury clamps required the establishment of new model injury parameters. Since the eventual goal was to implement a dislocation injury with residual compression, additional refinement was necessary. Spinal cord compression cannot be directly visualized in a closed-column model, thus electrophysiology techniques were implemented to determine a minimum residual compression depth that affects signal conduction following a traumatic injury. Parameters were identified to consistently produce a mild injury and consistently compress the spinal cord. The effect of holding residual compression immediately following a traumatic injury had a significant effect on SSEP conduction compared to injuries without immediate residual compression. Results were counterintuitive, suggesting initiation of different pathological responses at an acute time point, which emphasizes the importance of mimicking the clinical scenario. Behavioural outcome was used to assess dislocation severity following a range of displacements, and four hours of residual compression was survivable

following a ‘mild’ traumatic injury. These results identified suitable parameters for a full pre-clinical dislocation residual compression study.

5.2 Variability within the Dislocation Model

A common theme throughout this work has been the variability of injury outcome severity and how to minimize this variability. There are numerous factors that could introduce variability, such as injury kinematics due to the vertebral clamps, intervertebral disc properties, anatomical geometry, and intrinsic variables such as genetics, blood pressure, and respiration.

From an engineering perspective, the goal of any SCI model is to produce consistent spinal cord deformations. This is straightforward in a contusion model, where deformations are applied directly to the spinal cord. Producing consistent spinal cord deformations is more challenging in closed-column models such as dislocation and distraction. In these instances spinal cord deformations are caused by the kinematics of the vertebrae. In this dislocation model, the vertebrae are held by custom injury clamps, which are connected to the rigid stereotaxic frame and injury system actuator. It is critical that the interface between the clamps and the vertebrae remain rigid to produce consistent vertebral kinematics. High speed x-ray with fiducial markers attached to the clamps and vertebrae was used to measure vertebral kinematics, and to verify that relative motion was reduced when the self-aligning clamps were used. The deformation of the spinal cord however was not measured, and consistent vertebral kinematics do not guarantee consistent spinal cord deformation.

The variability of injury outcome severity from an animal care and survivability standpoint has been reduced with the self-aligning clamps compared to the existing clamps. The dislocation-injured animals (7 day group) from the Chapter 2 study demonstrated a wide range of injury severities, despite consistent actuator displacements (1.75 mm, SD: 0.04 mm). Behavioural outcome measures were not conducted, however, qualitative observations provide insight towards the differences (Table 5-1). Four animals had no apparent functional deficit, and were active and mobile following recovery from surgery. Eight animals had obvious functional deficits, including paw and/or limb paralysis. Five animals had severe injuries that were not survivable: one animal perished within 24 hours, and four animals required humane endpoint, demonstrating severe weight loss, respiratory issues, and/or porphyrin. The issue with

survivability introduced a ‘survival bias’ in the data, as animals of equivalent severity were able to survive until the earlier time points, and thus were included in the 3- and 24-hour groups. The animals injured using the self-aligning clamps in Chapter 4 demonstrated more consistent injuries, despite the intentionally wider range of actuator displacements to determine a displacement-severity relationship (1.46 mm, SD: 0.12). These animals were evaluated using the Martinez locomotor scale (Martinez et al., 2009), however these scores can be correlated to the equivalent qualitative observations from Chapter 2 injuries (Table 5-2). Animals with a score greater than 35 (out of a possible 40) would likely appear to have no functional deficits without the use of the objective behavioural scale, and scores of 35 or less typically have obvious deficits. Animals with injury displacements greater than 1.3 mm were included in the comparison. Of the fourteen animals included, only one animal had no obvious functional deficits, and one animal did not survive (perished immediately). The other twelve animals had obvious functional deficits in the first week post-injury, and survived for six weeks post-injury; five weeks longer than the survivability period of the existing clamps. The self-aligning clamps have effectively limited the range of possible outcomes, as injuries more consistently demonstrated obvious functional deficits with greater survivability. The comparison of results between these two studies are evidence of the reduced variability with the self-aligning clamps compared to the existing clamps. Further verification of the reduced variability using histological analysis is required, however this was outside of the scope of this thesis.

Table 5-1 – Qualitative outcome severity of dislocation injured animals from Chapter 2 (7 day group) using the existing clamps. Despite the consistent actuator displacements, four animals had no apparent functional deficits, while five animals did not survive to the 7 day time point.

Existing Clamps		Injury Severity		
Disp. (mm)	Force (N)	No deficit	Obvious deficit	Non-survivable
1.672	34.02		*	
1.687	32.26	*		
1.725	31.13	*		
1.749	23.47			*
1.753	24.16			*
1.753	24.16			*
1.768	26.06	*		
1.768	26.14			*
1.77	23.96		*	
1.772	22.64		*	
1.773	24.00		*	
1.778	24.02	*		
1.797	23.59		*	
1.798	26.88		*	
1.816	19.89			*
1.831	22.21		*	
1.833	23.51		*	
Ave: 1.767 SD: 0.044	Ave: 25.42 SD: 3.75	4	8	5

Table 5-2 – Outcome severity of dislocation injured animals from Chapter 4 using the self-aligning clamps. Martinez locomotor scores were converted to an equivalent outcome severity scale as Table 5-1, where scores greater than 35 likely would appear to have no obvious deficits without the use of the objective behavioural scale, and scores 35 or less typically have obvious deficits.

Self-Aligning Clamps		Injury Severity		
Disp. (mm)	Force (N)	No deficit	Obvious deficit	Non-survivable
1.309	19.95	*		
1.315	24.27		*	
1.331	22.86		*	
1.34	16.83		*	
1.379	22.35		*	
1.423	16.50		*	
1.436	15.31		*	
1.444	23.62		*	
1.464	16.23		*	
1.469	26.44		*	
1.569	21.96		*	
1.611	15.29		*	
1.655	15.44			*
1.657	16.50		*	
Ave: 1.457 SD: 0.122	Ave: 19.54 SD: 3.93	1	12	1

The anatomical variability of the spinal canal diameter is likely a contributing factor to injury outcome. Spinal canal diameters were measured to determine a correlation with rat weight to better understand the canal narrowing within the closed-column model. However, not only was there no correlation, there was substantial variability between rats of the same weight. The dorsoventral diameter differed by up to 0.42 mm at C5, and up to 0.26 mm at C6. These differences likely have a considerable effect considering the small injury displacements. A larger diameter C5 spinal canal requires greater displacement of the C6 vertebral body to produce an equivalent spinal cord deformation compared to the case where the C5 diameter is smaller. Further, spinal canal diameter and spinal cord diameter have been demonstrated to have

significant variability in humans, where the size of the spinal canal in particular has an effect on injury outcome in clinical studies (Eismont et al., 1984; Kang et al., 1994; Nouri et al., 2017).

The mechanical properties of the intervertebral disc affect the vertebral kinematics in a dislocation model. The intervertebral disc is the primary structure connecting the adjacent vertebrae at the dislocation level (following a facetectomy). Prior to injury, the rat is placed into the stereotaxic frame, which rigidly holds the rostral injury clamp, while the caudal injury clamp is secured to the actuator. When the clamps are secured to the vertebrae, the alignment of the clamp interface that attaches to the actuator may vary between animals (due to anatomic differences). A small residual force is often produced when the clamp is attached to the actuator, displacing the vertebrae from neutral alignment and introducing an arbitrary start location prior to injury. Our protocol has been to preload the caudal clamp to 2 N in tension in an attempt to provide a consistent starting location between animals at the intervertebral disc shear neutral zone boundary. This was increased to 3 N in Chapter 3, in an attempt to reduce variability by loading the disc further into the stiffer elastic zone. We have recently discovered in a small pilot study (n = 6) that there is variability in the mechanical properties of the intervertebral disc (Appendix B). For example, the shear neutral zone varied from 0.11 to 0.51 mm between rats, and the shear stiffness varied from 3.1 to 20.8 N/mm. Additionally, the same 3 N force would produce displacements that range as much as 0.40 mm across animals, simply due to variation in the mechanical stiffness of the disc. Ultimately, the displacement introduced due to preload affects the total displacement of the caudal vertebra relative to the rostral vertebra.

There may also be a compound effect of spinal canal diameter and intervertebral disc properties. Two animals could be injured by the exact same injury device parameters (i.e. actuator displacement), however experience different spinal cord deformations. If one animal had a stiff intervertebral disc (i.e. small preload displacement, and a large diameter spinal canal, it would experience less spinal cord deformation than an animal with a less-stiff disc, and small spinal canal diameter. From the observed differences, the combined magnitude of both of these factors could potentially be as large as 0.82 mm (0.42 mm canal diameter difference + 0.40 mm preload difference): greater than 50% of the maximum vertebral displacement of a 1.45 mm injury. This is likely an important source of variability to be addressed in the future.

Biological factors such as blood pressure, breathing cycle, and heart rate may also influence the severity of SCI in an animal model. During surgery prior to SCI, blood loss may result in changes in blood pressure, and hemorrhaging is a key component of traumatic SCI. Animals have individualistic responses to anesthesia, which may affect both breathing and heart rate. Breathing affects the oxygenation of the blood, and heart rate affects the rate of blood flow to tissues. Additionally, slight changes in force on the actuator are observed due to the breathing cycle prior to injury, but this has an unknown effect during injury. These factors are not unique to the dislocation model, but may also contribute to the injury outcome variability.

5.3 Clinical Relevance and Validation of Injury Models

It is important for SCI models to be clinically relevant to investigate injuries as similar as possible to those seen in the human population. Experimental findings are often judged based on the injury model used. From a survey amongst the SCI research community, 71% agreed that contusion was the most clinically relevant model, while 20% agreed that clip compression was the most relevant (Kwon et al., 2011). This is likely due to the high-speed nature of a contusion injury, an important characteristic of most traumatic injuries in the human population. However, one could argue that the dislocation animal model is the most clinically relevant injury model, as it is also induced at a high velocity and also simulates the dislocation injury pattern that is seen most frequently in humans. The mindset of 'the most clinically representative model' needs to shift in that each injury model should be evaluated with respect to the clinical injury it represents. Relying on a single injury model to represent the entire heterogeneous human population could lead to promising treatments being overlooked that may have otherwise been effective in a different model. Researchers should evaluate treatments in a variety of injury models not only to determine which patient populations may stand to benefit, but also to understand the underlying differences in pathological mechanisms that affect efficacy.

When developing injury models, the biomechanical and pathophysiological influence of assumptions must be understood as they relate to clinically observed injuries. The previous dislocation injury clamps were not evaluated using quantitative methods to determine if slipping between the clamp and vertebral interface occurred. Slipping results in increased variability and inconsistent injury displacements applied to the spinal cord. Previous studies involving residual

compression following a traumatic contusion injury involved a brief period of time when the spinal cord was unloaded between initial injury and residual compression (Dimar et al., 1999; Shields et al., 2005). This is a potentially critical time point at the onset of secondary pathological cascades. When the effect of immediately held residual compression on SSEPs was evaluated, it was significantly different than when the compression was removed. Experimental design decisions should be carefully justified to verify they represent the intended clinical scenario.

5.4 The Importance of Injury Mechanism

The development of animal SCI models has focused on the goal of producing injuries relevant to those seen clinically. Animal models have diverged from the original weight-drop model to address research questions relevant to specific clinical scenarios. The objectives from the original multi-mechanism study was to examine the effect of three clinically relevant injury mechanisms on the patterns of tissue damage (Choo et al., 2007). Mechanistic differences in animal models have also identified differences in behavioural, and treatment outcomes. Cellular level studies have reported responses based on mechanistic stresses. Finally, injury mechanism has demonstrated differences in neurological recovery in the human population. These findings emphasize the importance of continued development of robust models for the different injury mechanisms.

Spinal cord tissue is sensitive to the mechanical stresses and strains to which it is subjected. Neuronal cell cultures that were arranged in a 3-D configuration and subjected to heterogeneous strain fields representative of in vivo environments were shown to be significantly less viable than those subjected to homogeneous strains (Cullen & LaPlaca, 2006). This study also postulates that the heterogeneity in neuronal response to bulk mechanical loading may be due to local variations in stress and strain, influenced by factors such as cell orientation, morphology, cell and matrix viscoelastic properties, and cell-cell/cell-matrix adhesion properties (Cullen & LaPlaca, 2006). Neuronal-astrocytic cell cultures are also more sensitive to high strain rate deformations (Cullen et al., 2011). Further, cells demonstrated more sensitivity to bulk shear deformation than compression (Cullen et al., 2011). Cultures of human CNS cells subjected to high-pressure waves did not experience damage or excitation unless coupled with shear forces

(Ravin et al., 2012). Axons in white matter tissue have demonstrated distinct mechanical thresholds for morphological and physiological damage, in both compression and tension (Bain & Meaney, 2000; Bain et al., 2001; Shi & Blight, 1996; Shi & Pryor, 2002). Additionally, axons have demonstrated increased damage with increased strain rates (Shi, 2006). Strains along the same direction as white matter tracts have demonstrated to be better injury predictors than maximum principal strains, supporting the premise that traumatic axonal injury occurs due to tensile strain along the axon (Sullivan et al., 2015). Many of these studies have been driven by traumatic brain injury research, however the principles of heterogeneic forces causing variable injuries in CNS tissue likely remains valid in the spinal cord. It is clear that further research to investigate cellular vulnerabilities in the spinal cord orientation are warranted.

The previous work in animal models on the different patterns of tissue damage and functional outcomes due to contusion, dislocation, and distraction injury mechanisms has been reported in detail throughout this work (Chen et al., 2016A; Choo et al., 2007, 2009, 2008). Additionally, finite element models and in vivo MRI of these mechanisms have demonstrated distinct stress and strain fields (Greaves et al., 2008; Khuyagbaatar et al., 2016), which also correlate to tissue damage patterns (Bhatnagar, et al., 2016B; Russell et al., 2012).

Recently, preclinical models have demonstrated the effect of injury mechanism on treatment outcomes in rats. A treatment that reduces the membrane permeability to activated leukocytes into the spinal cord after injury (CD11d monoclonal antibody) improved neurological outcomes following a clip compression SCI, however not after a contusion SCI (Geremia et al., 2017). To confirm this result was not due to spinal level, the study was repeated at a different level with the same outcome. This result was thought to be attributed to the initiation of different pathomechansisms by each injury, where the hemorrhaging produced by contusion allowed infiltration of neutrophils. Importantly, this study is unique to demonstrate differences in treatment outcomes based on mechanism, and emphasizes the need to evaluate treatments across multiple injury models.

Clinical studies have reported mechanistic effects on patient populations. Individuals sustaining SCI due to a high-energy event (i.e. motor vehicle accident vs. falls from standing, sports-related, or blunt violence) are associated with a greater likelihood of complications during the

acute hospital period (Wilson, et al., 2012A). Patients with cervical facet dislocation SCIs presented with more severe injuries as a result of higher-energy injuries, had a longer duration of hospital stay, and experienced less motor recovery at 1-year follow-up compared with those with other SCI mechanisms – despite the earlier decompression times of the facet dislocation group (Wilson et al., 2013). The influence of these effects on neurological recovery in humans is particularly convincing of the relevance of injury mechanism.

The emerging results from cellular, preclinical, and clinical studies present a strong argument towards the effect of injury mechanism on primary injury pathologies and treatment options. This emphasizes the importance of developing robust injury models which closely represent the heterogeneous clinical SCI population to better understand these primary injury pathologies and evaluate treatment options.

5.5 Recommendations

5.5.1 Further Refinement of the Dislocation Model

An overall premise of this thesis work was to reduce outcome variability in the dislocation model so it could be more easily implemented in future studies, including treatment studies. The most apparent cause of variability, relative motion at the clamp-vertebrae interface, was addressed. Variability was reduced such that the range of injury outcomes was reduced – animals were no longer uninjured or injured severely to the point of humane endpoint from equivalent input parameters. Given the amount of time and resources required to perform SCI research, it is not feasible to simply increase animal numbers to obtain meaningful results. In order to refine the dislocation model, the influence of different biological and methodological variables must be evaluated to further reduce variability (e.g. animal weight, spinal canal size, injury start location, blood pressure, etc.). By investigating these variables using multiple outcomes (e.g. electrophysiology, spinal cord deformation, histology, behaviour), further relationships between outcome measures will help to deepen understanding of the dislocation injury mechanism. The next step would be to perform a study on a single group of animals, where injury input parameters are kept consistent, and the biological and methodological variables of interest are measured in detail. Regression analysis should be used to determine the influence of each of the variables measured.

Animals are typically controlled based on weight (which correlates approximately to age). Animals must be ordered to arrive at the research centre with enough time to adjust and settle into the environment, become comfortable with handling, and learn behavioural testing methods. Animals gain weight at different rates over this adaptation period, leading to a weight discrepancy (up to approximately 60 g) between animals at time of injury, which has not been directly investigated with respect to the dislocation model. Animals at time of injury also have variability in the size of vertebrae. Since a closed-column SCI model depends on the vertebrae to induce injury, the size will have a direct influence on the displacements imparted to the spinal cord.

Various methods could be applied to measure the vertebral geometries at the time of injury. In vivo micro CT would provide accurate geometries pre-injury. However this process is expensive, time consuming and would require extensive logistical planning for the animal to leave the animal vivarium and re-enter if further survival studies are desired. High-resolution ultrasound may also be possible. However this technique cannot image through bone so would need to be verified for feasibility (i.e. possibility of imaging between the spinal laminae to the ventral surface of the spinal canal) and validated for accuracy. Measuring these geometries post-injury would also be possible, but likely at the sacrifice of outcome data. In order to conduct histological analysis, the spinal column must be opened to harvest the spinal cord, typically destroying the vertebrae. Methodologies should be explored to leave C5 undamaged while removing the spinal cord. This would allow measurement of the spinal canal diameter, while preserving the spinal cord for histological analyses. To conduct behavioural outcomes, the animal must live beyond the date of injury, particularly the first few days when behavioural scores can be confounded by signs of pain from recent surgery and the effects of pain-killing drugs. Canal measurements taken at these later time points allow the vertebrae to potentially grow post-injury and may not be representative of the anatomical geometry at time of injury. Additionally, accurate measurements of spinal cord geometry should also be performed, which would likely involve MRI. Since the spinal column and spinal cord geometries directly affect the injury, careful consideration is imperative.

Determining an appropriate starting location for the dislocation injury remains a challenge. When the actuator is attached to the vertebral clamp, it is unknown if the vertebrae remain in

their neutral anatomical position, or if attachment forces have introduced displacement. Differences in intervertebral disc mechanical properties result in variable starting locations for equivalent preload forces (Appendix B). Further work is required to determine a method to ensure consistent injury starting locations between animals. If the spinal column is imaged pre-injury to determine the spinal canal diameter, markers could be used to determine the geometric relationship with the spinal canal. These markers could then be used during setup to align the spine in the neutral position prior to injury. The small scale would make this challenging, as high-accuracy measurement techniques would be needed to verify the positioning.

Electrophysiology techniques could be utilized to provide further insight. SSEP measured at the time of injury and acute time points could be used to correlate with histological and behavioural outcomes. Electrophysiology could also be used as an outcome measure to determine the effects of the dependent variables under evaluation.

Expanding on the kinematics of the clamps and vertebrae during a dislocation, the deformation of the spinal cord could be measured. The high-speed x-ray technique cannot observe soft tissues so an appropriate marker would need to be used, which presents distinct challenges. Tantalum beads, like those used as fiducial markers for the vertebrae and clamps, could be injected into the spinal cord or secured to the surface. However, the injection of too many beads inherently influences the mechanical properties of the tissue – due to the presence of the beads and damage introduced during injection. Perhaps a novel solution would be the injection of radiopaque liquid into the cerebrospinal fluid – similar to the use of a barium solution in a fluoroscopic swallowing exam. Visualization of a radiopaque spinal cord would allow for direct measurement of dynamic spinal cord deformation during injury. This approach would have challenges as well, including verifying that the fluoroscopic solution reliably migrates to the desired location in the spinal cord at an appropriate concentration. The solution would need to have minimal influence on the behaviour of the spinal cord, and the behaviour of the fluid during injury would need to be verified. If the CSF is essentially made radiopaque, it may be displaced when the cord is compressed during injury, making the most important aspect of the event invisible. Fluoroscopic cord visualization could potentially prevent the use of any histological or behavioural outcomes depending on the biocompatibility of the markers or fluid, limiting the study to only kinematic outcomes.

5.5.2 Perform Mechanistic Cellular Level Studies

The mechanism-specific temporal progression of damage observed in specific white matter tracts suggests that there are differences in the cellular response to specific mechanical stresses and strains. Many studies in the literature have reported the mechanistic force-dependent response of neural cells. Most of these studies have been conducted for traumatic brain injury purposes, but this cellular response is also relevant to spinal cord tissue. It is important to investigate how local spinal cord tissue regions behave at given stresses experienced during different injury mechanisms. Localized pathologies are initiated by primary injuries, and determining the mechanistic cause may help to inform treatment strategies. For example, how are cells damaged in the CST when under dynamic transverse compression (i.e. from a contusion)? How are cells in lateral white matter columns damaged when subjected to transverse shear forces (i.e. from a dislocation)? Further, how does the same region respond to different stresses? Are certain cells more sensitive to different stresses such as compression, shear or tension? The answers to these questions could potentially inform treatment strategies. For example, if microtubules in axons are the primary structures damaged in transverse compression, strategies could focus on repairing microtubules following a burst fracture. If oligodendrocytes are particularly vulnerable in shear, repopulating oligodendrocyte populations in the lateral white matter following a dislocation injury would be a priority.

Cell cultures representing specific cell populations or excised regions of spinal cord tissue could be subjected to the specific stresses typical of distinct injury mechanisms. As finite element models with spinal cord mechanical properties become more refined, localized stress magnitudes will be better approximated to increase the relevance of smaller scale tissue studies. Defining how specific cellular structures respond to specific forces will provide important information to the initiation of injury, and could define potential therapeutic targets.

5.6 Contributions

The overall objective of this thesis was to investigate the biomechanics of a high-speed cervical dislocation rat SCI model at acute stages, refine the model, and incorporate residual compression. Aspects of the biomechanical approach can be implemented to validate other SCI models, and to develop new robust models. The key contributions of this work are as follows:

1. This was the first study to investigate the temporal progression of SCI based on mechanism. The progression of damage to white matter tracts was shown to be dependent on injury mechanism, where dislocation injuries demonstrated significant white matter loss between 3 and 24 hours post-injury.
2. A high-speed x-ray technique was developed to measure vertebral kinematics during a closed-column SCI model, and verify clamp-vertebra relative motion.
3. Injury displacement parameters were measured to be different from injury input parameters, emphasizing the need to validate SCI injury models, particularly closed-column models, or where multiple interfaces exist between the measurement transducers and the spinal cord.
4. Vertebral injury clamps were designed for a rat model to allow the clamps to pivot and self-align to the vertebrae when attached to provide a secure grip. This design significantly reduced relative motion at the clamp-vertebra interface during a cervical dislocation SCI compared to previous injury clamps.
5. The acute response of continued residual compression was investigated for the first time, and observed to have significant physiological effects. Residual compression models should therefore maintain compression following the initial injury to properly replicate clinical injuries.
6. Rat vertebral anatomy and intervertebral disc properties were measured, and substantial variability was observed. These are important considerations for the development of closed-column SCI models.

5.7 Conclusions

This work has provided critical details regarding the biomechanics of a high-speed cervical dislocation rat SCI model at acute stages, refined the model, and incorporated residual compression. White matter damage progressed at different rates following different primary injury mechanisms, where dislocation demonstrated a faster pathological response compared to contusion or distraction injuries. The rapid pathological response and severe injury outcomes

associated with dislocation were analogous to clinical observations, further increasing the relevance of this model and justifying refinement. New dislocation injury clamps were developed to pivot and self-align to rigidly grip vertebrae of different widths. The new clamps were validated with high-speed x-ray and significantly reduced clamp-vertebrae slipping compared to the original clamps. Similar processes should be adopted by other injury models to verify that device input parameters produce desired injury kinematics. Specific parameters were independently determined to incorporate residual compression within the dislocation model, including initial injury displacement, residual compression displacement. Additionally, maintaining residual compression immediately following the initial trauma, mimicking clinical injuries, was found to have significant physiological effects. Finally, differences were observed in spinal canal geometry and mechanical properties of the intervertebral disc, which may be potential factors influencing the deformation experienced by the spinal cord. These developments provide an additional clinically relevant injury model to further investigate the biomechanics of SCI, and allow for more robust evaluation of potential treatments.

References

Ackery, A., Tator, C. H., & Krassioukov, A. (2004). A global perspective on spinal cord injury epidemiology. *Journal of Neurotrauma*, *21*(10), 1355–70. https://doi.org/10.1089/neu.2004.21.1355

Aebli, N., Rüegg, T. B., Wicki, A. G., Petrou, N., & Krebs, J. (2013). Predicting the risk and severity of acute spinal cord injury after a minor trauma to the cervical spine. *The Spine Journal*, *13*(6), 597–604. https://doi.org/10.1016/j.spinee.2013.02.006

Agrawal, G., Sherman, D., Maybhate, A., Gorelik, M., Kerr, D. A., Thakor, N. V., & All, A. H. (2010). Slope analysis of somatosensory evoked potentials in spinal cord injury for detecting contusion injury and focal demyelination. *Journal of Clinical Neuroscience*, *17*(9), 1159–1164. https://doi.org/10.1016/j.jocn.2010.02.005

Agrawal, G., Thakor, N. V., & All, A. H. (2009). Evoked potential versus behavior to detect minor insult to the spinal cord in a rat model. *Journal of Clinical Neuroscience*, *16*(8), 1052–1055. https://doi.org/10.1016/j.jocn.2008.08.009

Ahuja, C. S., Wilson, J. R., Nori, S., Kotter, M. R. N., Druschel, C., Curt, A., & Fehlings, M. G. (2017). Traumatic spinal cord injury. *Nature Reviews Disease Primers*, *3*, 17018. https://doi.org/10.1038/nrdp.2017.18

Aki, T., & Toya, S. (1984). Experimental Study on changes of the spinal-evoked potential and circulatory dynamics following spinal cord compression and decompression. *Spine*, *9*(8), 800–809.

Allen, A. (1911). Surgery of experimental lesion of spinal cord equivalent to crush injury of fracture dislocation of spinal column: a preliminary report. *Journal of the American Medical Association*. Retrieved from http://jamanetwork.com/data/Journals/JAMA/10834/jama_LVII_11_008.pdf

Allen, A. (1914). Remarks on the Histopathological changes in the Spinal Cord due to Impact. *Journal of American Medical Association*, *57*, 141–147.

Allen, B., Ferguson, R., Lehmann, T., & O'Brien, R. (1982). A mechanistic classification of closed, indirect fractures and dislocations of the lower cervical spine. *Spine*, *7*(1), 1–27. https://doi.org/10.1097/00007632-198200710-00001

American Electroencephalographic Society. (1994). Guideline eleven: guidelines forintraoperative monitoring of sensory evoked potentials. *J Clin Neurophysiol*, *11*, 77–87.

Anderson, M., Burda, J., Ren, Y., Ao, Y., O'Shea, T., Kawaguchi, R., Coppola, G., Khakh, B., Deming, T., Sofroniew, M. (2016). Astrocyte scar formation aids central nervous system axon regeneration. *Nature*, *532*(7598), 195–200. https://doi.org/10.1038/nature17623

Anderson, T. E. (1982). A controlled pneumatic technique for experimental spinal cord contusion. *Journal of Neuroscience Methods*, *6*(4), 327–33.

Andrade, M. S. R., Hanania, F. R., Daci, K., Leme, R. J. A., & Chadi, G. (2008). Contuse lesion of the rat spinal cord of moderate intensity leads to a higher time-dependent secondary neurodegeneration than severe one. An open-window for experimental neuroprotective interventions. *Tissue and Cell*, *40*(2), 143–156. https://doi.org/10.1016/j.tice.2007.11.002

Angel, A., & Mason, S. (1982). Brain noradrenaline and potentiation of barbituate anaesthesia: characterization of the receptor types. *Journal of Physiology, 328(Suppl)*, 13–14.

Anissipour, A. K., Agel, J., Bellabarba, C., & Bransford, R. J. (2017). Cervical facet dislocations in the adolescent population: a report of 21 cases at a Level 1 trauma center from 2004 to 2014. *European Spine Journal*, *26*(4), 1266–1271. https://doi.org/10.1007/s00586-017-5003-0

Arnold, P. M., Brodke, D. S., Rampersaud, Y. R., Harrop, J. S., Dailey, A. T., Shaffrey, C. I., Grauer, J., Dvorak, M., Bono, C., Wilsey, J., Lee, J., Nassr, A., Vaccaro, A. Spine Trauma Study Group. (2009). Differences between neurosurgeons and orthopedic surgeons in classifying cervical dislocation injuries and making assessment and treatment decisions: a multicenter reliability study. *American Journal of Orthopedics*, *38*(10), E156-61.

Bain, A., & Meaney, D. (2000). Tissue-level thresholds for axonal damage in an experimental model of central nervous system white matter injury. *Journal of Biomechanical Engineering*, *122*(6), 615–622. https://doi.org/10.1115/1.1324667

Bain, A., Raghupathi, R., & Meaney, D. (2001). Dynamic stretch correlates to both morphological abnormalities and electrophysiological impairment in a model of traumatic axonal injury. *Journal of Neurotrauma*, *18*(5), 499–511. https://doi.org/10.1089/089771501300227305

Barr, M., & Kiernan, J. (1988). *The Human Nervous System: An Anatomical Viewpoint* (Fifth Edit). Philadelphia: J.B. Lippincott Company.

Basso, D. M., Beattie, M. S., Bresnahan, J. C., Anderson, D. K., Faden, A. I., Gruner, J. A., Holford, T. R., Hsu, C. Y., Noble, L. J., Nockels, R., Perot, P. L., Salzman, S. K., Young, W. (1996). MASCIS Evaluation of Open Field Locomotor Scores: Effects of Experience and Teamwork on Reliability. *Journal of Neurotrauma*, *13*(7), 343–359. https://doi.org/10.1089/neu.1996.13.343

Bauze, R. J., & Ardran, G. M. (1978). Experimental production of forward dislocation in the human cervical spine. *The Journal of Bone and Joint Surgery. British Volume*, *60*(2), 239–45. Retrieved from http://www.ncbi.nlm.nih.gov/pubmed/659473

Bazley, F., Hu, C., Maybhate, A., Pourmorteza, A., Pashai, N., Thakor, N., … All, A. (2012). Electrophysiological evaluation of sensory and motor pathways after incomplete unilateral spinal cord contusion. *Journal of Neurosurgery: Spine*, *16*(April), 414–423. https://doi.org/10.3171/2012.1.SPINE11684

Beatson, T. (1963). Fractures and dislocations of the cervical spine. *Journal of Bone & Joint Surgery*, *45–B*(1), 21–35.

Beattie, M. S., Hermann, G. E., Rogers, R. C., & Bresnahan, J. C. (2002). Cell death in models of spinal cord injury. *Progress in Brain Research*, *137*, 37–47. Retrieved from http://www.ncbi.nlm.nih.gov/pubmed/12440358

Bell, J. E. S., Seifert, J. L., Shimizu, E. N., Sucato, D. J., & Romero-Ortega, M. I. (2017). Atraumatic Spine Distraction Induces Metabolic Distress in Spinal Motor Neurons. *Journal of Neurotrauma*, neu.2016.4779. https://doi.org/10.1089/neu.2016.4779

Bernal-Chico, A., Canedo, M., Manterola, A., Victoria Sánchez-Gómez, M., Pérez-Samartín, A., Rodríguez-Puertas, R., Matute, C., Mato, S. (2015). Blockade of monoacylglycerol lipase inhibits oligodendrocyte excitotoxicity and prevents demyelination in vivo. *Glia*, *63*(1), 163–176. https://doi.org/10.1002/glia.22742

Bhatnagar, T., Liu, J., & Oxland, T. (2014). Characterization of a novel, magnetic resonance imaging-compatible rodent model spinal cord injury device. *Journal of Biomechanical Engineering*, *136*(9), 95001. https://doi.org/10.1115/1.4027670

Bhatnagar, T., Liu, J., Yung, A., Cripton, P. A., Kozlowski, P., & Oxland, T. (2016A). In Vivo Measurement of Cervical Spinal Cord Deformation During Traumatic Spinal Cord Injury in a Rodent Model. *Annals of Biomedical Engineering*, *44*(4), 1285–1298. https://doi.org/10.1007/s10439-015-1412-6

Bhatnagar, T., Liu, J., Yung, A., Cripton, P., Kozlowski, P., Tetzlaff, T., & Oxland, T. (2016B). Relating Histopathology and Mechanical Strain in Experimental Contusion Spinal Cord Injury in a Rat Model. *Journal of Neurotrauma*, *33*, 1685–1695. https://doi.org/10.1089/neu.2015.4200

Bilston, L. (2016). The Influence of Microstructure on Neural Tissue Mechanics. In *Structure-Based Mechanics of Tissues and Organs* (pp. 1–469). https://doi.org/10.1007/978-1-4899-7630-7

Bilston, L., & Thibault, L. (1996). The Mechanical Properties of the Human Cervical Spinal Cord In Vitro. *Annals of Biomedical Engineering*, *24*, 67–74.

Blight, A. (1991). Morphometric analysis of a model of spinal cord injury in guinea pigs, with behavioral evidence of delayed secondary pathology. *Journal of the Neurological Sciences*, *103*(2), 156–71. Retrieved from http://www.ncbi.nlm.nih.gov/pubmed/1880533

Blight, A., & De Crescito, V. (1986). Morphometric analysis of experimental spinal cord injury in the cat : The relation of injury in density to survival of myelinated axons. *Neuroscience*, *19*(1), 321–341.

Boerger, T. O., Limb, D., & Dickson, R. A. (2000). Does "Canal Clearance" Affect Neurological Outcome after Thoracolumbar Burst Fractures? *The Journal of Bone and Joint Surgery*, *82–B*(5), 629–635.

Brainerd, E. L., Baier, D. B., Gatesy, S. M., Hedrick, T. L., Metzger, K. a, Gilbert, S. L., & Crisco, J. J. (2010). X-ray reconstruction of moving morphology (XROMM): precision, accuracy and applications in comparative biomechanics research. *Journal of Experimental Zoology. Part A, Ecological Genetics and Physiology*, *313*(5), 262–279. https://doi.org/10.1002/jez.589

Bresnahan, J. C., Beattie, M. S., Todd III, F. D., & Noyes, D. H. (1987). A behavioral and anatomical analysis of spinal cord injury produced by a feedback-controlled impaction device. *Experimental Neurology*, *95*(3), 548–70. Retrieved from http://www.ncbi.nlm.nih.gov/pubmed/3817079

Burke, J. F., Yue, J. K., Ngwenya, L. B., Winkler, E. A., Talbott, J., Pan, J., Ferguson, A., Beattie, M., Bresnahan, J., Haefeli, J., Whetstone, W., Suen, C., Huang, M., Manley, G., Tarapore, P., Dhall, S. S. (2016). Ultra-Early (<12 Hours) Decompression Improves Recovery After Spinal Cord Injury Compared to Early (12-24 Hours) Decompression. *Neurosurgery*, *63*, 172. https://doi.org/10.1227/01.neu.0000489751.59414.45

Cadotte, D., & Fehlings, M. (2011). Spinal cord injury: a systematic review of current treatment options. *Clinical Orthopaedics and Related Research*, *469*(3), 732–41. https://doi.org/10.1007/s11999-010-1674-0

Candès, E., Demanet, L., Donoho, D., & Ying, L. (2006). Fast Discrete Curvelet Transforms. *Multiscale Model. Simul.*, *5*(3), 861–899. https://doi.org/10.1137/05064182X

Carlson, G., Gorden, C., Nakazowa, S., Wada, E., Warden, K., & LaManna, J. (2000). Perfusion-limited recovery of evoked potential function after spinal cord injury. *Spine*, *25*(10), 1218–26. Retrieved from http://www.ncbi.nlm.nih.gov/pubmed/10806497

Carlson, G., Gordon, C., Oliff, H., Pillai, J., & LaManna, J. (2003). Sustained Spinal Cord Compression - Part I: Time-Dependent Effect on Long-Term Pathophysiology. *The Journal of Bone and Joint Surgery*, *85–A*(1), 86–94.

Carlson, G., Minato, Y., Okada, A., Gorden, C., Warden, K., Barbeau, J., Biro, C., Bahnuik, E., Bohlman, H., LaManna, J. (1997A). Early Time-Dependent Decompression for Spinal Cord Injury: Vascular Mechanisms of Recovery. *Journal of Neurotrauma*, *14*(12), 951–962.

Carlson, G., Warden, K., Barbeau, J., Bahnuik, E., Kutina-Nelson, K., Biro, C., Bohlman, H., LaManna, J. (1997B). Viscoelastic Relaxation and Regional Blood Flow Response to Spinal Cord Compression and Decompression. *Spine*, *22*(12), 1285–1291. Retrieved from http://www.ncbi.nlm.nih.gov/pubmed/9201829

Carlson, S., Parrish, M., Springer, J., Doty, K., & Dossett, L. (1998). Acute inflammatory response in spinal cord following impact injury. *Experimental Neurology*, *151*(1), 77–88. https://doi.org/10.1006/exnr.1998.6785

Carter, J. W., Mirza, S. K., Tencer, a F., & Ching, R. P. (2000). Canal geometry changes associated with axial compressive cervical spine fracture. *Spine*, *25*(1), 46–54. Retrieved from http://www.ncbi.nlm.nih.gov/pubmed/10647160

Casha, S., Yu, W. R., & Fehlings, M. G. (2001). Oligodendroglial apoptosis occurs along degenerating axons and is associated with FAS and p75 expression following spinal cord injury in the rat. *Neuroscience*, *103*(1), 203–18. Retrieved from http://www.ncbi.nlm.nih.gov/pubmed/11311801

Chang, D., Trencer, A., Ching, R., Treece, B., Senft, D., & Anderson, P. (1994). Geometric changes in the cervical spinal canal during impact. *Spine*, *19*(8), 973–980.

Chen, K., Liu, J., Assinck, P., Bhatnagar, T., Streijger, F., Zhu, Q., Dvorak, M., Kwon, B. K., Tetzlaff, W., Oxland, T. R. (2016A). Differential Histopathological and Behavioral Outcomes Eight Weeks after Rat Spinal Cord Injury by Contusion, Dislocation, and Distraction Mechanisms. *Journal of Neurotrauma*, *33*, 1–18. https://doi.org/10.1089/neu.2015.4218

Chen, Y., He, Y., & DeVivo, M. J. (2016B). Changing Demographics and Injury Profile of New Traumatic Spinal Cord Injuries in the United States, 1972-2014. *Archives of Physical Medicine and Rehabilitation*, *97*(10), 1610–1619. https://doi.org/10.1016/j.apmr.2016.03.017

Cheng, S., Clarke, E. C., & Bilston, L. (2008). Rheological properties of the tissues of the central nervous system: A review. *Medical Engineering and Physics*, *30*(10), 1318–1337. https://doi.org/10.1016/j.medengphy.2008.06.003

Cheriyan, T., Ryan, D. J., Weinreb, J. H., Cheriyan, J., Paul, J. C., Lafage, V., Kirsch, T., Errico, T. J. (2014). Spinal cord injury models: a review. *Spinal Cord*, *52*(8), 588–95. https://doi.org/10.1038/sc.2014.91

Choo, A., Liu, J., Dvorak, M., Tetzlaff, W., & Oxland, T. (2008). Secondary pathology following contusion, dislocation, and distraction spinal cord injuries. *Experimental Neurology*, *212*(2), 490–506. https://doi.org/10.1016/j.expneurol.2008.04.038

Choo, A., Liu, J., Lam, C. K., Dvorak, M., Tetzlaff, W., & Oxland, T. (2007). Contusion, dislocation, and distraction: primary hemorrhage and membrane permeability in distinct mechanisms of spinal cord injury. *Journal of Neurosurgery: Spine*, *6*(3), 255–66. https://doi.org/10.3171/spi.2007.6.3.255

Choo, A., Liu, J., Liu, Z., Dvorak, M., Tetzlaff, W., & Oxland, T. (2009). Modeling spinal cord contusion, dislocation, and distraction: characterization of vertebral clamps, injury severities, and node of Ranvier deformations. *Journal of Neuroscience Methods*, *181*(1), 6–17. https://doi.org/10.1016/j.jneumeth.2009.04.007

Clarke, E. C. (2011). Spinal Cord Mechanical Properties. In *Studies in Mechanobiology, Tissue Engineering and Biomaterials* (pp. 25–40). https://doi.org/10.1007/8415

Clarke, E. C., & Bilston, L. E. (2008). Contrasting biomechanics and neuropathology of spinal cord injury in neonatal and adult rats following vertebral dislocation. *Journal of Neurotrauma*, *25*(7), 817–32. https://doi.org/10.1089/neu.2007.0379

Clarke, E. C., Cheng, S., & Bilston, L. E. (2009). The mechanical properties of neonatal rat spinal cord in vitro, and comparisons with adult. *Journal of Biomechanics*, *42*(10), 1397–402. https://doi.org/10.1016/j.jbiomech.2009.04.008

Clarke, E. C., Choo, A., Liu, J., Lam, C. K., Bilston, L. E., Tetzlaff, W., & Oxland, T. (2008). Anterior fracture-dislocation is more severe than lateral: a biomechanical and neuropathological comparison in rat thoracolumbar spine. *Journal of Neurotrauma*, *25*(4), 371–83. https://doi.org/10.1089/neu.2007.0421

Clausen, J. D., Goel, V. K., Traynelis, V. C., & Scifert, J. (1997). Uncinate processes and Luschka joints influence the biomechanics of the cervical spine: Quantification using a finite element model of the C5-C6 segment. *Journal of Orthopaedic Research*, *15*(3), 342–347. https://doi.org/10.1002/jor.1100150305

Cloud, B. A., Ball, B. G., Chen, B. K., Knight, A. M., Hakim, J. S., Ortiz, A. M., & Windebank, A. J. (2012). Hemisection spinal cord injury in rat: The value of intraoperative somatosensory evoked potential monitoring. *Journal of Neuroscience Methods*, *211*(2), 179–184. https://doi.org/10.1016/j.jneumeth.2012.08.024

Clough, G. (1982). Environmental effects on animals used in biomedical research. *Biological Reviews*, *57*(3), 487–523. https://doi.org/10.1111/j.1469-185X.1982.tb00705.x

Coste, B., Mathur, J., Schmidt, M., Earley, T. J., Ranade, S., Petrus, M. J., Dubin, A., Patapoutian, A. (2010). Piezo1 and Piezo2 are essential components of distinct mechanically activated cation channels. *Science*, *330*(6000), 55–60. https://doi.org/10.1126/science.1193270

Courtine, G., Bunge, M. B., Fawcett, J. W., Grossman, R. G., Kaas, J. H., Lemon, R., Maier, I., Martin, J., Nudo, R., Ramon-cueto, A., Rouiller, E., Schnell, L., Wannier, T., Schwab, M., Edgerton, V. R. (2007). Can experiments in nonhuman primates expedite the translation of treatments for spinal cord injury in humans ? *Nature Medicine*, *13*(5), 561–566. https://doi.org/10.1038/nm1595

Croft, T. J., Brodkey, J. S., & Nulsen, F. E. (1972). Reversible spinal cord trauma: a model for electrical monitoring of spinal cord function. *Journal of Neurosurgery*, *36*(4), 402–6. https://doi.org/10.3171/jns.1972.36.4.0402

Crosby, E. T. (2006). Airway Management in Adults aftre Cervical Spine Trauma. *Anesthesiology*, *104*(6), 1293–1318. Retrieved from http://anesthesiology.pubs.asahq.org/article.aspx?articleid=1923133

Crowe, M. J., Bresnahan, J. C., Shuman, S. L., Masters, J. N., & Beattie, M. S. (1997). Apoptosis and delayed degeneration after spinal cord injury in rats and monkeys. *Nat Med*, *3*(1), 73–76. https://doi.org/10.1038/nm0197-73

Crowell, R. R., Shea, M., Edwards, W. T., Clothiaux, P. L., White, A. A., & Hayes, W. C. (1993). Cervical injuries under flexion and compression loading. *Journal of Spinal Disorders*, *6*(2), 175–81. https://doi.org/10.1097/00024720-199304000-00013

Cullen, D. K., & LaPlaca, M. C. (2006). Neuronal response to high rate shear deformation depends on heterogeneity of the local strain field. *Journal of Neurotrauma*, *23*(9), 1304–1319. https://doi.org/10.1089/neu.2006.23.1304

Cullen, D. K., Vernekar, V. N., & LaPlaca, M. C. (2011). Trauma-Induced Plasmalemma Disruptions in Three-Dimensional Neural Cultures Are Dependent on Strain Modality and Rate. *Journal of Neurotrauma*, *28*(11), 2219–2233. https://doi.org/10.1089/neu.2011.1841

Dabney, K. W., Ehrenshteyn, M., Agresta, C. A., Twiss, J. L., Stern, G., Tice, L., & Salzman, S. K. (2004). A model of experimental spinal cord trauma based on computer-controlled intervertebral distraction: Characterization of graded injury. *Spine*, *29*(21), 2357–2364. https://doi.org/10.1097/01.brs.0000143108.65385.74

Delamarter, R., Sherman, J., & Carr, J. (1991). 1991 Volvo Award in Experimental Studies. Cauda Equina Syndrome: Neurologic Recovery Following Immediate, Early, or Late Decompression. *Spine*, *16*(9), 1022–1029.

Delamarter, R., Sherman, J., & Carr, J. (1995). Pathophysiology of Spinal Cord Injury - Recovery After Immediate and Delayed Decompression. *The Journal of Bone and Joint Surgery*, *77–A*(7), 1042–1049.

Denis, F. (1983). The three column spine and its significance in the classification of acute thoracolumbar spinal injuries. *Spine*, *8*(8), 817–831.

Dickhaus, H., Pauser, G., & Zimmermann, M. (1985). Tonic descending inhibition affects intensity coding of nociceptive responses of spinal dorsal horn neurones in the cat. *Pain*, *23*(2), 145–58. Retrieved from http://www.ncbi.nlm.nih.gov/pubmed/4069718

Dimar, J. R., Glassman, S. D., Raque, G. H., Zhang, Y. P., & Shields, C. B. (1999). The influence of spinal canal narrowing and timing of decompression on neurologic recovery after spinal cord contusion in a rat model. *Spine*, *24*(16), 1623–33. Retrieved from http://www.ncbi.nlm.nih.gov/pubmed/10472095

Dobran, M., Iacoangeli, M., Nocchi, N., Di Rienzo, A., di Somma, L. G. M., Nasi, D., Colasanti, R., Al-Fay, M., Scerrati, M. (2015). Surgical treatment of cervical spine trauma: Our experience and results. *Asian Journal of Neurosurgery*, *10*(3), 207–11. https://doi.org/10.4103/1793-5482.161192

Dohrmann, G. J., Panjabi, M. M., & Banks, D. (1978). Biomechanics of experimental spinal cord trauma. *Journal of Neurosurgery*, *48*(6), 993–1001. https://doi.org/10.3171/jns.1978.48.6.0993

Dolan, E., Tator, C., & Endrenyi, L. (1980). The value of decompression for acute experimental spinal cord compression injury. *Journal of Neurosurgery*, *53*(6), 749–55. https://doi.org/10.3171/jns.1980.53.6.0749

Donnelly, D. J., & Popovich, P. G. (2008). Inflammation and its role in neuroprotection, axonal regeneration and functional recovery after spinal cord injury. *Experimental Neurology*, *209*(2), 378–388. https://doi.org/10.1016/j.expneurol.2007.06.009.Inflammation

Du, W., Wang, C., Tan, J., Shen, B., Ni, S., & Zheng, Y. (2014). Management of Subaxial Cervical Facet Dislocation Through Anterior Approach Monitored by Spinal Cord Evoked Potential. *Spine*, *39*(1), 48–52. https://doi.org/10.1097/BRS.0000000000000046

Dula, A. N., Gochberg, D. F., Valentine, H. L., Valentine, W. M., & Does, M. D. (2010). Multiexponential T2, magnetization transfer, and Quantitative histology in white matter tracts of rat spinal cord. *Magnetic Resonance in Medicine*, *63*(4), 902–909. https://doi.org/10.1002/mrm.22267

Dumont, R. J., Okonkwo, D. O., Verma, S., Hurlbert, R. J., Boulos, P. T., Ellegala, D. B., & Dumont, A. S. (2001). Acute Spinal Cord Injury , Part I : Pathophysiologic Mechanisms. *Clinical Neuropharmacology*, *24*(5), 254–264.

Durbin, F. (1957). Fracture-dislocations of the cervical spine. *The Journal of Bone and Joint Surgery*, *39B*(1), 23–38. Retrieved from http://bjj.boneandjoint.org.uk/content/39-B/1/23

Ebraheim, N. A., Patil, V., Liu, J., Haman, S. P., & Yeasting, R. A. (2008). Morphometric analyses of the cervical superior facets and implications for facet dislocation. *International Orthopaedics*, *32*(1), 97–101. https://doi.org/10.1007/s00264-006-0286-5

Edwards, W., Crowell, R., Coffee, M., & White, A. (1988). Mechanisms of injury in the cervical spine. In *Proceedings of a Special Symposium on Maturing Technologies and Emerging Horizons in Biomedical Engineering.* (pp. 123–129). IEEE. https://doi.org/10.1109/MTEHBE.1988.26415

Eismont, F. J., Clifford, S., Goldberg, M., & Green, B. (1984). Cervical sagittal spinal canal size in spine injury. *Spine*, *9*(7), 663–6. Retrieved from http://www.ncbi.nlm.nih.gov/pubmed/6505832

Elliott, H. C. (1945). Cross sectional diameters and areas of the human spinal cord. *The Anatomical Record*, *93*, 287–93. Retrieved from http://www.ncbi.nlm.nih.gov/pubmed/21008200

Engesser-Cesar, C., Anderson, A. J., Basso, D. M., Edgerton, V. R., & Cotman, C. W. (2005). Voluntary Wheel Running Improves Recovery from a Moderate Spinal Cord Injury. *Journal of Neurotrauma*, *22*(1), 157–171. https://doi.org/10.1089/neu.2005.22.157

Erbayraktar, Z., Gökmen, N., Yılmaz, O., & Erbayraktar, S. (2013). Experimental Traumatic Spinal Cord Injury. *Methods in Molecular Biology (Clifton, N.J.)*, *982*, 103–112. https://doi.org/10.1007/978-1-62703-308-4

Evans, T., Barkauskas, D., Myers, J., Hare, E., You, J., Ransohoff, R., Huang, A., Silver, J. (2014). High-resolution intravital imaging reveals that blood-derived macrophages but not resident microglia facilitate secondary axonal dieback in traumatic spinal cord injury. *Experimental Neurology*, *254*, 109–120. https://doi.org/10.1016/J.EXPNEUROL.2014.01.013

Fehlings, M., Tator, C., & Linden, R. (1989). The relationships among the severity of spinal cord injury, motor and somatosensory evoked potentials and spinal cord blood flow. *Electroencephalography and Clinical Neurophysiology*, *74*(4), 241–59. Retrieved from http://www.ncbi.nlm.nih.gov/pubmed/2471626

Fehlings, M., Vaccaro, A., Wilson, J., Singh, A., W Cadotte, D., Harrop, J., Aarabi, B., Shaffrey, C., Dvorak, M., Fisher, C., Arnold, P., Massicotte, E., Lewis, S., Rampersaud, R. (2012). Early versus Delayed Decompression for Traumatic Cervical Spinal Cord Injury: Results of the Surgical Timing in Acute Spinal Cord Injury Study (STASCIS). *PloS One*, *7*(2), e32037. https://doi.org/10.1371/journal.pone.0032037

Fehlings, M., & Wilson, J. (2010). Timing of surgical intervention in spinal trauma: what does the evidence indicate? *Spine*, *35*(21 Suppl), S159-60. https://doi.org/10.1097/BRS.0b013e3181f330f4

Fehlings, M., Wilson, J., Dvorak, M., Vaccaro, A., & Fisher, C. (2010). The challenges of managing spine and spinal cord injuries: an evolving consensus and opportunities for change. *Spine*, *35*(21 Suppl), S161-5. https://doi.org/10.1097/BRS.0b013e3181f352eb

Feir-walsh, B., & Toothaker, L. (1974). Assumptions Homogeneity Pendence. *Educational and Psychological Measurement*, *34*(4), 789–799. https://doi.org/10.1177/001316447403400406

Field, K. J., & Lang, C. M. (1988). Hazards of urethane (ethyl carbamate): a review of the literature. *Laboratory Animals*, *22*(3), 255–62. https://doi.org/10.1258/002367788780746331

Fiford, R., & Bilston, L. (2005). The mechanical properties of rat spinal cord in vitro. *Journal of Biomechanics*, *38*(7), 1509–15. https://doi.org/10.1016/j.jbiomech.2004.07.009

Fiford, R., Bilston, L., Waite, P., & Lu, J. (2004). A vertebral dislocation model of spinal cord injury in rats. *Journal of Neurotrauma*, *21*(4), 451–8. https://doi.org/10.1089/089771504323004593

Filli, L., & Schwab, M. E. (2012). The rocky road to translation in spinal cord repair. *Annals of Neurology*, *72*(4), 491–501. https://doi.org/10.1002/ana.23630

Fisher, C. G., Noonan, V. K., Smith, D. E., Wing, P. C., Dvorak, M. F., & Kwon, B. K. (2005). Motor recovery, functional status, and health-related quality of life in patients with complete spinal cord injuries. *Spine*, *30*(19), 2200–7. Retrieved from http://www.ncbi.nlm.nih.gov/pubmed/16205347

Fitzharris, M., Cripps, R. A., & Lee, B. B. (2014). Estimating the global incidence of traumatic spinal cord injury. *Spinal Cord*, *52*(2), 117–122. https://doi.org/10.1038/sc.2013.135

Flecknell, P. A. (2016). *Laboratory Animal Anaesthesia* (4th Ed.). Elsevier. Retrieved from https://books.google.ca/books?hl=en&lr=&id=2NuoBAAAQBAJ&oi=fnd&pg=PP1&ots=UWC8ctzo-8&sig=TScMmxMMBPUB49jYVt0UHdvxeD8#v=onepage&q&f=false

Flynn, J. R., & Bolton, P. S. (2007). Measurement of the vertebral canal dimensions of the neck of the rat with a comparison to the human. *Anatomical Record*, *290*(7), 893–899. https://doi.org/10.1002/ar.20523

Fradet, L., Cliche, F., Petit, Y., Mac-Thiong, J.-M., & Arnoux, P.-J. (2016). Strain rate dependent behavior of the porcine spinal cord under transverse dynamic compression. *Proceedings of the Institution of Mechanical Engineers, Part H: Journal of Engineering in Medicine*, *230*(9), 954411916655373. https://doi.org/10.1177/0954411916655373

Fredrickson, B. E., Edwards, W. T., Rauschning, W., Bayley, J. C., & Yuan, H. A. (1992). Vertebral burst fractures: an experimental, morphologic, and radiographic study. *Spine*, *17*(9), 1012–21. Retrieved from http://www.ncbi.nlm.nih.gov/pubmed/1411751

Fukuda, S., Nakamura, T., Kishigami, Y., Endo, K., Azuma, T., Fujikawa, T., Tsutsumi, S., Shimizu, Y. (2005). New canine spinal cord injury model free from laminectomy. *Brain Research Protocols, 14*(3), 171–180. https://doi.org/10.1016/j.brainresprot.2005.01.001

Furlan, J. C., Noonan, V., Cadotte, D. W., & Fehlings, M. G. (2011). Timing of decompressive surgery of spinal cord after traumatic spinal cord injury: an evidence-based examination of pre-clinical and clinical studies. *Journal of Neurotrauma*, *28*(8), 1371–99. https://doi.org/10.1089/neu.2009.1147

Gerber, A. M., & Corrie, W. S. (1979). Effect of impounder contact area on experimental spinal cord injury. *Journal of Neurosurgery*, *51*(4), 539–542.

Geremia, N., Hryciw, T., Bao, F., Streijger, F., Okon, E., Lee, J., … Brown, A. (2017). The effectiveness of the anti-CD11d treatment is reduced in rat models of spinal cord injury that produce significant levels of intraspinal hemorrhage. *Experimental Neurology*, *295*, 125–134. https://doi.org/10.1016/j.expneurol.2017.06.002

Grassner, L., Wutte, C., Klein, B., Mach, O., Riesner, S., Panzer, S., Weaver, L., Dekaban, G., Kwon, B. K., Maier, D. (2016). Early decompression (< 8 h) after traumatic cervical spinal cord injury improves functional outcome as assessed by Spinal Cord Independence Measure (SCIM) after 1 year. *Journal of Neurotrauma*, *1*(5), 1–47. https://doi.org/10.1089/neu.2015.4325

Greaves, C. Y., Gadala, M. S., & Oxland, T. (2008). A three-dimensional finite element model of the cervical spine with spinal cord: an investigation of three injury mechanisms. *Annals of Biomedical Engineering*, *36*(3), 396–405. https://doi.org/10.1007/s10439-008-9440-0

Grossman, S. D., Rosenberg, L. J., & Wrathall, J. R. (2001). Temporal–Spatial Pattern of Acute Neuronal and Glial Loss after Spinal Cord Contusion. *Experimental Neurology*, *168*(2), 273–282. https://doi.org/10.1006/exnr.2001.7628

Gruner, J. A. (1992). A monitored contusion model of spinal cord injury in the rat. *J.Neurotrauma*, *9*(0897–7151), 123–126.

Guha, A., Tator, C., Endrenyi, L., & Piper, I. (1987). Decompression of the Spinal Cord Improves Recovery after Acute Experimental Spinal Cord Compression Injury. *Paraplegia*, *25*(4), 324–339. https://doi.org/10.1038/sc.1987.61

Hagg, T., & Oudega, M. (2006). Neural Degeneration and Regeneration Myelin and Scar-Derived Inhibition. *Journal of Neurotrauma*, *23*(3/4), 264–280.

Hall, R. M., Oakland, R. J., Wilcox, R. K., & Barton, D. C. (2006). Spinal cord-fragment interactions following burst fracture: an in vitro model. *Journal of Neurosurgery. Spine*, *5*(3), 243–50. https://doi.org/10.3171/spi.2006.5.3.243

Harrington, J. F., & Park, M. C. (2007). Single level arthrodesis as treatment for midcervical fracture subluxation: a cohort study. *Journal of Spinal Disorders & Techniques*, *20*(1), 42–8. https://doi.org/10.1097/01.bsd.0000211255.05626.b0

Hashimoto, T., & Fukuda, N. (1990). New spinal cord injury model produced by spinal cord compression in the rat. *Journal of Pharmacological Methods*, *23*(3), 203–12. Retrieved from http://www.ncbi.nlm.nih.gov/pubmed/2329801

Hausmann, O. N. (2003). Review Post-traumatic inflammation following spinal cord injury. *Spinal*, *41*, 369–378. https://doi.org/10.1038/sj.sc.3101483

Hayton, S. M., Kriss, A., & Muller, D. P. R. (1999). Comparison of the effects of four anaesthetic agents on somatosensory evoked potentials in the rat. *Laboratory Animals*, *33*(February 1999), 243–251. https://doi.org/10.1258/002367799780578219

Herndon, W. A., & Galloway, D. (1988). Neurologic return versus cross-sectional canal area in incomplete thoracolumbar spinal cord injuries. *The Journal of Trauma*, *28*(5), 680–3. Retrieved from http://www.ncbi.nlm.nih.gov/pubmed/3367414

Hilton, B. J., Moulson, A. J., & Tetzlaff, W. (2016). Neuroprotection and secondary damage following spinal cord injury: concepts and methods. *Neuroscience Letters*. https://doi.org/10.1016/j.neulet.2016.12.004

Hoeijmakers, J. G., Faber, C. G., Lauria, G., Merkies, I. S., & Waxman, S. G. (2012). Small-fibre neuropathies—advances in diagnosis, pathophysiology and management. *Nature Reviews Neurology*, *8*(7), 369–379. https://doi.org/10.1038/nrneurol.2012.97

Holdsworth, F. (1963). Fractures, Dislocations, and Fracture-Dislocations of the Spine. *Journal of Bone & Joint Surgery*, *45–B*(1), 6–20. Retrieved from http://www.boneandjoint.org.uk/content/jbjsbr/45-B/1/6.full.pdf

Holdsworth, F. (1970). Review Article: Fractures, Dislocations, and Fracture-Dislocations of the Spine. *Journal of Bone & Joint Surgery*, *52–A*(8), 1534–1551. Retrieved from http://journals.lww.com/jbjsjournal/Abstract/1970/52080/Review_Article_Fractures,_Dislocations,_and.2.aspx

Hung, T. K., & Chang, G. L. (1981). Biomechanical and neurological response of the spinal cord of a puppy to uniaxial tension. *Journal of Biomechanical Engineering*, *103*(1), 43–7. Retrieved from http://www.ncbi.nlm.nih.gov/pubmed/7253612

Hung, T. K., Chang, G. L., Chang, J. L., & Albin, M. S. (1981A). Stress-strain relationship and neurological sequelae of uniaxial elongation of the spinal cord of cats. *Surgical Neurology*, *15*(6), 471–6. Retrieved from http://www.ncbi.nlm.nih.gov/pubmed/7280961

Hung, T. K., Chang, G. L., Lin, H. S., Walter, F. R., & Bunegin, L. (1981B). Stress-strain relationship of the spinal cord of anesthetized cats. *Journal of Biomechanics*, *14*(4), 269–76. Retrieved from http://www.ncbi.nlm.nih.gov/pubmed/7240289

Ichihara, K., Taguchi, T., Shimada, Y., Sakuramoto, I., Kawano, S., & Kawai, S. (2001). Gray matter of the bovine cervical spinal cord is mechanically more rigid and fragile than the white matter. *Journal of Neurotrauma*, *18*(3), 361–7. https://doi.org/10.1089/08977150151071053

Iggo, A., Steedman, W. M., & Fleetwood-Walker, S. (1985). Spinal processing: anatomy and physiology of spinal nociceptive mechanisms. *Philosophical Transactions of the Royal Society of London. Series B, Biological Sciences*, *308*(1136), 235–52. Retrieved from http://www.ncbi.nlm.nih.gov/pubmed/2858881

Isla, A., Alvarez, F., Perez-López, C., Budke, M., Moraleda, S., Martinez, M., & García-Reneses, J. (2002). Posterior approach for low cervical fractures with unilateral or bilateral facet dislocation. *European Journal of Orthopaedic Surgery & Traumatology*, *12*(3), 123–128. https://doi.org/10.1007/s00590-002-0039-0

Ito, S., Panjabi, M. M., Ivancic, P. C., & Pearson, A. M. (2004). Spinal canal narrowing during simulated whiplash. *Spine*, *29*(12), 1330–1339. https://doi.org/10.1097/01.BRS.0000127186.81814.4A

Ivancic, P. C., Panjabi, M. M., Tominaga, Y., Pearson, A. M., Elena Gimenez, S., & Maak, T. G. (2006). Spinal canal narrowing during simulated frontal impact. *European Spine Journal*, *15*(6), 891–901. https://doi.org/10.1007/s00586-005-0985-4

Ivancic, P. C., Pearson, A. M., Tominaga, Y., Simpson, A. K., Yue, J. J., & Panjabi, M. M. (2007). Mechanism of cervical spinal cord injury during bilateral facet dislocation. *Spine*, *32*(22), 2467–73. https://doi.org/10.1097/BRS.0b013e3181573b67

Ivancic, P. C., Pearson, A. M., Tominaga, Y., Simpson, A. K., Yue, J. J., & Panjabi, M. M. (2008). Biomechanics of cervical facet dislocation. *Traffic Injury Prevention*, *9*(6), 606–611. https://doi.org/10.1080/15389580802344804

Jakeman, L. B., Guan, Z., Wei, P., Ponnappan, R., Dzwonczyk, R., Popovich, P. G., & Stokes, B. T. (2000). Traumatic Spinal Cord Injury Produced by Controlled Contusion in Mouse. *Journal of Neurotrauma*, *17*(4), 299–319.

Jaumard, N. V., Leung, J., Gokhale, A. J., Guarino, B. B., Welch, W. C., & Winkelstein, B. A. (2015). Relevant Anatomic and Morphological Measurements of the Rat Spine. *Spine*, *40*(20), E1084–E1092. https://doi.org/10.1097/BRS.0000000000001021

Johnson, M. G., Fisher, C. G., Boyd, M., Pitzen, T., Oxland, T. R., & Dvorak, M. F. (2004). The radiographic failure of single segment anterior cervical plate fixation in traumatic cervical flexion distraction injuries. *Spine*, *29*(24), 2815–20. Retrieved from http://www.ncbi.nlm.nih.gov/pubmed/15599284

Jug, M., Kejžar, N., Vesel, M., Al Mawed, S., Dobravec, M., Herman, S., & Bajrović, F. F. (2015). Neurological Recovery after Traumatic Cervical Spinal Cord Injury Is Superior if Surgical Decompression and Instrumented Fusion Are Performed within 8 Hours versus 8 to 24 Hours after Injury: A Single Center Experience. *Journal of Neurotrauma*, *8*(18), 150422072921008. https://doi.org/10.1089/neu.2014.3767

Kang, J. D., Figgie, M. P., & Bohlman, H. H. (1994). Sagittal measurements of the cervical spine in subaxial fractures and dislocations. An analysis of two hundred and eighty-eight patients with and without neurological deficits. *The Journal of Bone and Joint Surgery. American Volume*, *76*(11), 1617–28. Retrieved from http://www.ncbi.nlm.nih.gov/pubmed/7962021

Kastner, A., & Gauthier, P. (2008). Are rodents an appropriate pre-clinical model for treating spinal cord injury? Examples from the respiratory system. *Experimental Neurology*, *213*(2), 249–56. https://doi.org/10.1016/j.expneurol.2008.07.008

Kearney, P. A., Ridella, S. A., Viano, D. C., Anderson, T. E. (1988). Interaction of contact velocity and cord compression in determining the severity of spinal cord injury. *Journal of Neurotrauma*, *5*(3), 187–208. Retrieved from http://www.ncbi.nlm.nih.gov/pubmed/3246693

Khuyagbaatar, B., Kim, K., Man Park, W., Hyuk Kim, Y. (2016). Biomechanical Behaviors in Three Types of Spinal Cord Injury Mechanisms. *Journal of Biomechanical Engineering*, *138*(8), 81003. https://doi.org/10.1115/1.4033794

Kim, J. H., Tu, T.-W., Bayly, P. V., Song, S.-K. (2009). Impact Speed Does Not Determine Severity of Spinal Cord Injury in Mice with Fixed Impact Displacement. *Journal of Neurotrauma*, *26*(8), 1395–1404. https://doi.org/10.1089/neu.2008.0728

Kjell, J., & Olson, L. (2016). Rat models of spinal cord injury: from pathology to potential therapies. *Disease Models & Mechanisms*, *9*(10), 1125–1137. https://doi.org/10.1242/dmm.025833

Kobrine, A. I., Evans, D., Rizzoli, H. V. (1979). Experimental acute balloon compression of the spinal cord: Factors affecting disappearance and return of the spinal evoked response, *51*, 841–845.

Kortelainen, J., Vipin, A., Thow Xin Yuan, Mir, H., Thakor, N., Al-Nashash, H., All, A. (2014). Effect of isoflurane on somatosensory evoked potentials in a rat model. In *2014 36th Annual International Conference of the IEEE Engineering in Medicine and Biology Society* (pp. 4286–4289). IEEE. https://doi.org/10.1109/EMBC.2014.6944572

Koser, D. E., Moeendarbary, E., Hanne, J., Kuerten, S., Franze, K. (2015). CNS cell distribution and axon orientation determine local spinal cord mechanical properties. *Biophysical Journal*, *108*(9), 2137–2147. https://doi.org/10.1016/j.bpj.2015.03.039

Koyanagi, I., & Tator, C. H. (1996). The effects of cortical stimulation, anesthesia and recording site on somatosensory evoked potentials in the rat. *Electroencephalography and Clinical Neurophysiology/Electromyography and Motor Control*, *101*(6), 534–542. https://doi.org/10.1016/S0921-884X(96)96007-5

Kroeker, S. G., & Ching, R. P. (2013). Coupling between the spinal cord and cervical vertebral column under tensile loading. *Journal of Biomechanics*, *46*(4), 773–779. https://doi.org/10.1016/j.jbiomech.2012.11.012

Kroeker, S. G., Morley, P. L., Jones, C. F., Bilston, L. E., Cripton, P. A. (2009). The development of an improved physical surrogate model of the human spinal cord--tension and transverse compression. *Journal of Biomechanics*, *42*(7), 878–83. https://doi.org/10.1016/j.jbiomech.2009.01.036

Krueger, H., Noonan, V. K., Trenaman, L. M., Joshi, P., Rivers, C. S. (2013). The economic burden of traumatic spinal cord injury in Canada. *Chronic Diseases and Injuries in Canada*, *33*(3), 113–22. Retrieved from http://www.ncbi.nlm.nih.gov/pubmed/23735450

Kuo, J. J., Lee, R. H., Johnson, M. D., Heckman, H. M., Heckman, C. J. (2003). Active Dendritic Integration of Inhibitory Synaptic Inputs In Vivo. *Journal of Neurophysiology*, *90*(6), 3617–3624. https://doi.org/10.1152/jn.00521.2003

Kwon, B., Ghag, A., Reichl, L., Dvorak, M., Illes, J., Tetzlaff, W. (2012). Opinions on the Preclinical Evaluation of Novel Therapies for Spinal Cord Injury: A Comparison between Researchers and Spinal Cord-Injured Individuals. *Journal of Neurotrauma*, *29*(14), 2367–74. https://doi.org/10.1089/neu.2012.2479

Kwon, B., Hillyer, J., & Tetzlaff, W. (2010). Translational research in spinal cord injury: a survey of opinion from the SCI community. *Journal of Neurotrauma*, *27*(1), 21–33. https://doi.org/10.1089/neu.2009.1048

Kwon, B., Okon, E., Tsai, E., Beattie, M., Bresnahan, J., Magnuson, D., Reier, P., McTigue, D., Popovich, P., Blight, A., Oudega, M., Guest, J., Weaver, L., Fehlings, M., Tetzlaff, W. (2011). A grading system to evaluate objectively the strength of pre-clinical data of acute neuroprotective therapies for clinical translation in spinal cord injury. *Journal of Neurotrauma*, *28*(8), 1525–43. https://doi.org/10.1089/neu.2010.1296

Kwon, B., Oxland, T., & Tetzlaff, W. (2002). Animal models used in spinal cord regeneration research. *Spine*, *27*(14), 1504–1510. https://doi.org/10.1097/00007632-200207150-00005

Laing, A. C., Brenneman, E. C., Yung, A., liu, J., Kozlowski, P., Oxland, T. (2014). The Effects of age on the morphometry of the cervical spinal cord and spinal column in adult rats: An MRI-based study. *Anatomical Record*, *297*(10), 1885–1895. https://doi.org/10.1002/ar.22995

Laing, A. C., Cox, R., Tetzlaff, W., Oxland, T. (2011). Effects of advanced age on the morphometry and degenerative state of the cervical spine in a rat model. *Anatomical Record*, *294*(8), 1326–36. https://doi.org/10.1002/ar.21436

Lam, C. J., Assinck, P., Liu, J., Tetzlaff, W., Oxland, T. R. (2014). Impact depth and the interaction with impact speed affect the severity of contusion spinal cord injury in rats. *Journal of Neurotrauma*, *1997*, 1985–1997. https://doi.org/10.1089/neu.2014.3392

Lantz, S. A., Lafferty, J. F., & Bowman, D. A. (1980). Response of the intervertebral disk of the rhesus monkey to P-A shear stress. *J Biomech Eng*, *102*(2), 137–140. https://doi.org/10.1115/1.3138209

LaPlaca, M. C., & Prado, G. R. (2010). Neural mechanobiology and neuronal vulnerability to traumatic loading. *Journal of Biomechanics*, *43*(1), 71–78. https://doi.org/10.1016/j.jbiomech.2009.09.011

Lau, N.-S. S., Gorrie, C. a, Chia, J. Y., Bilston, L. E., Clarke, E. C. (2013). Severity of spinal cord injury in adult and infant rats after vertebral dislocation depends upon displacement but not speed. *Journal of Neurotrauma*, *30*(15), 1361–73. https://doi.org/10.1089/neu.2012.2725

Leite, C. C., Escobar, B. E., Bazan, C., Jinkins, J. R. (1997). MRI of cervical facet dislocation. *Neuroradiology*, *39*(8), 583–588. https://doi.org/10.1007/s002340050472

Ling, X., Bao, F., Qian, H., Liu, D. (2013). The temporal and spatial profiles of cell loss following experimental spinal cord injury: effect of antioxidant therapy on cell death and functional recovery. *BMC Neuroscience*, *14*, 146. https://doi.org/10.1186/1471-2202-14-146

Ling, X., & Liu, D. (2007). Temporal and spatial profiles of cell loss after spinal cord injury: reduction by a Metalloporphyrin. *Journal of Neuroscience Research*, *85*(11), 2175–2185. https://doi.org/10.1002/jnr.21362

Liu, E., Wong, H., Chia, C., Lim, H., Chen, Z., Lee, T. (2005). Effects of isoflurane and propofol on cortical somatosensory evoked potentials during comparable depth of anaesthesia as guided by bispectral index. *British Journal of Anaesthesia*, *94*(2), 193–197. https://doi.org/10.1093/bja/aei003

Liu, Y., Shi, C., Wang, X., Chen, H., Wang, C., Cao, P., Gao, R., Ren, X., Luo, Z., Wang, B., Xu, J., Tian, J., Yuan, W. (2015). Timing of surgical decompression for traumatic cervical spinal cord injury. *International Orthopaedics*, *39*(12), 2457–2463. https://doi.org/10.1007/s00264-014-2652-z

Liverman, C., Altevogt, B., Joy, J., Johnson, R. (2005). *Spinal cord injury: progress, promise, and priorities*. Retrieved from https://books.google.ca/books?hl=en&lr=&id=fwtSAgAAQBAJ&oi=fnd&pg=PT17&dq=liverman+Spinal+cord+injury:+progress,+promise,+and+priorities+&ots=VKhQ_3nZEA&sig=jd22yy__Rm_onjkGziKaDtfurk8

Lubińska, L. (1977). Early course of Wallerian degeneration in myelinated fibres of the rat phrenic nerve. *Brain Research*, *130*(1), 47–63. https://doi.org/10.1016/0006-8993(77)90841-1

Luna, C., Detrick, L., Shah, S. B., Cohen, A. H., Aranda-Espinoza, H. (2013). Mechanical properties of the lamprey spinal cord: Uniaxial loading and physiological strain. *Journal of Biomechanics*, *46*(13), 2194–200. https://doi.org/10.1016/j.jbiomech.2013.06.028

Magerl, F., Aebi, M., Gertzbein, S. D., Harms, J., & Nazarian, S. (1994). A comprehensive classification of thoracic and lumbar injuries. *European Spine Journal*, *3*(4), 184–201. https://doi.org/10.1007/BF02221591

Maggi, C. A., & Meli, A. (1986). Suitability of urethane anesthesia for physiopharmacological investigations in various systems Part 1: General considerations. *Experientia*, *42*(2), 109–114. https://doi.org/10.1007/BF01952426

Maikos, J. T., Qian, Z., Metaxas, D., Shreiber, D. I. (2008). Finite element analysis of spinal cord injury in the rat. *Journal of Neurotrauma*, *25*(7), 795–816. https://doi.org/10.1089/neu.2007.0423

Maikos, J. T., & Shreiber, D. I. (2007). Immediate Damage to the Blood-Spinal Cord Barrier. *Journal of Neurotrauma*, *24*(3), 492–507. https://doi.org/10.1089/neu.2006.0149

Maiman, D. J., Coats, J., & Myklebust, J. B. (1989). Cord/Spine Motion in Experimental Spinal Cord Injury. *Journal of Spinal Disorders & Techniques*. Retrieved from http://journals.lww.com/jspinaldisorders/Fulltext/1989/03000/Cord_Spine_Motion_in_Experimental_Spinal_Cord.3.aspx

Marar, B. C. (1974). The pattern of neurological damage as an aid to the diagnosis of the mechanism in cervical-spine injuries. *The Journal of Bone and Joint Surgery. American Volume*, *56*(8), 1648–54. Retrieved from http://www.ncbi.nlm.nih.gov/pubmed/4434033

Marcol, W., Slusarczyk, W., Gzik, M., Larysz-Brysz, M., Bobrowski, M., Grynkiewicz-Bylina, B., Rosicka, P., Kalita, K., Weglarz, W., Barski, J., Kotulska, K., Labuzek, K., Lewin-Kowalik, J. (2012). Air gun impactor-a novel model of graded white matter spinal cord injury in rodents. *Journal of Reconstructive Microsurgery*, *28*(8), 561–568. https://doi.org/10.1055/s-0032-1315779

Martinez, M., Brezun, J., & Xerri, C. (2009). A New Rating Scale for Open-Field Evaluation of Behavioral Recovery after Cervical Spinal Cord Injury in Rats, *1053*(July), 1043–1053.

Mattucci, S., Liu, J., Fijal, P., Tetzlaff, W., Oxland, T. R. (2017). Repeatability of a Dislocation Spinal Cord Injury Model in a Rat—A High-Speed Biomechanical Analysis. *Journal of Biomechanical Engineering*, *139*(10), 104501. https://doi.org/10.1115/1.4037224

McCarthy, M., Gatehouse, S., Steel, M., Goss, B., Williams, R. (2011). The influence of the energy of trauma, the timing of decompression, and the impact of grade of SCI on outcome. *Evidence-Based Spine-Care Journal*, *2*(2), 11–17. https://doi.org/10.1055/s-0030-1267100

McKinley, M., & O'Loughlin, V. (2008). *Human Anatomy* (2nd Editio). New York: McGraw-Hill.

Mercer, S., & Bogduk, N. (1999). The ligaments and annulus fibrosus of human adult cervical intervertebral discs. *Spine*. Retrieved from http://www.ncbi.nlm.nih.gov/pubmed/10209789

Metz, G. A., Curt, A., van de, M. H., Klusman, I., Schwab, M. E., Dietz, V. (2000). Validation of the weight-drop contusion model in rats: a comparative study of human spinal cord injury. *Journal of Neurotrauma*, *17*(1), 1–17. Retrieved from http://www.ncbi.nlm.nih.gov/pubmed/10674754

Miele, V. J., Panjabi, M. M., & Benzel, E. C. (2012). Chapter 2 – Anatomy and biomechanics of the spinal column and cord. In *Handbook of Clinical Neurology* (Vol. 109, pp. 31–43). https://doi.org/10.1016/B978-0-444-52137-8.00002-4

Mohanty, S. P., & Venkatram, N. (2002). Does neurological recovery in thoracolumbar and lumbar burst fractures depend on the extent of canal compromise? *Spinal Cord*, *40*(6), 295–9. https://doi.org/10.1038/sj.sc.3101283

Moore, K. L., & Dalley, A. F. (1999). *Clinically oriented anatomy*. Lippincott Williams & Wilkins. Retrieved from https://books.google.ca/books/about/Clinically_Oriented_Anatomy.html?id=gn09DmSosW0C

Nashmi, R., Imamura, H., Tator, C., Fehlings, M. (1997). Serial recording of somatosensory and myoelectric motor evoked potentials: role in assessing functional recovery after graded spinal cord injury in the rat. *Journal of Neurotrauma*, *14*(3), 151–9. Retrieved from http://www.ncbi.nlm.nih.gov/pubmed/9104932

Nassr, A., Lee, J. Y., Dvorak, M. F., Harrop, J. S., Dailey, A. T., Shaffrey, C. I., Arnold, P., Brodke, D., Rampersaud, R., Grauer, J., Winegar, C.,Vaccaro, A. R. (2008). Variations in Surgical Treatment of Cervical Facet Dislocations. *Spine*, *33*(7), E188–E193. https://doi.org/10.1097/BRS.0b013e3181696118

Nesathurai, S., Graham, W. A., Mansfield, K., Magill, D., Sehgal, P., Westmoreland, S. V, Prusty, S., Rosene, D., Sledge, J. B. (2006). Model of traumatic spinal cord injury in Macaca fascicularis: similarity of experimental lesions created by epidural catheter to human spinal cord injury. *Journal of Medical Primatology*, *35*(6), 401–4. https://doi.org/10.1111/j.1600-0684.2006.00162.x

Nightingale, R., Doherty, B., Myers, B., McElhaney, J., Richardson, W. (1991). The influence of end condition on human cervical spine injury mechanisms. *STAPP Car Crash Journal*, *35*, 391–399. https://doi.org/10.4271/912915

Nightingale, R., McElhaney, J., Richardson, W., Best, T., Myers, B. (1996). Experimental impact injury to the cervical spine: relating motion of the head and the mechanism of injury. *The Journal of Bone and Joint Surgery. American Volume*, *78*(3), 412–21. Retrieved from http://www.ncbi.nlm.nih.gov/pubmed/8613449

Nightingale, R., Sganga, J., Cutcliffe, H., & Bass, C. (2016). Impact responses of the cervical spine: A computational study of the effects of muscle activity, torso constraint, and pre-flexion. *Journal of Biomechanics*, *49*(4), 558–564. https://doi.org/10.1016/j.jbiomech.2016.01.006

Nightingale, R., Winkelstein, B., Knaub, K., Richardson, W., Luck, J., Myers, B. (2002). Comparative strengths and structural properties of the upper and lower cervical spine in flexion and extension. *Journal of Biomechanics*, *35*(6), 725–32. Retrieved from http://www.ncbi.nlm.nih.gov/pubmed/12020991

Niu, J., Ding, L., Li, J. J., Kim, H., Liu, J., Li, H., Moberly, A., Badea, T. C., Duncan, I. D., Son, Y. J., Scherer, S., S.Luo, W. (2013). Modality-Based Organization of Ascending Somatosensory Axons in the Direct Dorsal Column Pathway. *Journal of Neuroscience*, *33*(45), 17691–17709. https://doi.org/10.1523/JNEUROSCI.3429-13.2013

Noonan, V. K., Fingas, M., Farry, A., Baxter, D., Singh, A., Fehlings, M. G., Dvorak, M. F. (2012). Incidence and prevalence of spinal cord injury in Canada: a national perspective. *Neuroepidemiology*, *38*(4), 219–26. https://doi.org/10.1159/000336014

Nordqvist, L. (1964). The Sagittal Diametter of the Spinal Cord and Subarachnoid Space in Different Age Groups. A Roentgenographic Post-Mortem Study. *Acta Radiologica: Diagnosis*, SUPPL 227:1-96. Retrieved from http://www.ncbi.nlm.nih.gov/pubmed/14150643

Norenberg, M. D., Smith, J., & Marcillo, A. (2004). The Pathology of Human Spinal Cord Injury: Defining the Problems. *Journal of Neurotrauma*, *21*(4), 429–440. https://doi.org/10.1089/089771504323004575

Norman, G. (2010). Likert scales, levels of measurement and the "laws" of statistics. *Advances in Health Sciences Education*, *15*(5), 625–632. https://doi.org/10.1007/s10459-010-9222-y

Norton, W. L. (1962). Fractures and dislocations of the cervical spine. *Journal of Bone & Joint Surgery, 44–A*(1), 115–139.

Nouri, A., Montejo, J., Sun, X., Virojanapa, J., Kolb, L. E., Abbed, K. M., Cheng, J. (2017). Cervical Cord-Canal Mismatch: A New Method for Identifying Predisposition to Spinal Cord Injury. *World Neurosurgery*, *108*, e88–e88. https://doi.org/10.1016/j.wneu.2017.08.018

Noyes, D. (1987). Electromechanical Impactor for Producing Experimental Spinal Cord Injury in Animals. *Medical & Biological Engineering & Computing*, *25*(May), 335–340.

NSCISC. (2016). *Facts and Figures at a Glance*. *National Spinal Cord Injury Statistical Center*. https://doi.org/10.1080/10790268.2016.1210925

Nuwer, M. R., Daube, J., Fischer, C., Schramm, J., Yingling, C. D. (1993). Neuromonitoring during surgery. Report of an IFCN Committee. *Electroencephalography and Clinical Neurophysiology*, *87*(5), 263–76. Retrieved from http://www.ncbi.nlm.nih.gov/pubmed/7693437

Oakland, R. J., Hall, R. M., Wilcox, R. K., Barton, D. C. (2006). The biomechanical response of spinal cord tissue to uniaxial loading. *Proceedings of the Institution of Mechanical Engineers. Part H, Journal of Engineering in Medicine*, *220*(4), 489–92. https://doi.org/10.1243/09544119JEIM135

Ong, H. H., Wright, A. C., Wehrli, S. L., Souza, A., Schwartz, E. D., Hwang, S. N., Wehrli, F. W. (2008). Indirect measurement of regional axon diameter in excised mouse spinal cord with q-space imaging: Simulation and experimental studies. *NeuroImage*, *40*(4), 1619–1632. https://doi.org/10.1016/j.neuroimage.2008.01.017

Onwuama, K. T., Salami, S. O., Ali, M., Nzalak, J. O. (2012). Effect of Different Methods of Bone Preparation on the Skeleton of the African Giant Pouched Rat (Cricetomys gambianus). *International Journal of Morphology*, *30*(2), 425–427. https://doi.org/10.4067/S0717-95022012000200011

Ordonez, B. J., Benzel, E. C., Naderi, S., Weller, S. J. (2000). Cervical facet dislocation: techniques for ventral reduction and stabilization. *Journal of Neurosurgery*, *92*(1 Suppl), 18–23. Retrieved from http://www.ncbi.nlm.nih.gov/pubmed/10616053

Orr, M. B., Simkin, J., Bailey, W. M., Kadambi, N. H., McVicar, A. L., Veldhorst, A. K., Gensel, J. (2017). Compression Decreases Anatomical and Functional Recovery and Alters Inflammation after Contusive Spinal Cord Injury. *Journal of Neurotrauma*, *34*(15), 2342–2352. https://doi.org/10.1089/neu.2016.4915

Ouyang, H., Galle, B., Li, J., Nauman, E., Shi, R. (2008). Biomechanics of spinal cord injury: a multimodal investigation using ex vivo guinea pig spinal cord white matter. *Journal of Neurotrauma*, *25*(1), 19–29. https://doi.org/10.1089/neu.2007.0340

Ouyang, H., Galle, B., Li, J., Nauman, E., Shi, R. (2009). Critical roles of decompression in functional recovery of ex vivo spinal cord white matter. *Journal of Neurosurgery: Spine*, *10*(2), 161–170. https://doi.org/10.3171/2008.10.SPI08495

Oxland, T., Bhatnagar, T., & Choo, A. (2011). Biomechanical Aspects of Spinal Cord Injury. In *Neural Tissue Biomechanics* (Vol. 3, pp. 159–180). https://doi.org/10.1007/8415

Oyinbo, C. A. (2011). Secondary injury mechanisms in traumatic spinal cord injury : a nugget of this multiply cascade. *Acta Neurobiologiae Experimentalis*, *71*, 281–299.

Oza, A. L., Vanderby, R., Lakes, R. S. (2006). Creep and Relaxation in Ligament: Theory, Methods and Experiment. In *Mechanics of Biological Tissue* pp. 379–397. Berlin/Heidelberg: Springer-Verlag. https://doi.org/10.1007/3-540-31184-X_27

Ozawa, H., Matsumoto, T., Ohashi, T., Sato, M., Kokubun, S. (2001). Comparison of spinal cord gray matter and white matter softness: measurement by pipette aspiration method. *Journal of Neurosurgery*, *95*(2 Suppl), 221–4. https://doi.org/10.3171/spi.2001.95.2.0221

Panjabi, M., Duranceau, J., Goel, V., Oxland, T., Takata, K. (1991). Cervical human vertebrae. Quantitative three-dimensional anatomy of the middle and lower regions. *Spine*, *16*(8), 861–9. Retrieved from http://www.ncbi.nlm.nih.gov/pubmed/1948369

Panjabi, M., Kifune, M., Wen, L., Arand, M., Oxland, T., Lin, R., Yoon, W., Vasavada, A. (1995). Dynamic Canal Encroachment During Thoracolumbar Burst Fractures. *Journal of Spinal Disorders*, *8*(1), 39–48.

Panjabi, M., Oxland, T., Lin, R., McGowen, T. (1994). Thoracolumbar burst fracture. A biomechanical investigation of its multidirectional flexibility. *Spine*. Retrieved from http://www.ncbi.nlm.nih.gov/pubmed/8184353

Panjabi, M., Simpson, A., Ivancic, P., Pearson, A., Tominaga, Y., Yue, J. (2007). Cervical facet joint kinematics during bilateral facet dislocation. *European Spine Journal*, *16*(10), 1680–1688. https://doi.org/10.1007/s00586-007-0410-2

Perey, O. (1957). Fracture of the vertebral end-plate in the lumbar spine: An experimental biochemical investigation. *Acta Orthopaedica Scandinavica*, *18*(25), 1–101. https://doi.org/10.3109/ort.1957.28.suppl-25.01

Pickett, G. E., Campos-Benitez, M., Keller, J. L., Duggal, N. (2006). Epidemiology of traumatic spinal cord injury in Canada. *Spine*, *31*(7), 799–805. https://doi.org/10.1097/01.brs.0000207258.80129.03

Plemel, J. R., Duncan, G., Chen, K. W. K., Shannon, C., Park, S., Sparling, J. S., Tetzlaff, W. (2008). A graded forceps crush spinal cord injury model in mice. *Journal of Neurotrauma*, *25*(4), 350–70. https://doi.org/10.1089/neu.2007.0426

Popovich, P. G., & Longbrake, E. E. (2008). Can the immune system be harnessed to repair the CNS? *Nature Reviews. Neuroscience*, *9*(6), 481–93. https://doi.org/10.1038/nrn2398

Purves, D., Augustine, G., Fitzpatrick, D., Katz, L., LaMantia, A., McNamara, J., Williams, S. (2001). *Neuroscience* (2nd Ed.). Sunderland, MA: Sinauer Associates.

Rabinowitz, R. S., Eck, J. C., Harper, C. M., Larson, D. R., Jimenez, M. A, Parisi, J. E., Friedman, J., Yaszemski, M., Currier, B. L. (2008). Urgent surgical decompression compared to methylprednisolone for the treatment of acute spinal cord injury: a randomized prospective study in beagle dogs. *Spine*, *33*(21), 2260–8. https://doi.org/10.1097/BRS.0b013e31818786db

Ravin, R., Blank, P. S., Steinkamp, A., Rappaport, S. M., Ravin, N., Bezrukov, L., Guerrero-Cazares, H., Quinones-Hinojosa, A., Bezrukov, S., Zimmerberg, J. (2012). Shear forces during blast, not abrupt changes in pressure alone, generate calcium activity in human brain cells. *PLoS ONE*, *7*(6), 0–7. https://doi.org/10.1371/journal.pone.0039421

Reinhold, M., Knop, C., Lange, U., Rosenberger, R., Schmid, R., Blauth, M. (2006). Reduction of traumatic dislocations and facet fracture-dislocations in the lower cervical spine. *Der Unfallchirurg*, *109*(12), 1064–1072. https://doi.org/10.1007/s00113-006-1188-0

Rivlin, A. S., & Tator, C. H. (1978). Effect of duration of acute spinal cord compression in a new acute cord injury model in the rat. *Surgical Neurology*, *10*(1), 38–43. Retrieved from http://www.ncbi.nlm.nih.gov/pubmed/684604

Roaf, R. (1960). A Study of the Mechanics of Spinal Injuries. *Bone & Joint Journal*, *42–B*(4), 810–823. https://doi.org/FOUND

Rolyan, H., Liu, S., Hoeijmakers, J. G., Faber, C. G., Merkies, I. S., Lauria, G., Black, J., Waxman, S. G. (2016). A painful neuropathy-associated Nav1.7 mutant leads to time-dependent degeneration of small-diameter axons associated with intracellular Ca2+ dysregulation and decrease in ATP levels. *Molecular Pain*, *12*. https://doi.org/10.1177/1744806916674472

Rowland, J. W., Hawryluk, G. W., Kwon, B., Fehlings, M. G. (2008). Current status of acute spinal cord injury pathophysiology and emerging therapies: promise on the horizon. *Neurosurgical Focus*, *25*(November), 1–3. https://doi.org/10.3171/FOC.2008.25.11.E2

Russell, C. M., Choo, A. M., Tetzlaff, W., Chung, T. E., & Oxland, T. R. (2012). Maximum principal strain correlates with spinal cord tissue damage in contusion and dislocation injuries in the rat cervical spine. *Journal of Neurotrauma*, *29*(8), 1574–85. https://doi.org/10.1089/neu.2011.2225

Saari, A., Itshayek, E., & Cripton, P. A. (2011). Cervical spinal cord deformation during simulated head-first impact injuries. *Journal of Biomechanics*, *44*(14), 2565–2571. https://doi.org/10.1016/j.jbiomech.2011.06.015

Scheff, S. W., Rabchevsky, A. G., Fugaccia, I., Main, J. A, Lumpp, J. E. (2003). Experimental modeling of spinal cord injury: characterization of a force-defined injury device. *Journal of Neurotrauma*, *20*(2), 179–93. https://doi.org/10.1089/08977150360547099

Schmider, E., Ziegler, M., Danay, E., Beyer, L., Bühner, M. (2010). Is It Really Robust?: Reinvestigating the robustness of ANOVA against violations of the normal distribution assumption. *Methodology*, *6*(4), 147–151. https://doi.org/10.1027/1614-2241/a000016

Schmidt, H., Häussler, K., Wilke, H. J., Wolfram, U. (2015). Structural behavior of human lumbar intervertebral disc under direct shear. *Journal of Applied Biomaterials & Functional Materials*, *13*(1), 66–71. https://doi.org/10.5301/jabfm.5000176

Seifert, J. L., Bell, J. E., Elmer, B. B., Sucato, D. J., Romero, M. I. (2011). Characterization of a novel bidirectional distraction spinal cord injury animal model. *Journal of Neuroscience Methods*, *197*(1), 97–103. https://doi.org/10.1016/j.jneumeth.2011.02.003

Sekhon, L., & Fehlings, M. (2001). Epidemiology, demographics, and pathophysiology of acute spinal cord injury. *Spine*, *26*(24 Suppl), S2-12. Retrieved from http://www.ncbi.nlm.nih.gov/pubmed/11805601

Sengupta, P. (2013). The Laboratory Rat: Relating Its Age With Human's. *International Journal of Preventive Medicine*, *4*(6), 624–30. Retrieved from http://www.ncbi.nlm.nih.gov/pubmed/23930179

Shahrokni, M., Zhu, Q., Liu, J., Tetzlaff, W., Oxland, T. (2012). Design and biomechanical evaluation of a rodent spinal fixation device. *Spinal Cord*, *50*(7), 543–7. https://doi.org/10.1038/sc.2011.185

Shi, R. (2006). Conduction Deficits and Membrane Disruption of Spinal Cord Axons as a Function of Magnitude and Rate of Strain. *Journal of Neurophysiology*, *95*(6), 3384–3390. https://doi.org/10.1152/jn.00350.2005

Shi, R., & Blight, A. (1996). Compression injury of mammalian spinal cord in vitro and the dynamics of action potential conduction failure. *Journal of Neurophysiology*, *76*(3), 1572–1580.

Shi, R., & Borgens, R. (1999). Acute Repair of Crushed Guinea Pig Spinal Cord by Polyethylene Glycol Acute Repair of Crushed Guinea Pig Spinal Cord by Polyethylene Glycol. *Journal of Neurophysiology*, *81*(5), 2406–2414.

Shi, R., & Pryor, J. (2002). Pathological changes of isolated spinal cord axons in response to mechanical stretch. *Neuroscience*, *110*(4), 765–777. https://doi.org/10.1016/S0306-4522(01)00596-6

Shields, C. B., Zhang, Y. P., Shields, L. B. E., Han, Y., Burke, D. a, & Mayer, N. W. (2005). The therapeutic window for spinal cord decompression in a rat spinal cord injury model. *Journal of Neurosurgery. Spine*, *3*(4), 302–7. https://doi.org/10.3171/spi.2005.3.4.0302

Shuman, S. L., Bresnahan, J. C., & Beattie, M. S. (1997). Apoptosis of microglia and oligodendrocytes after spinal cord contusion in rats. *Journal of Neuroscience Research*, *50*(5), 798–808. https://doi.org/10.1002/(SICI)1097-4547

Silverthorn, D. (2010). *Human Physiology: An Integrated Approach* (Fifth Edit). San Francisco: Pearson.

Sjovold, S., Mattucci, S. F. E., Choo, A. M., Liu, J., Dvorak, M. F., Kwon, B. K., Tetzlaff, W., Oxland, T. R. (2013). Histological effects of residual compression sustained for 60 minutes at different depths in a novel rat spinal cord injury contusion model. *Journal of Neurotrauma*, *30*(15), 1374–84. https://doi.org/10.1089/neu.2013.2906

Smith, L. J., Nerurkar, N. L., Choi, K. S., Harfe, B. D., Elliott, D. M. (2010). Degeneration and regeneration of the intervertebral disc: lessons from development. *Disease Models & Mechanisms*, *4*(1). Retrieved from http://dmm.biologists.org/content/4/1/31.article-info

Somerson, S. K., & Stokes, B. T. (1987). Functional analysis of an electromechanical spinal cord injury device. *Experimental Neurology*, *96*(1), 82–96. Retrieved from http://www.ncbi.nlm.nih.gov/pubmed/3556519

Sparrey, C. J., Choo, A., Liu, J., Tetzlaff, W., Oxland, T. (2008). The distribution of tissue damage in the spinal cord is influenced by the contusion velocity. *Spine*, *33*(22), E812-9. https://doi.org/10.1097/BRS.0b013e3181894fd3

Sparrey, C. J., & Keaveny, T. M. (2011). Compression behavior of porcine spinal cord white matter. *Journal of Biomechanics*, *44*(6), 1078–1082. https://doi.org/10.1016/j.jbiomech.2011.01.035

Speidel, J. (2017). *Effect of velocity and timing of residual compression in a dislocation spinal cord injury rat model*. (M.A.Sc. Thesis) University of British Columbia.

Steward, O., Popovich, P. G., Dietrich, W. D., Kleitman, N. (2012). Replication and reproducibility in spinal cord injury research. *Experimental Neurology*, *233*(2), 597–605. https://doi.org/10.1016/j.expneurol.2011.06.017

Stokes, B. (1992). Experimental spinal cord injury: a dynamic and verifiable injury device. *Journal of Neurotrauma*, *9*(2), 129-31–4. https://doi.org/10.1089/neu.1992.9.129

Stokes, B., Noyes, D., & Behrmann, D. (1992). An Electromechanical Spinal Injury Technique with Dynamic Sensitivity. *Journal of Neurotrauma*, *9*(3), 187–195.

Streijger, F., Beernink, T. M. J., Lee, J. H. T., Bhatnagar, T., Park, S., Kwon, B. K., Tetzlaff, W. (2013). Characterization of a cervical spinal cord hemicontusion injury in mice using the infinite horizon impactor. *Journal of Neurotrauma*, *30*(10), 869–83. https://doi.org/10.1089/neu.2012.2405

Sullivan, S., Eucker, S. A., Gabrieli, D., Bradfield, C., Coats, B., Maltese, M. R., Lee, J., Smith, C., Margulies, S. S. (2015). White matter tract-oriented deformation predicts traumatic axonal brain injury and reveals rotational direction-specific vulnerabilities. *Biomechanics and Modeling in Mechanobiology*, *14*(4), 877–896. https://doi.org/10.1007/s10237-014-0643-z

Susuki, K. (2010). Myelin: A Specialized Membrane for Cell Communication. *Nature Education*, *9*(3), 59.

Talac, R., Friedman, J. A., Moore, M. J., Lu, L., Jabbari, E., Windebank, A. J., Currier, B., Yaszemski, M. J. (2004). Animal models of spinal cord injury for evaluation of tissue engineering treatment strategies. *Biomaterials*, *25*(9), 1505–1510. https://doi.org/10.1016/S0142-9612(03)00497-6

Tarlov, I., & Klinger, H. (1954). Spinal Cord Compression Studies- Part II: Time Limits for Recovery After Acute Compression in Dogs. *Archives of Neurology and Psychiatry*, *71*(3), 271–290.

Tarlov, I., Klinger, H., & Vitale, S. (1953). Spinal Cord Compression Studies- Part I: Experimental Techniques to Produce Acute and Gradual Compression. *Archives of Neurology and Psychiatry, 70(6),* 813-9.

Tator, C. (1983). Spine-spinal cord relationships in spinal cord trauma. *Clinical Neurosurgery*, *30*, 479–94. Retrieved from http://www.ncbi.nlm.nih.gov/pubmed/6667588

Tator, C. (1995). Update on the pathophysiology and pathology of acute spinal cord injury. *Brain Pathology*, *5*(4), 407–13. Retrieved from http://www.ncbi.nlm.nih.gov/pubmed/8974623

Tator, C. (2006). Review of treatment trials in human spinal cord injury: issues, difficulties, and recommendations. *Neurosurgery*, *59*(5), 957-82–7. https://doi.org/10.1227/01.NEU.0000245591.16087.89

Tator, C., Duncan, E., Edmonds, V., Lapczak, L., Andrews, D. (1987). Comparison of surgical and conservative management in 208 patients with acute spinal cord injury. *Can J Neurol Sci*, *14*(0317–1671 (Print)), 60–69.

Tator, C., & Fehlings, M. (1991). Review of secondary injury theory of acute sci with emphasis on vascular mechanisms. *Journal of Neurosurgery*, *75*, 15–26.

Taylor, M. P., Wrenn, P., & O'Donnell, A. D. (2017). Presentation of neurogenic shock within the emergency department. *Emergency Medicine Journal*, *34*(3), 157–162. https://doi.org/10.1136/emermed-2016-205780

Torg, J. S., Naranja, R. J., Pavlov, H., Galinat, B. J., Warren, R., Stine, R. A. (1996). The relationship of developmental narrowing of the cervical spinal canal to reversible and irreversible injury of the cervical spinal cord in football players. *The Journal of Bone and Joint Surgery. American Volume*, *78*(9), 1308–14. Retrieved from http://www.ncbi.nlm.nih.gov/pubmed/8816644

Tran, N. T., Watson, N. A., Tencer, A. F., Ching, R. P., Anderson, P. A. (1995). Mechanism of the Burst Fracture in the Thoracolumbar Spine. The Effect of Loading Rate. *Spine*, *20*(18), 1984–1988.

Tunturi, A. R. (1978). Elasticity of the spinal cord, pia, and denticulate ligament in the dog. *Journal of Neurosurgery*, *48*(6), 975–9. https://doi.org/10.3171/jns.1978.48.6.0975

Tunturi, A. R. (1980). Viscoelasticity of dog spinal cord. *Physiological Chemistry and Physics*, *12*(4), 373–8. Retrieved from http://www.ncbi.nlm.nih.gov/pubmed/7454859

Vaccaro, A., Hulbert, R., Patel, A., Fisher, C., Dvorak, M., Lehman, R., … Shainline, M. (2007). The subaxial cervical spine injury classification system: a novel approach to recognize the importance of morphology, neurology, and integrity of the disco-ligamentous complex. *Spine*, *32*(21), 2365–74. https://doi.org/10.1097/BRS.0b013e3181557b92

Vaccaro, A., Koerner, J., Radcliff, K., Oner, F., Reinhold, M., Schnake, K., Anderson, P., Harrop, J., Oner, F., Arnold, P., Fehlings, M., Hedlund, R., Madrazo, I., Rechtine, G., Aarabi, B., Vialle, L. (2016). AOSpine subaxial cervical spine injury classification system. *European Spine Journal*, *25*(7), 2173–2184. https://doi.org/10.1007/s00586-015-3831-3

Vaccaro, A., Lehman, R., Hurlbert, R., Anderson, P., Harris, M., Hedlund, R., Harrop, J., Dvorak, M., Wood, K., Fehlings, M., Fisher, C., Zeiller, S., Anderson, D., Bono, C., Stock, G., Brown, A., Kuklo, T., Oner, F. (2005). A new classification of thoracolumbar injuries: the importance of injury morphology, the integrity of the posterior ligamentous complex, and neurologic status. *Spine*, *30*(20), 2325–33. https://doi.org/10.1016/S0276-1092(08)70533-9

Vaccaro, A., Madigan, L., Schweitzer, M., Flanders, A., Hilibrand, A., Albert, T. (2001). Magnetic resonance imaging analysis of soft tissue disruption after flexion-distraction injuries of the subaxial cervical spine. *Spine*, *26*(17), 1866–72. Retrieved from http://www.ncbi.nlm.nih.gov/pubmed/11568695

Vaccaro, A., Oner, C., Kepler, C., Dvorak, M., Schnake, K., Bellabarba, C., Reinhold, M., Aarabi, B., Kandziora, F., Chapman, J., Rajasekaran, S., Fehlings, M., Vialle, L. (2013). AOSpine Thoracolumbar Spine Injury Classification System. *Spine*, *38*(23), 2028–2037. https://doi.org/10.1097/BRS.0b013e3182a8a381

van Middendorp, J. J. (2012). Letter to the editor regarding: "Early versus delayed decompression for traumatic cervical spinal cord injury: results of the Surgical Timing in Acute Spinal Cord Injury Study (STASCIS)". *The Spine Journal : Official Journal of the North American Spine Society*, *12*(6), 540; author reply 541-2. https://doi.org/10.1016/j.spinee.2012.06.007

van Middendorp, J. J., Hosman, A. J. F., & Doi, S. A. R. (2013). The Effects of the Timing of Spinal Surgery after Traumatic Spinal Cord Injury: A Systematic Review and Meta-Analysis. *Journal of Neurotrauma*, *30*(21), 1781–94. https://doi.org/10.1089/neu.2013.2932

Vanický, I., Urdzíková, L., Saganová, K., Cízková, D., Gálik, J. (2001). A simple and reproducible model of spinal cord injury induced by epidural balloon inflation in the rat. *Journal of Neurotrauma*, *18*(12), 1399–407. https://doi.org/10.1089/08977150152725687

Wang, H., Sorenson, E. J., Spinner, R. J., Windebank, A. J. (2008). Electrophysiologic findings and grip strength after nerve injuries in the rat forelimb. *Muscle and Nerve*, *38*(4), 1254–1265. https://doi.org/10.1002/mus.20971

Ward, R. E., Huang, W., Kostusiak, M., Pallier, P. N., Michael-Titus, A. T., Priestley, J. V. (2014). A characterization of white matter pathology following spinal cord compression injury in the rat. *Neuroscience*, *260*(December), 227–239. https://doi.org/10.1016/j.neuroscience.2013.12.024

Watson, C., Paxinos, G., Kayalioglu, G., & Christopher & Dana Reeve Foundation. (2009). *The Spinal Cord : A Christopher and Dana Reeve Foundation Text and Atlas*. Elsevier/Academic Press.

White, A. A., & Panjabi, M. M. (1990). *Clinical Biomechanics of the Spine* (Second Edi). Lippincott Williams & Wilkins.

Wilcox, R. K., Allen, D. J., Hall, R. M., Limb, D., Barton, D. C., Dickson, R. A. (2004). A dynamic investigation of the burst fracture process using a combined experimental and finite element approach. *European Spine Journal*, *13*(6), 481–8. https://doi.org/10.1007/s00586-003-0625-9

Wilcox, R. K., Boerger, T. O., Allen, D. J., Barton, D. C., Limb, D., Dickson, R. A., Hall, R. M. (2003). A dynamic study of thoracolumbar burst fractures. *The Journal of Bone and Joint Surgery. American Volume*, *85–A*(11), 2184–9. Retrieved from http://www.ncbi.nlm.nih.gov/pubmed/14630851

Wilcox, R. K., Boerger, T. O., Hall, R. M., Barton, D. C., Limb, D., & Dickson, R. A. (2002). Measurement of canal occlusion during the thoracolumbar burst fracture process. *Journal of Biomechanics*, *35*(3), 381–4. Retrieved from http://www.ncbi.nlm.nih.gov/pubmed/11858815

Wilke, H. J., Wenger, K., & Claes, L. (1998). Testing criteria for spinal implants: Recommendations for the standardization of in vitro stability testing of spinal implants. *European Spine Journal*, *7*(2), 148–154. https://doi.org/10.1007/s005860050045

Willén, J., Lindahl, S., Irstam, L., Aldman, B., Nordwall, A. (1984). The thoracolumbar crush fracture. An experimental study on instant axial dynamic loading: the resulting fracture type and its stability. *Spine*, *9*(6), 624–31. Retrieved from http://www.ncbi.nlm.nih.gov/pubmed/6495033

Wilson, J., Arnold, P., Singh, A., Kalsi-Ryan, S., Fehlings, M. (2012A). Clinical prediction model for acute inpatient complications after traumatic cervical spinal cord injury: a subanalysis from the Surgical Timing in Acute Spinal Cord Injury Study. *Journal of Neurosurgery. Spine*, *17*(1), 46–51. https://doi.org/10.3171/2012.4.AOSPINE1246

Wilson, J., & Fehlings, M. (2011). Emerging approaches to the surgical management of acute traumatic spinal cord injury. *Neurotherapeutics : The Journal of the American Society for Experimental NeuroTherapeutics*, *8*(2), 187–94. https://doi.org/10.1007/s13311-011-0027-3

Wilson, J., Singh, A., Craven, C., Verrier, M. C., Drew, B., Ahn, H., Ford, M., Fehlings, M. G. (2012B). Early versus late surgery for traumatic spinal cord injury: the results of a prospective Canadian cohort study. *Spinal Cord*, *50*(11), 840–3. https://doi.org/10.1038/sc.2012.59

Wilson, J., Vaccaro, A., Harrop, J., Aarabi, B., Shaffrey, C., Dvorak, M., Fisher, C., Arnold, P., Massicotte, E., Lewis, S., Rampersaud, R., Okonkwo, D., Fehlings, M. (2013). The Impact of Facet Dislocation on Clinical Outcomes after Cervical Spinal Cord Injury: Results of a Multicenter North American Prospective Cohort Study. *Spine*, *38*(2), 97–103. https://doi.org/10.1097/BRS.0b013e31826e2b91

Woo, S. H., Ranade, S., Weyer, A. D., Dubin, A. E., Baba, Y., Qiu, Z., Petrus, M., Miyamoto, T., Reddy, K., Lumpkin, E., Stucky, C., Patapoutian, A. (2014). Piezo2 is required for Merkel cell mechanotransduction. *Nature*, *509*(7502), 622–626. https://doi.org/10.1038/nature13251.Piezo2

Wu, J., Xue, J., Huang, R., Zheng, C., Cui, Y., Rao, S. (2016). A rabbit model of lumbar distraction spinal cord injury. *Spine Journal*, *16*(5), 643–658. https://doi.org/10.1016/j.spinee.2015.12.013

Yingling, V. R., & McGill, S. M. (1999). Anterior Shear of Spinal Motion Segments. *Spine*, *24*(18), 1882–89. https://doi.org/10.1097/00007632-199909150-00004

Yoganandan, N., Kumaresan, S., & Pintar, F. A. (2001). Biomechanics of the cervical spine Part 2. Cervical spine soft tissue responses and biomechanical modeling. *Clinical Biomechanics*, *16*(1), 1–27. Retrieved from http://www.ncbi.nlm.nih.gov/pubmed/11114440

Yousefifard, M., Rahimi-movaghar, V., Baikpour, M., Ghelichkhani, P. (2016). Early versus Late Decompression for Traumatic Spinal Cord Injuries ; a Systematic Review and Meta-analysis. *Emergency*, *5*(1 e37), 1–12.

Zandieh, S., Hopf, R., Redl, H., Schlag, M. G. (2003). The effect of ketamine/xylazine anesthesia on sensory and motor evoked potentials in the rat. *Spinal Cord*, *41*(1), 16–22. https://doi.org/10.1038/sj.sc.3101400

Zhang, N., Fang, M., Chen, H., Gou, F., Ding, M. (2014). Evaluation of spinal cord injury animal models. *Neural Regeneration Research*, *9*(22), 2008–12. https://doi.org/10.4103/1673-5374.143436

Zhang, Y., Burke, D., Shields, L., Chekmenev, S., Dincman, T., Zhang, Y., Zheng, Y., Smith, R., Benton, R., DeVries, W., Hu, X., Magnuson, D., Whittemore, S., Shields, C. (2008). Spinal cord contusion based on precise vertebral stabilization and tissue displacement measured by combined assessment to discriminate small functional differences. *Journal of Neurotrauma*, *25*(10), 1227–40. https://doi.org/10.1089/neu.2007.0388

Zhu, Q., Lane, C., Ching, R. P., Gordon, J. D., Fisher, C. G., Dvorak, M. F., Cripton, P., Oxland, T. R. (2008). Translational constraint influences dynamic spinal canal occlusion of the thoracic spine: An in vitro experimental study. *Journal of Biomechanics*, *41*(1), 171–179. https://doi.org/10.1016/j.jbiomech.2007.06.030

Appendices

Appendix A : Complete Axon and Myelinated Axon Graphs and ANOVA Tables

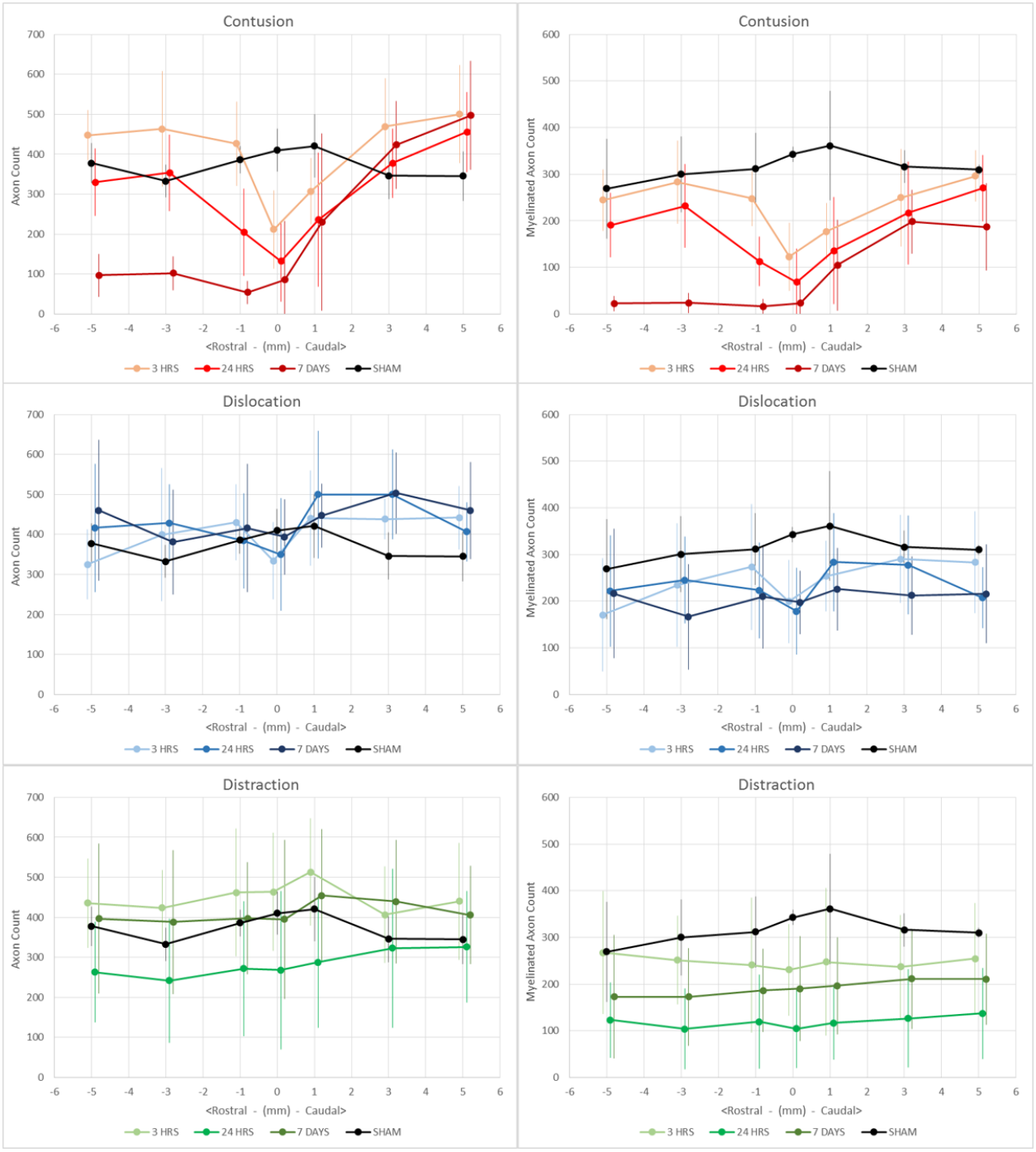

Figure A-1 – Gracile Fasciculus – Axon and myelinated axon count (per 3278 µm^2) along the length of the spinal cord from rostral (-) to caudal (+).

Table A-1 - Two-way mixed ANOVA summary - Gracile Fasciculus

Axon Count						
Injury Mechanism	**Effect**	**SS**	**DF**	**MS**	**F**	**P value**
Contusion	Interaction	1.07e+006	18	59703	4.94	P < 0.0001
	Spinal Location	900405	6	150068	12.4	P < 0.0001
	Time Point	1.16e+006	3	386484	32.0	P < 0.0001
	Error	2.02e+006	167	12096		
Dislocation	Interaction	191683	18	10649	0.7761	P = 0.7264
	Spinal Location	132586	6	22098	1.610	P = 0.1463
	Time Point	88897	3	29632	2.160	P = 0.0943
	Error	2.566e+006	187	13721		
Distraction	Interaction	91017	18	5056	0.2193	P = 0.9997
	Spinal Location	67678	6	11280	0.4891	P = 0.8160
	Time Point	930276	3	310092	13.45	P < 0.0001
	Error	4.335e+006	188	23061		
Myelinated Axon Count						
Injury Mechanism	**Effect**	**SS**	**DF**	**MS**	**F**	**P value**
Contusion	Interaction	315261	18	17514	3.16	P < 0.0001
	Spinal Location	259494	6	43249	7.80	P < 0.0001
	Time Point	1.08e+006	3	360238	65.0	P < 0.0001
	Error	925723	167	5543		
Dislocation	Interaction	115443	18	6414	0.6191	P = 0.8820
	Spinal Location	75485	6	12581	1.214	P = 0.3006
	Time Point	204259	3	68086	6.573	P = 0.0003
	Error	1.937e+006	187	10359		
Distraction	Interaction	32980	18	1832	0.1656	P > 0.9999
	Spinal Location	12342	6	2057	0.1859	P = 0.9805
	Time Point	821776	3	273925	24.76	P < 0.0001
	Error	2.080e+006	188	11062		

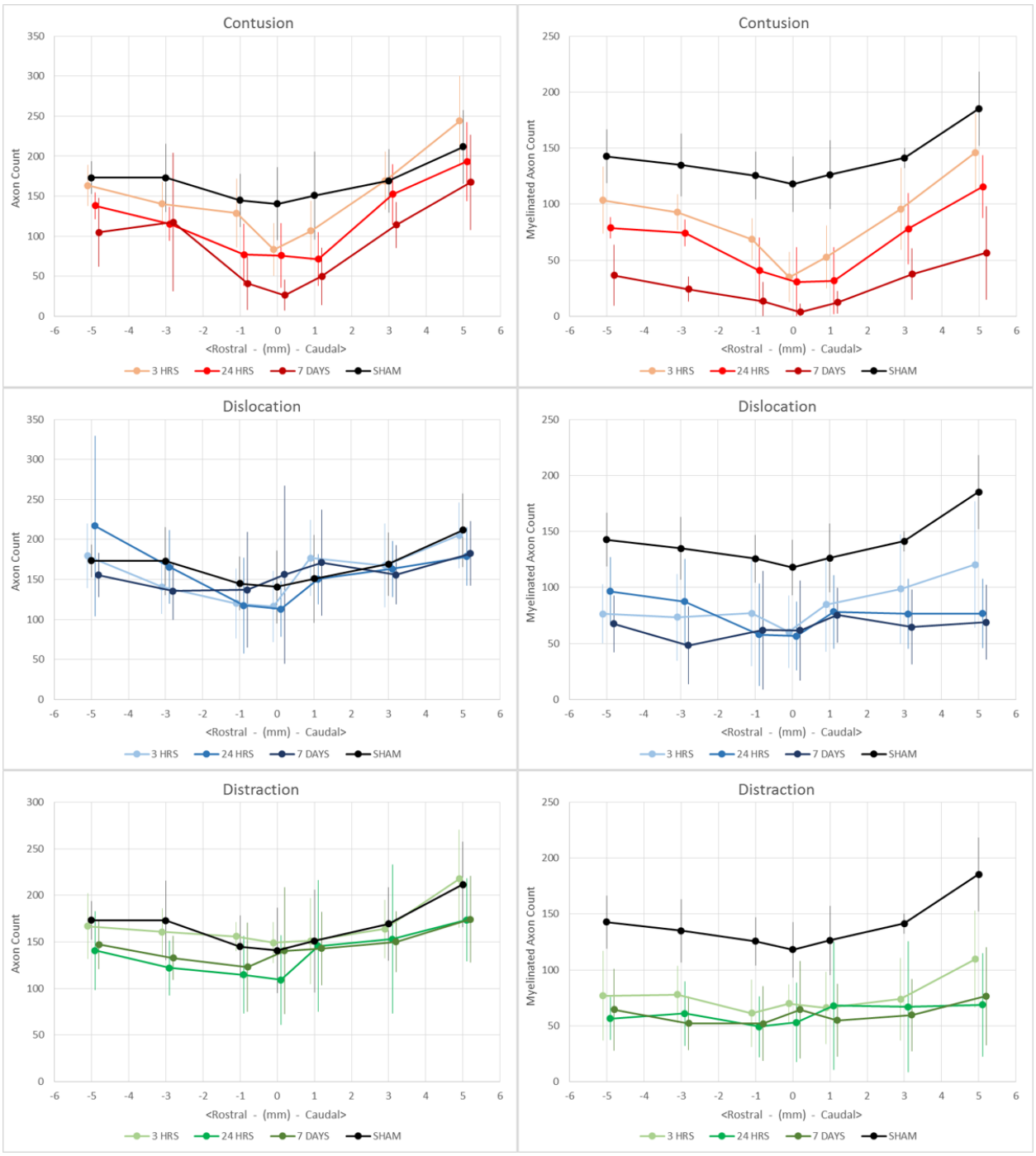

Figure A-2 - Cuneate Fasciculus – Axon and myelinated axon count (per 3278 µm2) along the length of the spinal cord from rostral (-) to caudal (+).

Table A-2 - Two-way mixed ANOVA summary - Cuneate Fasciculus

Axon Count						
Injury Mechanism	**Effect**	**SS**	**DF**	**MS**	**F**	**P value**
Contusion	Interaction	26858	18	1492	0.892	P = 0.5884
	Spinal Location	249149	6	41525	24.8	P < 0.0001
	Time Point	144639	3	48213	28.8	P < 0.0001
	Error	279215	167	1672		
Dislocation	Interaction	48265	18	2681	0.8814	P = 0.6016
	Spinal Location	82231	6	13705	4.505	P = 0.0003
	Time Point	1670	3	556.6	0.1830	P = 0.9079
	Error	568860	187	3042		
Distraction	Interaction	11766	18	653.7	0.3327	P = 0.9956
	Spinal Location	59194	6	9866	5.021	P < 0.0001
	Time Point	33494	3	11165	5.682	P = 0.0010
	Error	369384	188	1965		
Myelinated Axon Count						
Injury Mechanism	**Effect**	**SS**	**DF**	**MS**	**F**	**P value**
Contusion	Interaction	12719	18	707	1.09	P = 0.3694
	Spinal Location	98560	6	16427	25.3	P < 0.0001
	Time Point	220356	3	73452	113	P < 0.0001
	Error	108572	167	650		
Dislocation	Interaction	23337	18	1297	0.9415	P = 0.5296
	Spinal Location	22430	6	3738	2.715	P = 0.0150
	Time Point	95131	3	31710	23.03	P < 0.0001
	Error	257514	187	1377		
Distraction	Interaction	9701	18	538.9	0.4114	P = 0.9844
	Spinal Location	21767	6	3628	2.769	P = 0.0133
	Time Point	114363	3	38121	29.10	P < 0.0001
	Error	246303	188	1310		

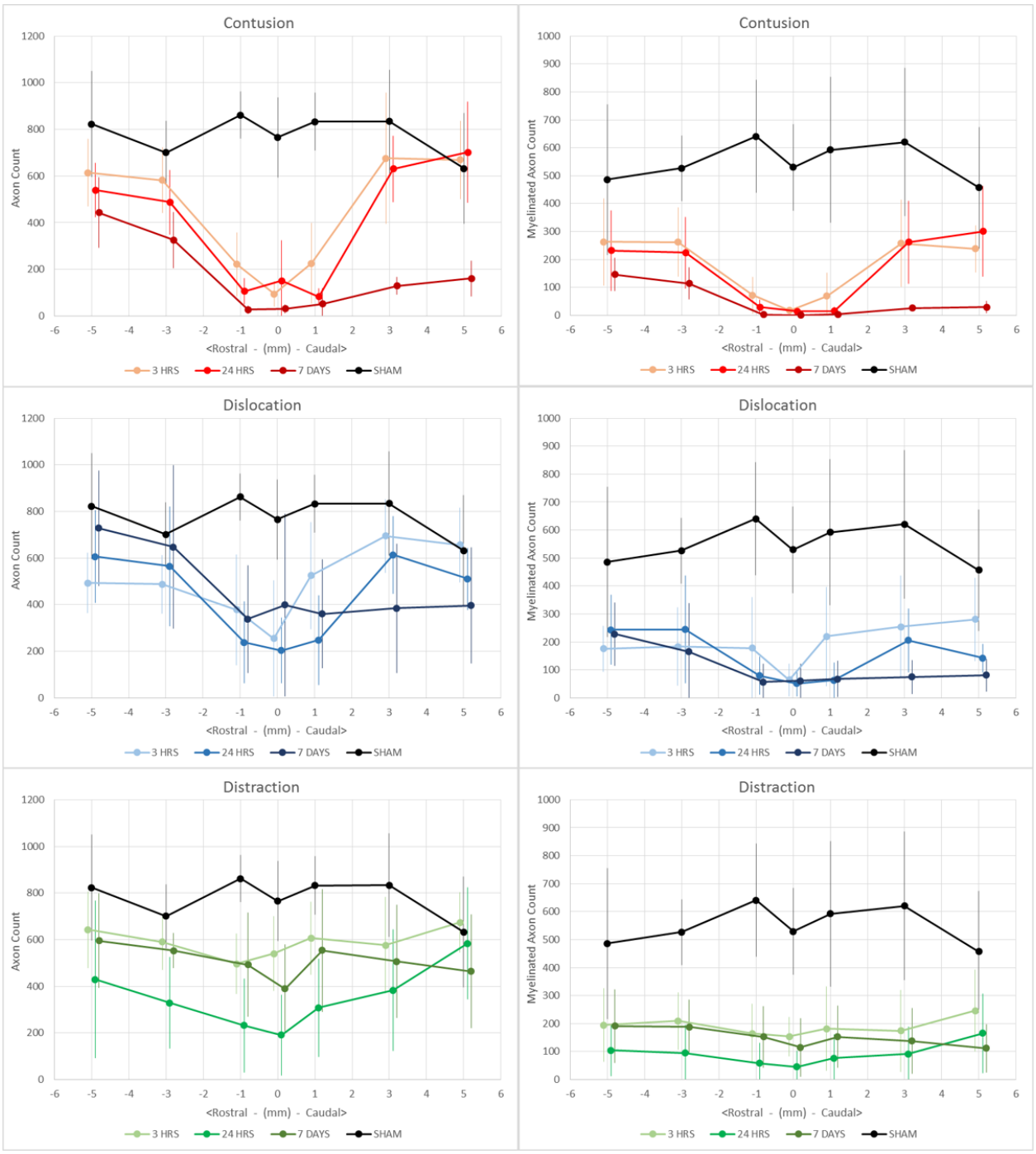

Figure A-3 – Dorsal Corticospinal Tract - Axon and myelinated axon count (per 3278 µm^2) along the length of the spinal cord from rostral (-) to caudal (+).

Table A-3 - Two-way mixed ANOVA summary – Dorsal Corticospinal Tract

Axon Count						
Injury Mechanism	**Effect**	**SS**	**DF**	**MS**	**F**	**P value**
Contusion	Interaction	2.39e+006	18	132806	6.67	P < 0.0001
	Spinal Location	3.03e+006	6	504259	25.3	P < 0.0001
	Time Point	6.06e+006	3	2.02e+006	101	P < 0.0001
	Error	3.33e+006	167	19916		
Dislocation	Interaction	2.146e+006	18	119220	2.260	P = 0.0035
	Spinal Location	1.318e+006	6	219589	4.163	P = 0.0006
	Time Point	2.048e+006	3	682613	12.94	P < 0.0001
	Error	9.759e+006	185	52750		
Distraction	Interaction	839104	18	46617	1.105	P = 0.3500
	Spinal Location	356958	6	59493	1.410	P = 0.2126
	Time Point	3.463e+006	3	1.154e+006	27.36	P < 0.0001
	Error	7.930e+006	188	42183		
Myelinated Axon Count						
Injury Mechanism	**Effect**	**SS**	**DF**	**MS**	**F**	**P value**
Contusion	Interaction	621715	18	34540	2.91	P = 0.0002
	Spinal Location	536427	6	89404	7.54	P < 0.0001
	Time Point	3.90e+006	3	1.30e+006	110	P < 0.0001
	Error	1.98e+006	167	11860		
Dislocation	Interaction	538501	18	29917	1.905	P = 0.0177
	Spinal Location	224909	6	37485	2.387	P = 0.0303
	Time Point	3.375e+006	3	1.125e+006	71.65	P < 0.0001
	Error	2.905e+006	185	15703		
Distraction	Interaction	214086	18	11894	0.8131	P = 0.6835
	Spinal Location	35819	6	5970	0.4081	P = 0.8731
	Time Point	3.456e+006	3	1.152e+006	78.75	P < 0.0001
	Error	2.750e+006	188	14628		

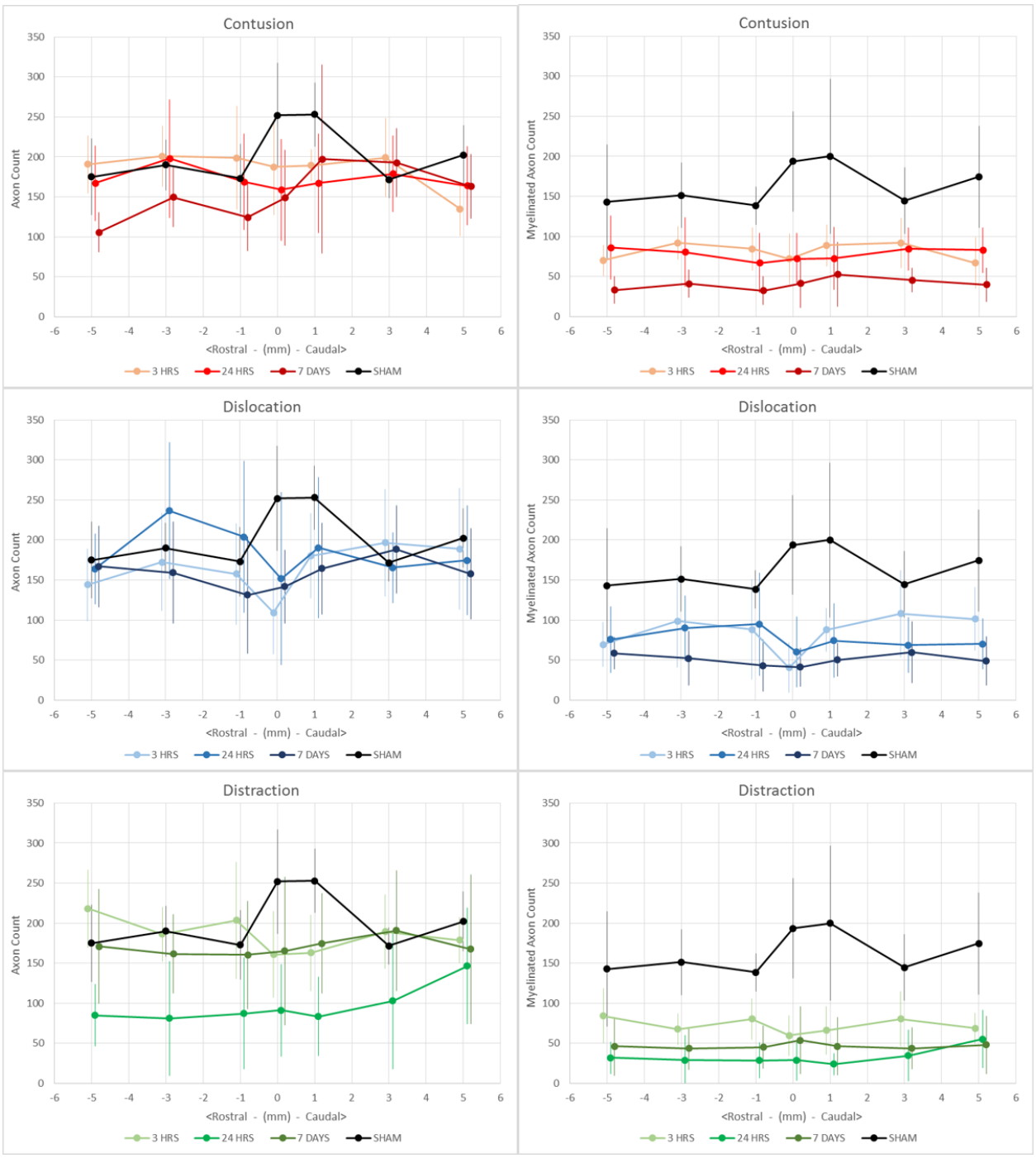

Figure A-4 - Ventrolateral White Matter - Axon and myelinated axon count (per 3278 µm^2) along the length of the spinal cord from rostral (-) to caudal (+).

Table A-4 - Two-way mixed ANOVA summary – Ventrolateral White Matter

Axon Count						
Injury Mechanism	**Effect**	**SS**	**DF**	**MS**	**F**	**P value**
Contusion	Interaction	79797	18	4433	1.54	P = 0.0810
	Spinal Location	31095	6	5182	1.80	P = 0.1012
	Time Point	46813	3	15604	5.43	P = 0.0014
	Error	479837	167	2873		
Dislocation	Interaction	92150	18	5119	1.221	P = 0.2478
	Spinal Location	26051	6	4342	1.036	P = 0.4036
	Time Point	45248	3	15083	3.597	P = 0.0146
	Error	784061	187	4193		
Distraction	Interaction	69296	18	3850	0.9436	P = 0.5271
	Spinal Location	6722	6	1120	0.2746	P = 0.9483
	Time Point	329523	3	109841	26.92	P < 0.0001
	Error	767012	188	4080		
Myelinated Axon Count						
Injury Mechanism	**Effect**	**SS**	**DF**	**MS**	**F**	**P value**
Contusion	Interaction	17813	18	990	0.897	P = 0.5825
	Spinal Location	7889	6	1315	1.19	P = 0.3128
	Time Point	230495	3	76832	69.7	P < 0.0001
	Error	184173	167	1103		
Dislocation	Interaction	36759	18	2042	1.195	P = 0.2689
	Spinal Location	6939	6	1157	0.6766	P = 0.6687
	Time Point	214219	3	71406	41.77	P < 0.0001
	Error	319641	187	1709		
Distraction	Interaction	19688	18	1094	0.9946	P = 0.4677
	Spinal Location	4794	6	799.0	0.7266	P = 0.6287
	Time Point	292889	3	97630	88.78	P < 0.0001
	Error	206732	188	1100		

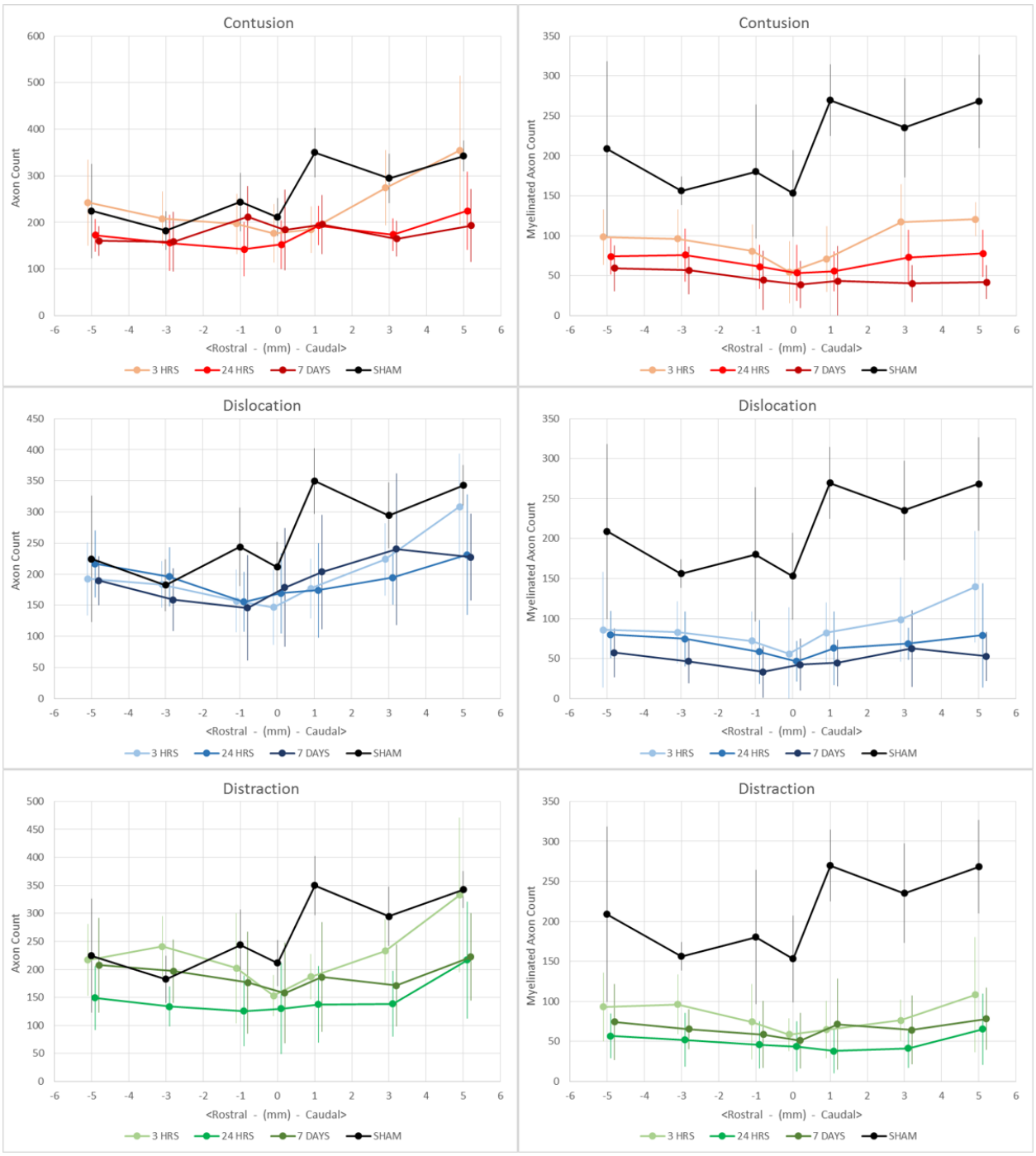

Figure A-5 - Lateral White Matter - Axon and myelinated axon count (per 3278 µm^2) along the length of the spinal cord from rostral (-) to caudal (+).

Table A-5 - Two-way mixed ANOVA summary – Lateral White Matter

Axon Count						
Injury Mechanism	**Effect**	**SS**	**DF**	**MS**	**F**	**P value**
Contusion	Interaction	171722	18	9540	1.93	P = 0.0163
	Spinal Location	174702	6	29117	5.90	P < 0.0001
	Time Point	212641	3	70880	14.4	P < 0.0001
	Error	818866	166	4933		
Dislocation	Interaction	111176	18	6176	1.260	P = 0.2184
	Spinal Location	211258	6	35210	7.185	P < 0.0001
	Time Point	96512	3	32171	6.565	P = 0.0003
	Error	916418	187	4901		
Distraction	Interaction	112485	18	6249	1.101	P = 0.3543
	Spinal Location	188623	6	31437	5.538	P < 0.0001
	Time Point	291612	3	97204	17.12	P < 0.0001
	Error	1.067e+006	188	5677		
Myelinated Axon Count						
Injury Mechanism	**Effect**	**SS**	**DF**	**MS**	**F**	**P value**
Contusion	Interaction	50474	18	2804	2.04	P = 0.0100
	Spinal Location	41619	6	6937	5.06	P < 0.0001
	Time Point	430432	3	143477	105	P < 0.0001
	Error	227623	166	1371		
Dislocation	Interaction	45821	18	2546	1.302	P = 0.1905
	Spinal Location	63144	6	10524	5.381	P < 0.0001
	Time Point	445595	3	148532	75.95	P < 0.0001
	Error	365703	187	1956		
Distraction	Interaction	41106	18	2284	1.312	P = 0.1837
	Spinal Location	42962	6	7160	4.115	P = 0.0007
	Time Point	431744	3	143915	82.70	P < 0.0001
	Error	327141	188	1740		

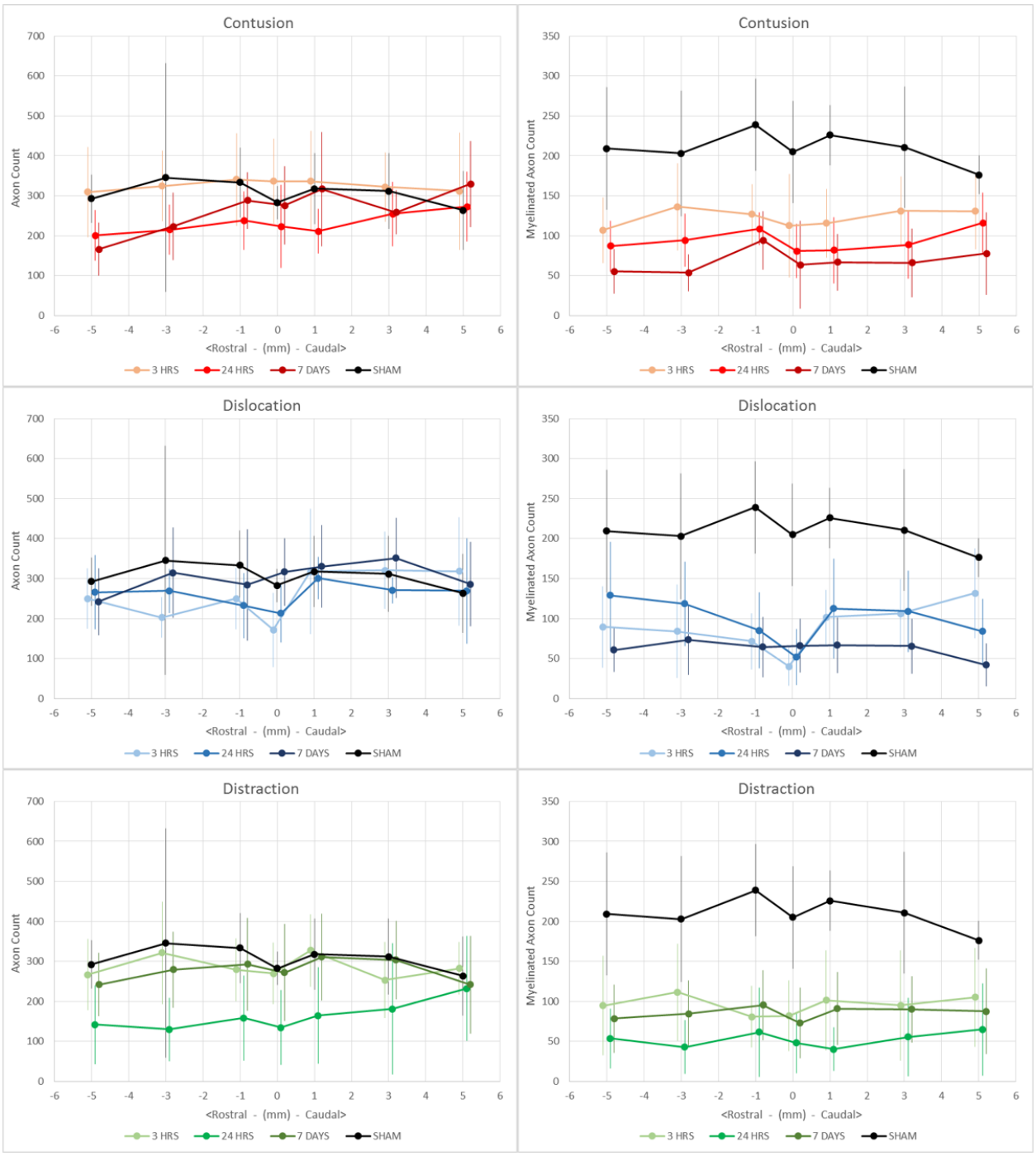

Figure A-6 - Dorsolateral White Matter - Axon and myelinated axon count (per 3278 µm^2) along the length of the spinal cord from rostral (-) to caudal (+).

Table A-6 - Two-way mixed ANOVA summary – Dorsolateral White Matter

Axon Count						
Injury Mechanism	**Effect**	**SS**	**DF**	**MS**	**F**	**P value**
Contusion	Interaction	124102	18	6895	0.689	P = 0.8192
	Spinal Location	53341	6	8890	0.888	P = 0.5050
	Time Point	295197	3	98399	9.83	P < 0.0001
	Error	1.67e+006	167	10011		
Dislocation	Interaction	169314	18	9406	0.9396	P = 0.5319
	Spinal Location	94875	6	15812	1.579	P = 0.1552
	Time Point	100265	3	33422	3.338	P = 0.0205
	Error	1.872e+006	187	10011		
Distraction	Interaction	121934	18	6774	0.5832	P = 0.9088
	Spinal Location	36919	6	6153	0.5298	P = 0.7852
	Time Point	667729	3	222576	19.16	P < 0.0001
	Error	2.184e+006	188	11615		
Myelinated Axon Count						
Injury Mechanism	**Effect**	**SS**	**DF**	**MS**	**F**	**P value**
Contusion	Interaction	16658	18	925	0.482	P = 0.9628
	Spinal Location	11457	6	1910	0.995	P = 0.4302
	Time Point	330188	3	110063	57.4	P < 0.0001
	Error	320359	167	1918		
Dislocation	Interaction	60048	18	3336	1.636	P = 0.0550
	Spinal Location	21967	6	3661	1.795	P = 0.1022
	Time Point	358746	3	119582	58.63	P < 0.0001
	Error	381389	187	2040		
Distraction	Interaction	17166	18	953.7	0.3897	P = 0.9886
	Spinal Location	4199	6	699.8	0.2859	P = 0.9431
	Time Point	393579	3	131193	53.61	P < 0.0001
	Error	460093	188	2447		

Appendix B : Mechanical Properties of the Intervertebral Disc, and Soft Tissue Injury Characteristics

A pilot study was conducted to explore several items of interest that were not addressed in the main thesis study components. Preloading the spinal column prior to a dislocation injury was performed prior to previous dislocation injury tests in attempt to ensure a consistent starting location before injury. This assumes a neutral zone of the intervertebral disc in shear, providing an injury start location at the neutral zone boundary. However the response of the intervertebral disc to low shear loading had not been investigated. Identifying a shear neutral zone of the intervertebral disc may help to inform more consistent testing protocols. The closed-column nature of the dislocation model limits the understanding of damage to the spinal cord and surrounding tissues following injury. This characteristic damage often cannot be directly observed in animals as part of long term survival studies. Qualitative observations of spinal cord and spinal column damage produced by the dislocation injury may help to better understand the mechanism of injury.

The main objectives of this pilot study were as follows:

i. Investigate the force-displacement characteristics of the rat intervertebral disc under low cyclic shear loads to identify a shear neutral zone, and the variability of preloading to a constant force;
ii. Qualitatively investigate the external spinal cord damage following a severe dislocation injury, and;
iii. Determine the damage to surrounding spinal column tissues following a severe dislocation injury.

B.1 Determination of a Shear Neutral Zone

Six animals were used for this study (male, Sprague-Dawley, 352 ± 9 g). Dislocation injury clamps were surgically attached to the rat vertebrae as described in Chapters 3 and 4. The actuator was attached to the caudal vertebral clamp with care to induce a minimal load on the spine, and this location was defined as zero displacement. Cyclic loading in the dorsoventral direction was applied to the caudal clamp (± 3 N, 0.5 Hz, 10 cycles) to determine the force-displacement response. Plots are shown both individually (Figure B-1) and grouped (Figure B-2)

for cycles 2 – 5. Neutral zone was defined as the difference in displacement at zero load between the two phases of motion (the two places the curve crosses the y-axis) (Wilke et al., 1998). The displacement at 3 N (typical preload force) during loading phase was identified, and stiffness was measured as the linear portion of the loading phase (Table B-1).

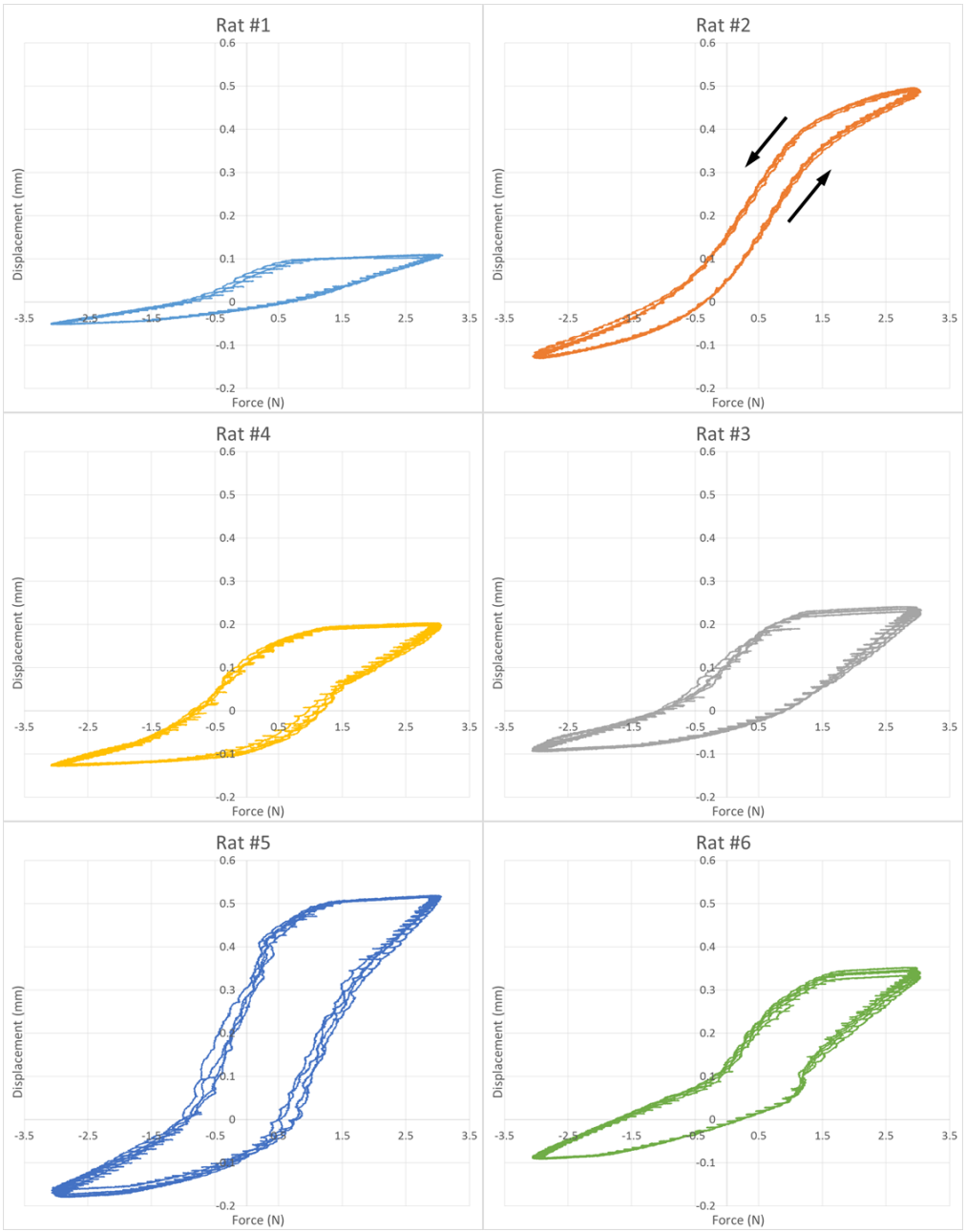

Figure B-1 - Individual force-displacement curves for rat intervertebral discs loaded in cyclic shear (±3 N). The loading cycles correspond to counterclockwise production of the force displacement curves.

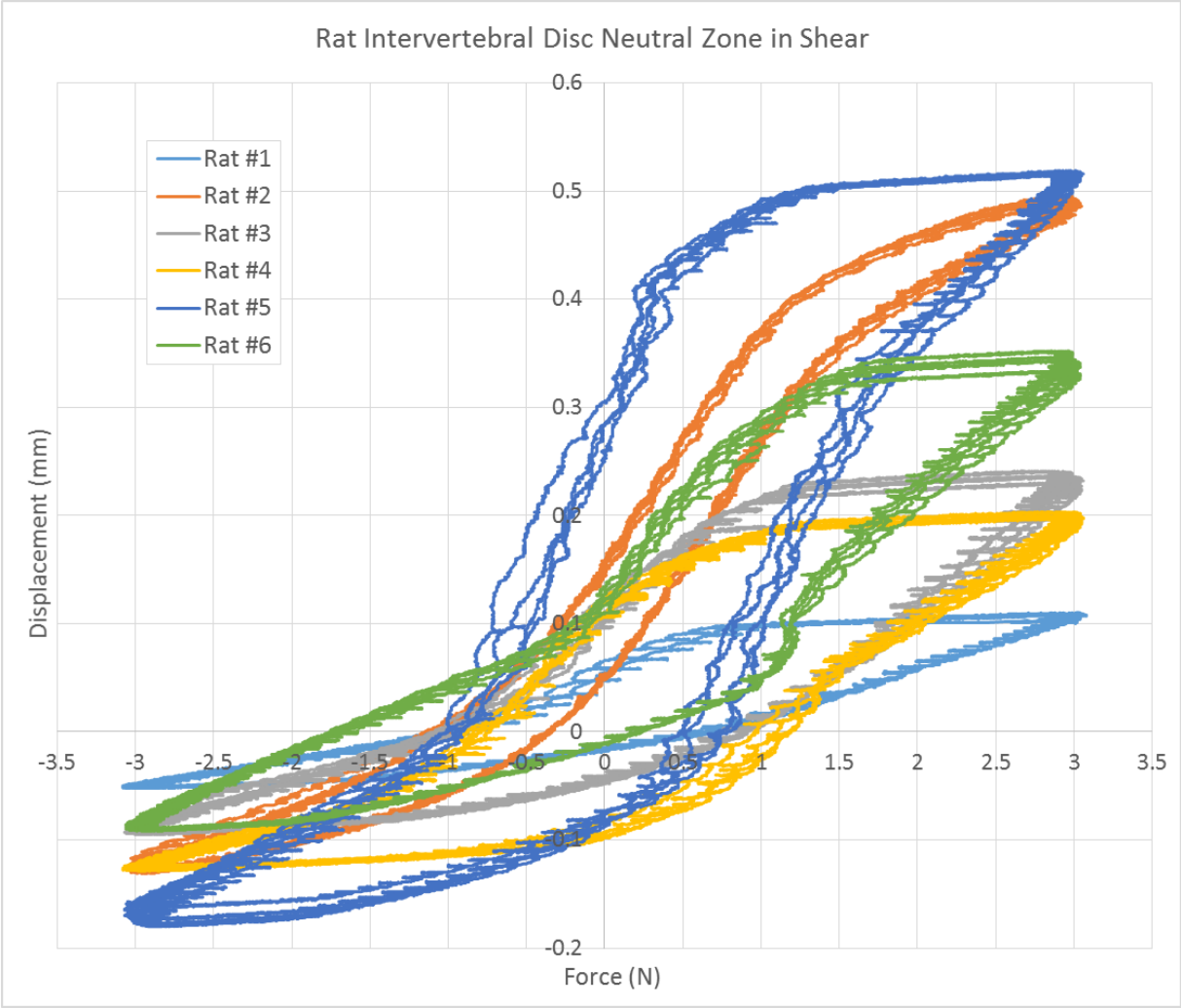

Figure B-2 - Combined force-displacement curves for rat intervertebral discs loaded in cyclic shear (±3 N). Intervertebral discs exhibited different biomechanical characteristics including range of motion, neutral zone, and stiffness.

Table B-1 - Neutral zone (NZ) of rat intervertebral discs in shear, and the displacement corresponding to 3 N of loading, the typical preload force prior to a dislocation injury.

	NZ (mm)	*d at 3 N (mm)*	*Stiffness (N/mm)*
Rat #1	0.08	0.11	20.83
Rat #2	0.11	0.49	4.44
Rat #3	0.15	0.23	8.62
Rat #4	0.21	0.19	7.87
Rat #5	0.37	0.51	3.09
Rat #6	0.16	0.34	8.00
Average (SD)	0.18 (0.10)	0.31 (0.16)	8.81 (6.29)

The mechanical characteristics of the rat intervertebral discs under low shear loading cycles were different between animals. Different neutral zones, and different disc stiffness properties indicate that preloading to a constant force would lead to different relative starting locations for injuries of equivalent injury input parameters. These findings identify another source of variability, and justify the need for redefining a consistent injury starting location between animals.

B.2 External Spinal Cord Injury Pattern and Spinal Column Tissue Damage

Following the intervertebral disc cyclic shear testing, severe dislocation injuries were produced (Table B-2) to allow for qualitative investigation of the spinal cord and spinal column damage.

Table B-2 - Dislocation injury parameters.

Rat	Weight (g)	Injury Disp. (mm)	Injury Force (N)
1	349	1.75	28.4
2	358	1.86	29.2
3	344	1.99	18.8
4	363	1.89	21.9
5	356	1.97	18.7
6	340	2.01	18.9
Average (SD)	352 (9)	1.91 (0.10)	22.65 (4.9)

Dislocation produced a characteristic injury pattern on the dorsal surface of the spinal cord: two distinct lesions lateral to midline (Figure B-3). The lesions were approximately 2 mm long, beginning slightly rostral from the caudal edge of the C5 lamina, and extending further rostrally. Four of five animals demonstrated this injury pattern, one spinal cord appeared uninjured (Rat #4), and one rat perished prior to injury so was not included (Rat #6). The dura mater and dorsal vasculature remained intact in each animal.

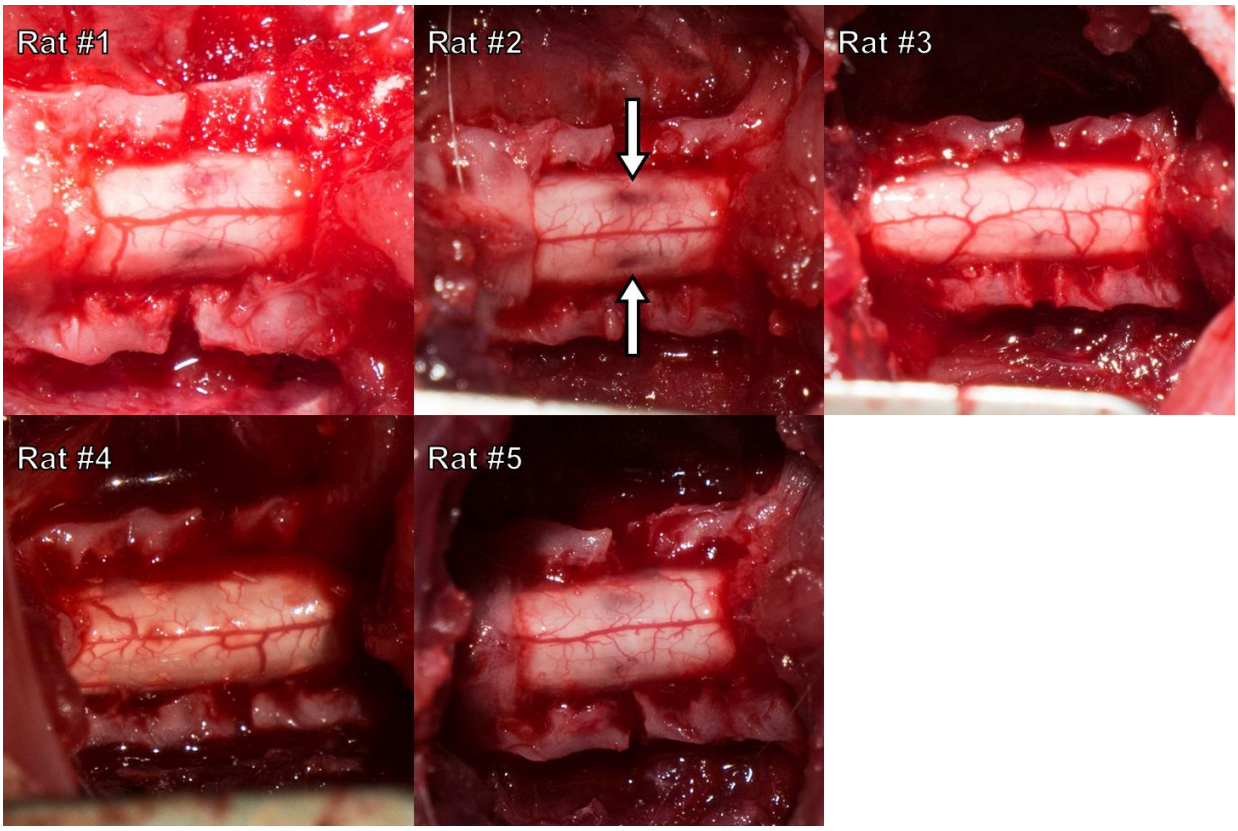

Figure B-3 - Lesion patterns from severe dislocation injuries typically exhibit a 'snake-bite' shape pattern (arrows on Rat #2). These lesions are hidden from sight in the closed-column model until sacrifice. Lesions exhibited consistent symmetrical patterns extending rostrally on the spinal cord from the C5 lamina caudal edge. The dura mater and dorsal vasculature remained intact in each animal.

All six spinal columns exhibited identical damage from the dislocation injury. The ventral dura mater and the posterior longitudinal ligament (PLL) were intact in every instance, however the PLL had been pulled from the dorsal surface of the C5 vertebral body, as evidenced by the underlying blood (Figure B-4.a). The intervertebral disc ruptured entirely from the C5 endplate, as confirmed both dorsally (Figure B-4.b) and ventrally (Figure B-4.c). All ventral soft tissues remained intact, except for the disc rupturing from the C5 endplate.

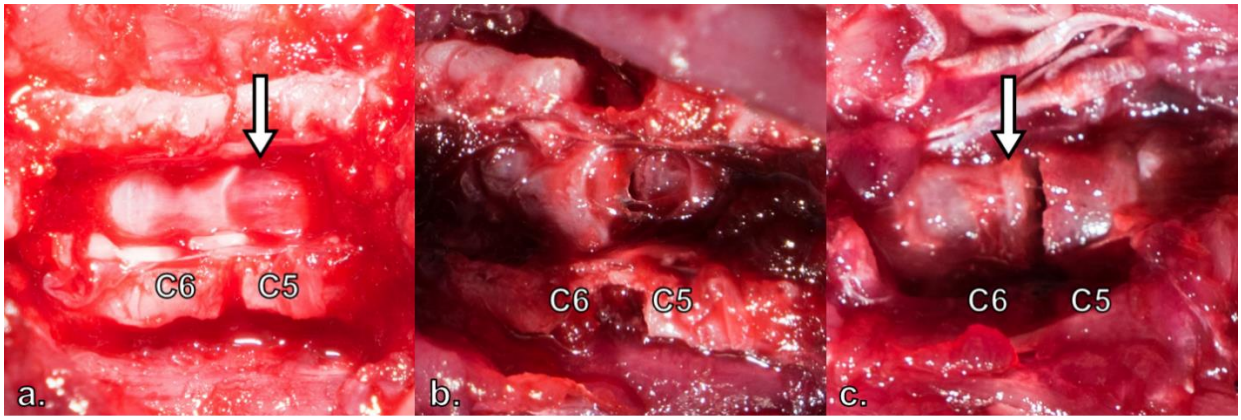

Figure B-4 - Spinal column damage following dislocation injury. a. the ventral dura mater and PLL remained intact following injury in each instance. The underlying hemorrhaging indicate the PLL was pulled from the dorsal surface of the C5 vertebral body (arrow). b. After careful dissection of the dura mater and PLL, the intervertebral disc was seen ruptured from the C5 endplate. c. Ventral approach identified all soft tissues remained intact, except the intervertebral disc which ruptured from the C5 vertebral endplate, indicating complete rupture from the endplate.

Appendix C : Lessons Learned and Development of a Large Animal Dislocation Model

With the increased use of large animal models to more accurately represent human SCI, the future development of a dislocation model is likely. This development should proceed with caution given the difficulties and lack of understanding still present in the small-scale rat dislocation model. Large animal studies typically involve fewer animals, with each animal requiring a significant investment of resources such as time, personnel, and funding. Additionally, there are greater ethical requirements for large animals. Therefore the risks are greater for each experiment, and injuries need to be performed reliably with confidence. Researchers are keen to implement novel methods; however, a large animal dislocation model should be systematically developed to avoid unexpected challenges and wasted resources. Differences between large animal models and the rat model may introduce unknown challenges. The larger size will also relieve certain challenges that exist in the rat dislocation model, such as the manufacture of small yet precise components and limited imaging capabilities.

Researchers will have their own motivations for which animal model to use (e.g. pig, non-human primate), likely due to similarities to the human, and the ability to address specific research questions. The purpose of this section is not to discuss which animal would be the most appropriate model, but to outline considerations in developing a dislocation model in any animal species.

A thorough understanding of the relevant spinal anatomy is required. This includes the shape of the vertebrae, the variability of anatomy between subjects, and surgical limitations. These factors will help inform functional design requirements of the injury system. The shape of the anatomy will provide insight towards the best methods to manipulate the vertebrae to induce injury. Anatomical features may be identified as structures to act as interfaces to the actuator or guide directions of motion (i.e. some structures may be better to push instead of trying to pull). Variability between subjects means it is important to design for adjustability to ensure the components will be compatible with any specimen. Surgical limitations will also influence the design – components may have size requirements to access the anatomy. Injury components must be designed so as to not interfere with other surgical tools or measurement instruments. A closed-column model relies on the vertebral anatomy to induce injury, so the anatomy of the

vertebrae contacting the spinal cord should produce injuries similar to those seen in humans (i.e. no shapes that may cause different types of injury, such as an edge of the lamina sharp enough to puncture the spinal cord).

Extensive pilot testing using cadaveric specimens should be performed to inform design requirements. This will provide insight about the feasibility of various methods of manipulating the vertebrae. Clamps that grip vertebrae may be used, or screws may be inserted into bone. These methods need to be evaluated to determine failure limits. A large animal will require significant force to fracture the intervertebral disc. When manipulating the vertebrae, it should be ensured that the gripping method will not cause fracture of the vertebrae. Limits should be established for any component that requires tightening for both consistency between tests and to avoid inadvertent fracture. This was implemented in the rat dislocation by using a torque screwdriver to tighten the clamps, as several laminae failed during pilot testing. The torque limit was progressively reduced after each failed lamina, until 2.7 cN·m no longer produced any fractures.

The biomechanics of the injury should be well understood to inform the selection of a device to induce injury. Equivalent relative motion kinematics at the dislocation level can be achieved in different ways (i.e. pull caudal vertebra, vs. push rostral vertebra), and all methods should be considered. The desired injury kinematics should first be determined, including the magnitude of translation, degrees of freedom of the vertebrae at the dislocation level, and the required forces to achieve these kinematics. The surrounding hard and soft tissues may have an effect on the motion of the vertebrae. For example, if a vertebra is translated about the centre of gravity the intervertebral disc will resist motion in the form of a moment, which will cause additional loading at the actuator interface. The magnitudes of the forces to cause injury must be determined to inform device functional requirements. A device should be selected that is capable of performing the desired motions, rather than the desired motions limited by the capabilities of the device. Surgical procedures which improve injury consistency should also be explored. The original UBC dislocation model introduced a facetectomy to allow the vertebrae to more easily return to anatomical alignment, but this also reduced the required force to produce the injury. One potential strategy could be to introduce an initiation point for failure of the intervertebral disc via surgical incision. This would reduce the failure force of the disc and provide a consistent

mode of failure. However it is important to properly evaluate risks associated with additional surgical procedures. An intervertebral disc incision would likely involve a ventral surgical site, which would risk damage to the ventral organs and increase risk of infection.

Following a dislocation injury and the failure of intervertebral connecting soft tissues, the spinal column is unstable and requires fixation to prevent further injury. This is not a trivial aspect and should not be overlooked. However, one advantage of larger models is the potential implementation of human spine fixation techniques, such as pedicle screws and rods. The fixation method should be considered during all design phases as it may introduce limitations to producing the injury, especially post-injury when the spine is unstable and requires fixation.

After the system has been designed and manufactured, validation tests are required to confirm the desired kinematics, and consistency between tests.